Comprehensive analysis of peptidoglycan hydrolases in *Caulobacter crescentus*

Dissertation
zur Erlangung des Doktorgrades
der Naturwissenschaften
(Dr. rer. nat.)

dem
Fachbereich Biologie
der Philipps-Universität Marburg

von
Aleksandra Zielińska
aus Świdnica, Polen

Marburg (Lahn), Februar 2016

ABSTRACT

The peptidoglycan (PG) sacculus is a large macromolecule enclosing most bacterial cells. During progression of the cell cycle, it needs to be continuously remodelled to enable elongation of the cell body and, finally, cell division. This process requires a delicate balance between synthetic and hydrolytic reactions, which are executed by an array of different enzymes. However, the roles of individual components in this complex machinery and the mechanisms underlying their temporal and spatial regulation are still incompletely understood. In particular, the functional significance of many PG hydrolases is still unclear.

While acting at all stages of cell wall biogenesis, PG hydrolases have a particularly important role during cell division, facilitating the coordinated invagination of the PG layer as constriction proceeds. Previous work has identified the putative PG hydrolase DipM as a key component of the *Caulobacter crescentus* divisome. However, the extent to which other hydrolases contribute to PG remodelling during the constriction process in this species has remained unknown. To identify the major players and elucidate their function, I have analysed the full set of putative amidases, lytic transglycosylases (LTs), endopeptidases (EPases) and LD-transpeptidases (LD-TPases) encoded in the *C. crescentus* genome. For this purpose, I generated a variety of fluorescent fusions and deletion mutants and characterized them using microscopic and biochemical approaches.

The results obtained indicate that the PG hydrolases of *C. crescentus* have highly redundant functions. Based on the observation of changes in cell morphology, localization dynamics, stress and antibiotic resistance I have identified a particularly important role of EPases in maintaining cell wall integrity. Deletion of the *amiC* and *chap* genes encoding proteins with PG amidase activity had no detectable effect. In contrast, mutants lacking multiple EPases of the NlpC/P60 or LytM subgroups formed either long smooth filaments or occasionally cell chains. Furthermore, the presence of either NlpC/P60 domain containing EPase NlpA, or the Chap amidase is essential to maintain proper growth. Inactivation of all soluble lytic transglycosylases (SLTs), led to cell filamentation accompanied by outer-membrane blebbing. Depletion of DipM, an EPase homologue lacking catalytic activity in strains lacking either all SLTs or all of the remaining LytM factors (a subgroup of EPases), led to a complete block in cell division and finally to cell death. Interestingly, a similar morphological defect was observed upon depletion of a DipM in a strain lacking another LytM factor with degenerated active site, LdpF. Cultivation in stress conditions revealed critical functions of LdpF, SdpA (falling into the SLTs group) and Chap in cell envelope biogenesis, since single deletions of the respective genes led to either osmo- or antibiotic sensitivity. Moreover, SdpA displayed a dynamic localization pattern, characteristic for the divisome components implicated in the final stages of cell wall remodelling, indication a role in the cell division.

Collectively, this work provides the first comprehensive analysis of PG hydrolases in *C. crescentus* and underscores the key role of the catalytically inactive EPase homologues DipM and LdpF in the autolytic system of this species.

ZUSAMMENFASSUNG

Der Peptidoglucan-Sacculus ist ein (einzelnes) großes Makromolekül, welches die meisten bakteriellen Zellen umhüllt. Während des Zellzyklus muss dieser kontinuierlich remodelliert werden, um den Elongationsprozess und letztlich auch die Zellteilung zu ermöglichen. Dieser Prozess benötigt ein empfindliches Gleichgewicht aus synthetischen und hydrolythischen Reaktionen, welche von einer Vielzahl an verschiedenen Enzymen durchgeführt werden. Jedoch sind die Aufgaben der einzelnen Komponenten dieser komplexen Maschinerie, noch deren zeitliche und räumliche Regulation bisher vollständig aufgeklärt. Insbesonders die Funktion und die Signifikanz der meisten PG-Hydrolasen ist noch weitgehend unbekannt.

Während PG-Hydrolasen in allen Phasen der Zellwand-Biogenese beteiligt sind, besitzen sie eine besonders wichtige Rolle während der Zellteilung, bei der sie die streng regulierte Invagination der Zellwand, während des Abschnürprozesses, ermöglichen. Frühere Arbeiten identifizierten das PG-Hydrolase Homolog DipM als eine Schlüsselkomponente des *Caulobacter crescentus* Divisoms. Indes ist der Umfang, in dem Hydrolasen an der PG-Remodelierung bei dieser Spezies beitragen, noch unklar. Um die zentralen Faktoren zu identifizieren und ihre Funktion zu beleuchten, wurden in dieser Arbeit alle Amidasen, lytische Transglycosylasen (LTasen), Endopeptidasen (EPasen) und LD-Transpeptidasen (LD-TPasen) die im Genom von *C. crescentus* kodiert sind, analysiert. Dazu generierte ich eine Vielzahl an Fluoreszenzfusionen und Deletionsmutanten und analysierte diese mit mikroskopischen und biochemischen Methoden.

Die daraus gewonnenen Erkenntnisse zeigten, dass die PG-Hydrolasen von *C. crescentus* hochgradig redundante Funktionen aufweisen. Basierend auf der Analyse der Zellmorphologien, Lokalisierungsdynamiken, Stress- und Antibiotika-Resistenz, konnte eine besonders wichtige Rolle der EPasen bei der Sicherstellung des korrekten Zellwachstums identifiziert werden. Die Deletion der amiC- und chap-Gene, welche Proteine mit Amidase-Aktivität kodieren, hatten keinerlei Effekt. Im Gegensatz dazu bildeten Mutanten mit multiplen Deletionen in EPase Genen, welche in die NlpC/P60- oder LytM-Familie fallen, lange glatte Filamente und gelegentlich Zellketten. Darüber hinaus ist die NlpC/P60 artige EPase NlpA zusammen mit Chap Amidasen redundant essentiell für das Zellwachstum. Eine Inaktivierung aller löslichen lytischen Transglycosylasen (SLTasen) führt zu einer Filamentierung zusammen mit der Bildung von Membranvesikeln. Depletion von DipM in Stämmen, in denen die SLTasen oder die verbleibenden LytM-Faktoren deletiert worden waren, führt zu einem kompletten Stillstand der Zellteilung und schließlich zum Zelltod. Interessanterweise wurde ein ähnlicher Phänotyp, auch bei Depletion von DipM in Zellen erhalten, denen die katalytisch inaktive EPase LdpF, fehlt. Eine Kultivierung unter Stress-Bedingungen zeigte eine eindeutige Funktion von LdpF, SdpA (einer SLTasen) und Chap bei der Zellhüllen-Biogenese, denn Deletionen in den entsprechenden Genen führten einerseits zu einer Osmo- oder Antibiotika-Sensitivität. Ferner zeigt SdpA ein dynamisches, Zellzyklus abhängiges Lokalisierungmuster, das dem von Divisom-assoziierten Proteinen entspricht, die an den finalen Schritten der Zellwandremodellierung beteiligt sind, was eine Funktion bei der Zellteilung unterstützt.

Insgesamt stellt diese Arbeit die erste Umfassende Analyse von PG-Hydrolasen von *C. crescentus* dar und unterstreicht die Schlüsselfunktionder katalytisch inaktiven EPase-Homologe DipM und LdpF im autolytischen System in diesem Organismus.

ABBREVIATIONS

aa	amino acid
APS	ammonium persulfate
ATP	adenosine triphosphate
BAC2H	bacterial two-hybrid
bp	base pairs
BSA	bovine serum albumine
C-	carboxy-
CFP -	cyan fluorescent protein
d	day/s
DAPI	4', 6-diamidino-2-phenylindole
DIC	differential interference contrast
DMSO	dimethyl sulfoxide
DNA	deoxyribonucleic acid
dNTPs	deoxyribonucleoside triphosphate
EDTA	ethylendiaminetetraacetic acid
gent	gentamicin
GFP	green fluorescent protein
kan	kanamycin
kb	kilobase pairs
kDa	kilo Dalton
N-	amino-
LB	Luria-Bertani medium
Ldps	LytM domain-containing proteins
mCherry-	monomeric red fluorescent protein Cherry
OD_{600}	optical density at 600 nm
o/n	overnight
PBP	penicillin binding protein
PCR	polymerase chain reaction
PVDF	polyvinylidene fluoride
RFP	red fluorescent protein
rpm	revolutions per minute
RT	room temperature
SAP	shrimp alkaline phosphatase
SDS	sodium dodecylsulfate
Tat	twin-arginine translocation
TEM	transmission electron microscopy
TEMED	N, N, N', N'-tetramethylethylenediamine
WT	wild-type
YFP	yellow fluorescent protein

TABLE OF CONTENTS

1. INTRODUCTION

From the moment when microorganisms appeared on Earth, the planet was changed in an irreversible way by appearance of oxygen, and the diversification of species. Considering the fact that about 80 % of the evolutionary history of life is limited to microorganisms, an understanding of basic cellular processes in this group of organisms, may be a key for understanding mechanism organizing more sophisticated cellular assemblies. This is one of the reasons why bacteria became excellent model systems to study a variety of physiological processes including cell division. For decades, the machinery responsible for this fundamental process has been investigated extensively, nevertheless its function is still waiting to be unraveled in full details. Cell division is intimately tied to the presence and properties of the cell wall, which ensures the cell shape, its stability and integrity. The mechanistic principles of how exactly the cell wall remodeling is orchestrated with cell division processes are incompletely understood. Considering the complexity of the process, reaching way beyond visible septum formation and separation of the progeny, it must be executed with remarkable fidelity. Intensive studies, which produced an impressive amount of data, characterized an array of conserved and species-specific factors guiding and driving the division mechanism. And this work will contribute to this knowledge.

1.1 Bacterial cell wall

Bacterial cells display an enormous variety of shapes, which are established and maintained by the cell wall. The majority of bacterial species possess a cell wall composed of peptidoglycan (PG, murein) (Weidel & Pelzer, 1964), which together with lipid membrane/s, secondary polymers, and proteins forms the cell envelope. PG is the structural equivalent of an exoskeleton encapsulating the cell, protecting from the unpredictable and often hostile environment. Therefore, cell wall not only preserves the cell's shape and integrity but also provides the mechanical strength to withstand constant changes in turgor/osmotic pressure, thereby protecting the cell from uncontrolled rupture. The PG sacculus is a gigantic (several MDa molecular mass), bag-shaped macromolecule, which can be readily isolated in intact form (Figure 1AB). Surprisingly, the cell wall is not essential for survival. Cell wall deficient variants (CWD, L- forms) of bacteria that normally possess a wall were firstly described in 1935 (Klieneberger, 1935). L-forms, which lost their shape form either unstable, round spheroplasts, or stable, misshaped protoplasts, characterized by anunusual mode of proliferation, including blebbing, tabulation, and vesiculation (Allan *et al.*, 2009).

Back in 1884, the staining method invented by Hans Christian Gram allowed to group bacterial species based on fundamental differences in the structure and thickness of their cell envelope. This staining method is still in wide use, classifying bacterial species as either Gram-positive or Gram-negative. Years later, it has been established that the cell envelope of all bacterial lineages shares a common structural basis, although the architecture and properties of the cell wall can differ significantly. Precisely, Gram-positive species are characterized by a bipartite cell envelope composed of a single lipid membrane topped with 40 nm thick murein layer, often decorated with attached to it proteins

(Neuhaus & Baddiley, 2003). This massive coat is additionally divided into two zones with diverse density based on the presence of teichoic acids (Matias & Beveridge, 2007; Matias & Beveridge, 2005).

In contrast, Gram-negative bacteria are enclosed with tripartite cell envelope composed of an inner (cytoplasmic) membrane (IM), a mostly single-layered (2.5–6 nm) sacculus (Gan *et al.*, 2008; Labischinski *et al.*, 1991; Matias *et al.*, 2003), and an outer membrane (OM), forming a vital permeability barrier (Nikaido, 2003). The cell wall is located in the space between these two membranes, in the so called periplasm (Hobot *et al.*, 1984). Free passage through the murein layer is possible for small proteins up to 25 kDa (Demchick & Koch, 1996), whereas bigger macromolecules require specialized transporter to cross the cell wall. Notably, the IM and OM are structurally divergent. The IM is symmetric and largely consists of phospholipids, while OM is asymmetric, made of a phospholipid-based inner leaflet and an outer lipopolysaccharide (LPS) –based outer leaflet (Duong *et al.*, 1997; Raetz & Whitfield, 2002). LPS is a unique Gram-negative structure, essential for survival in most species, made of glucosamine-based glycolipids (Doerrler, 2006; Raetz & Whitfield, 2002). OM stability is maintained by covalent and non-covalent interactions between OM proteins (Lpp, Pal, OmpA) and PG (Hantke & Braun, 1973; Parsons *et al.*, 2006).
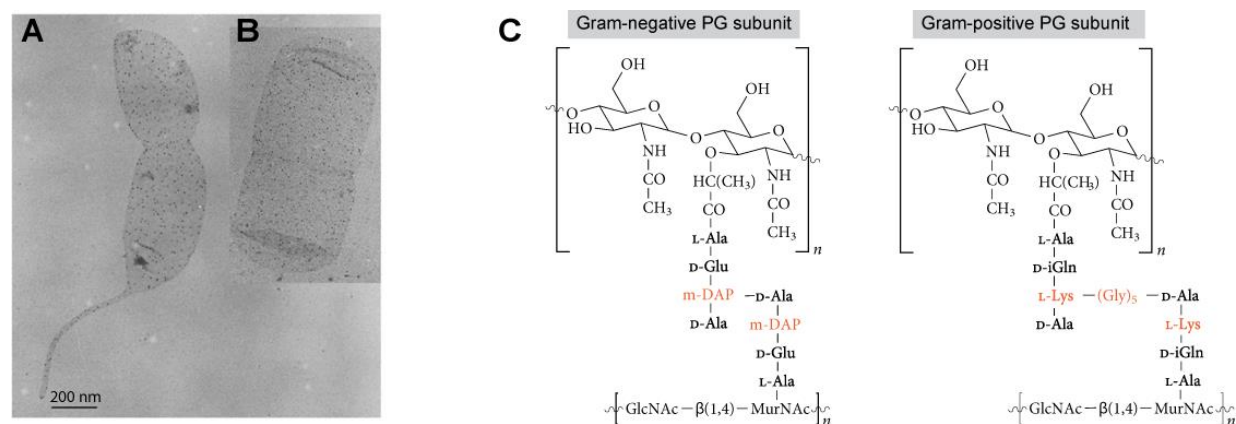
Figure 1. **Structure and architecture of peptidoglycan (PG) in Gram-positive and Gram-negative bacteria. (A)** Electron micrographs of peptidoglycan sacculus isolated from *Caulobacter crescentus* (Vollmer *et al.*, 2008) and *Escherichia coli* **(B)** (den Blaauwen *et al.*, 2008). **(C)** Comparison of the PG subunits composition between Gram-positive and Gram-negative bacteria. Adapted from Royet & Dziarski (2007). On orange were labeled residues characteristic for distinct type of PG.

The chemical composition of PG has been studied intensively for decades. Due to its non-crystalline, relatively flexible arrangement, direct structure determination is impossible. Nevertheless, intensive biochemical studies have revealed a conserved chemical composition, featuring linear, perpendicularly running (Yao *et al.*, 1999) glycan strands of alternating, β1,4-linked N-acetylglucosamine (GlcNAc) and N-acetylmuramic acid (MurNAc) residues (disaccharide subunit) that are cross-linked by short peptides (stem peptides)(Vollmer, 2008; Vollmer *et al.*, 2008) (Figure 1C). MurNAc is a unique monosaccharide found exclusively in the bacterial world, which is an attachment site for the so-called stem peptides, which help condense the murein mesh. Canonical stem peptide subunit consists of five amino acids, including D-stereoisomers that are otherwise rare in nature.

2

Noteworthy, this uncommon composition ensures resistance towards classical peptidases, protecting from unwanted digestion (Cava *et al.*, 2011). Chemical degradation is prevented additionally by the strong ether bond between MurNAc and the peptide chain. Apart from sharing a basic PG precursor, the chemistry and architecture of the cell wall is firstly, specie specific and secondly, cell cycle dependent (Turner *et al.*, 2014).

The current model of the architecture of Gram-negative PG is based on cryo-transmission electron microscopy (cryo-TEM) imaging, atomic force microscopy (AFM) or small angle neutron scattering (SANS) data. AFM imaging revealed conservation of the Gram-negative PG, showing no difference between the sacculi from *Escherichia coli* (*E. coli*), *Caulobacter crescentus* (*C. crescentus*), and *Campylobacter jejuni* (*C. jejuni*) (Turner *et al.*, 2013). The cryo-TEM analyses performed for *E. coli* confirmed the presence of multi-layered PG (Brown *et al.*, 2012; Vollmer & Seligman, 2010). In the current model, the stem peptides stick out from the glycan strands in a helical pattern, with roughly four disaccharide units being required for one complete turn (Vollmer, 2008). The length of the glycan filaments shows great diversity due to species-specific differences in the processivity and of the glycosyltransferases (GTases), the enzymes polymerizing the glycan chains (Wang *et al.*, 2008) and differential PG turnover. For example, the length of the glycan strands of *Bacillus subtilis* (*B. subtilis*) reaches up to 5000 disaccharide subunits (Braun, 1973), whereas in *E. coli* the strands are on average 25 to 40 units long (Glauner *et al.*, 1988). In *C. crescentus*, the glycans are even shorter and only reach 7 disaccharide subunits on average (Takacs *et al.*, 2013). Glycan strands are mainly terminated with GlcNAc or, more rarely with 1,6-anhydro muramic acid (anhydroMurNAc), which is a MurNAc derivative with an intra-molecular ether-linkage between C-1 to C-6 (Holtje *et al.*, 1975). The presence of anhydroMurNAc is essential for murein metabolism, firstly because it marks the end of the glycan strands, preventing further polymerization (Holtje *et al.*, 1975; Park, 1993) and secondly because it fulfills a 'signaling' role, crucial for induction of the PG recycling pathway (Johnson *et al.*, 2013) and β-lactamase synthesis in *E. coli* (Jacobs *et al.*, 1994; Jacobs *et al.*, 1997). In *E. coli*, anhydroMurNAc represent 3-6 % (Glauner, 1988), whereas in *C. crescentus* up to 14 % of the glycan termini (Takacs *et al.*, 2013). Generation of anhydroMurNAc relies on hydrolytic cleavage of the glycan strands by lytic transglycosylases (LTs) (Holtje *et al.*, 1975).

The cell wall is a rather flexible structure. Furthermore, it can reversibly expand and shrink up to three-fold without rupture (Koch & Woeste, 1992), preferentially in the direction of its longer axis in *E. coli* (Yao *et al.*, 1999). It is speculated that the flexibility of murein depends on the developmental stage, where longer, pre-divisional cells have a stretched cell wall due to the high turgor pressure, whereas newly generated offspring has a packed and relaxed one (Vollmer & Bertsche, 2008). Thus, under 'stretched' conditions, the peptides maintain a relatively straight conformation, allowing relaxation of the mesh (Oldmixon *et al.*, 1974; Virudachalam & Rao, 1979). This relaxation is postulated to be crucial for proper PG growth, since only in the stretched state PG is recognized by its biosynthetic complexes (Typas *et al.*, 2012) (for more details see section 1.3.4 and Figure 6).

The variations in PG structure come mostly from the composition of the stem peptides and the type of crosslinking. As mentioned before, the chemical structure of the initial disaccharide pentapeptide

subunit is shared by almost all Gram-negative bacteria as well as the Gram-positive species *B. subtilis* and *Listeria monocytogenes* (*L. monocytogenes*) (Schleife.Kh & Kandler, 1972)(Figure 1C). The classical pentapeptide subunit of the stem peptides consists of L-alanine (L-Ala)–D-iso-glutamate (D-Glu) – diaminopimelic acid (mDAP)–D-alanine (D-Ala)–D-alanine (D-Ala). mDAP is achiral derivative of lysine participating in the formation of the crosslinks between adjacent peptide chain(s), leading to two/three dimensional net-like arrangement. For all bacterial species, the stem peptide terminates with two D-Ala, which are recognized and cleaved by DD-transpeptidases (DD-TPases). DD-TPases catalyze the cleavage of the terminal D-Ala, which energizes the synthesis of the peptide bond (crosslink) linking two neighboring stem peptides (Vollmer & Bertsche, 2008). Interestingly, the fourth and the fifth D-Ala can be substituted with glycine (Gly) and D-phenylalanine or D-tryptofan and D-methionine, respectively, which modulates the possibility for hydrolytic cleavage (Caparros *et al.*, 1991). The exchange of the terminal D-Ala to glycine in the pentapeptide PG precursor is a rather rare event in *E. coli* (in about 1 %), unlike in *C. crescentus* where this substitution occurs in about 19 % of the PG stems, if glycine is available in the growth media (Takacs *et al.*, 2013). Pentapeptide stems are characteristic for newly synthesized (nested) murein, which was not yet subjected to maturation through proteolytic cleavage by DL- and LD-EPases. Therefore, the mature *E. coli* PG is built mostly out of tetra- (L-Ala-D-Glu-mDAP-D-Ala) and to small extent, tri-(L-Ala-D-Glu-mDAP) and di- (L-Ala-D-Glu) peptides (Vollmer *et al.*, 2008).

In *E. coli*, approximately 20-30 % of the stem peptides in PG are cross-linked. Interestingly, murein is cross-linked not only by dimeric peptide bridges between two sugar strands, but in 4.6 % of cases by trimeric bridges connecting three glycan strands (Holtje, 1998). The amount of cross-links relies on the growth conditions, and their number increases with time as result of PG maturation (Glauner *et al.*, 1988). Notably, the degree of cross-linking differs significantly between bacterial species: in *E. coli* 31–61 % of stem peptides are bridged (Vollmer & Seligman, 2010), in *C. crescentus* the degree of crosslinking was shown to be 34 % (Takacs *et al.*, 2013), in *B. subtilis* 3 % (in spores) or 64 % (stationary phase) (Atrih *et al.*, 1996) and in the Gram-positive coccus *Staphylococcus aureus* (*S. aureus*) 74–92 % (Snowden & Perkins, 1990). There are two distinct types of crosslinks, created by two different types of enzymatic reactions in the Gram-negative bacteria. The majority of the inter-bridges condensing the mesh is generated by the PBPs (**P**enicillin-**b**inding **p**roteins), which have DD-transpeptidase (DD-TPase) activity, and catalyze the formation of the 4-3 cross-links between the mDAP moiety of one stem peptide and the D-Ala at position 4 of an adjacent stem peptide.

An alternative type of linkage (3-3), formed between two mDAP residues in the peptide stems, is catalyzed by LD-TPases, the novel (discovered in 2002), penicillin-insensitive group of PG biosynthetic enzymes (Mainardi *et al.*, 2002). LD-TPases from the YkuD superfamily were first described in enterococci, but they are widespread among bacterial lineages (Mainardi *et al.*, 2002). It has been shown that LD-TPases are anchoring Braun's lipoprotein (Lpp) to PG (Magnet *et al.*, 2008) and are central components of PG synthetic machinery of Gram-positive *Agrobacterium tumefaciens* (*A. tumefaciens*) (Cameron *et al.*, 2014). Moreover, in *Enterococcus faecium* (*E. faecium*), LD-TPases can bypass the action of PBPs, resulting in increased β-lactam resistance (Mainardi *et al.*, 2005). The fraction of 3-3 cross-links differs significantly between bacterial species reaching 3-5 % (Sanders &

Pavelka, 2013) in *E. coli*, but more than 50 % in *S. meliloti* and *A. tumefaciens* (Brown *et al.*, 2012) and 60-80 % in *M. tuberculosis* (Kumar *et al.*, 2012). A current study of *A. tumefaciens* reported that all four LD-TPase homologues are recruited from the growing cell pole to the midcell with the onset of cell division, indicating that the unipolar growth of *Rhizobiales* is a dynamic process (Cameron *et al.*, 2014). Interestingly, the lack of LD-TPases in *E. coli* does not affect the morphology of the cells, in contrast to *A. tumefaciens*, suggesting a possible correlation with the polar mode of growth (Sanders & Pavelka, 2013).

1.2   Cell wall biogenesis

The exact molecular mechanisms coordinating PG biogenesis are still enigmatic. Current hypotheses assume that cell wall biosynthesis relies on the formation of multienzyme complexes comprising both synthetic and hydrolytic activities. There are several suggestions describing possible scenarios of the growth of the murein sacculus. The common 'make before break' model suggests that the newly synthesized subunits of nested PG are inserted into the existing sacculus, which is beforehand nicked by specialized PG hydrolases (Koch *et al.*, 1981). The growth model suggested by Burman & Park presumes first PG hydrolysis, followed by incorporation of the new strands with concomitant cross-linking exclusively between new and old glycan strands (Burman & Park, 1984; Park, 1995). The 3-for-1 model assumes incorporation of the three new glycan strands with concurrent removal of one old one (Holtje, 1998). Positioning of the cell wall biogenesis complex is thought to be controlled by the cytoskeletal elements and OM proteins (Holtje, 1998; Typas *et al.*, 2010).

In every generation, the synthesis of new PG and its incorporation into the sacculus is accompanied by the removal of old material in a process called PG turnover. The soluble turnover products are transported into the cytoplasm where they are recycled for *de novo* murein synthesis (Goodell & Schwarz, 1985).

1.2.1   Synthesis of the peptidoglycan precursor

In general, PG biosynthesis consists of three main stages taking place in three different cell compartments: the cytoplasm, the IM and the periplasm, respectively. The PG precursor is first synthesized in the cytoplasm. It is then attached to the lipid and completed, yielding lipid II, which is flipped through the membrane. Finally, and thirdly, PG subunits are inserted into the existing PG mesh, resulting in nested PG formation. The reactions driving these processes are carried out by a specialized group of enzymes, best described for *E. coli*.

Synthesis of the soluble PG precursor starts in the cytoplasm with the MurA-catalyzed transfer of an enolpyruvyl residue from phosphoenolpyruvate (PEP) to uridine diphosphate (UDP)-N-acetylglucosamine (GlcNAc) resulting in the formation of enolpyruvyl UDP-GlcNAc (Barreteau *et al.*, 2008). The next step in PG synthesis requires the reductase MurB to catalyze the NADPH-dependent conversion of enolpyruvyl UDP-GlcNAc to UDP-MurNAc. Subsequently, the pentapeptide side chain is synthesized by the series of ligation reactions, catalyzed by the ATP-dependent ligases MurC, MurD, MurE and MurF. MurC catalyzes addition of the first L-Ala onto the UDP-MurNAc precursor. Next,

MurD mediates the addition of D- Glu to UDP-MurNAc-L-Ala, followed by the action of MurE ligating the third peptidyl residue, mesodiaminopimelic acid (mDAP) in the Gram-negative *E. coli* or L-Lys in the Gram-positive *S. aureus*. MurF catalyses the next cytoplasmic step with the addition of D-Ala-D-Ala. D-Ala is made by the alanine racemase from L-Ala, and condensation of two molecules leads to the final product. Stem peptide can be inhibited by the action of D- cycloserine, a structural analogue of the D-Ala that inhibits both the racemase and D-Ala ligase.

In the second step, the lipid I precursor is assembled by a transfer of the muramyl pentapeptide onto an undecaprenyl phosphate carrier (bactoprenol or UP), catalyzed by the IM protein MraY (Bouhss *et al.*, 2008), yielding lipid I. The pool of lipid I molecules has been estimated at 700 molecules/cell (Mravljak *et al.*, 2011). Next, the IM glycosyltransferase MurG converts lipid I in a lipid-anchored disaccharide-pentapeptide subunit (lipid II). In the last, third step, the lipid II precursor is flipped over the membrane to the periplasm, most likely by the FtsW or RodA or MurJ flippase (Sham *et al.*, 2014), and polymerized, releasing the lipid carrier. The resulting glycan precursor is then ready to be inserted into the existing sacculus.

The third stage of PG expansion comprises lipid II polymerization and peptide stem crosslinking, which are carried out in the periplasm by specialized synthases- the penicillin binding proteins (PBPs), named after their ability to bind penicillin (Suginaka *et al.*, 1972). Notably, PBPs are classified according to their molecular weight (Spratt, 1977). PBPs are divided into three classes, based on their predicted activity: bifunctional glycosyltransferases/transpeptidases (class A GTase/TPase), monofunctional TPases (class B PBPs), and monofunctional GTase (Sauvage *et al.*, 2008). Transglycosylases elongate the sugar backbone by catalysing formation of the 1,4-β-glycosidic bond between an existing glycan strand and lipid II, while transpeptidases catalyze peptide bond formation between adjacent stem peptides. The *E. coli* genome encodes three bifunctional PBPs (PBP1A, PBP1B, and PBP1C, which have partially redundant functions in the biosynthetic process), two TPases (PBP2, crucial for elongation events, and PBP3, also known as FtsI, essential for cell division) and one GTase, MgtA. The function of PBP1C and MgtA is not known. The set of *E. coli* PG synthases is anchored to the cytoplasmic membrane (Egan & Vollmer, 2013). The TP and TG activities of the class A PBPs were investigated *in vitro* with lipid II as a substrate, revealing efficient glycan strand formation by PBP1A and PBP1B with an average length of 23 disaccharide units, and with 18–50 % of stem peptides crosslinked respectively. It has been proposed that the TPase and GTase activities of PBP1A and PBP1B are coordinated and require successful GTase reactions for TPase activity (Bertsche *et al.*, 2006; Born *et al.*, 2006).

The monofunctional TPases PBP2 and PBP3 are essential for elongation and division respectively. Likewise, the bifunctional TPases PBP1A and PBP1B specifically interact with the elongation and division machineries, respectively, although they can substitute for each other (Yousif *et al.*, 1985). Studies on *E. coli* demonstrated TP activity of PBP2 in the presence of PG and PBP1A. The localization pattern of PBP2 in *E. coli* supports the idea that it is particularly active during elongation and early septation (Den Blaauwen *et al.*, 2003). Interestingly, in *C. crescentus*, an osmotic upshift causes relocation of PBP2 to midcell, implying an adaptation of growth in response to the fluctuating

environmental conditions (Hocking *et al.*, 2012). A recent report proposed that in *E. coli* PG synthesis is also regulated by the OM lipoproteins LpoA and LpoB, which stimulate *in vitro* the activity of PBP1A and PBP1B respectively (Paradis-Bleau *et al.*, 2010; Typas *et al.*, 2010). The Lpo activators span the periplasm and traverse the cell wall to reach the cognate PBPs and form active synthase complex (Egan *et al.*, 2014; Jean *et al.*, 2015).

1.3   Bacterial cell division

The precise order and coordination of fundamental cell cycle events must be maintained to assure survival of the cell. Three sequential processes a DNA replication, chromosome segregation, and cell division, must be completed to prevent premature onset of division and inappropriate partitioning of DNA between the progeny.

Rod-shaped bacteria undergo two phases of growth: elongation and division (Figure 2). During the elongation phase, the cell grows longitudiually while keeping its width, whereas the division phase leads to formation of the septum and the new cell poles. The precursors for cell wall biosynthesis are synthesized in the cytoplasm. Therefore, bacteria assemble IM-associated multiprotein complexes facilitating growth events in a cell cycle-dependent rhythm. These temporarily built complexes named elongasome and divisome are guided by cytoskeletal elements.
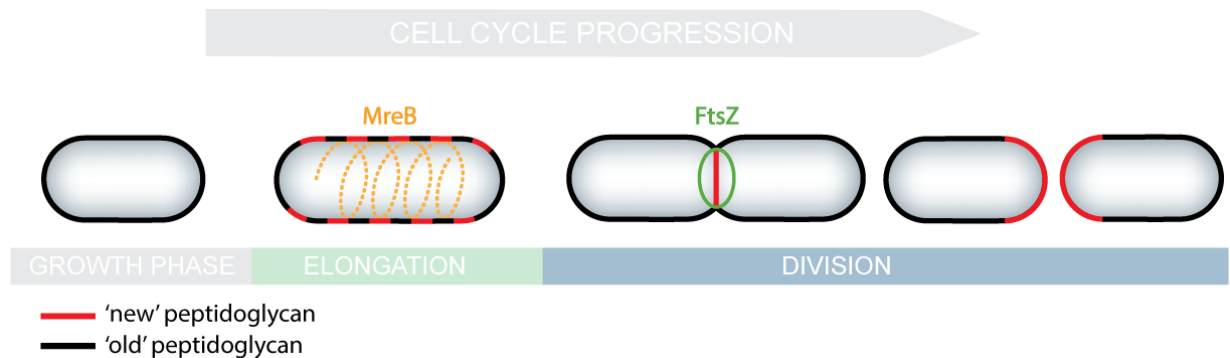
Figure 2. **Modes of the PG synthesis are dictated by the cell cycle.** The process of growth in rod-shaped bacteria is divided into the elongation phase and the division phase. The elongation phase is controlled by the actin-like MreB protein (orange dashed helix), which guides the patchy-like insertion of the PG subunits (red dashed line) along the sidewalls, except of the poles. The division phase is controlled by the tubulin homologue FtsZ (green circle), which assembles into a ring-like structure at the site of division promoting zonal PG synthesis and septal cross-wall formation (red line). Next, the septum is split between the daughter cells, forming the new polar caps.

1.3.1   Biosynthesis of the cell wall is driven by the cell cycle

The elongation and the division events involve distinct modes of PG insertion. However, both require synthesis of the new PG subunits and concurrent hydrolysis of the existing matrix to allow expansion. The common view suggests that during elongation, the newly synthesized PG subunits are inserted in patchy like pattern at the sidewalls, excluding the poles (Figure 2). It is believed that the actin-like protein MreB ensures constant cell width by guiding elongasome assembly and activity. The precise

localization pattern of polymerized MreB filaments is still subject to discussions since the dynamic nature and the resolution limit of light microscopy gave rise to opposing observations. Previously, it was stated that MreB forms mobile patches moving perpendicularly to the long axis of the cell, attracted by ongoing PG synthesis (van Teeffelen *et al.*, 2011). However, results based on recent high-resolution imaging question this statement and rather support the model in which MreB forms dynamic arcs (Errington, 2015; Olshausen *et al.*, 2013)(Figure 2).

In majority of rod-shaped bacteria, including *E. coli,* once the cell reaches twice its initial length, a visible constriction is formed at the midcell, indicating the initiation of the septation phase. At this point, PG synthesis switches from dispersed to zonal growth at the division site. Synthesis of the septum is guided by the tubulin homologue FtsZ, which polymerizes in a GTP-dependent manner into a ring-like structure at the future division plane (Erickson *et al.*, 2010). The septum, which is a cross-wall between the dividing cells, will ultimately be split and form the new cell poles of mother cell and its progeny. The exact trigger for the switch between the elongation and division mode is not known.

E. coli's divisome is composed of ten essential (FtsA, B, I, K, L, Q, N, W, Z and ZipA), conserved proteins and about twenty redundant ones, which have important roles during the fission process, but individually are not crucial for survival (de Boer, 2010; Egan & Vollmer, 2013; Lutkenhaus *et al.*, 2012). Loss of any core component results in the formation of long, smooth, multi-nucleate filaments that ultimately die. The complexity of the septal ring reflects the intricacy of tasks, which must be fulfilled to successfully go through the division process.

The precise position of the Z-ring at the midcell is controlled by specialized molecular mechanisms, preventing polymerization in the aberrant location. Two negative Z-ring regulators were characterized for *E. coli*: the Min system and nucleoid occlusion (de Boer *et al.*, 1989; Levin *et al.*, 1998), whereas in *C. crescentus* it is gradient-forming regulator MipZ (Thanbichler & Shapiro, 2006). The exact pattern formed by the FtsZ polymers has been studied for years, resulting in two main hypotheses. Studies based on cryo-TEM both *in vitro* and *in vivo* in *E. coli* and *C. crescentus* support a model where single-layered filaments create a continuous ring (Szwedziak *et al.*, 2014). The alternative analysis, obtained for *C. crescentus* via photoactivated localization microscopy (PALM), favored a model where the ring was rather built out of patchy bundles, rarely forming a continuous ring (Holden *et al.*, 2014).

FtsZ forms a basis of all division apparatus, and is believed to coordinate septation by generation inwardly directed constrictive force (most likely coming out of the bending filaments) (Osawa *et al.*, 2009). Moreover, it was published that FtsA and FtsZ are sufficient to generate contractile rings *in vitro* in liposomes (Osawa and Erickson, 2014).
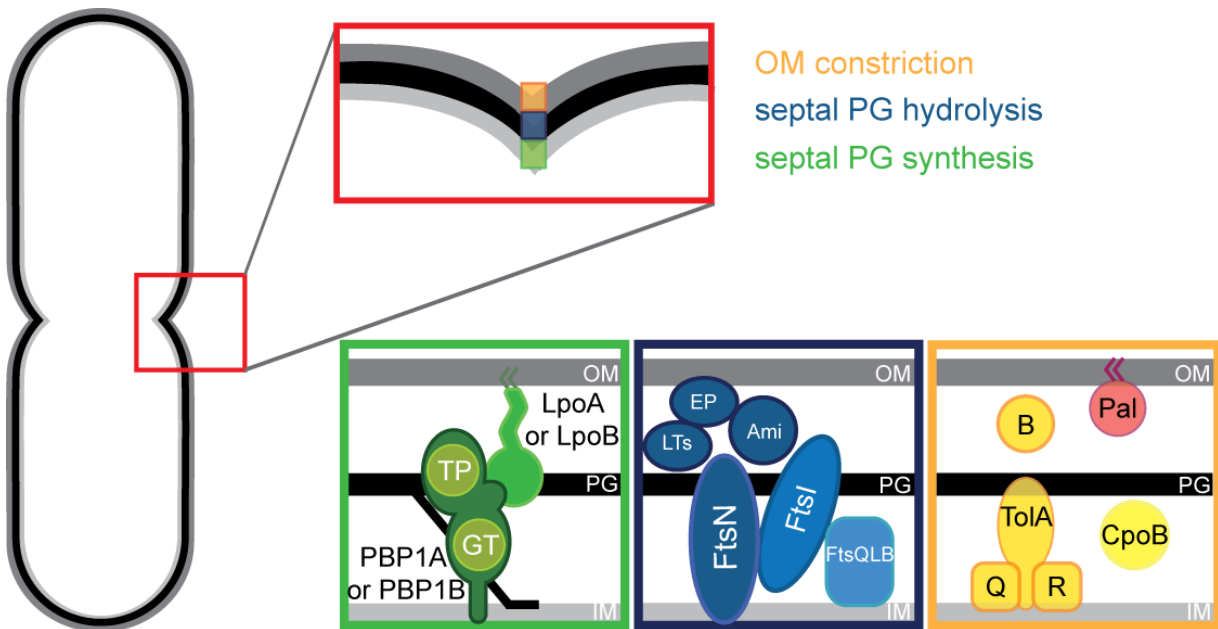
Figure 3. **Machineries involved in cell envelope constriction in Gram-negative bacteria.** Schematic of the Gram-negative cell envelope. The upper panel illustrates the processess involved in remodelling of the tripartie Gram-negative cell envelope (light grey color represents the inner membrane (IM), black represents peptidoglycan (PG), and dark grey represents the outer membrane (OM)). The lower panels show the main components involved in the particular stage of the cell envelope remodelling process in *E. coli*. PG synthesis (green frame) is facilitated by bifunctional High-Molecular Mass (HMM) PBPs with both glycosyltransferase (GT) and transpeptidase (TP) activity, which form a trans-complex with their cognate Lpo activators, required for PBP activity. PG hydrolysis (blue frame) is carried out by the essential late recruits of the cell division apparatus (explanation in text) along with PG hydrolases: lytic transglycosylases (LTs), endopeptidases (EP) and amidases (Ami). OM constriction (yellow frame) is conducted by the Tol-Pal complex, comprising TolA, TolQ (Q), TolR (R), TolB (B), Pal and accessory CpoB protein. Modified from (Gray *et al.*, 2015).

In *E. coli,* cell division starts when FtsZ assembles into a ring-shaped complex (Z-ring) on the cytoplasmic side of the IM, driven by its GTP-dependent polymerization and depolymerization, way before the cell visibly invaginates the cell envelope. The essential components of the divisome attracted by FtsZ, show almost linear dependency, where the absence of one key factor prevents the recruitment of the respective 'downstream' proteins. Analysis of divisome assembly, based mostly on fluorescence microscopy, revealed two recruitment waves: early and late, separated by a significant time interval termed preseptal elongation. Z-ring assembly is followed by almost simultaneous recruitment of FtsA, ZipA, ZapB, ZapC, ZapD (YacF), ZapA, FtsEX, and FtsK (Aarsman *et al.*, 2005), the early associates, driving preseptal elongation. FtsA and/or ZipA are the first two proteins arriving at the division plane to tether the Z-ring to the membrane via interaction with the conserved C-terminal region of FtsZ (Haney *et al.*, 2001; Ma & Margolin, 1999; Pichoff & Lutkenhaus, 2002; Szwedziak *et al.*, 2014). FtsA is a bacterial actin-like protein, forming membrane-associated protofilaments (Pichoff & Lutkenhaus, 2007), whereas ZipA is a bitopic membrane protein fulfilling most likely a ring-stabilizing function (Hale & deBoer, 1997; Pazos *et al.*, 2013). Homo-polymeric filaments formed by FtsA are believed to help tethering longer FtsZ filaments to the membrane (Lara *et al.*, 2005; Szwedziak *et al.*, 2012). Interestingly, mutations in FtsA can bypass the lack of the normally essential protein ZipA (Bernard *et al.*, 2007; Geissler *et al.*, 2003; Pichoff *et al.*, 2012). The assembly of the divisome then continues with the arrival of the ZapA-D proteins, which possess partially overlapping functions in

9

stabilizing and regulating FtsZ ring dynamics (Durand-Heredia *et al.*, 2012; Gueiros-Filho & Losick, 2002; Hale *et al.*, 2011).

The FtsEX complex, which is composed of the ATPase (FtsE) and the transmembrane (TM) part (FtsX) is homologous to ABC transporter (ATP-binding cassette), and conditionally essential for cell division in *E. coli* (Schmidt *et al.*, 2004). In a medium with low salinity, FtsEX is crucial to keep cells alive (de Leeuw *et al.*, 1999; Schmidt *et al.*, 2004). The division defect caused by the loss of FtsEX can be partially aleviated by the overproduction of FtsZ or FtsN, as well as increased osmolality and cultivation at the lower temperature (Reddy, 2007; Schmidt *et al.*, 2004). Recent studies showed that rather than transporting an unknown substrate, FtsEX modulates PG cleavage by regulating PG amidases in *E. coli* (Yang *et al.*, 2011), *B. subtilis* (Meisner *et al.*, 2013), and *S. aureus* (Sham *et al.*, 2011) respectively (for details see section 1.4.4).

After assembly of the early divisome componens, a multi-functional protein FtsK arrives at the midcell, with a well-defined role in the resolution and segregation of the sister chromosomes. This polytopic IM protein is composed of cytoplasmic, C-terminal domain forming homohexameric DNA translocase and periplasmic N-terminal part. The cytoplasmic part is not crucial for survival (Sherratt *et al.*, 2010), whereas the latter one is essential to sustain proper division events (Aussel *et al.*, 2002; Lowe *et al.*, 2008). Apart from its DNA pumping role, FtsK stabilizes the Z-ring and is required for the localization of the downstream FtsQLB complex (Buddelmeijer & Beckwith, 2004; Chen & Beckwith, 2001).

1.3.2 Final stages of the cell division

Invagination of the OM at the midcell in Gram-negative species is usually coordinated with the ongoing septation. Septation in turn, is initiated after successful duplication and segregation of the nucleoid. In order to start the septation process, six core 'late cell division' proteins are recruited in a linear hierarchy to complete the divisome assembly: FtsQ, FtsL, FtsB, FtsW, FtsI and FtsN. All of these are integral IM proteins. Most of the decorating, non-essential Z-ring components arrive to the division site once the constriction process is initiated (Figure 3).

FtsQ, FtsL, and FtsB form an essential complex, which is well-conserved throughout the bacterial kingdom (Buddelmeijer & Beckwith, 2004; Goehring & Beckwith, 2005). In *E. coli,* FtsB and FtsL are mutually dependent on each other. In *E. coli* FtsQ is a low abundance periplasmic protein (22 copies) with a bitopic topology (Carson *et al.*, 1991). FtsL forms unstable dimers *in vitro* and heterodimers with FtsQ and FtsB (Buddelmeijer *et al.*, 2002; Buddelmeijer & Beckwith, 2004; Ghigo & Beckwith, 2000). Previously, it has been stated that FtsQLB does not have any enzymatic activity but rather is an assembly factor, forming a scaffold for other Z-ring components such as FtsW or FtsI, whose recruitment relies on their presence (Gonzalez & Beckwith, 2009; Gonzalez *et al.*, 2010). In *B. subtilis,* DivIC (FtsB homologue) and FtsL are unstable until fixed by the contact with each other and DivIB (FtsQ homologue) at the septum, suggesting that an FtsQLB might be a control point for divisome assembly (Daniel & Errington, 2000; Robson *et al.*, 2002). Indeed, a current report postulates that FtsL together with FtsQ and FtsB, rather than being an inactive scaffold, function as a sensing complex disclosing divisome maturity to trigger septal cross-wall synthesis in *E. coli* (Tsang & Bernhardt,

2015a). Studies in *S. aureus* suggest a PG binding ability of FtsQ, implying a direct influence on the cell wall remodeling and thus an active contribution of FtsQLB to the division process (Bottomley, 2014).

FtsW is thought to be a flippase, transporting the lipid II precursor through the cytoplasmic membrane to the periplasm, where it is used as a substrate for PG synthesis (described in chapter 1.1.2.1). FtsW is member of the SEDS (**s**hape, **e**longation, **d**ivision, and **s**porulation) protein family, possessing 10 transmembrane segments, where the fourth one is essential for activity (Mohammadi *et al.*, 2014). It has been shown that FtsI and FtsW form a sub-complex, based on *in vivo* and *in vitro* experiments (Fraipont *et al.*, 2011). Interestingly, FtsW interacts with both septal PG synthases, FtsI and PBP1B, suggesting a pivotal role in PG biogenesis linking both elongation and septation (Bertsche *et al.*, 2006). Nevertheless, recently, the membrane transporter homologue MurJ, has been proposed as a new flippase candidate as an alternative to FtsW in *E. coli* (Sham *et al.*, 2014).

Out of all known divisome components, only a monofunctional TPase FtsI (PBP3) has a clearly defined and direct role in septal PG synthesis in *E. coli* (Adam *et al.*, 1997; Pisabarro *et al.*, 1986; Wang *et al.*, 1998). Besides its synthetic activity, it additionally binds the murein biosynthetic complex to the septal ring. Moreover, it interacts with PBP1B with its N-terminal part, supporting the hypothesis that there is interplay between these two different PG biosynthetic machineries (Vollmer & Bertsche, 2008).

The last essential component of the divisome is FtsN, which in contrast to other essential components is not conserved in Gram-positive bacteria and was firstly identified as a suppressor of a *ftsA*, *ftsQ* and *ftsI* in *E. coli* (Dai *et al.*, 1993). FtsN is an abundant PG binding protein triggering septation (Addinall *et al.*, 1997), widely distributed among the proteobacteria (Moll & Thanbichler, 2009). It is composed of a short cytoplasmic part, a TM domain, and a C-terminal SPOR domain, which is believed to recognize and bind specifically septal PG (Gerding *et al.*, 2009; Ursinus *et al.*, 2004). Indeed, based on the results obtained in recent study the SPOR-domains are attracted to the Z-ring by septal PG, which is enriched in the glycan strands but not stem peptides (Yahashiri *et al.*, 2015). However, the essential part of FtsN does not include the SPOR domain, but instead comprises a 35 aa long N-terminal periplasmic region (Duncan *et al.*, 2013). Because FtsN is a last in the divisome recruitment pathway, it was thought that its primary role is to initiate the constriction phase and subsequent septum synthesis. Recent studies demonstrated that the early recruit FtsA interacts directly with the cytoplasmic domain of FtsN and by that creates a basis for the initial localization of FtsN to the division plane (Busiek & Margolin, 2014). It was speculated that trace amounts of FtsN are triggering septal PG synthesis and the initiation of constriction. Another, newly published report showed functional dependence of the FtsQLB, FtsA and FtsN, where FtsN is proposed to work through both: FtsA and FtsQLB (Liu *et al.*, 2015; Tsang & Bernhardt, 2015b; Weiss, 2015).
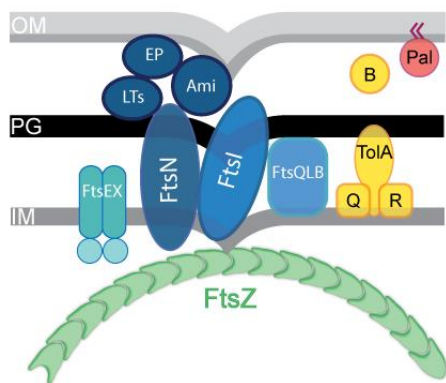
Figure 4. **Divisome architecture during late stages of the cell division in *E. coli*.** The FtsZ ring (green) recruits the elements crucial to control (turquoise) and facilitate (blue) septal PG remodeling along with components taking part in OM constriction (yellow Tol-Pal complex TolA, TolQ (Q), TolR (R), TolB (B), Pal and accessory CpoB protein). IM-inner membrane, PG - peptidoglycan, OM – outer membrane. Details in the text.

OM constriction is stimulated by the energy-transducing Tol system, which is conserved across Gram-negative bacteria (Sturgis, 2001). The Tol-Pal complex in *E. coli* is composed of at least five proteins, localized to the division site: TolA, TolQ, TolR, which form a complex in the IM (Derouiche *et al.*, 1995; Journet *et al.*, 1999), TolB (a periplasmic protein) and Pal (**p**eptidoglycan-**a**ssociated **l**ipoprotein), which is an OM lipoprotein (Gerding *et al.*, 2007). All these components are encoded in two adjacent operons. The Tol-Pal complex is not essential for survival, but crucial to maintain OM integrity. Inactivation or mutations in any of the Tol-Pal components impair OM constriction and cause defects in OM integrity leading to blebbing, periplasmic leakage, and multiple drug and stress sensitivities (Bernadac *et al.*, 1998; Cascales *et al.*, 2002; Gerding *et al.*, 2007). Recent studies in *E. coli* also linked PG synthesis with OM constriction machineries through PBP1B and LpoB (OM lipoprotein, required for PBPs activity–see chapter 1.2.1) (Paradis-Bleau *et al.*, 2010; Typas *et al.*, 2010).

1.4 Sculpturing of the new cell poles – hydrolysis of the septal cross-wall

Successful completion of the divisome assembly promotes septal PG hydrolysis, separation of the daughter cells, and formation of the new cell poles (den Blaauwen *et al.*, 2008). Simple incorporation of the new PG subunits into the already existing cell wall would result in thickening but not elongation of the PG polymer. For that reason, it is suggested that murein must be concominantly cleaved to allow insertion of the newly synthesized PG subunits (Koch, 1990).

A specialized group of PG-degrading enzymes, called PG hydrolases (autolysins), arriving at midcell concurrent with visible constriction, is known to be responsible for septal PG cleavage (Fan, 1970; Holtje, 1998). Despite clearly assigned biochemical function, the exact physiological roles of autolysins are still unknown. Studies in various prokaryotes have drawn attention to a common characteristic - a high redundancy. Hitherto, any single inactivation of a putative autolysin failed to cause bacteriolysis, with the exception of AmiB, a PG amidase in *Pseudomonas aeruginosa* (Yakhnina *et al.*, 2015). Furthermore, cell growth continues fairly fine in the absence of multiple hydrolases (Heidrich *et al.*, 2002).
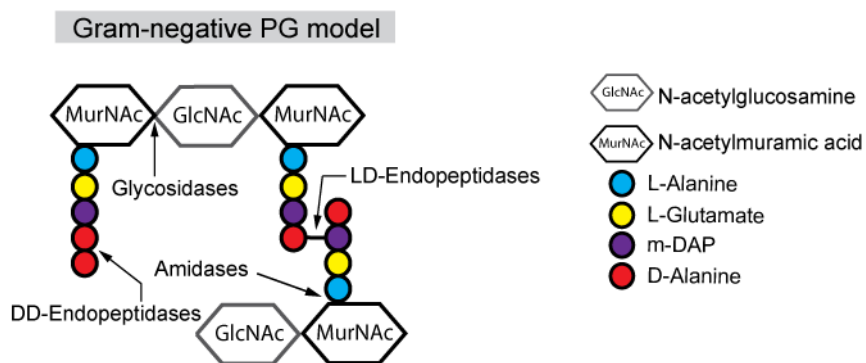
Figure 5. **Clevage specificity of PG hydrolases.** Model of Gram-negative peptidoglycan showing the cleavage specificity of autolysins indicated by arrows.

The heteropolymeric PG network requires several enzymatic activities to be efficiently digested (Figure 5). This set of autolysins includes enzymes belonging to the group of: (I) glycosidases, comprising N-acetylglucosaminidases, lysosymes and lytic transglycosylases (LTs), which target the β1-4 glicosidic bonds between MurNAc and GlcNAc (Holtje *et al.*, 1975), (II) DD- and LD- endopeptidases (EPases) cleaving various bonds within the stem peptides, and (III) N-acetylmuramyl-L-alanine amidases with specificity for the amide bond connecting the stem peptide with the sugar backbone (Heidrich *et al.*, 2001; Holtje, 1998) (Figure 5).

1.4.1 N-acetylmuramyl-L-alanine amidases

N-acetylmuramyl-L-alanine amidases are specialized in cleaving the amide bond between MurNAC and L-Ala, liberating the sugar strands from the peptide side chains in PG. Two types of catalytic domains, Ami_3 and CHAP are reported to be particularly important for septum cleavage in many bacterial species.

LytC-type amidases with a demonstrated ability to cleave septal PG were identified in *E. coli*, *Salmonella typhimurium*, *Vibrio cholerae* (*V. cholerae)*, and *Neisseria gonorrhoeae* (*N. gonorrhoeae*) (Garcia & Dillard, 2006; Heidrich *et al.*, 2001; Moll *et al.*, 2014; Priyadarshini *et al.*, 2007; Weatherspoon-Griffin *et al.*, 2011). The AmiB homologue found in *P. aeruginosa* turned out to be essential for viability, cell division, and antibiotic resistance (Yakhnina *et al.*, 2015). The *E. coli* genome encodes five LytC type amidases, AmiA, AmiB, AmiC, AmiD, and AmpD. AmiABC are soluble in the periplasm (Heidrich *et al.*, 2001), AmiD is a lipoprotein anchored to the OM, whereas AmpD resides in the cytoplasm (Jacobs *et al.*, 1995). AmiA-C target specifically septal PG with some preference for anhydroMurNAc, in contrast to AmiD, which displays a broader specificity (Kerff *et al.*, 2010). AmpD is characterized by its specificity towards 1,6-anhydromuropeptides (Holtje *et al.*, 1994; Jacobs *et al.*, 1995). Furthermore, AmiD and AmpD were stated to resemble structurally Zn^{2+} metallo-amidases, based on NMR data (Liepinsh *et al.*, 2003). Physiologically, AmiA, AmiB and AmiC are the main enzymes cleaving the septum between the daughter cells, whereas AmpD is involved directly in PG turnover and activation of β-lactamase activity in *E. coli* (Jacobs *et al.*, 1995). The deletion of *amiA*,

amiB and *amiC* promotes formation of chains of unseparated cells with completely synthesized septa (Heidrich *et al.*, 2002). Loss of amidase function additionally enhances sensitivity towards antibiotics and detergents, which is associated with a dysfunction of the OM compromising its function as a permeability barrier (Craig *et al.*, 2013; Ize *et al.*, 2003; Weatherspoon-Griffin *et al.*, 2011). The crystal structure of AmiC revealed the presence of novel PG binding domain named AMIN (PF11441), which mediates the accumulation at the division site (Rocaboy *et al.*, 2013). The recruitment of AmiA and AmiB is FtsN-dependent, suggesting that the presence of a mature divisome is required for triggering the activity of amidases (Bernhardt & de Boer, 2003; Peters *et al.*, 2011). Moreover, an experiment using cephalexin to block the synthesis of PG abolished septal recruitment of AmiA and AmiB, suggesting that active murein synthesis is also necessary to promote amidases action (Peters *et al.*, 2011). Consistent with their low basal activity *in vitro*, PG amidases the AmiA-C in *E. coli* must be activated by the divisome-associated LytM factors NlpD and EnvC, which structurally fall into the M23 metallopeptidase family (see chapter 1.3.2) (Uehara et al., 2009). Interestingly, EnvC and NlpD were found to be catalytically inactive and to serve as regulatory factors instead (Uehara *et al.*, 2010). The proposed regulatory mechanism assumes release of an autoinhibitory alpha helix occluding the active center of amidases upon binding of the respective LytM factor (Rocaboy *et al.*, 2013; Yang *et al.*, 2012a). The specificity of LytM factors are precisely assigned so that NlpD activates AmiC and EnvC activates AmiA and AmiB (Uehara *et al.*, 2010). Activation of LytC type amidases by LytM factors was also stated for other gamma-proteobacteria, such as *V. cholerae*, *H. influenzae* and *P. aeruginosa*, suggesting a class-specific regulatory mechanism (Ercoli *et al.*, 2015; Moll *et al.*, 2014; Yakhnina *et al.*, 2015). The precise mechanism that in turn controls the activity of EnvC and NlpD is still incompletely understood. However, it has been postulated that EnvC-mediated amidase regulation is driven by ATP-dependent conformational changes in the divisome associated ABC transporter homologue FtsEX (Yang *et al.*, 2011).

The CHAP superfamily is a recently characterized group of enzymes harboring, among the others, two different PG cleavage activities, N-acetylmuramoyl-L-alanine amidase or EPase. CHAP amidases structurally resemble papain proteases (Bateman & Rawlings, 2003; Rigden *et al.*, 2003) and are found mainly in bacteria and bacteriophages, along with few homologues identified in Archaea and Eukaryotes (Rigden *et al.*, 2003). The CHAP (**c**ysteine, **h**istidine-dependent **a**midohydrolases/**p**eptidases) domain is often coupled with other domains that hydrolyze PG. So far, only a few CHAP-domain containing proteins have a characterized function (Barendt *et al.*, 2009; Layec *et al.*, 2009). Some of these proteins, such as Sle1 from *S. aureus* and PcsB homologues in *S. pneumoniae,* play a fundamental role in cell division (Kajimura *et al.*, 2005; Sham *et al.*, 2011). Interestingly, the hydrolytic activity of PcsB was proposed to be dependent on FtsEX interaction (Sham *et al.*, 2011).

1.4.2   Endopeptidases (EPases)

Autolysins classified as autolytic EPases comprise two groups of enzymes: DD, DL or LD carboxypeptidases (DD, DL or LD-CPases), which remove the terminal amino acid from the stem peptide, and EPases, which cleave crosslinks between dimuropeptides in mature murein. The specificity of the cleavage process is based on the stereochemistry described in the name of the

particular peptidase: DD-enzymes target the bond between two amino acids in D-configuration, LD-enzymes the bond between an L- and a D-amino acid, and DL- the bond between a D- and an L-amino acid (Holtje, 1995). The *E. coli* genome encodes more than 20 peptidases cleaving within PG, PG precursors, or muropeptides (van Heijenoort, 2011).

DD-EPases cleave the mDAP-D-Ala crosslinks in the stem peptides, created by the high-molecular weight (HMW) PBPs in the DD-transpeptidation reaction (Sauvage *et al.*, 2008). There are two types of DD-EPases in *E. coli*: low-molecular weight (LMW) PBPs (PBP4 and PBP7), which are inhibited by β lactam antibiotics, and EPases unrelated to PBPs (MepA). Interestingly, PBP4 additionally possess CPase activity (Iwaya & Strominger, 1977), confirmed by studies examining its overproduction (Korat *et al.*, 1991). PBP7 is stated to be important for septum cleavage and biofilm formation (Typas *et al.*, 2012). There is another set of CPases identified in *E. coli* that belong to a group of LMW PBPs (PBP5, PBP4b, PBP6 and PBP6B with hydrolytic activity, but more than being needed for septum hydrolysis, they are important for the PG maturation process and the regulation of cross-linking (van Heijenoort, 2011). Among all five CPases, PBP5 (DacA) is reported to be the most active one, and its deletion causes slight morphological defects. Interestingly, the morphology is radically changed to branched and kinked cells, when PBP5 and additional PBPs are deleted (de Pedro *et al.*, 2003; Nelson & Young, 2001). PBP5 localizes to the sites of active PG synthesis, where it reduces the number of D-Ala-D-Ala bonds usable for transpeptidation. As much as for the *E. coli* D-Ala cleavage is physiologically relevant, it is not the case for many other bacterial species including *C. crescentus*. Interestingly, the *C. crescentus* genome encodes only one putative DD-CPase, most likely inactive (Markiewicz *et al.*, 1983), consistent with its naturally high fraction of pentapeptides in its murein. Collectively, this bacterium must possess unique, pentapeptide-rich PG growth mechanism.

Lysostaphin-like metalloproteases (LytM factors) from the M23 peptidase family comprise a widely distributed group of EPases found in bacteria and bacteriophages, known to cleave crosslinks within murein stem peptides. However, their cleavage specificity is broader than targeting the meso-DAP-D-Ala bond in Gram-negative or Penta-Gly inter-bridges in Gram-positive bacteria, since LytH from *B. subtilis* was reported to target L-Ala-D-Glu in dimurotetrapeptides (Horsburgh *et al.*, 2003). Structurally, LytM factors belong to the group of the LAS enzymes (**l**ysostaphin, D-**A**la, D-Ala–CPase and **s**onic hedgehog), characterized by HXH and HXXXD motif and active site architecture coordinating zinc ion (Zi^{2+}) (Bochtler *et al.*, 2004). The first LAS-type EPase, lysostaphin, cleaving the pentaglycine bridge in the PG stem peptides was identified as an anti-microbial agent in *S. aureus* (Schindler & Schuhardt, 1964). Although, LytM factors have been implicated in the division process in *E. coli* (Uehara *et al.*, 2009), *B. subtilis* (Cohen *et al.*, 2009), *P. aeruginosa* (Yakhnina *et al.*, 2015), *V. cholerae* (Moll *et al.*, 2014), and *H. influenza* (Ercoli *et al.*, 2015), not all of them possess enzymatic activity (Levdikov *et al.*, 2012; Meisner & Moran, 2011; Yang *et al.*, 2012a). Interestingly, apart from their contribution in the regulation to PG cleavage during cell division events, recent studies discovered an association of LytM factors with the pathogenicity of *H. influenza*, *N. gonorrhoeae*, and *Y. pestis* (Ercoli *et al.*, 2015; Stohl *et al.*, 2012; Tidhar *et al.*, 2009). *E. coli* possesses four LytM factors with recognizable LytM motif: NlpD, EnvC, YebA and YgeR, where NlpD and EnvC are characterized by an incomplete active site (Uehara *et al.*, 2009). These enzymatically passive LytM factors were

demonstrated to specifically activate their cognate amidases (see chapter 1.3.1), in contrast to their catalytically active paralogues, whose role has not been elucidated. A quadruple deletion of all genes encoding LytM factors leads to cell separation defects, comparable to the one observed upon the loss of all PG amidases (Uehara *et al.*, 2009). Interestingly, fluorescently tagged versions of EnvC and NlpD arrive at the septum before their cognate amidases, serving as a fail-safe mechanism preventing potentially lethal amidase activity (Peters *et al.*, 2011). Noteworthy, even though the EnvC, NlpD and YebA homologues were identified in several bacterial species, they seem to fulfill different roles, not always directly associated with the division process. For example, EnvC in *H. influenza* does not contribute to the division process at all (Ercoli *et al.*, 2015).

The NlpC/P60 family is the second group of EPases with demonstrated hydrolytic activity against PG. Phylogenetically, the group of NlpC/P60 belongs to the CHAP superfamily and is widely spread within the bacterial lineages (Anantharaman & Aravind, 2003). Structurally, these enzymes possess the classical papain-like folds with an active site composed of a His-Cys-His/Asn/Gln triad and are often fused with an SH3 domain presumably facilitating PG binding or enzymatic function (Anantharaman & Aravind, 2003; Aramini *et al.*, 2008; Whisstock & Lesk, 1999). Three homologues carrying an NlpC/P60 domain, Spr, YebA, and YdhO, were characterized in *E. coli* as redundantly essential (Singh *et al.*, 2012). All three cleave the D-Ala-mDAP peptide crosslink *in vitro*, and their absence leads to cell lysis due to inhibition of the insertion of new PG subunits (Singh *et al.*, 2012). Interestingly, two NlpC/P60 homologues, CwlO and LytE, were described as first ever autolysins essential for survival in *B. subtilis* (Bisicchia *et al.*, 2007).

1.4.3 Glycosidases

The glycosidic bond linking GlcNAc with MurNAc is cleaved in two ways: either by lysozymes, with MurNAc as the terminal residue, or by the lytic transglycosylases (LTs), with the concomitant formation of an intramolecular ether bond resulting in a terminal non-reducing 1,6-anhydroMurNAc residue (anhydroMurNAc). In contrast to lysozymes, LTs are hydrolyzing the substrate with no water molecule required (Holtje *et al.*, 1975).

Lysozymes are the best biochemically characterized enzymes across all kingdoms of life. Interestingly, there are only few well-studied examples with proven specificity in bacteria. *E. coli* possess only one lysozyme paralogue, NagZ (Cheng *et al.*, 2000), which is not essential for proper growth but required for PG turnover (Park & Uehara, 2008).

LTs are exoglycosidases, ubiquitous among bacteria, with the exception of the species lacking a typical cell wall, such as *Chlamydiaceae* or *Mycoplasmaceae* (Tatusov *et al.*, 2001). These hydrolytic enzymes are often termed 'space-makers', since their predominant function in PG metabolism (cleavage for its synthesis and recycling) and cell division. Apart from their autolytic function, LTs are implicated in various cellular processes such as spore germination, pathogenicity (Cloud-Hansen *et al.*, 2006), and incorporation of the multi-protein complexes spanning the cell envelope, including pili and flagellum (Koraimann, 2003). As mentioned before, the LTs are required for PG turnover and recycling in Gram-negative bacteria with anhydroMurNAc being reused in the cytoplasm to generate new PG precursor.

At the same time anhydroMurNAc serves as signaling molecule inducing β-lactamase genes (Jacobs *et al.*, 1994). The reactions of all seven *E. coli's* LTs were characterized in a quantitative manner, supporting their primary role in the modulation of the cell wall recycling (Lee *et al.*, 2013).

LTs are divided into four families, based on sequence similarities and consensus motifs (Blackburn & Clarke, 2001). The *E. coli* genome encodes seven identified and characterized LTs: Slt70 and MltA-F, where Slt70 is soluble, and the remaining five are OM bound (Holtje, 1995; Kraft *et al.*, 1998). Most of the LTs act as exoenzymes, releasing anhydromuropeptides from the ends of the glycan strands, with the exception of endo-specific MltE (Kraft *et al.*, 1998). The specificity of LTs is additionally underlined by preferential cleavage of crosslinked or non-crosslinked PG (Lee *et al.*, 2013). Crystal structures were successfully solved for Slt70 (van Asselt *et al.*, 1999b; van Straaten *et al.*, 2005), MltA (van Straaten *et al.*, 2005; van Straaten *et al.*, 2007), a soluble proteolytic fragment of MltB (Slt35) (van Asselt *et al.*, 1999a; van Asselt *et al.*, 2000), MltE (Artola-Recolons *et al.*, 2011), and MltF (Madoori & Thunnissen, 2010). Studies of these structures confirmed that all LTs, except for MltA, share a goose-type lysozyme fold in the active domain (Thunnissen *et al.*, 1995).

Despite an increasing amount of data collected for *E. coli's* LTs, their precise role in murein metabolism is still unclear (Heidrich *et al.*, 2002). Notably, MltD contains tandem of LysM domains, which are known for their PG-binding ability and coexistence with other PG hydrolytic domains (Bateman & Bycroft, 2000). MltE is implied in triggering cell wall recycling (Artola-Recolons *et al.*, 2011). The analysis of the single and multiple mutants revealed overlapping functions, since single knock-outs did not result in visible morphological aberrations. However, the deletion of six LTs (Slt70 in combination with MltA-E) yielded cells growing as chains, composed of three to eight compartments in 50 % of the population (Heidrich *et al.*, 2002).

1.4.4 Regulation of autolytic activity

The action of PG hydrolases must be carefully coordinated since any uncontrolled action may lead to sacculus breakage and cell disintegration. Apart from the extremely selective cleavage specificities of autolysins, several mechanisms modulating autolysins activity have been proposed.

One of them is the existence of multienzyme PG biosynthetic complexes stretching from the IM-located synthases to the OM-localized hydrolases, so that hydrolytic cleavage is directed specifically to murein synthesis sites, preventing random cleavage (Holtje, 1998). These complexes have never been isolated, since their dynamic nature results in only transient interactions. However, several interactions between the PBPs and/or divisome components were reported (Vollmer & Bertsche, 2008). A few years back, an *in vitro* interaction of PBP1B and FtsI from *E. coli* was reported, and verified by crosslinking and bacterial two-hybrid (BACT2H) experiments (Bertsche *et al.*, 2006). Recently, a genetic link between PBP1B-LpoB and Tol (Typas *et al.*, 2010) was identified, consistent with the notion that OM invagination and murein synthesis must be perfectly synchronized to coordinate the division process (Gray *et al.*, 2015). This coordination is maintained by newly

characterized protein CpoB (**C**oordinator of **P**G synthesis and **O**M constriction, associated with PBP1**B**), which is needed for both PBP1B function *in vivo* and proper OM architecture (Gray *et al.*, 2015).

A mechanism modulating directed murein hydrolysis has recently been identified in *E. coli*, *B. subtilis* and *S. pneumoniae*. Published reports point out FtsEX as a bridge coupling cell division with murein remodeling by conserved regulatory mechanism. It has been proposed that ATP hydrolysis drives conformational changes of FtsEX, which in turn activate (directly or indirectly) cell wall hydrolases to initiate cleavage of septal PG (Meisner *et al.*, 2013). So far, FtsEX was demonstrated to coordinate the activity of AmiA/AmiB/AmiC in *E. coli* (see section 1.1.3.2) (Yang *et al.*, 2011), CwlO, harboring an NlpC/P60 domain, in *B. subtilis* (Sham *et al.*, 2011), and PcsB from *S. pneumoniae*, carrying a CHAP domain (Meisner *et al.*, 2013). A detailed mechanism of activation was proposed for *E. coli*, where conformational changes of FtsE promote the recruitment of the respective LytM factor, followed by the release of the inhibitory helix from the active site of the amidases and promotion of the septal PG hydrolysis (Yang *et al.*, 2012b). Recently, a structural basis of cell wall hydrolysis mediated by *S. pneumoniae* PcsB was also uncovered. The crystal structure of PcsB, suggests that PcsB dimerizes with the V-shaped coiled–coil domain of each monomer locking the catalytic domain of each dimeric partner in passive state. The release of the catalytic domains, resulting in cell wall cleavage, depends on the conformational change in the FtsEX complex (Bartual *et al.*, 2014).
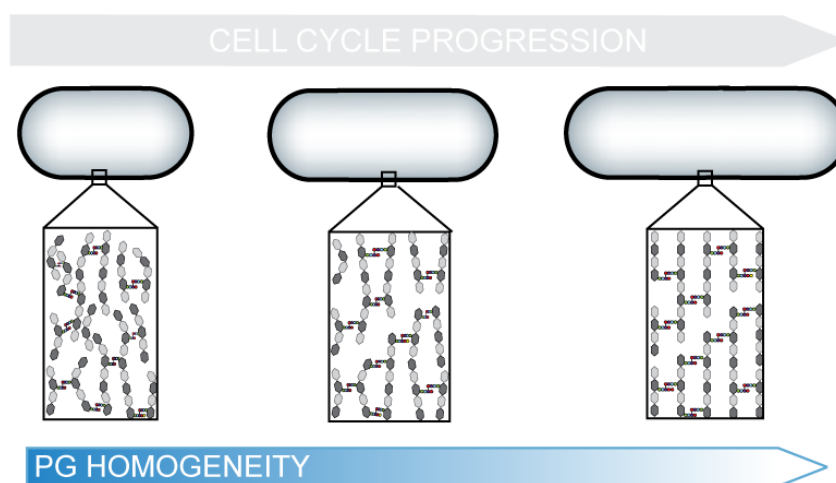
Figure 6. **Elongation of the cell body stretches the cell wall organizing its structure.** Growth of the cell bodies serves as a natural mechanism enhancing homogeneity of the peptidoglycan, which is next recognized by its bioynthetic enzymes.

The third parameter speculated to have an impact on PG growth rate is a mechanical force - the turgor pressure. Sacculi isolated from *E. coli* are elastic in the direction of the longer axis (Yao *et al.*, 1999), which agrees with the orientation of the peptides confering the described elasticity. This means that the osmotic pressure changes significantly the length but not the diameter of the cells (van den Bogaart *et al.*, 2007). Accordingly, the sacculus is 'more organized' when stretched and 'less organized' when relaxed. It has been speculated that murein biosynthetic complexes may recognize and/or require stretched cell wall structure (Figure 6) (Vollmer & Bertsche, 2008). Particularly, hydrolases

were termed as 'smart autolysins' by Arthur Koch, owing to their ability to recognize and cleave cell wall in stretched conformation (Koch, 1983; Koch, 1990).

1.5   *Caulobacter crescentus* - the model organism

Caulobacter crescentus is non-pathogenic, aerobic, fresh water, alpha-proteobacterium, serving as a model organism in cellular biology for over 50 years now (Poindexter, 1964). The strain, to which scientists refer to as the 'wild type' (CB15N, NA1000), in fact, is a derivative of the ancestor strain that has evolved after years of cultivation in laboratory conditions (Evinger & Agabian, 1977). *C. crescentus* is a rod-shaped bacterium characterized by its asymmetric cell division, generating daughter cells morphologically and physiologically different from each other (Figure 7) (Curtis & Brun, 2010). One of the daughter cells is sessile and attached to the surface with a thin polar protrusion, called the stalk. The other daughter cell, the swarmer cell is motile and equipped with single, polar flagellum. At the tip of the stalk, *C. crescentus* synthesizes one of the world's strongest glues, called holdfast (Bodenmiller *et al.*, 2004).

Based on the described asymmetry, the phenotype of *C. crescentus* is tightly connected to the actual developmental stage the cells are currently in. This convenient feature coupled with the existence of only one copy of a chromosome, duplicated once per cell cycle, makes *C. crescentus* a perfect choice to study many aspects of the cell biology, including the mechanisms of the chromosome segregation and cell division.
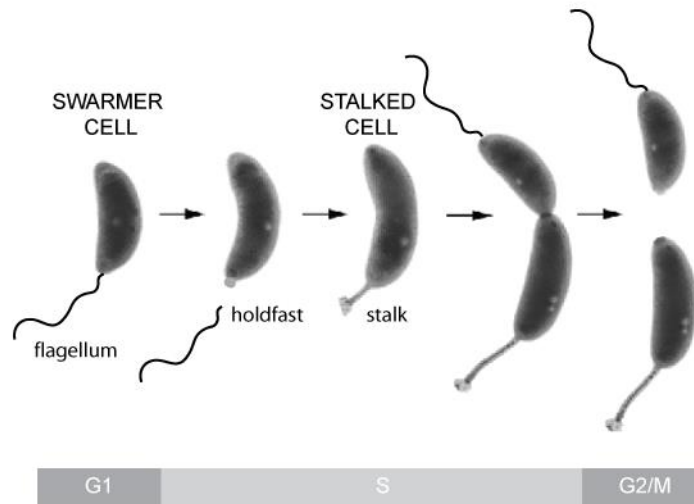
Figure 7. **Cell cycle of the *Caulobacter crescentus*.** The cell cycle of *C.crescentus* starts from the flagellated swarmer cell, which differentiates into the division-proficient stalked cell. Duplication and segregation of the chromosome triggers invagination of the cell envelope, and finally division. The stalked cell may directly enter next round of replication, while the swarmer cell must differentiate beforehand. For more information, see text. Adapted from Y. Brun (unpublished).

Based on the DNA replication state, the cell cycle of *C. crescentus* can be easily compared to the phases known from eukaryotic cells (Figure 7). It is composed of three parts: G1 phase –phase in which proteins needed for the following replication are synthesized, S phase in which DNA is

replicated, and G2 phase, in which the cell ultimately divides. The *C. crescentus* at swarmer stage is trapped in G1 phase until it loses the flagellum and generates a stalk instead. Stalk formation is a sign for upcoming DNA replication (S-phase) during which the cell elongates approximately twice and segregates the duplicated chromosome. Meanwhile, a flagellum grows at the pole opposite the stalked pole, and the constriction emerges at the middle of the cell, followed by cell division and progeny release (G2 phase) (Figure 7). After division, the swarmer cell must differentiate into a stalked cell before it can enter the division phase, whereas the stalked mother cell is immediately ready for a new round of cell division.

Over the years, a comprehensive set of biochemical techniques and genetic tools have been developed, for *C. crescentus*, making this organism an excellent model to study bacterial biology. The genome of *C. crescentus* has been sequenced and annotated (Marks *et al.*, 2010; Nierman *et al.*, 2001). Additionally, a set of plasmids containing inducible promoters for switching on and off the transcription of the desired genes is available (Thanbichler *et al.*, 2007). Moreover, a synchronized population of swarmer cells can easily be isolated via density gradient centrifugation, based on differences in the buoyant density of the different cell types. On top of this, a large amount of data describing polar factors, master regulators and many other aspects of *Caulobacter's* biology provides an excellent starting point for future research.

1.5.1 Cell division in *C. crescentus*

During the last two decades, a remarkable amount of data has revealed the basis of *Caulobacter's* cell division. Many homologues of proteins building and guiding the divisome in *E. coli* were found and characterized in *C. crescentus*. Recent data have shed light not only onto the conserved core divisome components, but also onto the diversifications mediating PG biosynthesis during cell constriction.

The guidance of the divisome components is conducted by MreB and FtsZ homologues. Consequently, also in *C. crescentus* MreB appeared to be a cell shape determination factor (Figge *et al.*, 2004). Based on its cell cycle-orchestrated localization pattern, oscillating between patchy/helical and midcell arrangement, it is believed that MreB has a role in the coordination of cell wall biogenesis (Figge *et al.*, 2004). Cell division in *C. crescentus* relies on FtsZ-based divisome assembly, which temporal order was established using fluorescently tagged divisome components. Unlike in *E. coli*, *C. crescentus* is building the divisome in seven, not two recruitment waves (Goley *et al.*, 2011). The essential set of the divisome components in *C. crescentus* includes FtsZ, FtsI, FtsN, FtsE, FtsK, FtsA and FtsQ, whose all are transcriptionally regulated in a cell cycle dependent manner (Costa *et al.*, 2008; Goley *et al.*, 2011; Martin *et al.*, 2004; Wang *et al.*, 2006).

Based on localization studies, the gradient-forming negative regulator MipZ positions the Z-ring, which arrives at the midcell in the first minutes of the cell cycle (Thanbichler & Shapiro, 2006). The architecture of the Z-ring was analyzed by several research groups, resulting in two major models. The first model was obtained by a 3D PALM study in live *C. crescentus* cells, suggesting that the Z-ring is composed of a loosely packed, continuous band (Biteen *et al.*, 2012). The second idea describing the Z-ring architecture was provided via high-throughput PALM (HDPALM), and suggests a patchy band as

a most common arrangement (Holden *et al.*, 2014). Early cell division components, including FzlA, ZapA, FtsE and FzlC, are recruited to the midcell shortly after FtsZ, presumably to stabilize the ring. FzlA and FzlC are Z-ring-bound proteins, where the first one is essential for cell division and proper FtsZ filaments organization (Goley *et al.*, 2010b). FtsE is proposed to be essential for survival, forming together with FtsX an ABC transporter-like complex (Goley *et al.*, 2011). Factors involved in PG remodeling, including MurG (PG glycosyltransferase) (Aaron *et al.*, 2007) and DipM (see chapter 1.4.2.1), reach midcell together with MreB (Aaron *et al.*, 2007; Goley *et al.*, 2011). After another 10 min gap, the membrane-tethering Tol-Pal complex is recruited to the midcell to ensure OM invagination (Goley *et al.*, 2011). The very late recruitment of the Tol-Pal complex in *E. coli* represents another interesting difference in divisome assembly between *E. coli* and *C. crescentus* (Yeh *et al.*, 2010). In *C. crescentus*, it localizes to the division site prior to division and remains at the newly generated poles of the daughter cells, anchoring TipN (Huitema *et al.*, 2006; Lam *et al.*, 2006). TipN is a polar marker, playing a critical role in cell asymmetry and polar development (Lam *et al.*, 2006). Remarkably, in *C. crescentus* the Tol-Pal complex is composed of TolR, TolQ, TolA, TolB and Pal and is essential for survival (Yeh *et al.*, 2010). It has been proposed that Tol-Pal in *C. crescentus* maintains cell envelope integrity similarily to Lpp (the Braun lipoprotein) in *E. coli* (Weigand *et al.*, 1976; Yeh *et al.*, 2010). This idea was based on the fact, that *C. crescentus* lacks an Lpp homolog. Surprisingly, the actin homolog FtsA arrives late at the midcell, suggesting that in *C. crescentus* the membrane tethering function of FtsA is either dispensable or different from that in *E. coli*. The late arrival of FtsA to the division site was also noted in *A. tumefaciens*, suggesting that the recruitment mechanism may be conserved among alpha-proteobacteria (Cameron *et al.*, 2014). It was proposed that FtsA is not essential for survival of *C. crescentus*, but its depletion causes abnormal, shallow constrictions, suggesting a role in the cell division (Martin *et al.*, 2004; Ohta *et al.*, 1997). The core divisome components FtsN, FtsQ, FtsI (PBP3), FtsK, and FtsL reach the division plane almost simultaneously to FtsA. An FtsN homologue has been identified in *C. crescentus* despite poor sequence conservation (Möll and Thanbichler, 2009). Even trace amounts of FtsN are sufficient to support cell division, and its depletion results in extreme filamentation and eventual lysis (Moll & Thanbichler, 2009). An FtsQ was found to localize at midcell or additionally at the stalked pole in pre-divisional and stalked cells, suggesting its role in stalk biogenesis (Martin *et al.*, 2004). Interestingly, the arrival of FtsN, FtsI and FtsW to the midell was thought to trigger constriction of the cytokinetic ring, together with the proteins forming a subcomplex within the ring (Modell *et al.*, 2011). The dynamic localization of FtsI begins with the formation of the polar focus at the new cell pole in the swarmer cells. A midcell focus of FtsI then appears right before constriction in predivisional cells (Costa *et al.*, 2008). The invagination of the cell envelope is coupled with the recruitment of FtsW and FtsB. Interestingly, in *E. coli*, FtsW is essential for FtsI localization, while in *C. crescentus* it seems not to be the case, since FtsI reaches midcell way before the putative flippase (Modell *et al.*, 2011). The last known of component *C. crescentus* divisome, the polarity factor TipN, reaches the division plane right before division, concurrently with relocalization of MreB from a midcell to a sidewalls. Once the cell divides, TipN keeps its position, marking the newly shaped poles of the daughter cells (Lam *et al.*, 2006).

1.5.2   PG biosynthesis in *C. crescentus*

Several studies have shed light on the PG remodeling machinery in *C. crescentus*. Nevertheless, not much is known about the details concerning the architecture of the system and the regulation of the PG synthases and hydrolases. It was suggested that both MreB and FtsZ have a significant influence on the regulation of cell wall metabolism. This idea was supported by the fact that MreB depletion results in synthesis of longer glycan strands, implying either positive regulation of PBPs or negative regulation of LTs (Takacs *et al.*, 2010). Additionally, a recent report by Sundarajan at. al., suggests that a Z-ring gives a physical signal to promote PG remodeling (Sundararajan *et al.*, 2015). The published data also include primarily an initial characterization of the PBPs and reports describing the hydrolase homologue DipM (Moll *et al.*, 2010; Salje *et al.*, 2011; Strobel *et al.*, 2014) (Goley *et al.*, 2010a; Poggio *et al.*, 2010).

The *C. crescentus* genome encodes seven PBPs, including two monofunctional PBPs, PBP2 and PBP3, and five bifunctional GT/TPases Pbp1A, PbpC, PbpX, PbpY, and PbpZ. PBP2 and PBP3 are essential for survival (Costa *et al.*, 2008), in contrast to Pbp1A, PbpC, PbpX, PbpZ, and PbpX (Strobel *et al.*, 2014; Yakhnina & Gitai, 2013). PbpX is thought to function as the main GTase, since the absence of this protein causes loss of cell wall integrity and increased sensitivity to cell wall-targeting antibiotics (Yakhnina & Gitai, 2013). However, the exact function of the five bPBPs is difficult to determine due to their high redundancy. PbpY and PbpX localize to the division site and likely interact with early and late divisome components, implying an activity throughout the division process (Strobel *et al.*, 2014).

1.5.3   PG hydrolysis in *C. crescentus*

Three independent studies were published in 2010 describing the PG hydrolase DipM (**Di**vision and **p**olarity **m**etallopeptidase) as crucial for the division process in *C. crescentus* (Goley *et al.*, 2010a; Moll *et al.*, 2010; Poggio *et al.*, 2010). DipM is a periplasmic protein, falling into the group of LytM factors, with a C-terminally located M23 metallopeptidase domain. Additionally, it is contains two tandem repeats of LysM modules with PG-binding capacity. LysM units are widely spread in both the microbial and eukaryotic world. They are characterized by their ability to recognize polysaccharides containing GlcNAc and usually appear in tandem or multiple repeats. LysM motifs are composed out of 43-50 amino with the high conservation of the first sixteen residues (Bateman & Bycroft, 2000; Buist *et al.*, 2008). Prokaryotic LysM domains are specific mostly for PG, while the eukaryotic ones mostly recognize chitin (de Jonge *et al.*, 2010). Structural studies of the multimodular LysM-domain containing PG hydrolase AltA from *Enterococcus faecalis* revealed the recognition motif and the structural basis of its binding specificity. It has been proposed that LysM motifs do not form higher-order assemblies but rather act in an additive manner, binding GlcNAc and, to a lesser extent stem peptides (Mesnage *et al.*, 2014).

DipMs association with the divisome was analyzed by fluorescence miscroscopy, showing that the protein has a dynamic, cell cycle-dependent localization pattern. Spatiotemporal studies of this dynamic localization revealed that DipM relocalizes to the division site concominant with FtsN forming additionally a small focus at a stalked pole, at the beginning of the stalk synthesis. Consistently, DipMs

localization is FtsN-dependent. Other interaction partners, determined by bacterial two-hybrid analysis (BACT2H) and include TolR, AmiC and TipN (Moll *et al.*, 2010). It was shown that C-terminal M23 peptidase domain is sufficient for DipM function, whereas at least two LysM modules (one tandem) are needed for proper localization at the division site (Goley *et al.*, 2010a; Moll *et al.*, 2010).

Based on deletion studies, DipM is a critical component of the cell division apparatus, since the cells lacking a functional *dipM* copy grow as filaments, with a significantly reduced growth rate. Microscopy studies of Δ*dipM* mutant revealed not only cell division defects but also significant polarity disorders, as reflected by branching, blebbing, and ectopic stalk formation (Goley *et al.*, 2010a; Moll *et al.*, 2010). The origin of these defects may come from misplacement of the polarity factor TipN in the Δ*dipM* background. Labeling of the periplasm revealed membrane vesicle formation (blebbing) together with an enlargement of the periplasmic space at the division site. Cryo-TEM data of a Δ*dipM* strain suggested dysfunction of OM invagination and septation, indicating abnormalities in PG architecture (thickening) and delayed remodeling of the division sites (Goley *et al.*, 2010a; Moll *et al.*, 2010; Poggio *et al.*, 2010).

1.6 Scope

The knowledge about the molecular basis and the regulation of elementary cellular processes is expanding extremely fast. Bacterial cell division and accompanying cell wall biosynthesis are one of the most intensively studied topics, particularly relevant for the medical field, where multiresistance of pathogenic species triggers the urge for novel antibiotics, often targeting synthesis of the cell wall. Despite an enormous amount of published data obtained from different bacterial lineages, a comprehensive dataset exists only for *E. coli*. This dataset includes not only the information about the key players but also about the molecular mechanism controlling the cell wall remodeling events. Even though, the central components driving the PG remodeling process were identified, many open questions remain unanswered.

Since not much is known about cell wall biogenesis in Gram-negative bacteria other than *E. coli*, I decided to explore the field, focusing on murein hydrolysis during last stages of the cell division, in *C. crescentus*. Based on structural homology to the proteins implicated in PG hydrolysis in other bacterial species, I sought to characterize putative PG hydrolases in *C. crescentus*, assign their function, and examine their association with the divisome. Furthermore, I aimed to establish a regulatory network between them and assess the extent of their direct impact on PG biosynthesis.

DipM was identified as a core protein for PG hydrolysis in *C. crescentus*. The protein was characterized carefully however; its exact function has remained unknown. Therefore, my second goal is to shed light on DipM's precise role and its cooperation with other PG hydrolases.

2.   RESULTS

2.1 Bioinformatics screening of putative cell division factors involved in PG hydrolysis in *Caulobacter crescentus*

A Previous study performed by Andrea Möll revealed that *C. crescentus* possesses genes coding for canonical PG remodeling enzymes falling into the group of putative endopeptidases (LytM factors, named LdpA-F and DipM), carboxypeptidases (CP-ase), amidases (named AmiC) and soluble lytic transglycosylases (SLTs, named SdpA-C) (Möll, 2011). Single in-frame deletion of genes encoding these enzymes, with the exception of *dipM*, were neither affecting cells survival nor dramatically altered their morphology (Moll *et al.*, 2010). However, fluorescent labeling revealed midcell recruitment of SdpA during the division phase (Möll, 2011). Since a specific spatiotemporal localization pattern often reflects protein function in *C. crescentus*, I decided to further investigate the extent to which SdpA and other SLTs contribute to cell division.

Furthermore, I decided to re-screen the genome of *C. crescentus* and seek for novel factors involved in PG hydrolysis, reported to play a crucial role in PG remodeling in other bacterial species. This analysis resulted in the identification of two genes encoding putative LD-TPases (PF03734), one CHAP domain-harboring putative amidase (PF05257), two putative EPases belonging to NlpC/P60 family (PF00877) and four putative membrane-bound lytic transglycosylases (MLTs) harboring either a PG_binding_1 (PF01471) or MltA (PF03562) domain. Subsequently, the identified set of putative autolysins was subjected to localization and deletion studies, whereby individual outcomes determined further investigations.

2.2   Deciphering physiological role of lytic transglycosylases (LTs)

2.2.1   Soluble lytic transglycosylases (SLTs)

2.2.1.1   Subcellular localization of SdpABC

Together with Andrea Möll, I sought to investigate the subcellular localization of the three uncharacterized proteins SdpA (CCNA_01252), SdpB (CCNA_01393) and SdpC (CCNA_02498), which fall into the group of lytic transglycosylases (LTs), owing to their C-terminal SLT domain (PF01464) (Figure 8A). Interestingly, based on a transposon screen, SdpA was acknowledged as important for cellular fitness (Table S7) (Christen *et al.*, 2011). Bioinformatic analysis indicated that all three SLTs were soluble in the periplasm. To confirm the predicted subcellular localization of SdpABC, the candidate genes were fused C-terminally to *mCherry* and ectopically expressed from a xylose-inducible promoter (P_{xyl}). The fluorescent fusion of SdpC was unstable, with cleaved mCherry producing an even

fluorescent signal. In contrast, both SdpA and SdpB fusion proteins were stable and displayed a cell cycle-dependent localization pattern (Figure 8B).

2.2.1.2   Localization dynamics and characterization of SdpA

The precise localization dynamics of inducible SdpA-mCherry was examined via time-course microscopy for a synchronized population in rich medium (Figure 9A). In the swarmer cells, SdpA-mCherry resided in the periplasm, forming compressed zones during the transition to the S-phase. Once stalk synthesis has initiated, an SdpA-mCherry focus appeared at the non-flagellated pole, remaining there until the cells reached their maximum length. SdpA-mCherry signal was detectable at the pole until the stalk was completely synthesized, but gradually relocated to midcell. Over time, the brightest signal at the future division plane was observed right at the onset of cell constriction. The focus gradually decreased in intensity with ongoing invagination, until the protein was again largely dispersed throughout the cell (Figure 9A). An SdpA-mCherry fusion integrated at the native locus confirmed the fluorescence pattern observed for the inducible version (Figure 9D).
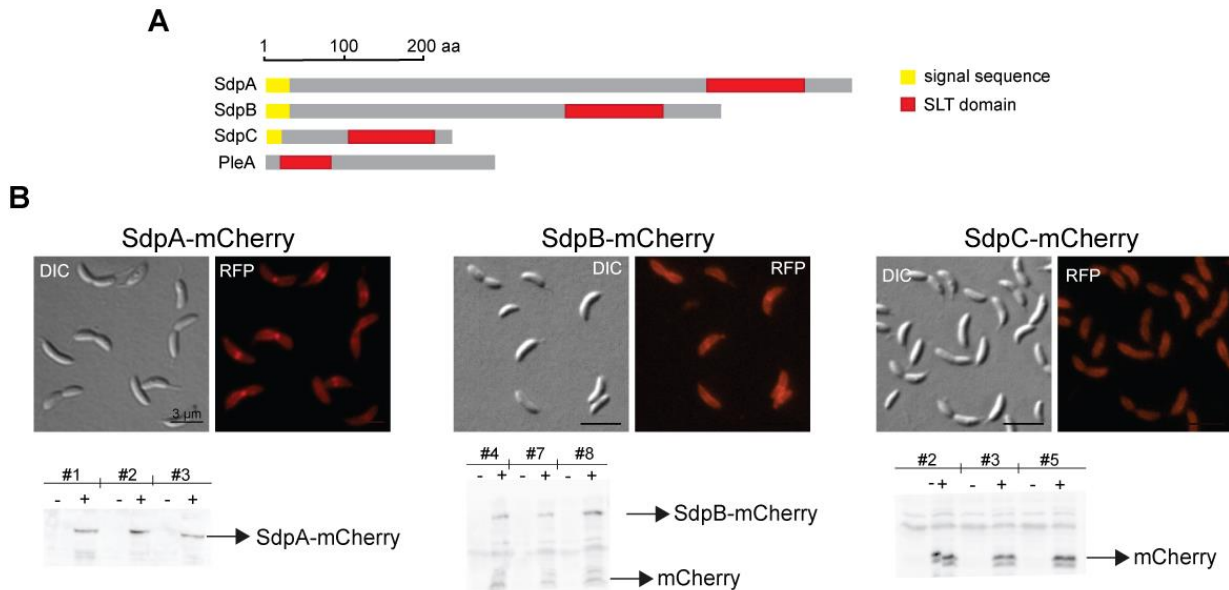
Figure 8. **SdpA and SdpB are late recruits to the divisome.** **(A)** Schematic representation of the soluble lytic transglycosylases (SLTs) based on SMART analysis (2014) (Letunic *et al.*, 2012; Schultz *et al.*, 1998). **(B)** Subcellular localization of SdpA, SdpB and SdpC fused C-terminally with mCherry. Strains AM480 (CB15N P$_{xyl}$-*sdpA-mCherry*), AZ127 (CB15N P$_{xyl}$-*torA-sdpB-mCherry*), and AZ12 (CB15N P$_{xyl}$-*sdpC-mCherry*) were grown to exponential phase in PYE medium, induced with 0.3 % xylose for 2 h and visualized with DIC and fluorescence microscopy. Immunoblot analyses of respective fluorescent fusion, using anti-mCherry antiserum, for three independent clones (#1, #2, #3) are shown below. The samples were collected concurrently with the microscopy experiment. Arrows indicate prominent bands, (-) indicate uninduced samples, (+) indicate samples induced for 2 h. Scale bars: 3 µm.

To place SdpA into the divisome assembly hierarchy, I compared the localization dynamics of the protein to those of well-known divisome components. For this purpose, identical time-course experiments were performed for the following inducible fusions: eGFP-FzlC, YFP-FtsZ, TolA-venus, FtsN-eGFP, and TipN-eGFP. Subsequently, the fraction of cells exhibiting a midcell focus was quantified for each time point for comparison. The data show that SdpA is recruited to the division

site at a similar timepoint as is FtsN, suggesting its contribution to septal PG biosynthesis and possibly final fission (Figure 9B).
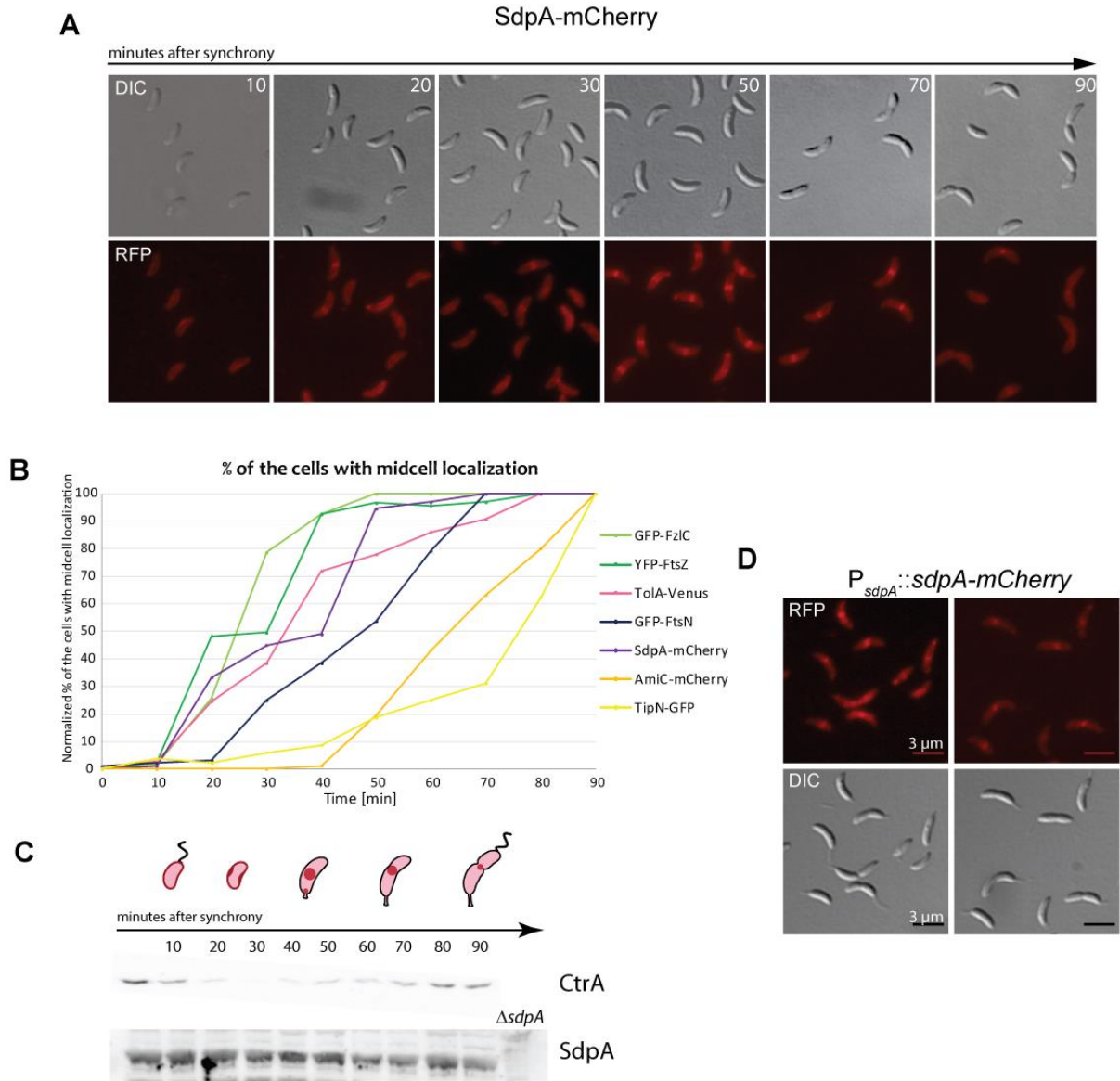
Figure 9. **SdpA is a constitutively produced late cell division protein with cell cycle-regulated localization dynamics. (A)** Cell cycle-dependent localization of SdpA. Strain AM480 (CB15N P$_{xyl}$-*sdpA-mcherry*) was grown in PYE medium to an OD$_{600}$ of 0.8. 2 h before synchronization, expression of SdpA-mCherry was induced by addition of 0.3 % xylose. Cells were synchronized followed by visualization through DIC and fluorescence microscopy at 10 min intervals for a total period of 90 min. **(B)** Temporal order of the assembly of divisome components at midcell. Percentage of the cells with midcell localization from seven individual strains plotted as function of time. Cells of strains SS255 (CB15N P$_{xyl}$-*gfp-fzlC*), MT248 (CB15N P$_{xyl}$-*amiC-mCherry*), MT46 (CB15N P$_{van}$-*ftsN-egfp*), MT196 (CB15N P$_{van}$-*yfp-ftsZ*), NR1371 (Δ*bla* P$_{xyl}$-*tipN-gfp*), MT289 (CB15N P$_{xyl}$-*venus-tolA*), and AM480 (CB15N P$_{xyl}$-*sdpA-mCherry*) were induced with either 0.3 % xylose or 0.5 mM vanillate, synchronized, and analyzed by time-course microscopy in PYE media. An average of 300 cells was counted for each time point per strain for each independent synchrony. **(C)** Cellular levels of SdpA over the cell cycle. Synchronized cells of strain CB15N were grown in PYE medium. Samples collected every 10 min and subjected to Western blot analysis using anti-SdpA and anti-CtrA antibodies. A parallel experiment analyzing the fluctuating levels of the cell cycle master regulator CtrA served as synchrony control is shown in the upper panel (Domian *et al.*, 1997). A graphical representation of SdpA-mCherry localization pattern (shown as a red line or dot) is shown at the top. **(D)** Localization of SdpA-mCherry expressed from its native promoter. Strain AZ45 (CB15N P$_{sdpA}$-*sdpA-mCherry*) was grown to exponential phase in PYE medium, induced with 0.3 % xylose for 2 h, and visualized by DIC and fluorescence microscopy. Scale bar: 3 μm.

Considering that the levels of many *C. crescentus* proteins are cell cycle-controlled, I decided to examine whether the dynamic localization of SdpA-mCherry is caused by fluctuating protein levels or active relocation of the molecules. An immunoblot analysis performed on a synchronized cell population demonstrated constitutive production of SdpA over the course of the cell cycle (Figure 9C), which agrees with previous microarray data (Laub *et al.*, 2000). Collectively, SdpA and SdpB are integral parts of the divisome recruited during the constriction phase, with SdpA additionally being involved in stalked biogenesis. Moreover, SdpA is a constitutively produced divisome component, arriving at the septal ring along with FtsN, suggesting a distinct role in the terminal stages of the cell division, consistent with its predicted hydrolytic activity directed against cell wall.

2.2.1.3 SdpA localization is FtsN, FtsZ and DipM dependent

The foundation of the septal ring is formed of polymerized FtsZ molecules, which are critical for the recruitment of all other downstream divisome component. Since the localization pattern of SdpA is characteristic for cell division proteins, I decided to test whether SdpA also needs FtsZ for localization. For that reason, I integrated an inducible copy of *sdpA-mCherry* at the *vanA* locus of a conditional *ftsZ* mutant and examined microscopically the fluorescence pattern. When depleted of FtsZ, the SdpA-mCherry signal was dispersed within the long, smooth filaments (Figure 10C). 80 minutes after re-induction of FtsZ synthesis, a discrete SdpA-mCherry focus appeared at the future division sites, followed by cell fission after a 40 min delay (Figure 10C).

Since SdpA localizes in an FtsZ-dependent manner, the question arose if its positioning also relies on other cell division components. To test this possibility, I integrated an *sdpA-mCherry* fusion under the control of a xylose-inducible promoter into the conditional *ftsN* mutant strain. Interestingly, in non-permissive conditions, the SdpA-mCherry signal was evenly distributed within the elongated cell bodies, mimicking the result observed for the experiment involving FtsZ (Figure 10A). Considering the key role of FtsN in coordinating cell constriction (Moll & Thanbichler, 2009), it is likely that SdpA is a part of cell wall remodeling machinery.

The precise role of DipM is so far unknown. Nevertheless, experimental data suggested that it is not catalytically active due to the absence of critical residues needed for coordination of the metal cofactor (Figure 32A). Therefore, I hypothesized that it might serve as a scaffold for the localization of other divisome recruits such as SdpA. To test whether SdpA localization is DipM-dependent, I introduced *sdpA-mCherry* at the *xylX* locus of a Δ*dipM* mutant and visualized its localization pattern via fluorescence microscopy. Interestingly, the focus typically formed by SdpA-mCherry was lost in the absence of DipM, suggesting a recruitment dependency (Figure 10B).

Next, I wondered whether other LytM factors (Ldps) may also play a role in the correct spatiotemporal positioning of SdpA since they fall into the same enzymatic family as DipM. For that reason, I generated a strain carrying a xylose-inducible version of SdpA-mCherry in a Δ*ldpABCDEF* background and analyzed the fluorescence signal. The Δ*ldpABCDEF* strain is characterized by mixed population of chaining and WT-like cells (see chapter 2.4.1) (Figure 10B). Unlike in the above experiments, the

distinct focus formed by tagged SdpA was detectable in almost every cell regardless of cell morphology. Therefore, I concluded that Ldps have no role in SdpA's recruitment mechanism.
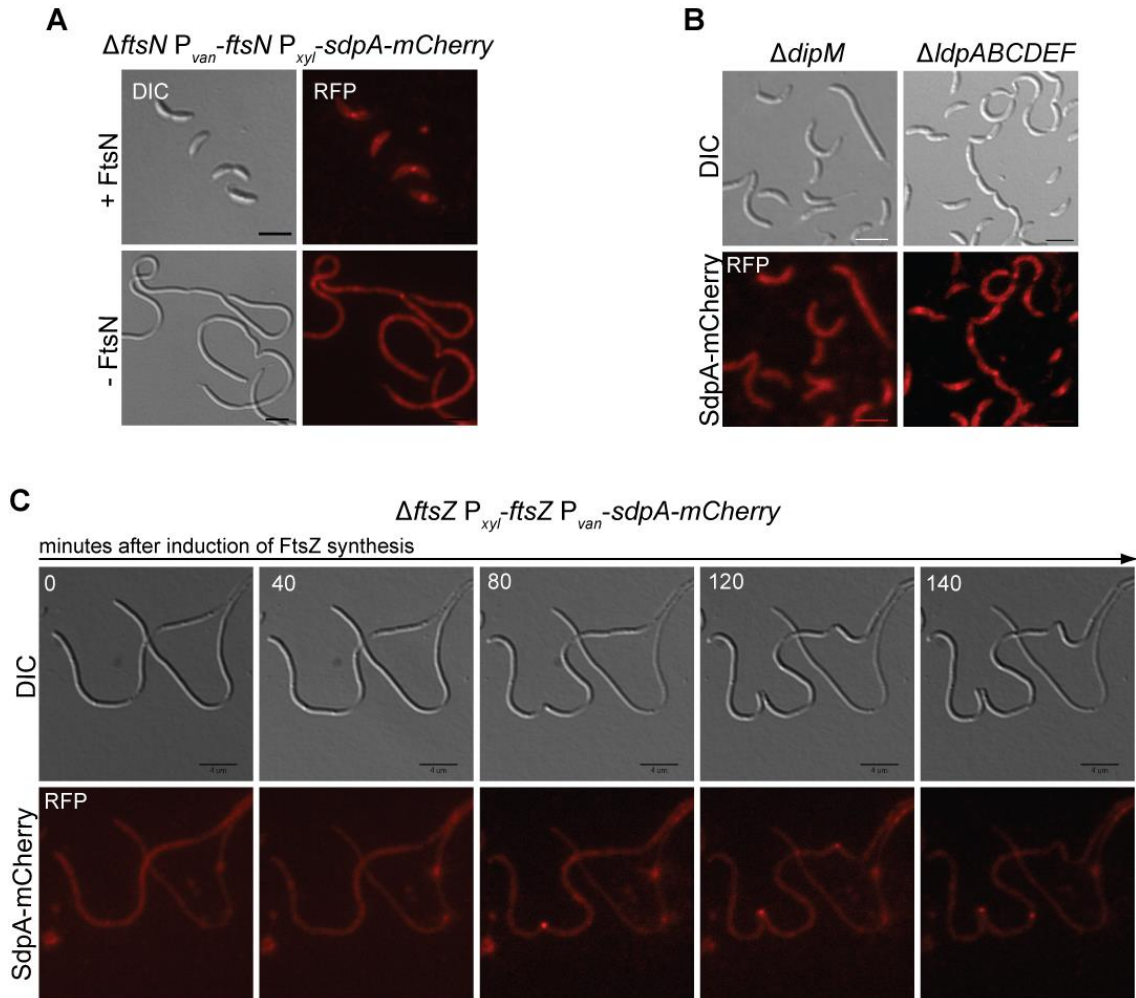
Figure 10. **Localization of SdpA is dependent on FtsN, FtsZ and DipM. (A)** Dependence of SdpA localization on FtsN. Strain AZ46 (Δ*ftsN* P$_{van}$::P$_{van}$-*ftsN* P$_{xyl}$-*sdpA-mCherry*) was grown to exponential phase in PYE medium containing 0.5 mM vanillate. The cells were washed and depleted of FtsN by cultivation for another 14 h in the absence of the inducer. 2 h before analysis, expression of SdpA-mCherry was induced by addition of 0.3 % xylose. Cells were visualized by DIC and fluorescence microscopy. Scale bar: 3μm. **(B)** Dependence of SdpA localization on DipM and LytM factors. Strains AZ67 (Δ*dipM* P$_{xyl}$-*sdpA-mCherry*) and AZ64 (Δ*ldpABCDEF* P$_{xyl}$-*sdpA-mCherry*) were grown to exponential phase in PYE medium following a 2 h expression of SdpA-mCherry triggered with 0.3 % xylose. Cells were visualized by DIC and fluorescence microscopy. Scale bar: 3 μm. **(C)** Dependence of SdpA localization on FtsZ. Strain AZ58 (Δ*ftsZ* P$_{xyl}$::P$_{xyl}$-*ftsZ* P$_{van}$::P$_{van}$-*sdpA-mCherry*) was depleted of FtsZ for 8 h followed by time-lapse fluorescence and DIC microscopy on agarose containing 0.3 % xylose. Images were taken every 20 min for a total period of 3 h. SdpA-mCherry expression was induced with 0.5 mM vanilate 2 h prior microscopy. Scale bar: 4 μm.

Taken together, the localization dependency studies confirm that SdpA's midcell recruitment relies on the presence of the master regulator FtsZ and the late cell divisome components FtsN and DipM. The dependence on factors implicated in cell wall biosynthesis supports the initial idea of SLT involvement in PG remodeling events.

2.2.1.4   Physiological role of SLTs

To more precisely assess the role of SLTs, single and multiple in-frame deletions of the respective genes were introduced into the WT strain. The morphology of strains lacking all possible combinations of *sdpA, sdpB*, and *sdpC* was analyzed microscopically. Neither the single nor the double SLT deletions affected cell morphology, except for a minor elongation of the cell body observed for the Δ*sdpAB* strain (data not shown). In contrast, the triple *sdpABC* mutant displayed evident filamentation accompanied by stalk deformations including shortening and misplacement. Moreover, the cell bodies were elongated in 7 % of the population, reaching up to 23 μm. Together, these result imply difficulties in the division process and involvement of the SLTs in stalk positioning and/or biogenesis (Figure 11A). Intrigued by this observation, I decided to generate an SLT null mutant by introducing an in-frame deletion of *pleA*, fourth and last SLT encoded in the *C. crescentus* genome, into the Δ*sdpABC* background and then assess the morphological consequences. PleA is dispensable for cell division but required for flagellum and pili biogenesis (Viollier & Shapiro, 2003). The morphology of the strain lacking all hypothetical SLTs (Δ*sdpABC* Δ*pleA*) was similar to the one observed for the parental strain. However, a more frequent occurrence of smooth filaments reaching up to 15 μm was observed (Figure 11A). Interestingly, despite enhanced filamentation, the quadruple deletion did not affect the growth rate of the cells (data not shown).

The hydrolytic activity of SLTs is directed against the glycosidic bonds linking GlcNAc and MurNAc in PG. Based on the assumption that the Δ*sdpABC* strain partially or completely lost this activity, I wondered to which extent it alters the architecture of the cell envelope. For that reason, I decided to label the periplasm of the Δ*sdpABC* strain with the tdimer2 and visualize the cells by fluorescence microscopy. Fusion of the gene for the red fluorescent protein tdimer2 to the *torA* twin-arginine signal sequence (*torA*ss) from *E. coli*, assured exclusive translocation of the resulting protein to the periplasm (Judd *et al.*, 2005). Surprisingly, in addition to the cell bodies, very bright fluorescent signal in the periphery of the spots was detected in the surrounding milieu (Figure 11C). It turned out that cells were shedding membrane vesicles. The signal strength emitted from the blebs indicated a high accumulation of tdimer2, likely enclosed by OM but probably not PG. Some of these membrane protrusions were still attached to the cells. Careful examination showed that many of the vesicles were big enough to be visible by DIC microscopy (Figure 11D, vesicles indicated with white arrows).

To confirm that the observed vesicles originate from the OM, I stained the cell membranes of the Δ*sdpABC* strain with the green fluorescent membrane dye BODIPY®FL. Visualization by fluorescence microscopy confirmed the presence of the vesicles; however the signal was less intensive than the one obtained with tdimer2 (Figure 11D). Final validation of the membrane blebbing phenotype of the Δ*sdpABC* mutant was provided by negative staining TEM and cryo-TEM microscopy. Results gathered from both experiments clearly support the initial conclusion that the Δ*sdpABC* deletion leads to the shedding of membrane vesicles. The EM pictures revealed massive cell envelope bulges and stalk deformations (Figure 11F). Moreover, studies of the Δ*sdpABC* ultrastructure by cryo-TEM confirmed that the blebs are bounded by a single membrane (Figure 11G).
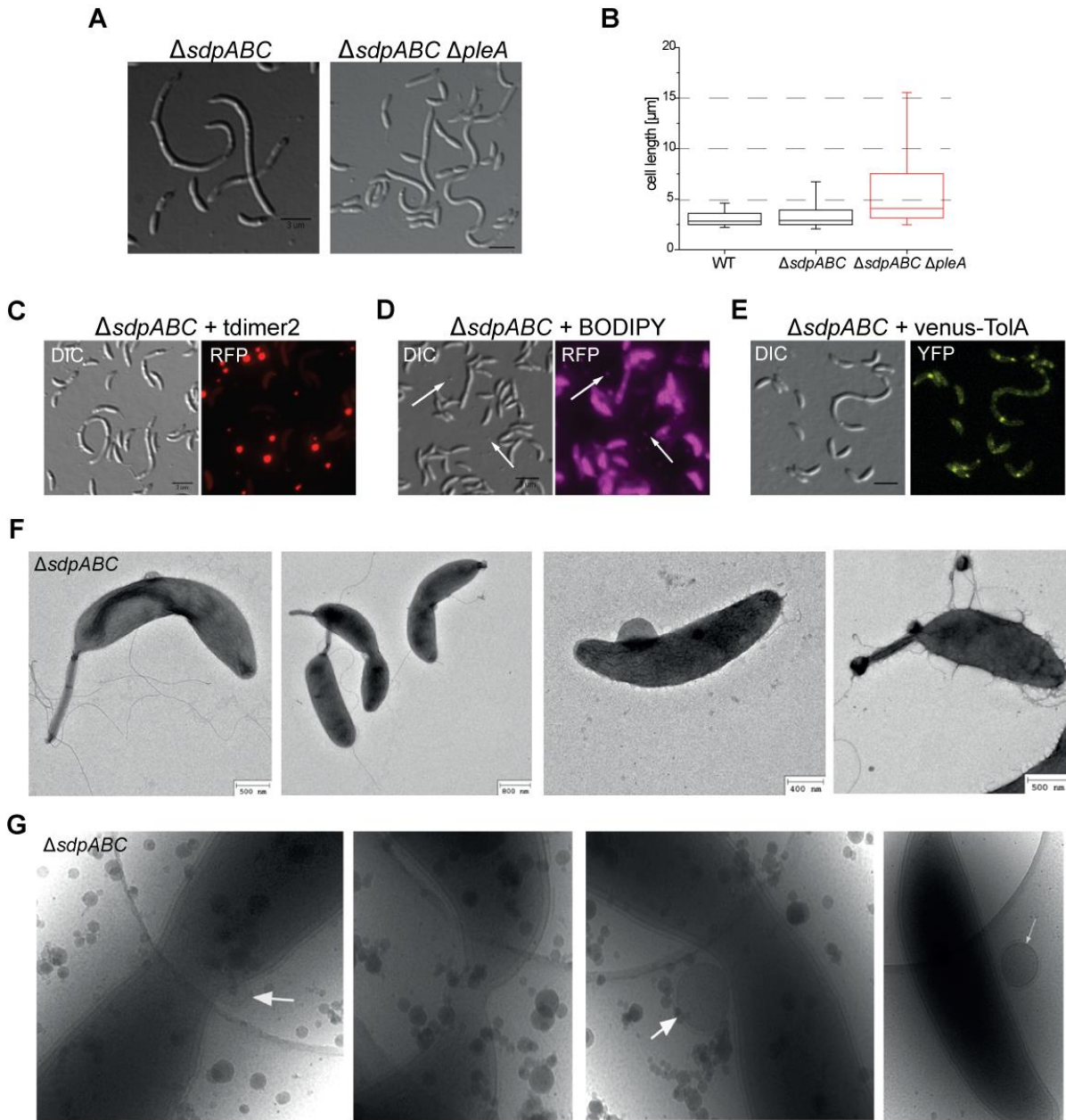
Figure 11. **The *ΔsdpABC* mutant displays a mild filamentous phenotype with concurrent blebbing. (A)** SLT-deficient strains show an elongated morphology. The strains AM440 (*ΔsdpABC*) and AZ93 (*ΔsdpABC ΔpleA*) were grown to exponential phase in PYE medium followed by DIC microscopy. Scale bar: 3 μm. **(B)** Cell length analysis of SLT-deficient strains. The cells described in (A) were analyzed in comparison to the wild-type (WT). Cell body lengths were measured for 150 cells per strain using the MetaMorph program. The results are presented in a box plot. Box plots show the median and the interquartile range (box), the 5th and 95th percentile (whiskers), outliers are excluded. **(C)** Labeling of the periplasmic space of *ΔsdpABC* strain with a red fluorescent protein. Strain AZ57 (*ΔsdpABC* pP$_{xyl}$-torA^{ss}-tdimer2) was grown in PYE to exponential phase and induced for 2 h with 0.3 % xylose, followed by DIC and fluorescence microscopy. **(D)** Labeling of the cell membrane with the lipid probe BODIPY. *ΔsdpABC* cells were grown in PYE to exponential phase followed by BODIPY® staining according to the manufacturer protocol and DIC and fluorescence microscopy. Arrows indicate membrane vesicles. **(E)** Localization pattern of TolA-venus in the *ΔsdpABC* background. Strain AZ63 (*ΔsdpABC* P$_{xyl}$-venus-tolA) was grown to exponential phase in PYE, supplemented with 0.3 % xylose for 2 h and visualized by DIC and fluorescence microscopy. Scale bar: 3 μm. **(F)** Blebbing phenotype of the *ΔsdpABC* mutant. Electron micrographs of AM440 (*ΔsdpABC*) cells grown in PYE to exponential phase. Analysis performed by Dr. Kathrin Bolte (Faculty of Biology, Philipps University of Marburg). **(G)** Ultrastructure of the division site of *ΔsdpABC* cells. Strain AM440 (*ΔsdpABC*) was grown in PYE medium and analyzed by electron cryo-tomography by Dr. Ariane Briegel (California Institute of Technology, USA). Arrows indicate formed vesicles.

The shedding of membrane vesicles is a common process of Gram-negative bacteria that is enhanced especially in strains with cell division disorders. In *C. crescentus*, depletion of the essential Pal protein, a component of Tol-Pal complex, leads to extensive blebbing, resulting from the detachment of the OM from the IM and the PG (Yeh *et al.*, 2010). Due to phenotype similarities between Δ*sdpABC* and the *pal* mutants, I wondered whether the lack of SLTs influences the localization of the Tol-Pal complex. To answer this question I integrated a copy of *venus-tolA* at the *xylX* locus of the Δ*sdpABC* strain, followed by fluorescence microscopy. The formation of venus-TolA foci was not affected, and the pattern known for the WT cells was maintained, unless cells became filamentous, in which accumulation occurred randomly over the cell body (Figure 11E). Therefore, I conclude that both SLTs and TolA might be involved in the OM biogenesis, albeit to a different extent.

Together, the analysis of the mutants lacking SLTs indicates a high functional redundancy of these proteins. To this point, SLTs turned out to be dispensable for cell survival. However, their lack causes filament formation coupled with excessive blebbing, suggesting an active involvement in the cell division process and in general cell envelope integrity.

2.2.1.5   SLTs are necessary for correct cell wall architecture

Homeostasis between synthesis and hydrolysis of the PG is crucial to maintain its correct architecture. Thus, the cell wall composition of an SLT-deficient strain may differ from the native one due to the absence of glycolytic activity and a lower abundance of 1,6-anhydroMurNAc termini. To test this hypothesis, I decided to explore the architecture and properties of the sacculus of the Δ*sdpABC* mutant. The PG composition was determined via fragmentation of the PG, followed by HPLC separation of the resulting muropeptides and their identification by electrospray mass spectometry. Notably, due to the lack of active carboxypeptidases (CPase) (Markiewicz *et al.*, 1983), the mature PG of *C. crescentus* features a high content of pentapeptide side chains, which in other bacterial species is characteristic for nascent PG. Moreover, the experiment confirmed a high percentage of penta-peptides terminated with glycine, instead of D-Ala as in other Gram-negative bacteria, which is only incorporated when present in the media (Takacs *et al.*, 2013). Comparison of the peaks between Δ*sdpABC* and wild type cells revealed a doubling in fraction of tetra-tetra muropeptides in the mutant strain. Further analysis of the chromatogram revealed no significant difference in any other fraction of the muropeptides (Figure 12).

2.2.2   Characterization of membrane bound lytic transglycosylases (MLTs)

C. crescentus possesses four MLTs, identified by Dr. Maria Billini, encoded by the ORFs CCNA_03856, CCNA_03431, CCNA_01579 and CCNA_02650. These proteins were named MbtA, MbtB (**M**embrane-**b**ound lytic **t**ransglycosylase A and B), MtyD (**M**embrane-bound lytic **t**ransglycosylase and **Y**ku**D** containing protein), and Mta2 (**M**embrane-bound lytic **t**ransglycosylase and **A**mi**2** domain-containing protein), respectively (Table S7, Figure 13). An analysis of the domain architecture shows that all four, except for MbtB, contain an additional domain with predicted activity towards PG. Specifically, MbtA

harbors an additional 3D domain (named after three conserved aspartates needed for catalytic activity of the MltA), whereas an Ami_2 (PF01510) domain is found in the N-terminal region of Mta2, confessing an N-acetyl-anhydromuramyl-L-alanine amidase activity. In contrast, MtyD possesses additionally YkuD domain (PF03734) in its C-terminal region with predicted LD-TPase activity, which generates alternative 3-3 crosslinks between mDAPs in the PG stem peptides (Figure 13A). Notably, a transposon screen revealed Mta2 as important for the cell viability, since its lack prompts a "high fitness costs" (Table S7) (Christen *et al.*, 2011).
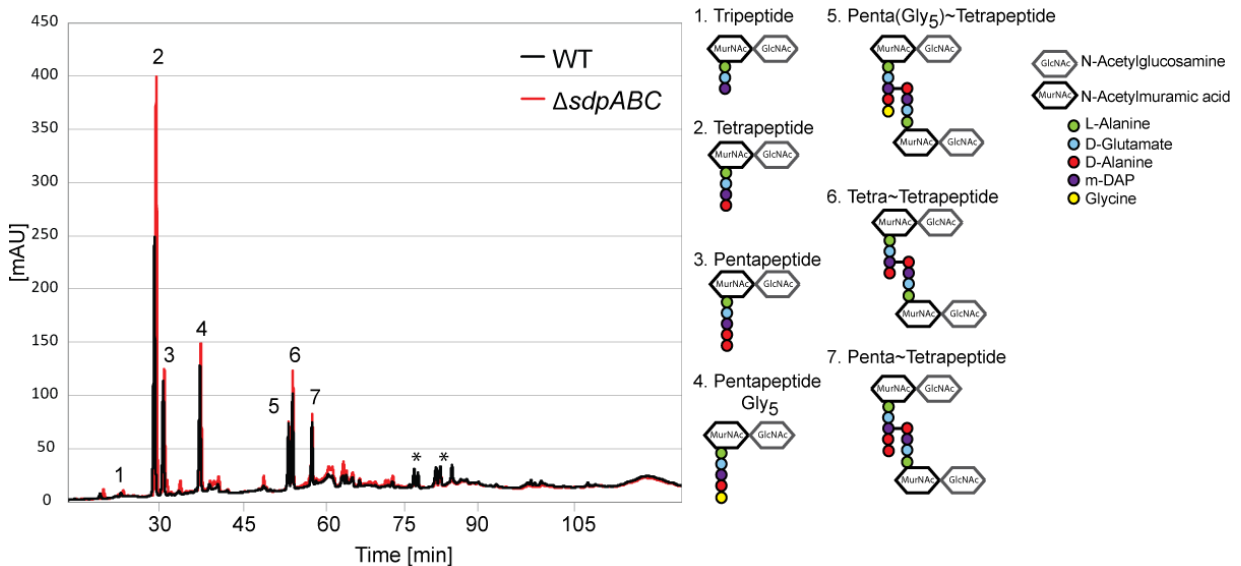
Figure 12. **Absence of SLTs affects cell wall architecture.** Overlay of the HPLC profiles of muropeptides obtained from AM440 (Δ*sdpABC*, red track) and the CB15N (WT, black track) strains. Strains were grown in minimal medium (M2G) to an OD_{600} of 0.7. Cells were lyophilized and cell walls were isolated (5-10 μg) and treated with muramidase. The resulting PG fragments were chromatographically separated and quantified. Their identity was determined by mass spectrometry (ESI-MS/MS). The numbers above the peaks are explained on the right side along with the graphical representations of the respective muropeptides. The asterisks indicate the fractions terminated with 1,6-anhydro-muropeptides.

MLTs are predicted to be membrane-bound proteins. To verify the subcellular localization of Mta2 and MtyD, I generated strains in which additional copies of *mta2* and *mtyD* were fused to *mCherry* and integrated at the *xylX* locus under the control of the xylose-inducible promoter. Resulting strains were analyzed via fluorescence microscopy. Unlike Mta2-mCherry, MtyD-mCherry was stable and showed the predicted localization, as a bright, periplasmic signal was detected. Interestingly, its distribution was rather patchy, suggesting that it may associate with zones of active PG synthesis. However, midcell localization, suggesting implication with the divisome was not observed (Figure 13B).

To define the function of MLTs, strains lacking functional copies of *mbtA*, *mbtB* and *mytD* were generated and studied microscopically. The construction of an *mta2* deletion was not possible, as the deletion procedure only yielded cells with WT phenotype, due to the absence of a second homologous recombination. Strain carrying single and the double deletion of mbtA and/or *mtaB*, were constructed by Maria Billini (unpublished) and exhibited a wild-type phenotype. Similarly, triple deletion of *mbtAB* and *mtyD* did not significantly affect cell morphology implying functional redundancy (Figure 13C). Notably, *mta2* is the only MLT gene so far, that could not be deleted, automatically raising the

question about its essentiality. To test this, a depletion strain was created, by integrating a vanillate-inducible promoter upstream of the only copy of the gene. Surprisingly, the physiology of the cells was unaffected after 24 hours of Mta2 depletion, suggesting that either also this enzyme also has a dispensable function or the critical enzyme activity was still sufficiently high at the basal levels achieved after depletion (data not shown).
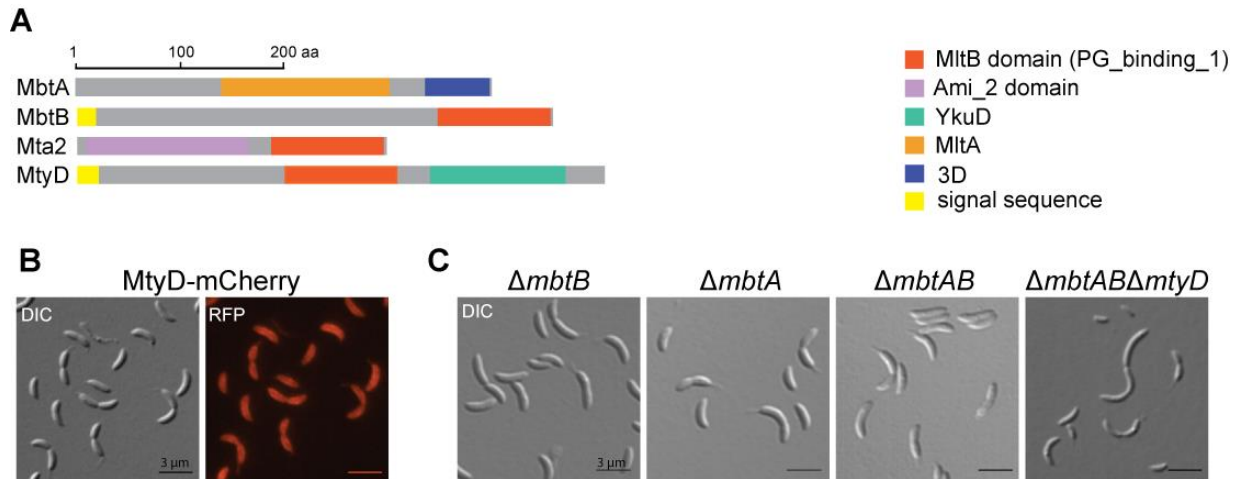
Figure 13. **MLT homologues have a minor contribution to cell division in *C. crescentus*.** **(A)** Schematic representation of MLTs including the domain organization and protein length based on SMART analyses (Letunic *et al.*, 2012; Schultz *et al.*, 1998). **(B)** Localization pattern of MtyD-mCherry. Strain AZ130 (CB15N P*xyl*– *mtyD–mCherry*) was grown to exponential phase in PYE medium, induced with 0.3 % xylose for 2 h, and analyzed by DIC and fluorescence microscopy. **(C)** Morphology of the MLT-deficient strains. DIC micrographs of the strains MAB233 (Δ*mbtB*), MAB239 (Δ*mbtA*), MAB251 (Δ*mbtAB*), and AZ164 (Δ*mbtAB* Δ*mtyD*) during exponential phase of growth. Bar: 3 μm.

Taken together, the results indicate that in contrast to MLTs, SLTs are more important for proper cell morphology. Interestingly, the spatiotemporal localization dynamics of SdpA and SdpB suggest an association with the divisome. Notably, the localization of SdpA is FtsZ-, FtsN- and DipM- dependent and it is constitutively produced over the cell cycle. Notably, the absence of SLTs causes OM alteration as reflected by the formation of blebs. Moreover, their presence is crucial to sustain correct cell wall architecture and most likely other cell envelope properties. Based on the microscopy data, MLTs seems to have a minor, if any, influence on the division process. The localization pattern of MtyD proved its association with the cell envelope, excluding any direct relation with the divisome.

2.3 Enigmatic role of N-acetylmuramoyl-L-alanine amidase homologues

N-acetylmuramoyl-L-alanine amidases have been long known to be crucial for final septum cleavage in *E. coli* (Heidrich *et al.*, 2001; Heidrich *et al.*, 2002; Priyadarshini *et al.*, 2007). Loss of amidase function results in the formation of multicellular chains of inseparable cells. A screen of the *C. crescentus* genome revealed only one homologue gene harboring an Ami_3 (CCNA_01952, named AmiC) domain, with hydrolytic activity against the amide bonds connecting the oligopeptide to MurNAc.

Based on localization studies performed by Andrea Möll, AmiC is part of the *C. crescentus* divisome (Möll, 2011). Surprisingly, deletion of *amiC* does not affect cell morphology, suggesting functional

redundancy (Möll, 2011). Based on the assumption that active amidases might still be unidentified I sought to characterize alternative candidate genes fulfilling this function. My attention was caught by the putative N-acetylmuramoyl-L-alanine amidase with a predicted CHAP domain (CCNA_00354, named Chap), known to be involved in various cellular processes including PG hydrolysis (Bateman & Rawlings, 2003). Interestingly, both genes are considered essential based on a previous transposon screen (Table S7) (Christen *et al.*, 2011).

2.3.1   AmiC is an integral part of the septal ring

The localization dynamics of a fluorescent AmiC-mCherry fusion controlled by the xylose-inducible promoter (P_{xyl}) was monitored via time-course microscopy. To this end, a synchronized population of cells was analyzed over the course of the cell cycle, followed by quantification of the cells that exhibited a characteristic midcell focus at every examined time point.

The fluorescent signal was largely dispersed in the cytoplasm until cells proceeded to final fission, concurrent with OM invagination (Figure 14B). In the very last minutes before daughter cells separation, a distinct AmiC-mCherry focus appeared in approximately 90 % of the cells (Figure 9B). Comparison of the localization dynamics between AmiC-mCherry and already characterized cell division proteins revealed temporal midcell assembly similar to TipN, one of the last Z-ring recruits (Figure 9B).

2.3.2   Chap belongs to the PG remodeling machinery

According to bioinformatic data, Chap is predicted to be soluble in the periplasm. To verify this hypothetical localization, an inducible C-terminal fluorescent protein fusion to mCherry was generated and integrated into the *C. crescentus* chromosome as an additional copy at the *xylX* locus. Unfortunately, proteolytic degradation of the fluorescent fusion resulted in a diffuse, cytoplasmic signal, leaving the true localization of Chap unclear (data not shown).

Next, an in-frame deletion of Chap was generated by double homologous recombination. The mutant strain exhibited very mild morphological changes reflected in cell body elongation and seldom branches formation in approx. 4 % of the population (Figure 14C). Nevertheless, the majority of Δ*chap* cells displayed a phenotype identical to that of the wild type (Figure 14D). Intrigued by the possible functional dependency of both hypothetical N-acetylmuramoyl-L-alanine amidases I went on to generate a double deletion by introducing the *chap* deletion into the Δ*amiC* background. Microscopic study of the resulting strain yielded a Δ*chap* phenotype, which excludes the possibility that these two proteins have critical but redundant functions (Figure 14C). Notably, growth capability was not impaired in any case (data not shown).

In summary, the results presented in this section indicate non-essential functions of both putative N-acetylmuramoyl-L-alanine amidases. Nevertheless, AmiC exhibited cell cycle-driven localization dynamics and association with the divisome, which may suggest an active, so far unknown role.

Inactivation of the second putative PG amidase, Chap, caused a very mild filamentous phenotype, coupled with polarity defects, implying that it likely plays a role in the division process.
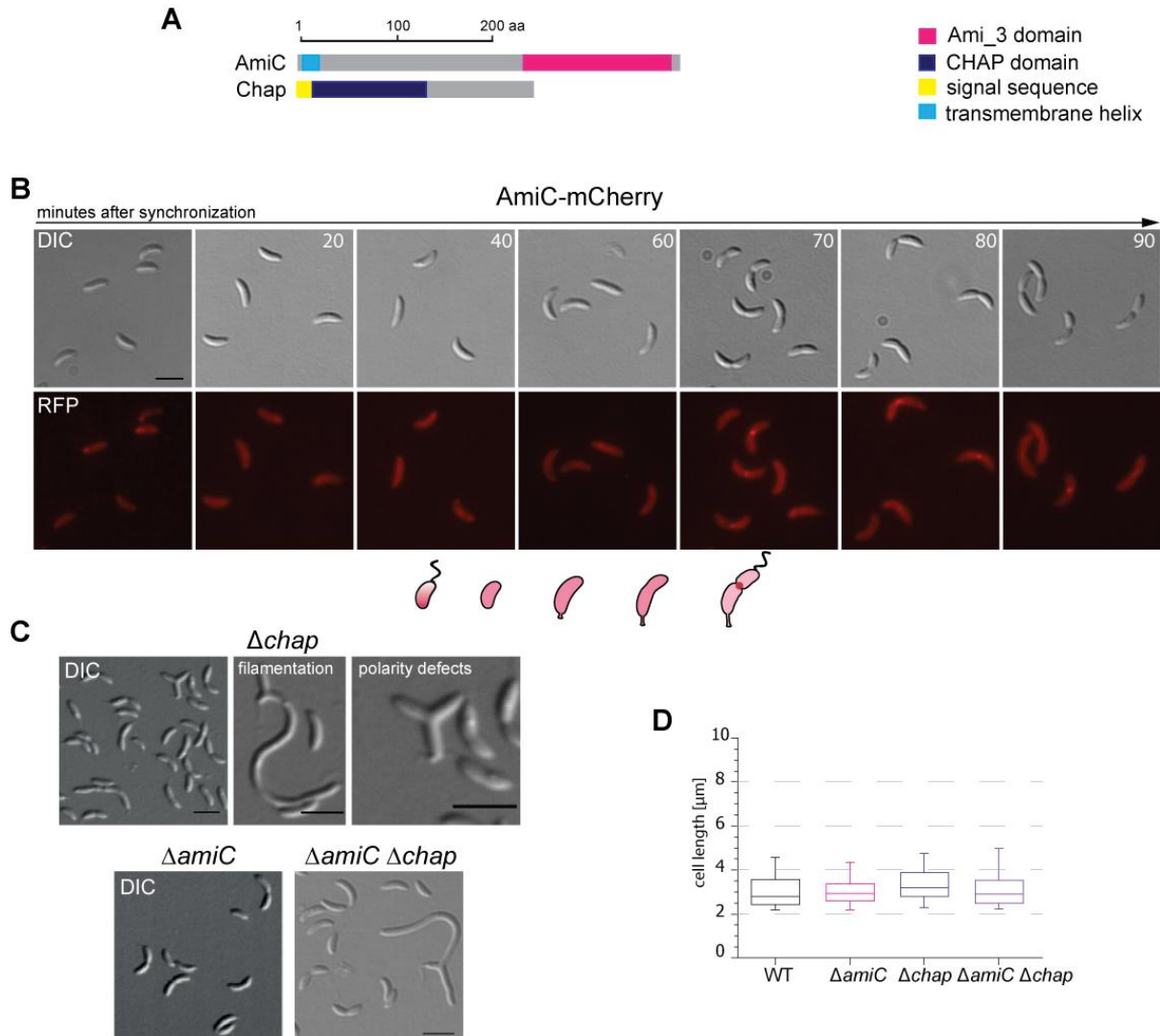
Figure 14. **Characterization of putative N-acetylmuramoyl-L-alanine amidase homologues. (A)** Schematic representation of PG amidases, including their domain organization and protein length based on NCBI and SMART analyses (Letunic *et al.*, 2012; Schultz *et al.*, 1998). **(B)** Cell cycle dependent localization of AmiC. Strain MT248 (CB15N P$_{xyl}$-*amiC-mCherry*) was grown in PYE medium to an OD$_{600}$ of 0.8. 2 h before synchronization, expression of SdpA-mCherry was induced by addition of 0.3 % xylose. Cells were synchronized followed by DIC and fluorescence microscopy visualization at 10 min intervals for a total period of 90 min. **(C)** Morphology of amidase-deficient strains. DIC micrographs of the strains AM338 (Δ*amiC*), AZ86 (Δ*chap*), and AZ165 (Δ*amiC* Δ*chap*) at the exponential phase of growth. Scale bars 3 μm. **(D)** Cell length comparison between amidase-deficient strains. The cells described in (C) were analyzed in comparison to the wild-type (WT). Cell body lengths were measured for 150 cells per strain using the MetaMorph program. The results are presented in a box plot. Box plots show the median and the interquartile range (box), the 5th and 95th percentile (whiskers), outliers are excluded.

2.4   Endopeptidases (EPases)

Catabolic activities required for murein disintegration during growth and division demand LD-EPase activity to cleave peptide bridges that link oligopeptide moieties in around 30 % of the mature murein mesh. There are two specialized groups of enzymes with this activity: intensively studied LytM factors,

which harbor an M23 peptidase domain and the newly identified NlpC/P60 (belonging to CHAP superfamily) hydrolases from Spr family, which contain a **c**ysteine, **p**eptidase domain.

2.4.1   Physiological role of LytM factors

LytM factors (Ldps) fall into the group of endopeptidases (EPases) owing to their characteristic M23 peptidase domain localted usually at C-terminus (Figure 15A). Initial data collected by Andrea Möll demonstrated functional redundancy, based on phenotypical studies of the deletion mutants (Möll, 2011). An exception was DipM, which is crucial for proper cell constriction and proper cell poles architecture in *C. crescentus* (Goley *et al.*, 2010a; Moll *et al.*, 2010; Poggio *et al.*, 2010). Ldps comprise either a partial (DipM, LdpB and LdpF) or a full (LdpA, LdpC, LdpD and LdpE) M23 peptidase motif, suggesting the lack or presence of catalytic activity, respectively (Figure 32A). Localization studies of LdpA-F (**L**ytM **d**omain containing **p**roteins **A-F**) were unsuccessful due to proteolytic degradation. Moreover, single and multiple deletions of Ldps had no effect on the phenotype and growth rate of the cells, with the exception a deletion of *ldpF* , which caused mild chaining morphology (Möll, 2011).

The mutant libraries constructed to this point lacked strains with lesions of both catalytically inactive enzymes (LdpB and LdpF) and with the deletions of all six Ldps. Construction of these strains may yield interesting insights because *ldpF* is the only gene that slightly affects morphology and, secondly, inactive LytM factors are important regulators of amidases in *E. coli* (Uehara *et al.*, 2009). Δ*ldpBF and* Δ*ldpABCDEF* (6ΔLytM) strains were generated, followed by visualization with DIC microscopy. Strikingly, the morphology of both strains was significantly altered, and very similar to each other (Figure 15B). The phenotype of the cells missing Δ*ldpBF and* Δ*ldpABCDEF* indicated a dysfunction of cell division, precisely final cell fission, as reflected by the formation of cell chains composed of up to 7 compartments (Figure 15). Statistical analysis of the cell lengths yielded an almost identical median for both strains (Figure 15C). Growth defect was not observed (Figure 33D). Therefore, I concluded that LdpF is the protein responsible for the observed separation defect. This conclusion is additionally supported by the fact that the lack of the five remaining Ldps affects neither cell morphology nor viability (Figure 15B).

2.4.1.1   LdpF plays a crucial role in the cell wall biogenesis

To better understand LdpF's contribution to cell division and the cell wall biosynthesis process, overexpression, localization and complementation studies were performed together with Katharina Kremer (Kremer, 2015).

If LdpF is directly involved in cell division, changes in the protein amount should cause a dysfunction in the process manifested by phenotypical and/or growth abnormalities. We speculated that the function of LdpF might be similar to that of DipM. To test theis possibility, an LdpF P_{xyl}-based overproduction construct was generated and transformed into wild-type and Δ*dipM* cells. Previous data clearly showed that DipM overexpression results in cellular lysis (Moll *et al.*, 2010). If LdpF is critical for cell division, the overexpression effect should be analogous to the one obtained for DipM. Furthermore, if both proteins fulfill the same function, LdpF overproduction should suppress the

filamentous phenotype of the Δ*dipM* strain. DIC microscopy of the resulting strains was performed after 3.5 hours of overproduction. The overproduction of LdpF did not affect morphology in either tested genetic background (Kremer, 2015). Therefore, we conclude that LdpF influences cell division rather indirectly and acts in a pathway alternative to the DipM.
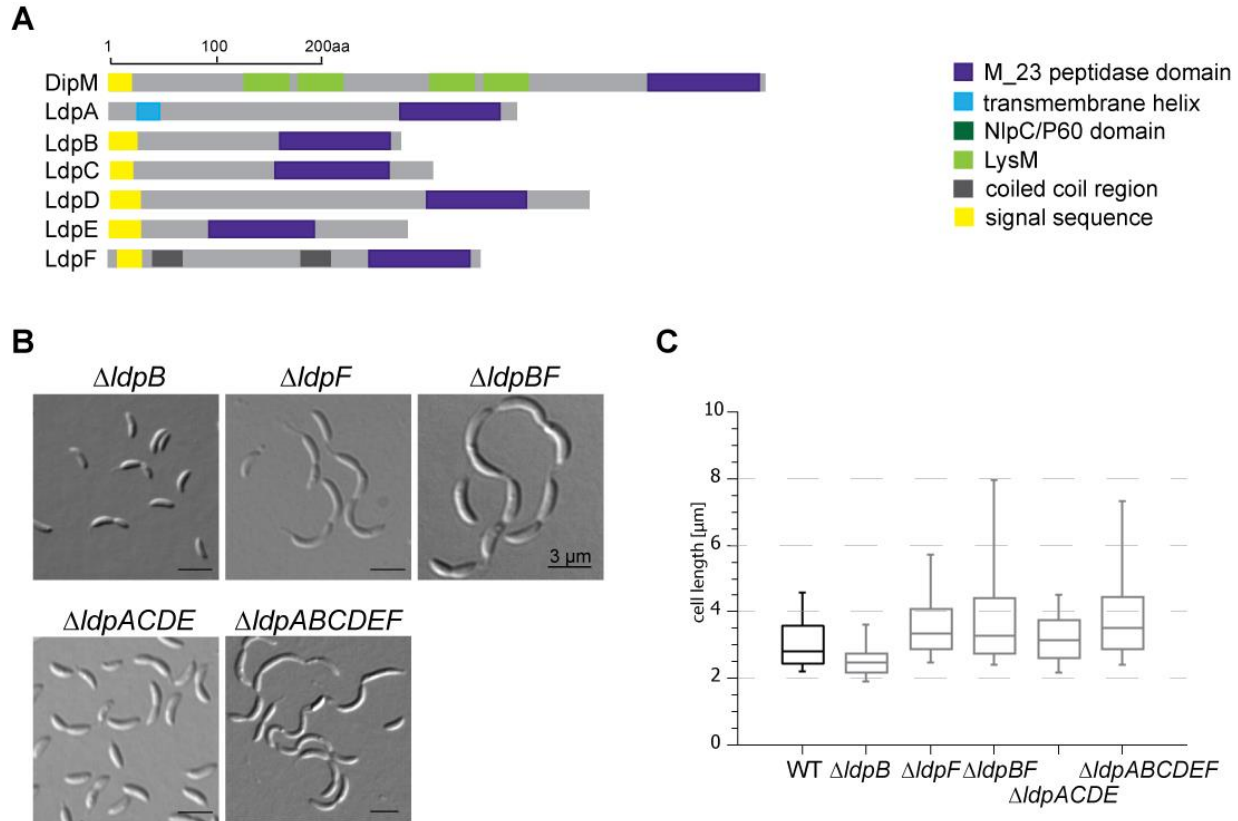
Figure 15. **Endopeptidases (EPases) from the LytM family have redundant functions.** **(A)** Schematic representation of LytM factors including their domain organization and protein length based on NCBI and SMART analyses (Letunic *et al.*, 2012; Schultz *et al.*, 1998). **(B)** Morphology of the LytM deficient strains. DIC micrographs of the strains AM365 (Δ*ldpB*), AM369 (Δ*ldpF*), AZ91 (Δ*ldpBF*), AM438 (Δ*ldpABCDE*), AM448 (Δ*ldpACDE*), and AZ52 (Δ*ldpABCDEF*) at the exponential phase of growth. Scale bar: 3 μm. **(C)** Cell length comparison between LytM-deficient strains. The cells described in (B) were analyzed in comparison to the wild-type (WT). Cell body lengths were measured for 150 cells per strain using the MetaMorph program. The results are presented as a box plot. Box plots show the median and the interquartile range (box), the 5th and 95th percentile (whiskers), outliers are excluded.

Localization studies, using an LdpF-mCherry fusion expressed under control of the xylose-inducible promoter (P$_{xyl}$), allow any conclusions on the subcellular localization of the protein, because the fluorescent fusion was not stable. In contrast, the complementation studies confirmed that the morphological aberrations observed for the Δ*ldpF* strain were a direct result of the lack of a functional copy of *ldpF* (Kremer, 2015).

2.4.2 LytM factors and their contribution to the cell wall architecture

The chaining phenotype of the Δ*ldpABCDEF* mutant implies either a direct influence of LytM factors on PG biosynthesis or a role in the regulation of cell division/PG remodeling. To directly examine the influence of LytM factors on cell wall composition, a muropeptide analysis of digested PG isolated from Δ*ldpABCDEF* cells was performed, as describe in section 2.2.1.5. The muropeptides pattern obtained for the mutant was almost identical to the one observed for the wild-type control (Figure 16). The variations of the peaks heights between the strains most likely resulted from slight differences in the amount of the cell walls used for analysis.
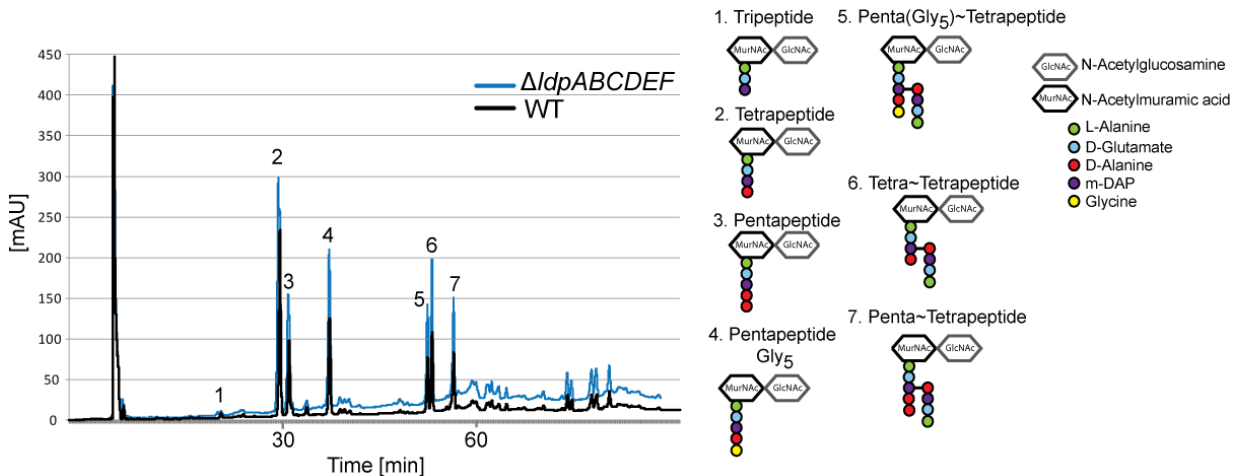
Figure 16. **A Sextuple deletion of LytM factor genes does not affect cell wall composition.** Overlay of HPLC profiles of muropeptides obtained from the strains AZ52 (Δ*ldpABCDEF*, blue track) and CB15N (WT, black track). Cells were grown in minimal medium (M2G) to an OD_{600} of 0.7, and lyophilized. Cell walls were isolated (5-10 µg) and treated with muramidase. The resulting PG fragments were chromatographically separated and quantified. Their identity was determined by mass spectrometry (ESI − MS/MS). The numbers above the peaks are given on the right side along with a graphical representations of the respective muropeptides.

Together, these results suggest that LytM factors are important but dispensable members of the PG biosynthetic machinery. Loss of the two catalytically inactive Ldps, LdpB and LdpF, results in the phenotype mimicking the absence of all of them, which highlights the physiological relevance of these proteins. Moreover, LdpF arose as a prominent candidate to fulfill significant role/s in the division process, but its precise function is so far unknown. In fact, it might be important to maintain the homeostasis of PG synthesis since its lack triggers a salt sensitive phenotype (see chapter 2.6). Even though the lack of Ldps as a group does not significantly affect overall PG composition, it still may influence the septal PG biosynthesis and/or architecture. Most importantly, DipM and LdpF seem to have an unquestionable influence on the division process, which makes them important players in cell wall biogenesis in *C. crescentus*.

2.4.3 DipM function

Despite intensive studies, the precise role of DipM in the division process has not been elucidated. Published data suggested that it is catalytically inactive and that it interacts with divisome

components recruited during the late stages of the cell division based on BAC2H studies (Moll *et al.*, 2010; Poggio *et al.*, 2010). Therefore, I speculated that DipM may be either a scaffold for other redundant cell division components (chapter 2.2.1.3) or a regulator of so far uncharacterized PG remodeling component. For that reason, I aimed to find DipM interaction partners via co-immunoprecipitation (Co-IP) followed by mass spectrometry (MS) analysis to provide additional support for the results obtained via BAC2H analysis.

The Co-IP experiment was carried out using a *C. crescentus* strain in which the native *dipM* copy was truncated and replaced with a gene encoding DipM variant tagged with a decahistidine tag (His10) under the control of the xylose-inducible promoter. Before the reactions, cells were treated with paraformaldehyde to preserve unstable/transient protein-protein interactions. As a control for every experiment, lysates from a Δ*dipM* strain expressing native (untagged) DipM from the xylose-inducible promoter were prepared in parallel under identical conditions.

Figure 17. DipM interaction studies based on coimmunoprecipitation analysis. Lysates of strains AM409 (Δ*dipM* P_{xyl}-*dipM*-his10) and SW59 (Δ*dipM* P_{xyl}-*dipM*) were incubated with either GE-Ni-Mag®**(A and C)** or anti-his antibody-coupled **(B)** magnetic beads probed with anti-his antibodies. Samples abbreviations stand from probed fractions: P- pellet, L-lysate, i-post-incubational, W123- washing steps 1, 2 and 3, E 1,2 – elution, B- beads cooked in the sampling buffer. Arrow indicates molecular weight corresponding to DipM-His10, asterisk indicates unspecific products. **(D)** Putative interaction partners identified via Co-IP. Schematic representation of CCNA_00398 and CCNA_02661 including their domain organization and protein length based on NCBI and SMART analyses (Letunic *et al.*, 2012; Schultz *et al.*, 1998).

In total, six independent Co-IP experiments were performed using various conditions. In three cases, I was able to confirm the presence of DipM-His10 in the elution fraction via immunoblot analysis using anti-His antibodies (Figure 17ABC). The MS analysis performed by Dr. Jörg Kahnt (Max-Planck-Institut für terrestrische Mikrobiologie, Marburg) identified a number of putative interaction partners bound to DipM-His10 (Table S5 and S6). Interestingly, among the identified hits, SdpA was found with the very low peptide score. Assuming that potential DipM interaction partners are residing in the periplasm and/or contain either domains with predicted catabolic activity or of unknown function (DUF), two interesting candidates were selected for further analysis: CCNA_00398 and CCNA_02661 (Figure 17D). Both putative DipM interaction partners, CCNA_00389 and CCNA_02661, were selected based on the presence of the signal peptide. Moreover, a CCNA_02661 additionally encoded a two repeats of M16- and M16C (PF05193) -peptidase domain, classified as zinc-metallopeptidases. Unfortunately, neither localization nor deletion analyses confirmed implications in the division and/or PG remodeling process (data not shown). Therefore, I concluded that it is unlikely that either CCNA_00398 or CCNA_02661 directly interact with DipM and modulate its activity.

To directly test how the absence of DipM influences cell wall of *C. crescentus*, the muropeptide profile of PG isolated from the Δ*dipM* strain was analyzed as described in section 2.2.1.5. The data revealed no significant change between the profiles obtained from the wild-type and the Δ*dipM* strain, suggesting that the activity of DipM or potential proteins regulated by it overlaps with that of other hydrolytic enzymes or only affects a minor fraction of the PG sacculus (Figure 18).
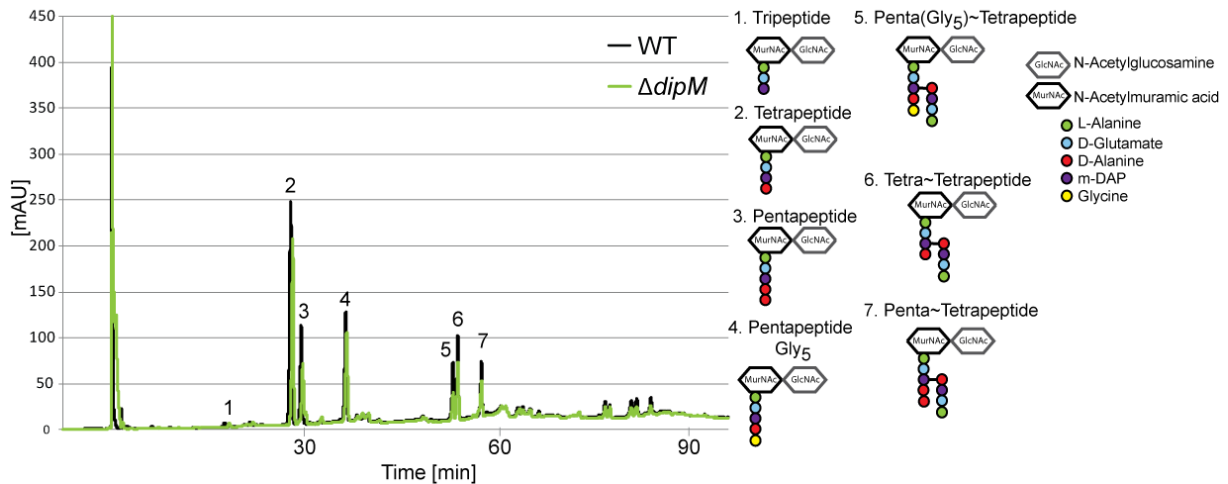
Figure 18. **Muropeptide profile of the Δ*dipM* mutant.** Shown is an overlay of the HPLC elution profiles of muropeptide samples obtained from strains MT258 (Δ*dipM*, green track) and CB15N (WT, black track). Cells were grown in minimal medium (M2G) to an OD_{600} of 0.7 and lyophilized. Cell walls were isolated (5-10 µg) and digested with muramidase. The resulting PG fragments were separated chromatographically and quantified. Their identity was determined by mass spectrometry (ESI–MS/MS). The numbers above the peaks are explained on the right side along with graphical representations of the respective muropeptides.

2.4.4 Physiological function of NlpC/P60 endopeptidases

C. crescentus possesses two homologues coding for EPases falling into the NlpC/P60 family and one CHAP-domain protein, as described in chapter 2.3.2. Despite their distinct catalytic activities, all three proteins are classified as CHAP superfamily.

A bioinformatics screen of the *C. crescentus* genome identified two open reading frames encoding NlpC/P60 domain-containing proteins with predicted peptidase activity directed against cross-links in murein. These so-far uncharacterized ORFs CCNA_03031 and CCNA_02863 were named NlpA and NlpB (**Nl**pC/**P**60 domain containing protein **A** and **B**) accordingly (Table S7, Figure 19A).

To assess the physiological function of the proteins from the CHAP superfamily, single and multiple in-frame deletions were generated, followed by visualization of the mutant cells with DIC microscopy. Inactivation of NlpB and Chap alone yielded morphologically normal cells and slightly elongated and/or branched cells, respectively. In contrast, loss of NlpA triggered the formation of significantly elongated cell bodies, implying a cell division defect (Figure 19B). Double deletion of *nlpB* and *chap* yielded a phenotype similar to that of the Δ*chap* mutant. Progressive filamentation was a dominant feature of the Δ*nlpA* Δ*chap*, and Δ*nlpAB* double and Δ*nlpAB* Δ*chap* triple mutants (Figure 19C). In fact, a double deletion of *nlpA* and *chap* resulted in the most severe elongation of the cell bodies observed

so far upon inactivation of only two proteins with hypothetical hydrolase activity. Notably, filamentation was accompanied by the formation of short appendixes outgrowing randomly from the cell bodies, as characteristic for the inactivation of Chap. This additive phenotype suggests a block of two independent pathways. The Δ*nlpAB* Δ*chap* triple deletion resulted in the formation of filaments, coupled with frequently observed spontaneous lysis of the cells (Figure 19C). Interestingly, the analysis of the cell lengths revealed that additional inactivation of NlpB in the Δ*nlpA* Δ*chap* background seemed to partially suppress the filamentation phenotype (Figure 19D).
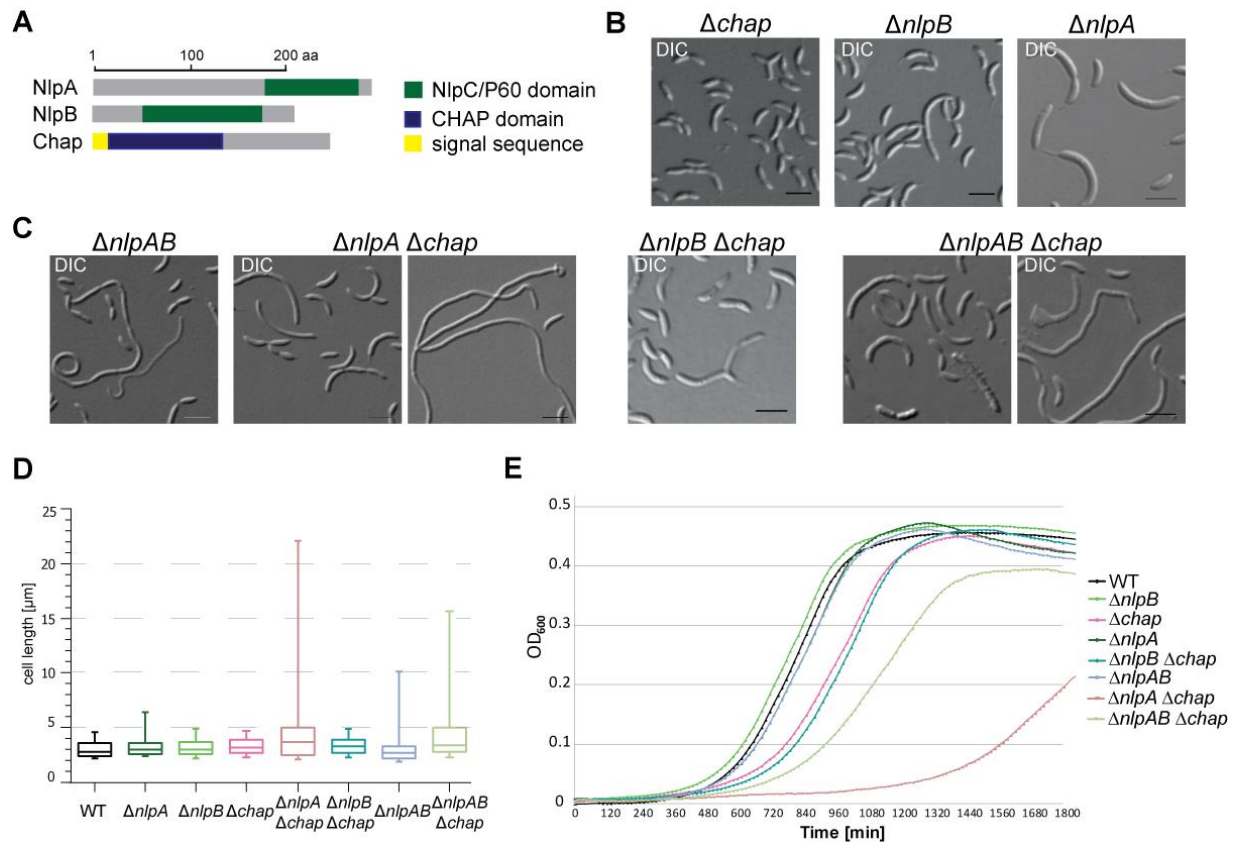
Figure 19. **EPases from the NlpC/P60 family are relevant for cell division in *C. crescentus*.** **(A)** Schematic representation of NlpC/P60 EPases and CHAP amidase including their domain organization and protein length based on NCBI and SMART analyses (Letunic *et al.*, 2012; Schultz *et al.*, 1998). Morphology of the strains lacking single **(B)** and multiple **(C)** copies of NlpC/P60 homologues. Strains AZ86 (Δ*chap*), AZ85 (Δ*nlpB*), AZ167 (Δ*nlpA*), AZ89 (Δ*nlpAB*), AZ121 (Δ*nlpB* Δ*chap*), AZ120 (Δ*nlpA* Δ*chap*), and MAB250 (Δ*nlpAB* Δ*chap*) were grown to exponential phase in PYE medium followed by DIC microscopy. Scale bar: 3 μm. **(D)** Cell length analysis of NlpC/P60 deficient strains. The cells described in (B and C) were analyzed in comparison to the wild-type (WT). Cell body lengths were measured for 150 cells per strain using the MetaMorph program. The results are presented in box plots. Box plots show the median and the interquartile range (box), the 5th and 95th percentile (whiskers), outliers are excluded. **(E)** Growth rate analysis of the NlpC/P60/CHAP deficient strains described in (B) and (C). Cells were grown o/n in rich medium, followed by inoculation into fresh PYE medium and OD_{600} measurements every 15 min for the total period of 31 h. Curves were color-codedi n correlation to the box plot diagrams in (D).

Since division defects often affect growth rate, the proliferation capacity of the NlpC/P60 deletion mutants was tested in liquid and on solid media. The assay, performed in rich liquid medium, revealed a highly aberrant proliferation rate for the Δ*nlpA* Δ*chap* and the Δ*nlpAB* Δ*chap* mutants (Figure 19E). As expected, the strongest growth inhibition correlated with the most severe phenotype as observed for the Δ*nlpA* Δ*chap* strain, which was approximately twofold slower than any other strain in the

tested conditions (Figure 19D). In agreement with the cell length analysis, additional loss of NlpB in the Δ*nlpA* Δ*chap* background indeed partially suppressed vitality loss of the Δ*nlpA* Δ*chap* double mutant (Figure 19E). Noteworthy, a strain carrying the tripe *nlpAB/chap* deletion reached stationary phase at a lower cell density. Additionally, every combination of deletions including mutation of *nlpA* and *chap* resulted in lysis in stationary phase (Figure 19E). Colony formation on solid media agreed with the results obtained in liquid conditions, indicating significantly or partially decreased vitality of the Δ*nlpA* Δ*chap* and Δ*nlpAB* Δ*chap* strain, respectively (Figure 25D).

In summary, the collected data show that NlpA and Chap from the NlpC/P60 EPase family are required to maintain correct cell division, growth rate and most likely cell envelope properties in *C. crescentus*. In contrast to this result, NlpB did not appear to have a detectable role in the division process.

2.5   Characterization of LD-Transpeptidases (LD-TPases)

Recent studies suggested a prominent role of LD-TPases in the PG synthesis and/or remodeling events in *A. tumefaciens* (Cameron *et al.*, 2014). Evolutionary proximity of *A. tumefaciens* to *C. crescentus* made me wonder how much LD-TPases contribute to the PG remodeling process in the latter one. To answer this question, I searched the *C. crescentus* genome for YkuD domain harboring genes, responsible for the described TP activity. Two uncharacterized LD-TPases homologues encoded by CCNA_03860 (named YkuD) and CCNA_01579 (named MtyD, as described before in section 2.2.2) were identified. YkuD was predicted to be a cytoplasmic protein, composed almost entirely of the single catalytic domain (Figure 20A).

To determine the physiological function of MtyD and YkuD, single and multiple deletion strains were generated and examined microscopically (Figure 20B). The morphology of the Δ*mtyD* strain was unaffected, whereas inactivation of YkuD triggered formation of elongated cells, featuring a significant length variation with a single cells reaching up to 17 μm (Figure 20C). The Δ*ykuD* Δ*mtyD* double deletion resembled the Δ*ykuD* phenotype, suggesting the same function, but acting in parallel.

In sum, the results indicate that LD-TPases are dispensable for cell division and most likely PG biogenesis. The reason behind the cell body elongation observed upon deletion of Δ*yku* needs to be clarified with additional experiments.

Altogether, I provided several lines of evidence that the known enzymes hydrolyzing PG at the division site are characterized by functional redundancy in *C. crescentus*. The comprehensive analysis of the autolysin-deficient strains revealed that none of the examined homologues is essential for cell survival. The dynamic localization pattern characteristic for divisome components was established for SdpA and SdpB, suggesting a role in the division process. Collectively, SLTs seems to play an important role in cell division as a group, but to which extent is not known so far. The *ldpB* and *ldpF* mutants emulated the morphological defects observed upon inactivation of all six LytM factors, pointing to their prominent role in the terminal stages of the cell division. Loss of function of three EPases LdpF, NlpA and YkuD, alone caused a defective morphology, suggesting a contribution of these proteins in the cell division process. Unfortunately, experiments aiming at gathering direct evidence for an

association with the divisome were unsuccessful. Noteworthy, NlpA and Chap together are essential to maintain the normal proliferation capacity, as their loss rendered serious vitality suppression. To unravel the precise role/s of the putative PG hydrolases, further experiments are required.
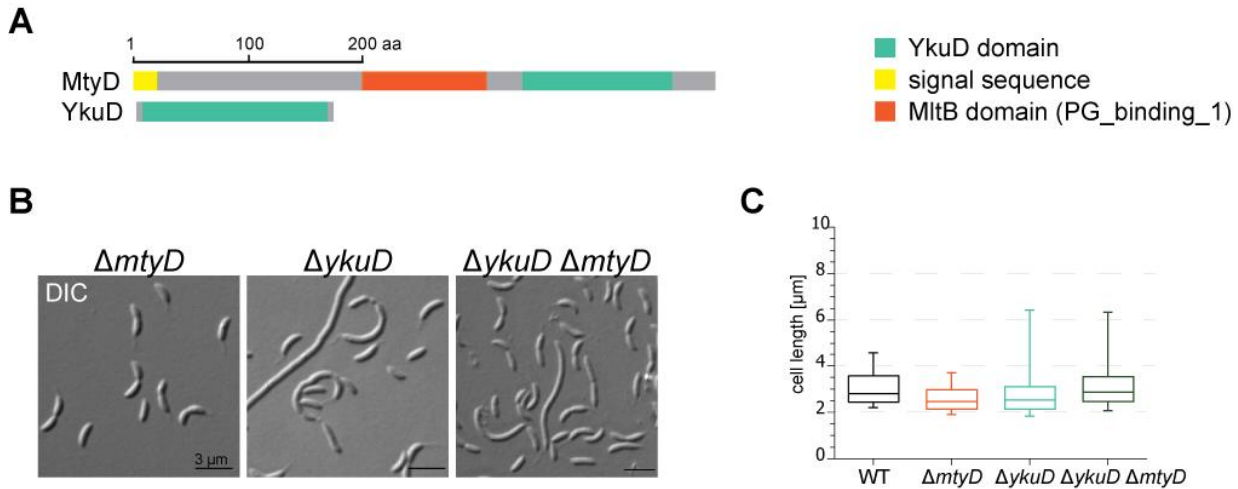
Figure 20. **YkuD may fulfill a cell division associated role. (A)** Schematic representation of LD-TPases including their domain organization and protein length based on NCBI and SMART analyses (Letunic *et al.*, 2012; Schultz *et al.*, 1998). **(B)** Morphology of the LD-TPase-deficient strains. DIC micrographs of strains AZ137 (Δ*mtyD*), AZ140 (Δ*ykuD*), and AZ138 (Δ*mtyD* Δ*ykuD*) during exponential phase of growth in PYE medium. Scale bars: 3 µm. **(C)** Cell length comparison between LD-TPase deficient strains. The cells described in (B) were analyzed in comparison to the wild-type (WT). Cell body lengths were measured for 150 cells per strain using the MetaMorph program. The results are presented in box plots. Box plots show the median and the interquartile range (box), the 5th and 95th percentile (whiskers), outliers are excluded.

2.6 Physiological response of PG hydrolase-deficient strains in stress conditions

Single and multiple in-frame deletions in genes encoding SLTs, LytMs and AmiC caused rather mild phenotype when analyzed in rich media (Figure 21ABC). These results are consistent with the fact that most (>90 %) of the annotated biosynthetic genes in the intensively studied model organism *E. coli* are dispensable under standard growth conditions (Baba *et al.*, 2006). Therefore, I decided to explore whether the respective murein hydrolases in *C. crescentus* would become more important in harsh environmental conditions. For that reason, I designed a series of experiments testing the physiological response of different mutants towards various stress factors. Thus, I analyzed the physiological response of the Δ*dipM*, Δ*amiC*, Δ*sdpABC* and Δ*ldpABCDEF* strains to elevated osmolality provoked by salt or sugar, elevated temperature, nutrient limitation, and exposure to the cell wall targeting antibiotic ampicillin.

To establish optimal concentrations of the solutes for the subsequent experiments, firstly, the osmotolerance of the wild-type strain was tested in rich, liquid media supplemented with a range of 0.1-10 % of either sodium chloride or sucrose (Figure 23A). Complete growth inhibition and cell lysis, were observed for 0.7 % of salt and 7.5 % sucrose in the rich media (data not shown). Notably, supplementation of 5 % sucrose yielded swollen cells, suggesting upcoming lysis. Filament formation

began in the presence of 0.3 % sodium chloride and became more severe with raising concentrations (Figure 22B), indicating an extremely low salt tolerance of *C. crescentus* and a strong influence into the cell division process.
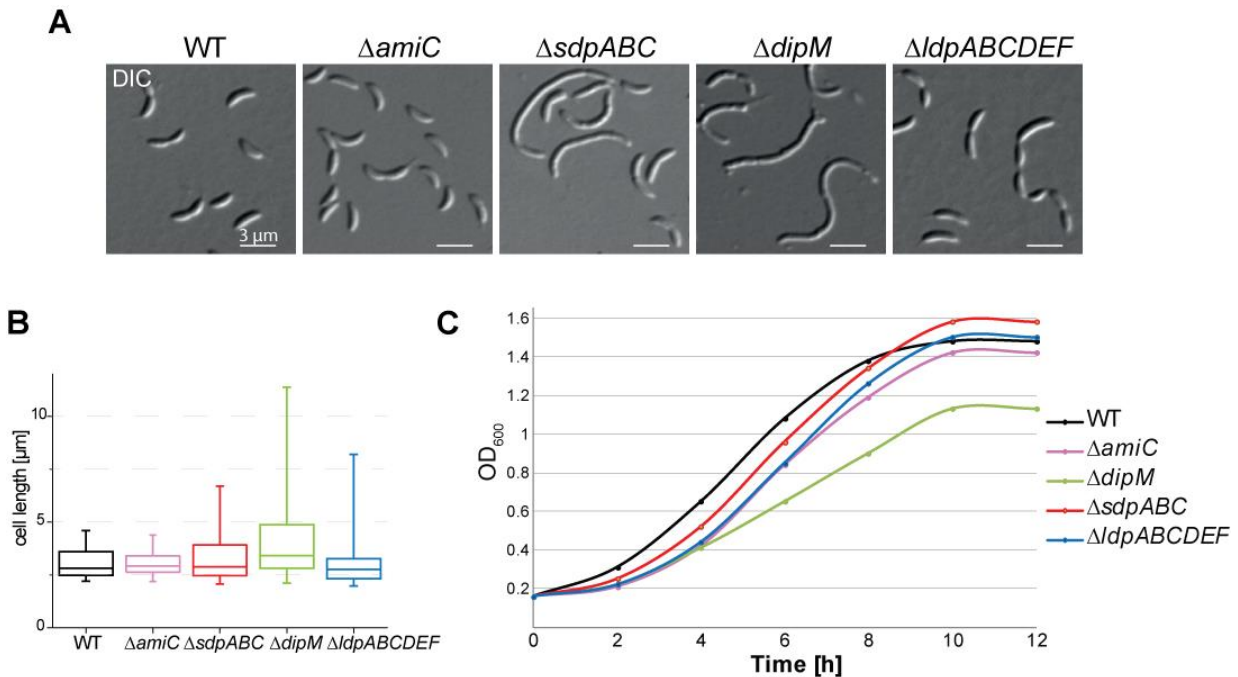
Figure 21. **The set of putative PG hydrolases is highly redundant. (A)** Morphology of deletion strains lacking whole enzymatic families. DIC micrographs of CB15N (WT), AM338 (Δ*amiC*), AM440 (Δ*sdpABC*), MT258 (Δ*dipM*), and AZ52 (Δ*ldpABCDEF*) strains during the exponential phase of growth. Scale bars: 3 μm. **(B)** Statistical analysis of the cell lengths of putative PG hydrolase-deficient strains. The cells described in (B) were analyzed in comparison to the CB15N (WT). Cell body lengths were measured for 150 cells per strain using the MetaMorph program. The results are presented in box plots. Box plots show the median and the interquartile range (box), the 5th and 95th percentile (whiskers), outliers are excluded. **(C)** Growth rate analysis of the PG hydrolase deficient strains described in (A). Cells were grown o/n in rich medium, followed by inoculation into fresh PYE medium and OD_{600} measurements every 2 h for the total period of 12 h. Curves were color-coded in correlation to the box plot diagrams in (B).

The minimal concentrations triggering a response in wild-type cells were established to be 0.3 % sodium chloride and 4 % sucrose (Figure 23AC). Nevertheless, to ensure a phenotypical response of the deletion strains, a higher concentration of 0.47 % sodium chloride was included in the microscopy experiments, which was raised to 0.82 % for growth tests on solid media.

When subjected to salt stress, the Δ*amiC* and Δ*sdpABC* strains did not display significant changes in either morphology or vitality, when compared to the wild-type control (Figure 22DF). Moreover, based on cell length analysis and a comparison of growth rates, the solute seemed to affect the wild-type cells more than any other strain able to grow in tested conditions (Figure 22E). In contrast, vitality of the Δ*ldpABCDEF* was completely abolished in the presence of sodium chloride regardless of the media state (Figure 22F, data not shown). Notably, a higher solute concentration was needed in the solid media, to achieve the same growth inhibition as in liquid medium (Figure 22C).
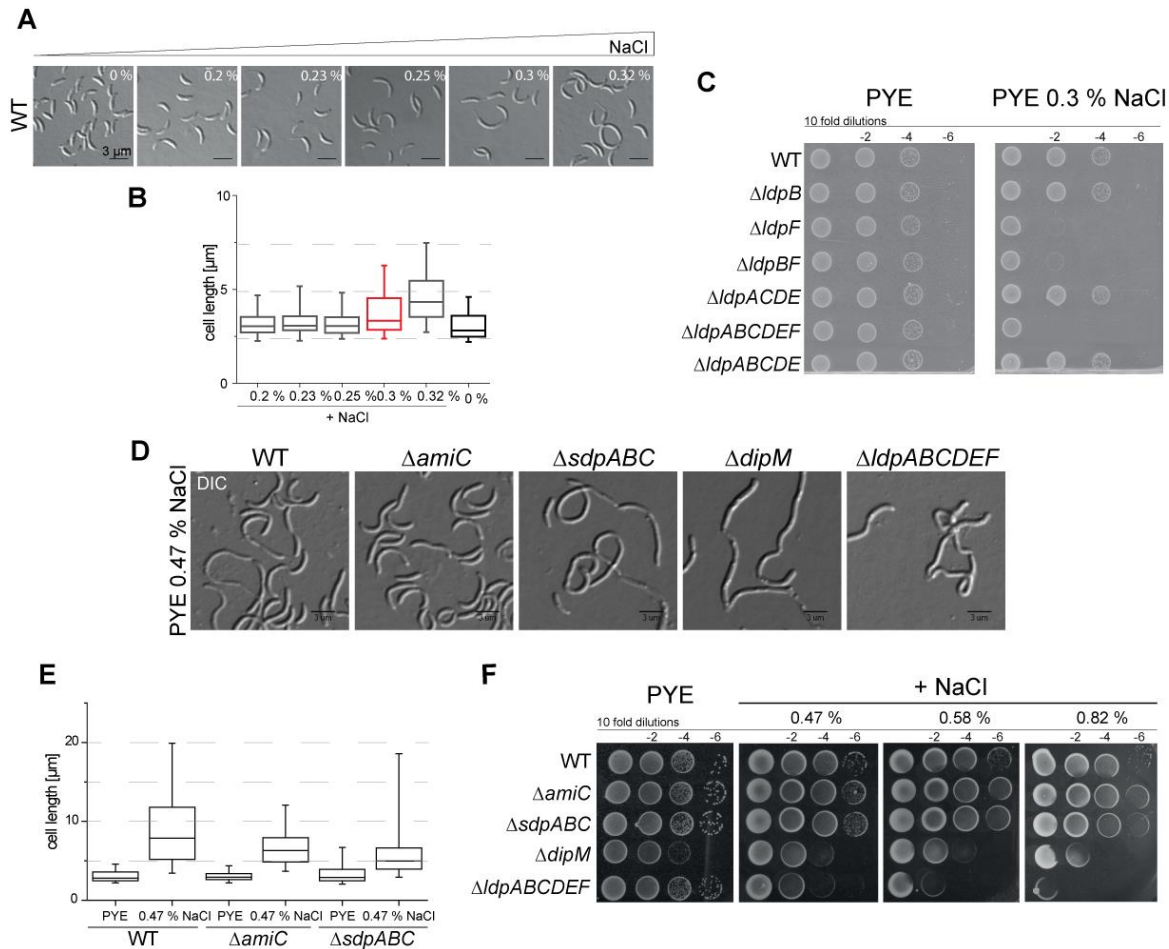
Figure 22**. Increased salinity triggers filamentation and gradual viability loss of DipM- and LdpF-deficient strains. (A)** 0.3 % salinity is a threshold concentration triggering filamentation of the wild-type (WT) strain. WT cells grown in the PYE medium supplemented or not with increased sodium chloride concentrations (0-0.32 %), followed by DIC microscopy after 24 h of incubation. **(B)** Cell length comparison between WT cells grown in the presence of increased concentrations of salt. Cell body lengths from (A) were measured for 150 cells using the MetaMorph program. The results are shown as box plots. Box plots show the median and the interquartile range (box), the 5th and 95th percentile (whiskers), outliers are excluded. **(C)** The viability of strains lacking native *ldpF* is impaired in the presence of 0.3 % sodium chloride. Serial dilutions of wild-type (WT), MT258 (Δ*dipM*), AM365 (Δ*ldpB*), AM369 (Δ*ldpF*), AZ91 (Δ*ldpBF*), AM438 (Δ*ldpABCDE*), AM448 (Δ*ldpABCD*), and AZ52 (Δ*ldpABCDEF*) were spotted on PYE or PYE agar supplemented with 0.3 % NaCl and incubated for 2 days. Performed by Katharina Kremer. **(D)** Filamentation is a common phenotype in the presence of sodium chloride at concentrations higher than 0.3 %. DIC micrographs of the wild-type (WT), AM338 (Δ*amiC*), AM440 (Δ*sdpABC*), MT258 (Δ*dipM*), and AZ52 (Δ*ldpABCDEF*) strains during exponential phase of growth cultivated in the presence of 0.47 % sodium chloride (NaCl) for 24 h. **(E)** Cell length comparison between wild-type (WT), AM338 (Δ*amiC*), and AM440 (Δ*sdpABC*) strains cultivated in PYE medium with and without 0.47 % NaCl addition. Cell body lengths from (D) were measured for 150 cells using the MetaMorph program. The results are shown as box plots. **(F)** Viability effect of 0.47 % sodium chloride in single and multiple in-frame knock outs of autolysins. Serial hundred fold dilutions of the cells described in (D) and of wild-type, were plated on PYE agar and PYE agar supplemented with 0.47 %, 0.58 %, 0.82 % NaCl, and incubated for 2 days.

To test whether the observed halosensitivity was triggered by the absence of all or particular Ldps, single and multiple deletion strains were spotted on media supplemented with salt, followed by comparison of their capacity to form colonies. Interestingly, every tested strain lacking a copy of *ldpF* was hypersensitive towards sodium chloride, which clearly indicates that LdpF, directly or indirectly, modulates osmotolerance in *C. crescentus* (Figure 22C) (Kremer, 2015). The Δ*dipM* strain exhibited moderate halotolerance on solid media, which decreased with increasing salt concentrations.

Furthermore, the presence of a sodium chloride in liquid medium significantly inhibited growth of the strain lacking DipM (Figure 22F, data not shown).
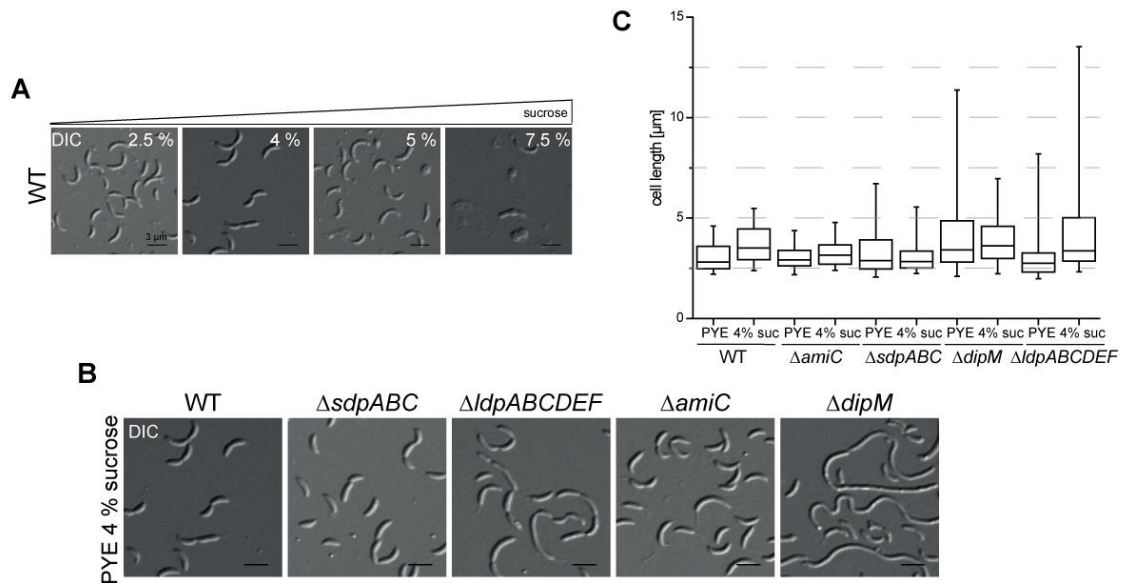
Figure 23. **High osmolality caused by increased sucrose concentration affects morphology of strains lacking LytM factors. (A)** Morphological response of the WT (CB15N) to increased sucrose concentrations in the environment. WT strain was grown in the PYE medium supplemented with increased sucrose concentrations (2.5-7.5 %) following with DIC microscopy after 24 h. **(B)** Sucrose enhances filamentous phenotype of the Δ*ldpABCDEF* and Δ*dipM* strains. DIC micrographs of the wild-type (WT), AM338 (Δ*amiC*), AM440 (Δ*sdpABC*), MT258 (Δ*dipM*), and AZ52 (Δ*ldpABCDEF*) cells during exponential phase of growth cultivated in the presence of 0.4 % sucrose for 24 h. Scale bar: 3 µm. **(C)** Cell length comparison between WT and strains described in (B) cultivated in PYE medium with and without 0.4 % sucrose. Cell body lengths from (B) were measured for 150 cells using the MetaMorph program. The results are shown as box plots. Box plots show the median and the interquartile range (box), the 5th and 95th percentile (whiskers), outliers are excluded.

The influence of increased osmolality, induced by the 4 % sucrose in rich medium was tested, followed by DIC visualization and statistical analysis of the cell lengths. In every case, changes in the doubling rate were observed (data not shown). In addition, elevated amounts of sugar significantly altered the morphology of the Δ*ldpABCDEF* strain, resulting in more frequent filamentation when compared to the standard conditions (Figure 23C). The morphology of the Δ*amiC* strain remained unaffected in the tested conditions. In contrast, the filamentation of the Δ*dipM* and Δ*sdpABC* strains was slightly suppressed by the presence of sucrose, when comparing cell length variation with and without the solute. Notably, the median value did not change for both mentioned deletion mutants (Figure 23B).

Since temperature is a critical physical factor able to dramatically influence the efficiency of enzymes, I asked whether sub-optimal incubation conditions in elevated temperature of 42 °C would affect the physiology of Δ*dipM*, Δ*amiC*, Δ*sdpABC* and Δ*ldpABCDEF* mutated strains. Interestingly, only strains carrying either single (Δ*dipM*) or multiple deletions of genes encoding LytM factors (Δ*ldpABCDEF*) were characterized by a temperature-sensitive phenotype, as manifested by slightly elongated cell bodies (Figure 24 AB). The growth rate of the tested strains was unaffected by elevated temperatures (data not shown).
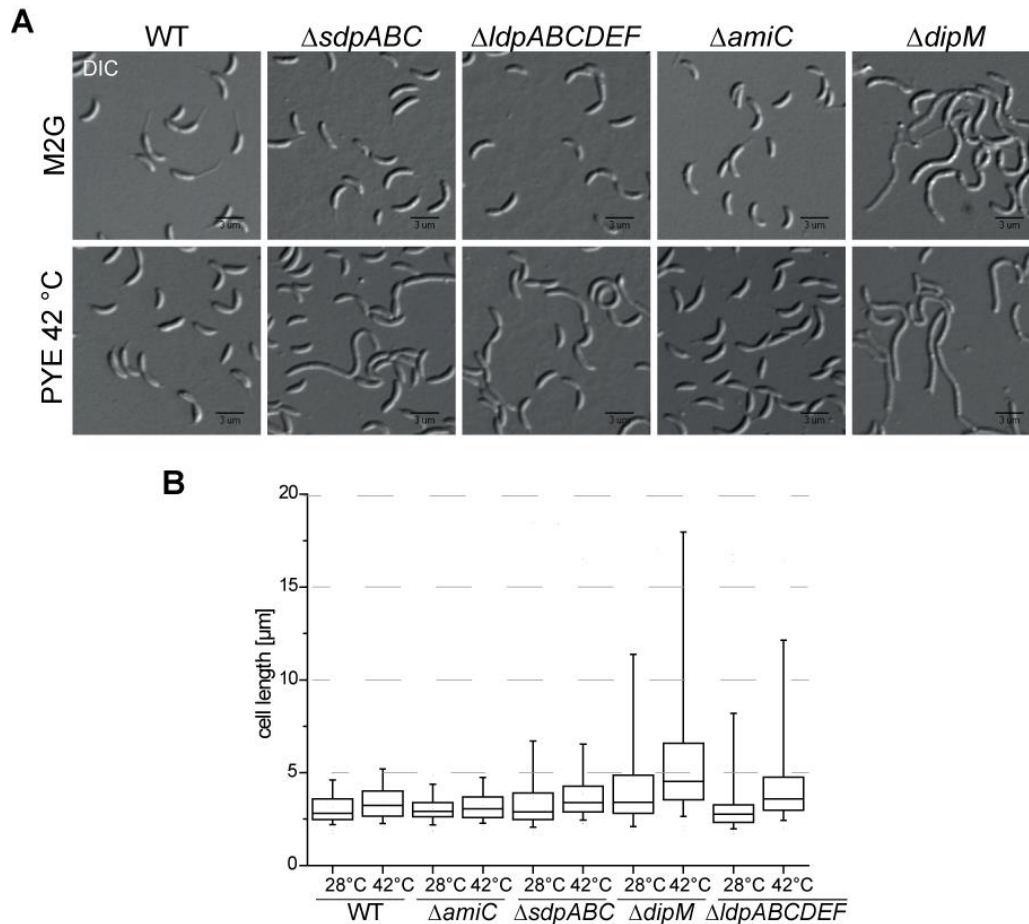
Figure 24. **Elevated temperature prompts significant cell body elongation in the LytM factors-deficient strains. Cultivation in minimal medium (M2G) suppresses the filamentous phenotype of Δ*sdpABC* and enhances filamentation of the Δ*ldpABCDEF* and Δ*dipM* mutants.** **(A)** DIC micrographs of CB15N (WT), AM338 (Δ*amiC*), AM440 (Δ*sdpABC*), MT258 (Δ*dipM*), and AZ52 (Δ*ldpABCDEF*) cells during exponential growth in the minimal medium (M2G) or in PYE at 42 °C for 24 h. (B) Cell length comparison between WT and strains described in (A) cultivated in M2G or the temperature elevated to 42 °C. Cell body lengths were measured for 150 cells using the MetaMorph program. The results are shown as box plots. Box plots show the median and the interquartile range (box), the 5th and 95th percentile (whiskers), outliers are excluded.

The morphological response to nutrients limitation was analyzed by cultivation in minimal M2G medium. Upon starvation, cell division is slowed down and a complete life cycle is extended to 120 minutes. DIC microscopy revealed rather minor effects on the Δ*amiC* and Δ*dipM* strains (Figure 24A). In contrast, Δ*sdpABC* and Δ*ldpABCDEF* cells lost their typical phenotype and reverted to the regular wild-type morphology (Figure 24A).

Taken together, the collected data point to an increased sensitivity of strains carrying in-frame deletion/s of the M23 EPase genes to environmental stresses. Ldps seem to play a crucial role in stress resistance, and they may also specifically contribute to cell division, since their lack triggers filamentation in hyper- and hypo-osmotic conditions.

2.7 Analysis of the cell envelope properties and sites of active PG incorporation

Inactivation of autolysins may not only render morphological abnormalities resulting from division dysfunctions but also directly influence the general properties of the cell envelope. Since the precise role of PG hydrolytic enzymes is not clear yet, the alterations most likely influence primarily the murein but may also affect the properties of the surrounding membrane/s and/or the periplasm.

The absence of hydrolytic activities necessary for growth of murein should theoretically strongly influence the properties and/or architecture of the cell wall. There is a whole spectrum of antibiotics inhibiting various steps in cell wall assembly. For the upcoming experiments, I decided to test sensitivity towards ampicillin. Ampicillin is one of the best-studied antibiotics belonging to β-lactam group, acting as an irreversible cell wall synthesis inhibitor, which covalently modifies the catalytic residue of the TP domain. I speculated that altered murein architecture and/or turnover sensitize towards the antibiotics, since activation of β-lactamases is triggered by 1,6-anhydroMurNAc, a certain type of PG degradation product (Jacobs *et al.*, 1997). I took advantage from the fact that wild-type *C. crescentus* is naturally resistant towards ampicillin due to the presence of β-lactamase (*bla*) genes scattered throughout its chromosome.

To test this hypothesis, the respective hydrolase mutants were cultivated with the presence of ampicillin and analyzed. The threshold level of ampicillin causing strong filamentation was 100 µg/ml, whereas significant growth inhibition was observed at 150 µg/ml (Figure 25AC). Microscopy experiments combined with cell length measurements revealed that inactivation of AmiC and six LytM factors led to no visible morphological or growth defects, when compared to the wild-type (Figure 25AB). A significant deviation in the cell length was observed for Δ*ldpABCDEF* strain when compared to standard conditions without antibiotic (Figure 25B). Inactivation of SLTs and DipM, by contrast resulted in ampicillin-sensitive phenotype, as reflected by complete growth inhibition (Figure 25C). Interestingly, even trace amounts of ampicillin in the media were able to block the proliferation of Δ*dipM* cells (data not shown). To test whether the observed sensitivity of the Δ*sdpABC* mutant results from inactivation of SLTs as a group or from the lack of specific protein, single, double and triple SLT mutants were spotted on media containing antibiotic, followed by comparison of their growth. Every strain lacking *sdpA*, triggered ampicillin sensitivity. This result suggests that SdpA is an important factor keeping endogenous resistance towards β-lactam antibiotics, likely by sustaining the sufficient amount of 1,6-MurNAc moieties triggering PG turnover.

Based on the physiological defects of mutants lacking NlpC/P60 homologues and the hypothesis that these disorders resulted from a dysfunction of cell wall metabolism, I decided to test these mutants for their resilience towards ampicillin. Strains carrying single and multiple NlpC/P60 gene deletions were spotted on a plate with and without antibiotic followed by an analysis of their growth ability. Notably, ampicillin sensitivity was observed for every tested strain, with the exception of the wild-type control and the Δ*nlpB* mutant (Figure 25D).
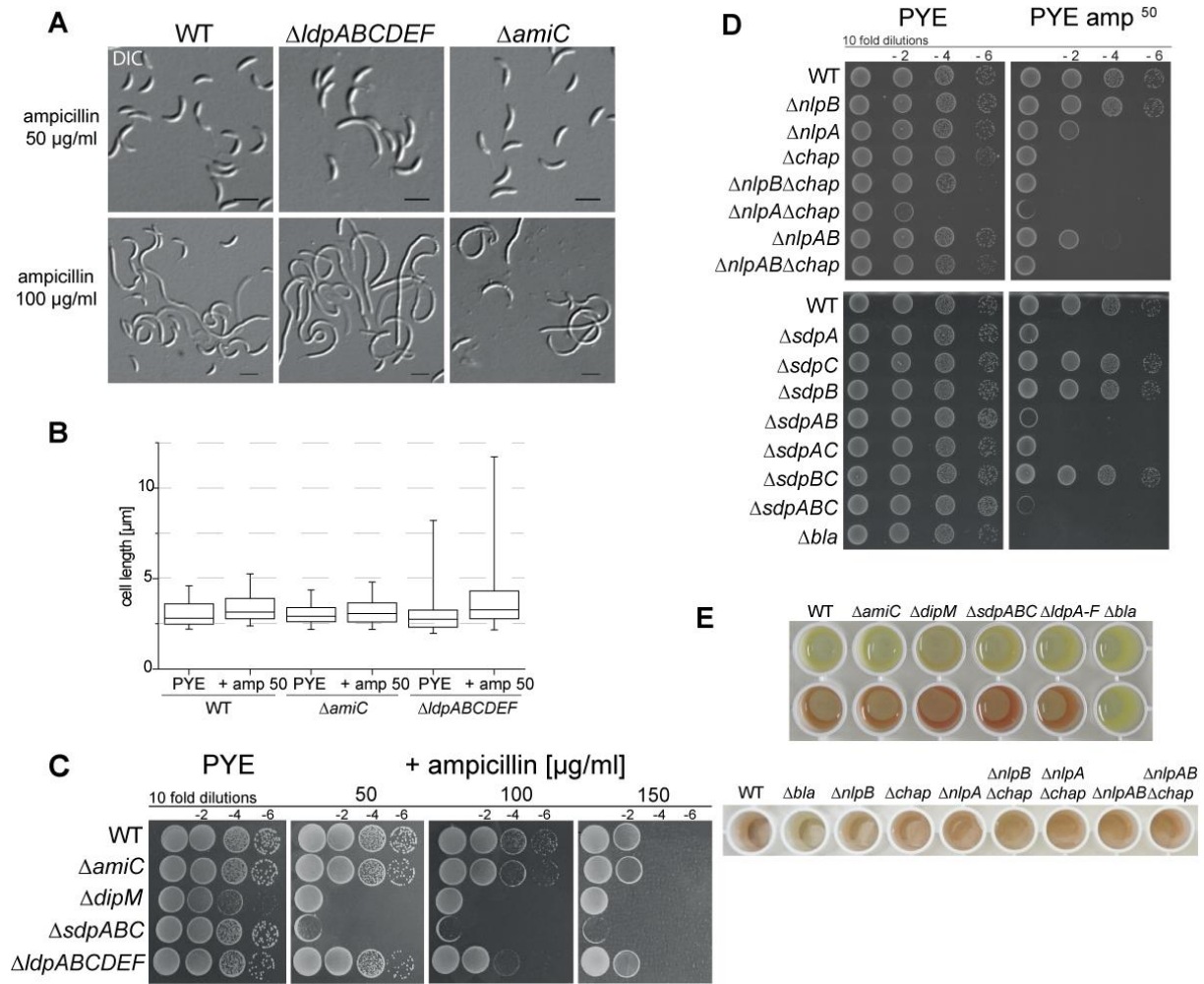
Figure 25. **Cells lacking DipM, SdpA or Chap show an ampicillin-sensitive phenotype.** **(A)** High ampicillin concentration provokes extreme filamentation of *C. crescentus*. DIC micrographs of strains CB15N (WT), AM338 (Δ*amiC*), and AZ52 (Δ*ldpABCDEF*) during exponential phase of growth cultivated in the presence of either 50 μg/ml or 100 μg/ml ampicillin in PYE medium for 24 h. **(B)** Comparison of the cell lengths of the strains from (A) grown with (amp 50) or without (PYE) ampicillin. Cell body lengths were measured for 150 cells using the MetaMorph program. The results are shown in box plots. Box plots show the median and the interquartile range (box), the 5th and 95th percentile (whiskers), outliers are excluded. **(C)** Effect of single and multiple deletions of PG hydrolases on viability in the presence of elevated ampicillin concentrations. Serial hundred-fold dilutions of cells of AM338 (Δ*amiC*), AM440 (Δ*sdpABC*), MT258 (Δ*dipM*), AZ52 (Δ*ldpABCDEF*), and wild-type (WT), were plated on PYE agar and PYE agar supplemented either with 50 μg/ml or 100 μg/ml or 150 μg/ml of ampicillin, and incubated for 2 days. **(D)** Effect of single and multiple NlpC/P60 (upper panel) and SLTs (lower panel) in-frame gene deletions on viability in the presence of 50 μg/ml ampicillin. Serial hundred-fold dilutions of cells CB15N (WT), AZ86 (Δ*chap*), AZ85 (Δ*nlpB*), (Δ*nlpA*), AZ89 (Δ*nlpAB*), AZ121 (Δ*nlpB* Δ*chap*), AZ120 (Δ*nlpA* Δ*chap*), MAB250 (Δ*nlpAB* Δ*chap*), AM399 (Δ*sdpA*), AM400 (Δ*sdpC*), AM418 (Δ*sdpB*), AM419 (Δ*sdpAB*), AZ28 (Δ*sdpAC*), AZ29 (Δ*sdpBC*), AM440 (Δ*sdpABC*), and CS606 (Δ*bla*) were plated on PYE agar and PYE agar ampicillin 50 μg/ml, and incubated for 2 d. **(E)** Single and multiple deletions of PG hydrolases genes do not affect natural β-lactamase activity. Cells of the strains described in (C) and (D) hydrolyze synthetic β-lactamase substrate Nitrocefin, as indicated by a change in color from yellow to red after incubation with the compound. Exponentially growing cells in PYE medium were supplemented with Nitrocefin and incubated for 20 min.

Interestingly, every strain in which Chap was inactivated displayed ampicillin intolerance, implying either an important role in cell wall biogenesis or in the regulation of the expression of the *bla* genes. The most dramatic reaction on antibiotic was observed for Δ*nlpA* Δ*chap* cells, which correlates with their defective morphology and reduced growth rate (Figure 25D, Figure 19CE). Moreover, the

tolerance of the Δ*nlpA* and Δ*nlpAB* strains towards ampicillin was significantly reduced, most likely because of inactivation of NlpA (Figure 25D). These findings suggest that NlpA and Chap are involved either directly or indirectly in the cell wall metabolism.

To clarify the origin of the observed sensitivity, I tested whether the natural β-lactamase activity of *C. crescentus* cells was affected in the mutant cells. To this end, I used the chromogenic cephalosporin Nitrocefin®, a substrate for β-lactamases undergoing a color change, from yellow (λ=390 nm) to red (λ=468 nm) upon hydrolysis. The test revealed β-lactamase activity in every tested sample, excluding the possibility that the increased ampicillin sensitivity of the hydrolase mutants results from the failure to induce β-lactamase gene expression (Figure 25E). Therefore, more experiments need to be performed to clarify origin of observed results.

Disruption of the murein biosynthesis equilibrium between synthetic and hydrolytic events may lead to lesions in its thickness and ultimately to the abnormal periplasm architecture, as it was shown for the Δ*dipM* mutant (Goley *et al.*, 2010a; Möll *et al.*, 2010). To test whether the inactivation of other PG hydrolases affects width of the periplasmic space, I labeled the PG hydrolase deficient cells with red fluorescent protein tdimer2 exported to the periplasm via the *E. coli* TorA, Tat signal sequence (Judd *et al.*, 2005).
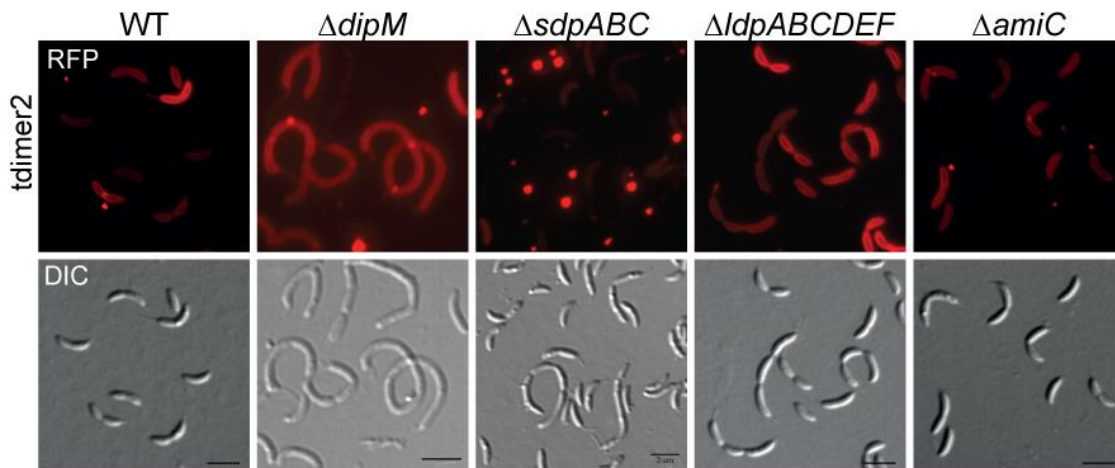
Figure 26. **The architecture of the periplasm is altered upon SLTs and DipM deactivation.** The strains AZ96 (CB15N pP*xyl*-*tdimer2*), AZ57 (Δ*sdpABC* pP*xyl*-*tdimer2*), AZ97 (Δ*amiC* pP*xyl*-*tdimer2*), and AZ98 (Δ*ldpABCDEF* pP*xyl*-*tdimer2*) were grown in PYE to exponential phase and induced with the 0.3 % xylose for 2 h, followed by DIC and fluorescence microscopy. Bar 3 μm.

Fluorescence microscopy analysis of the Δ*amiC* and Δ*ldpABCDEF* mutants transformed with a plasmid encoding *torA*$_{ss}$-*tdimer2* revealed a wild-type localization pattern, with no visible swelling or narrowing of the periplasm (Figure 26). The Δ*sdpABC* mutant was characterized by OM vesicle formation, as described in section 2.2.1, whereas the strain lacking functional copy of *dipM* formed bright foci at the division sites, which have been reported to feature an enlarged periplasmic space (Moll *et al.*, 2010). Notably, the intensity of the blebbing varied significantly between the Δ*sdpABC* and Δ*dipM*, as shown in Figure 26.

Cell wall biosynthesis relies on constant cooperation between PG synthases and hydrolases, likely clustering into multienzyme complex/es assembled and orchestrated in a cell-cycle dependent manner. Therefore, I asked whether PG synthesis is altered in strains with inactivated murein hydrolases. To test this prediction, the cells were stained with the fluorescent D-Ala analogue, HADA (hydroxycoumarin-carbonyl-amino-D-alanine), which is incorporated into the lipid II precursor (Kuru *et al.*, 2012; Siegrist *et al.*, 2013). Thus, HADA labeling coupled with fluorescence microscopy selectively highlights sites of ongoing PG synthesis.
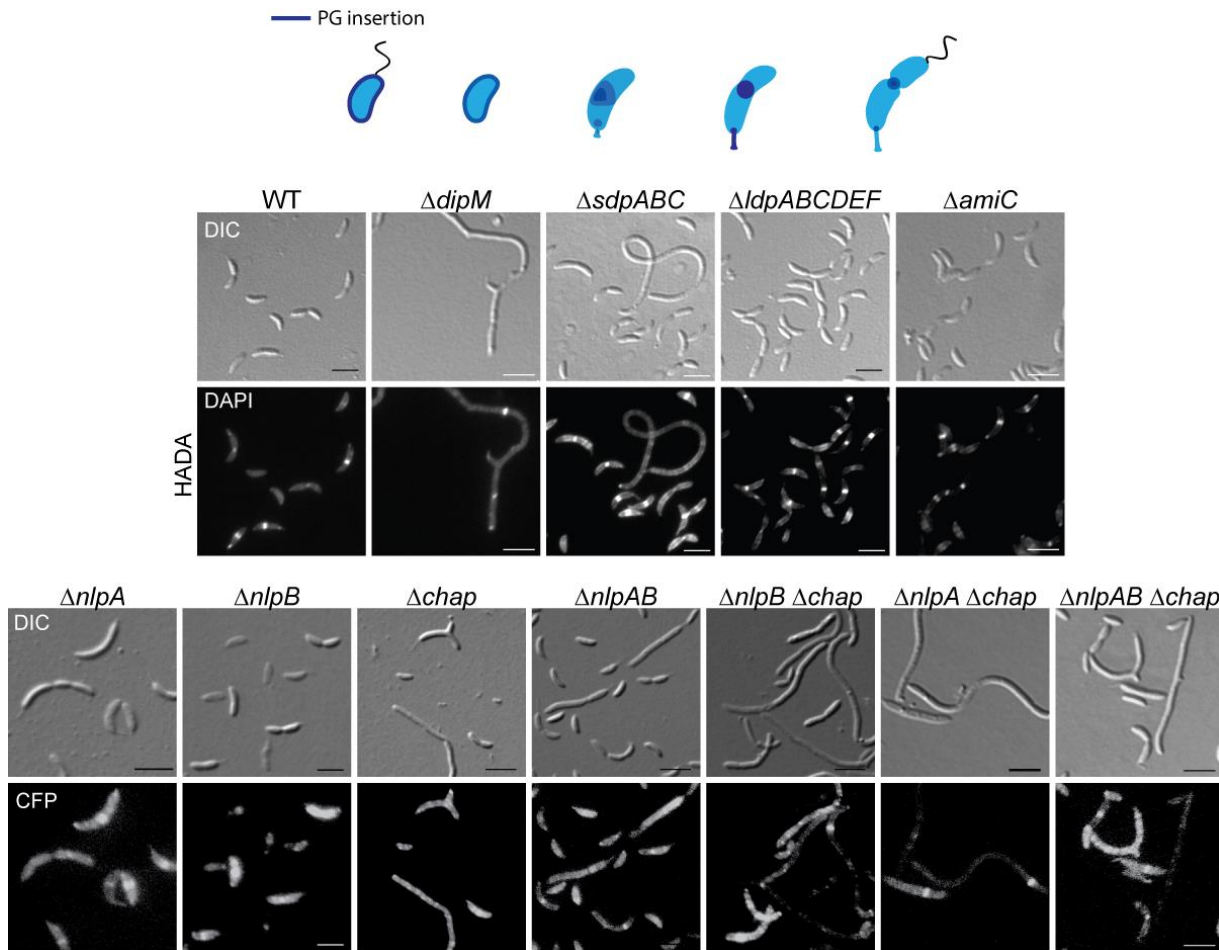
Figure 27. **Active sites of PG insertion are ectopically distributed in the filamentous cells.** Graphical representation of sites of active PG incorporation (blue line or dot) over the course of the cell cycle in wild-type *C. crescentus* (upper panel). Exponentially growing cells from the strains CB15N (WT), AM338 (Δ*amiC*), AM440 (Δ*sdpABC*), MT258 (Δ*dipM*), AZ52 (Δ*ldpABCDEF*), AZ86 (Δ*chap*), AZ85 (Δ*nlpB*), AZ167 (Δ*nlpA*), AZ89 (Δ*nlpAB*), AZ121 (Δ*nlpB* Δ*chap*), AZ120 (Δ*nlpA* Δ*chap*), and MAB250 (Δ*nlpAB* Δ*chap*) were incubated with HADA, followed by fixation in ethanol and fluorescence microscopy. Scale bars: 3 μm.

As expected, pulse-labeling of the wild-type cells yielded a pattern of most intensive PG synthesis at the midcell in predivisional cells, along with the additional, smaller focus at the stalked pole, appearing upon initiation of the stalk synthesis. The swarmer cells yielded mostly diffused, cytoplasmic signal with more intense circumferential zones (Figure 27, upper panel). The chaining phenotype of Δ*ldpABCDEF* cells did not prevent assembly of active zones of PG incorporation, and the fluorescent foci were clearly visible (Figure 27). The same was true for *amiC* and *nlpB* mutant, suggesting that in

both cases the PG biosynthetic clusters were regulary formed. The populations of the Δ*sdpABC*, Δ*dipM*, Δ*nlpA*, and Δ*nlpAB* mutants were composed of two morphologically different types of cells, with wild type-like and filamentous morphology. The latter ones showed mostly multiple, irregularly distributed fluorescent zones with a variable intensity. Distinct foci were formed within the filaments of the Δ*dipM* and Δ*nlpA*Δ*chap*, whereas inactivation of SLTs led to more dispersed and less dense foci formation (Figure 27). Interestingly, the inactivation of Chap seemed to prevent formation of the distinct murein growth zones in the cells with branched morphology.

In sum, I provided several lines of evidence that inhibition of the putative cell wall hydrolases may promote changes in the cell wall structure that lead to its weakening/modification, thereby sensitizing cells towards β-lactam antibiotics. In particular, the absence of SdpA, DipM and Chap triggered ampicillin intolerance. The mutations did not cause a down-regulation of β-lactamase activity, which leaves the mechanistic basis for this effect unknown. Fluorescent labeling of the periplasm revealed no changes in its architecture, except for the Δ*sdpABC* and Δ*dipM* strains, which both shed OM vesicles, with the Δ*dipM* strain additionally showing a widening of the periplasm at the division sites. The assembly of the PG biosynthesis complex was intact in the absence of AmiC, NlpB and LytM factors, and delocalized in elongated cells suffering from the loss of DipM, SLTs and NlpA. Inactivation of SdpA-C and Chap led to mostly diffused, irregular signal suggesting that these proteins are necessary to maintain correct architecture of the PG biosynthetic clusters. In contrast, cells lacking DipM and NlpA were able to form distict zones of active PG incorporation within the cells yielding elongated morphology.

2.7.1 DipM is active in a pathway independent of any other PG hydrolase

Functional characterization of non-essential proteins is not easy due to the absence of a phenotype under normal and often harsh growth conditions. In the previous chapters, I provided data, which give an idea about the function of the autolysins homologues. However, they did not shed light onto the regulatory mechanism that controls them. Until now, I was generating deletion mutants within particular enzyme family, theoretically depriving the cells of a certain activity. To gain insight into the functional dependency between studied enzymes, I decided to generate mutant strains lacking more than one enzyme family, to identify further redundancies and learn about regulatory interactions.

2.7.1.1 DipM does not regulate amidase activity in C. *crescentus*

The first question I aimed to answer was whether DipM regulates amidase activity in *C. crescentus*. This idea was based on the fact that it lacks catalytic activity and on recent findings on the role of catalytically inactive LytM factors in other bacteria. Studies in *E. coli* revealed a regulatory pathway in which amidases and LytM factors cooperate with FtsEX to trigger septation by stimulating amidase activity (Yang *et al.*, 2012a). Interestingly, BLAST analysis revealed that DipM has 34 % similarity to NlpD, which is an inactive LytM factor regulating the activity of AmiC in *E. coli* (Yang *et al.*, 2011; Yang *et al.*, 2012a). The deletion strains Δ*amiC* and Δ*dipM* resulted in different phenotypes, thus it is

unlikely that DipM is simply the activator of amidase. To test a functional interaction between DipM and AmiC, I performed epistasis experiment, where a double Δ*amiC* Δ*dipM* mutant was generated and examined microscopically to assess morphological consequences. Surprisingly, the cells lacking both DipM and AmiC did not resemble the phenotype of Δ*dipM* but rather the wild-type cells (Figure 28C).
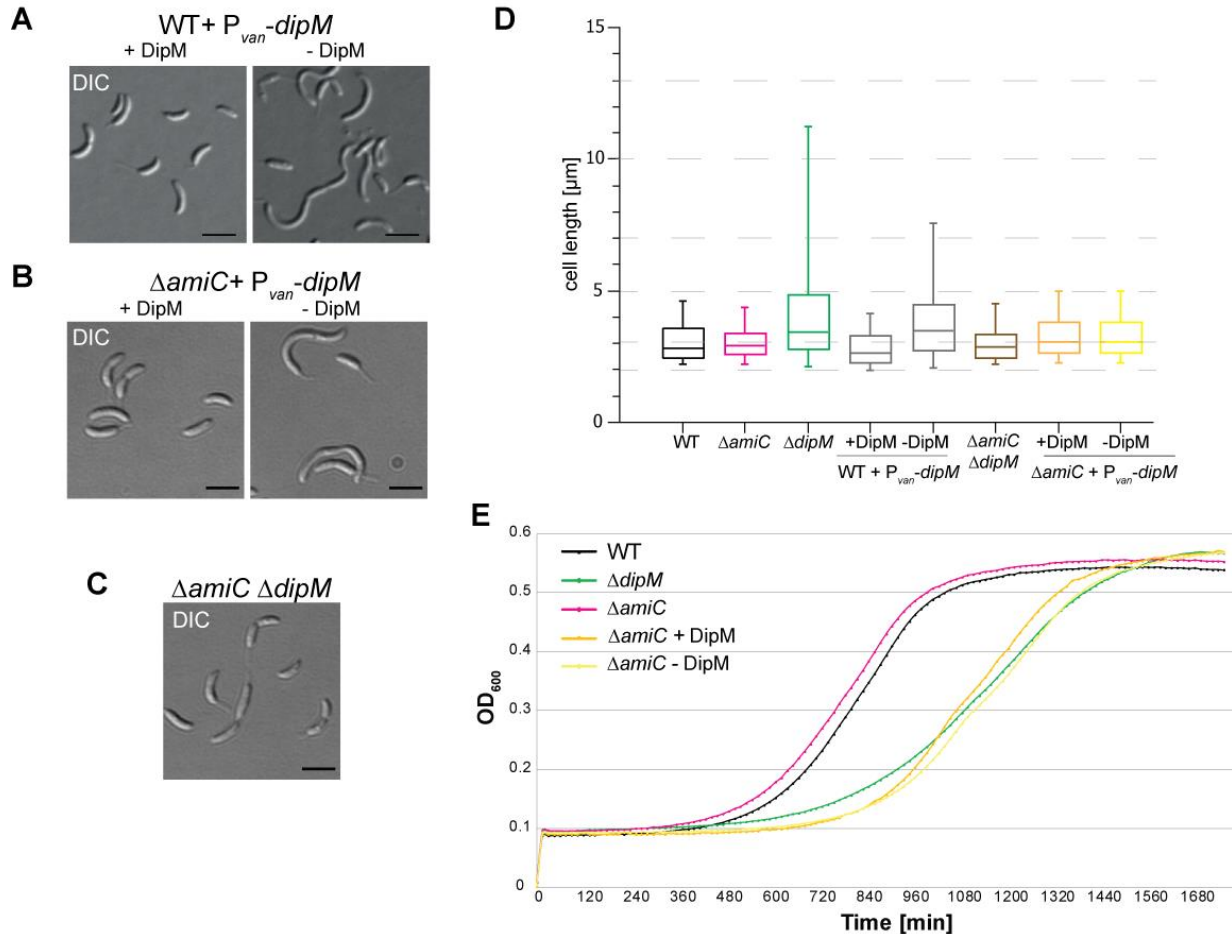
Figure 28. **AmiC and DipM are active in independent pathways.** Morphology of the wild-type (WT) **(A)** or Δ*amiC* strain with or without DipM depletion **(B)** or with *dipM* deletion **(C)**. DIC micrographs of the strains AZ35 (CB15N P$_{dipM}$::P$_{van}$-*dipM*), AZ39 (Δ*amiC* Δ*dipM*), and AZ38 (Δ*amiC* P$_{dipM}$::P$_{van}$-*dipM*) during exponential phase of growth in either PYE medium or PYE supplemented with 0.5 mM vanillate. To induce DipM depletion, the cells were washed and incubated for 22 h in the absence of inducer. Scale bars: 3μm. **(D)** Effects of DipM depletion in Δ*amiC* background on the cell length. Strains CB15N (WT), AM338 (Δ*amiC*), MT258 (Δ*dipM*), and AZ39 (Δ*amiC* Δ*dipM*) were grown to exponential phase in PYE medium. In addition, strains AZ35 (CB15N P$_{dipM}$::P$_{van}$-*dipM*) and AZ38 (Δ*amiC* P$_{dipM}$::P$_{van}$-*dipM*) were grown in the same conditions in media containing 0.5 mM vanillate. Cell body lengths were measured for 150 cells per strain using the MetaMorph program and visualized in box plots. Box plots show the median and the interquartile range (box), and the 5th and 95th percentile (whiskers), outliers are excluded. **(E)** Growth capacity of the strains described in (D). Cells were grown o/n in rich medium supplemented with inducer if necessary, followed by inoculation into fresh PYE medium and OD$_{600}$ measurements every 15 min for a total period of 31 h. Curves were color coded in correlation to the box plot diagrams in (C).

To exclude the possibility that last observation was caused by the presence of spontaneous suppressor mutation, I decided to construct a DipM depletion strain in the Δ*amiC* background. To this end, *dipM* was exchanged at its native locus for a vanillate-inducible version. Microscopic and cell length measurements revealed the presence of elongated cells as typical upon loss of DipM albeit, in a significantly lower fraction of the cell population (Figure 28BD). Additionally, characteristic, aberrantly localized stalk was observed in a frequent manner. Next, I analyzed the proliferation capacity by cultivating the strains in liquid media with or without the inducer and monitoring growth for a total period of 31 hours. Interestingly, concurrent DipM depletion did not affect the doubling time of the Δ*amiC* mutant, suggesting either incomplete depletion or compensatory effects Figure 28E). Although the mechanistic basis of the observed effects remains unclear, *dipM* does not appear epistatic to *amiC*. Therefore, I conclude that there is no functional dependency between AmiC and DipM of *C. crescentus*.

Since DipM does not regulate AmiC, I wondered whether it regulates any other group of autolysins in *C. crescentus*. To test this idea, I created a library of single and multiple deletions of LytM factor and SLT genes and then combined with DipM depletion, since an in-frame *dipM* deletion was impossible to obtain in the respective backgrounds. DipM depletion constructs were carrying a short vanillate promoter fragment upstream of an N-terminal part of the *dipM* gene, introduced via single homologous integration. In this way, the native *dipM* gene was truncated and exchanged for a version fused with a vanillate promoter (P$_{van}$). The resulting strains were characterized first microscopically by comparing the morphology of the cells before and after the depletion of DipM. A decrease in the DipM levels resulted in synthetic lethality in the Δ*ldpABCDEF* and Δ*sdpABC* genetic backgrounds, since the proliferation of cell population ceased after several hours of depletion (Figure 29F). Subsequent microscopy experiments illustrated the variety of defects that result from the absence of particular hydrolytic enyzmes (Figure 30A).

The Δ*sdpABC* mutant depleted of DipM, developed rather smooth filaments reaching up to 57 μm, accompanied by the loss of stalks and progressive lysis (Figure 29BC). DIC microscopy indicated that after 22 hours of DipM depletion almost all cells were severely damaged, since they were not motile and secondly, mostly showed large membrane extrusions indicating considerable envelope defects (Figure 30A). Similarly, the Δ*ldpABCDEF* deletions coupled with DipM depletion resulted in massive filamentation, with the cells elongating up to 65 μm, and visible lysis (Figure 29AC). The culture frequently contained elongated compartments or mini cells and cells with stalk deformations (Figure 30A). Notably, the strain did not show any motility when cultivated in non-permissive conditions, when observed under the light microscope, suggesting that by this time they were metabolically compromised (data not shown).
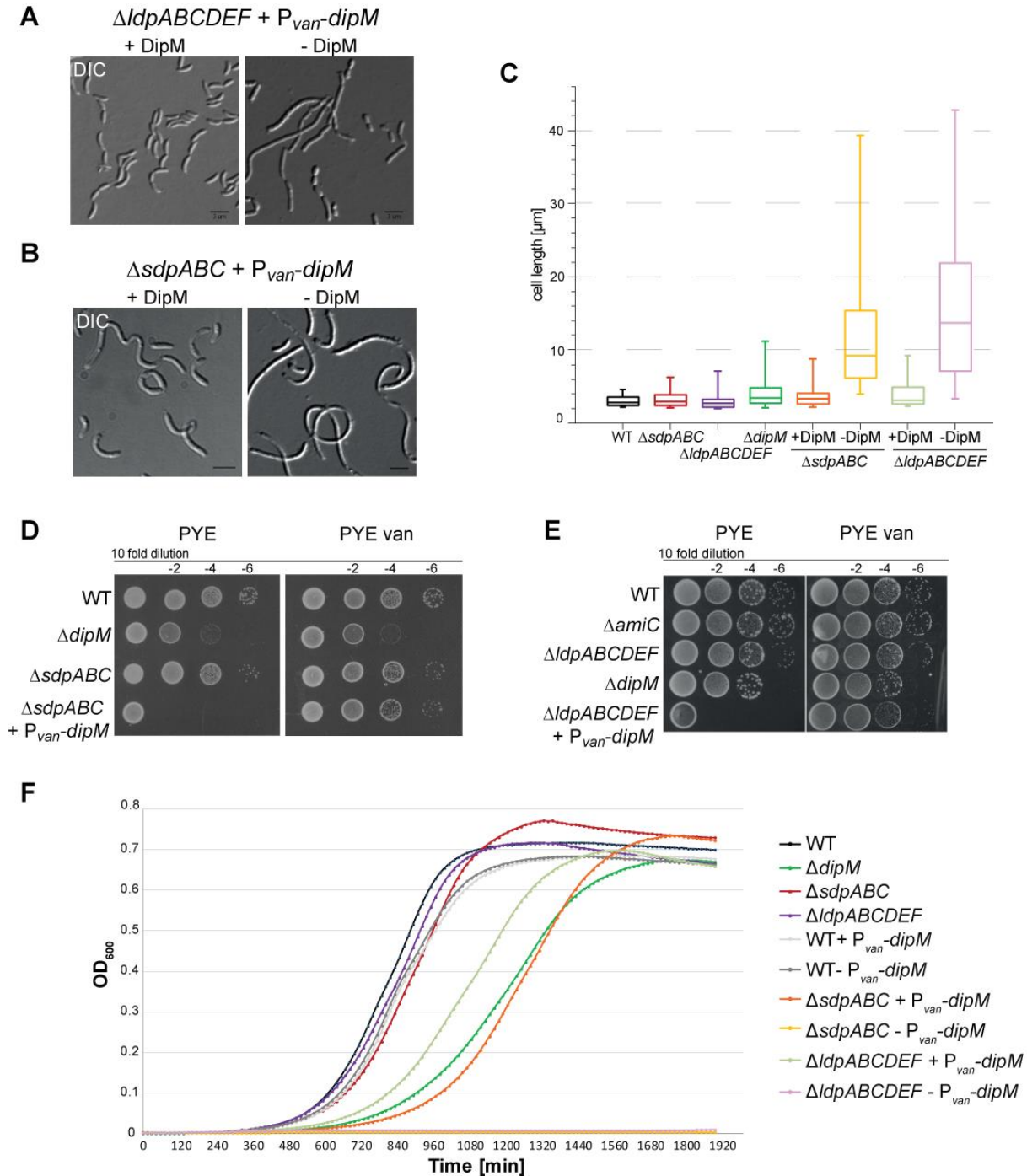
Figure 29. **Inactivation of SLTs and LytM factors coupled with DipM depletion is synthetically lethal. (A, B)** Block in the cell division in Ldps- (A) or SLT- (B) deficient strains when depleted of DipM. DIC micrographs of strains AZ65 (Δ*ldpABCDEF* P$_{dipM}$::P$_{van}$-*dipM*) and AZ41 (Δ*sdpABC* P$_{dipM}$::P$_{van}$-*dipM*). The strains were grown to exponential phase in PYE medium supplemented with 0.5 mM vanillate. Next, the cells were washed and depleted of DipM by incubation for 22 h in the absence of inducer, followed by DIC microscopy. Scale bars 3 μm. **(C)** Synthetic effects on cell lengths. Statistical evaluation of cell lengths of the strains analyzed in (D) and (E) in relation to WT (CB15N). Strains CB15N (WT), AM338 (Δ*amiC*), AZ21 (Δ*sdpABC*), MT258 (Δ*dipM*), AZ52 (Δ*ldpABCDEF*), AZ65 (Δ*ldpABCDEF* P$_{dipM}$::P$_{van}$-*dipM*) and AZ41 (Δ*sdpABC* P$_{dipM}$::P$_{van}$-*dipM*) were grown in PYE to exponential phase and/or analyzed for their cell lenghts before and after 22 h of DipM depletion. Cell body lengths were measured for 150 cells per strain using the MetaMorph program and visualized as box plots. Box plots show the median and the interquartile range (box), and the 5th and 95th percentile (whiskers), outliers are excluded. **(D, E)** Growth comparison of the strains depicted in (A) and (B). Serial hundred-fold dilutions of cells described in (C) and CB15N (WT) were plated on PYE agar and PYE agar supplemented with 0.5 mM vanillate, and incubated for 2 d. **(F)**

Proliferation of the Δ*ldpABCDEF* and Δ*sdpABC* cells deprived of DipM is completely inhibited. Cells of the strains described in (C) were grown o/n in rich medium supplemented with inducer if necessary, and transferred into fresh PYE medium. Growth was monitored by measuring the OD_{600} every 15 min for the total period of 31 h. Curves are color-coded to correlate with the box plots diagrams in (C).

To assess the extent to which DipM depletion affects the vitality of the strains additionally carrying the multiple Ldps- and SLTs- deletions, I tested their proliferation ability in liquid and on solid media. The results clearly indicated growth inhibition on solid media without inducer, revealing DipM as critical for survival in the two mutant backgrounds (Figure 29DE). By contrast, growth of the depletion strains was restored in the permissive conditions. These results were supported by real-time growth assays acquired with an automated plate reader system in liquid media. The growth curves showed complete proliferation inhibition of the conditional mutants in non-permissive conditions (Figure 29F).
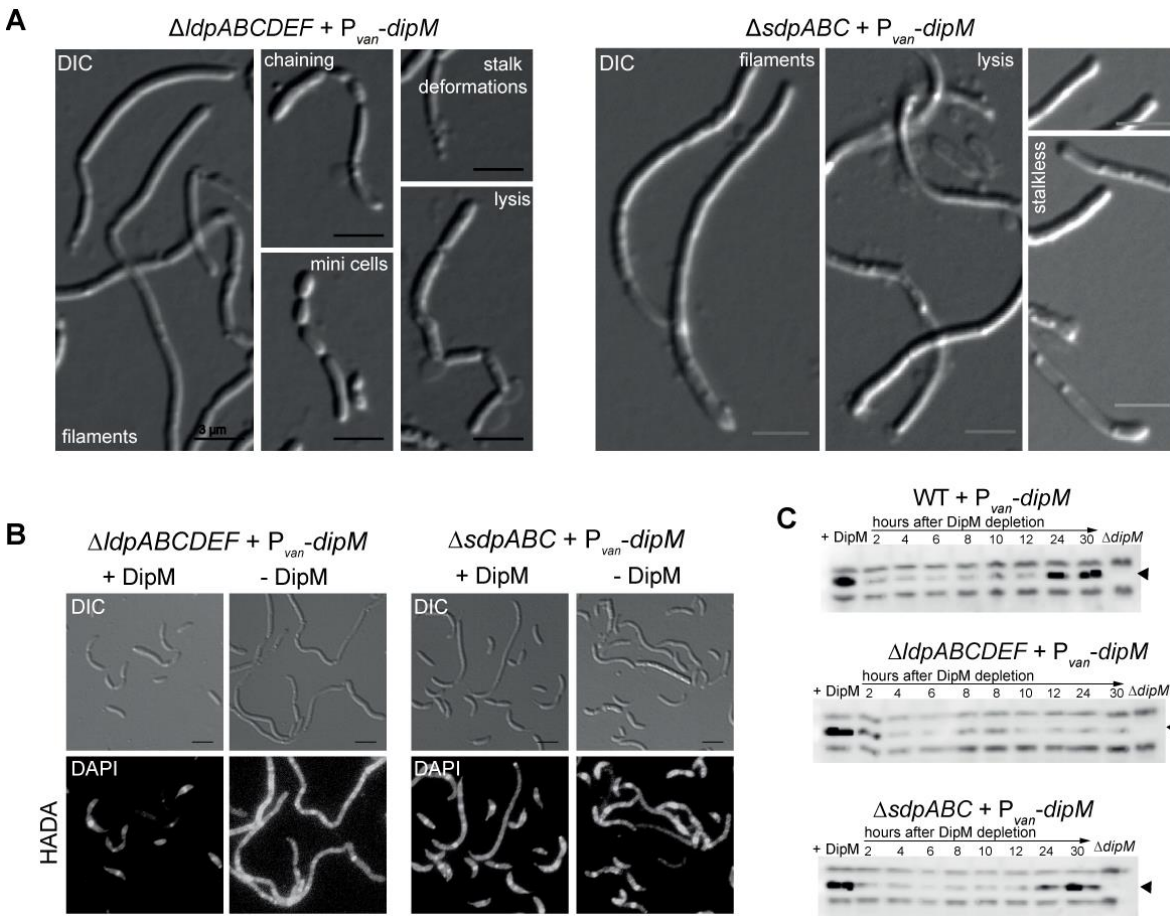
Figure 30. **Synthetically lethal strains display variable morphologies. (A)** DIC micrographs of strains AZ65 (Δ*ldpABCDEF* P$_{dipM}$::P$_{van}$-*dipM*) and AZ41 (Δ*sdpABC* P$_{dipM}$::P$_{van}$-*dipM*). Cells were grown to exponential phase in PYE medium supplemented with 0.5 mM vanillate. Next, cultures were washed and depleted of DipM by incubation for 22 h in the absence of inducer, followed by DIC microscopy. **(B)** Labeling of PG incorporation active sites. Cells from (A) were incubated with HADA, followed with fixation in ethanol, DIC and fluorescence microscopy. Scale bar 3 µm. **(C)** DipM levels in the strains from (A) in comparison to that in AZ35 (CB15N P$_{dipM}$::P$_{van}$-*dipM*). Samples were taken at 2 h intervals for a total period of 30 h and analyzed by immunoblotting using anti-DipM antiserum. Arrowhead indicates molecular weight corresponding to DipM.

The effect caused by DipM depletion was observed immediately in Δ*sdpABC* cells, as the population hardly show any increase in cell density, indicating complete block in cell division (yellow line,

Figure 29F). Similarly, the cells with depleted DipM in Δ*ldpABCDEF* background stop dividing after the first few rounds of duplication (pale purple line, Figure 29F).

To clarify the positioning of the cell wall biosynthetic complexes in both synthetically lethal strains, before and after DipM depletion, staining with HADA (described in section 2.7), was performed. As expected, in both cases, upon depletion of DipM the fluorescent clusters indicating ongoing PG synthesis were spread along the filaments, forming rather randomly distributed zones with higher intensity than distinct foci (Figure 30B). Therefore, observed synthetic lethality was likely triggered by the dysfunction of the cell wall biosynthetic machinery.

To determine whether the observed changes in the physiology of the cells were indeed caused by the gradual loss of DipM, the depletion efficiency was tested of both Δ*ldpABCDEF* and Δ*sdpABC* deletion backgrounds (Figure 30C). Lysates for Western blot analysis were collected over the course of DipM depletion and probed with anti-DipM antiserum. A progressive loss of DipM was detected for up to six hours after transfer into non-permissive conditions in every tested strain. However, in the wild-type and the Δ*sdpABC* background pointed out re-accumulation of DipM was observed after 24 hours of depletion (Figure 30C). It is likely that this increase is caused by the leakiness of the vanillate promoter combined with the cessation of growth, which slows down dilution of the cytoplasm. Leaky expression of *dipM* under the control of P$_{van}$ is additionally supported by microscopy experiments, which showed that depletion in the wild-type background still yields a cell population with largely normal morphology, suggesting presence of DipM (Figure 28A).
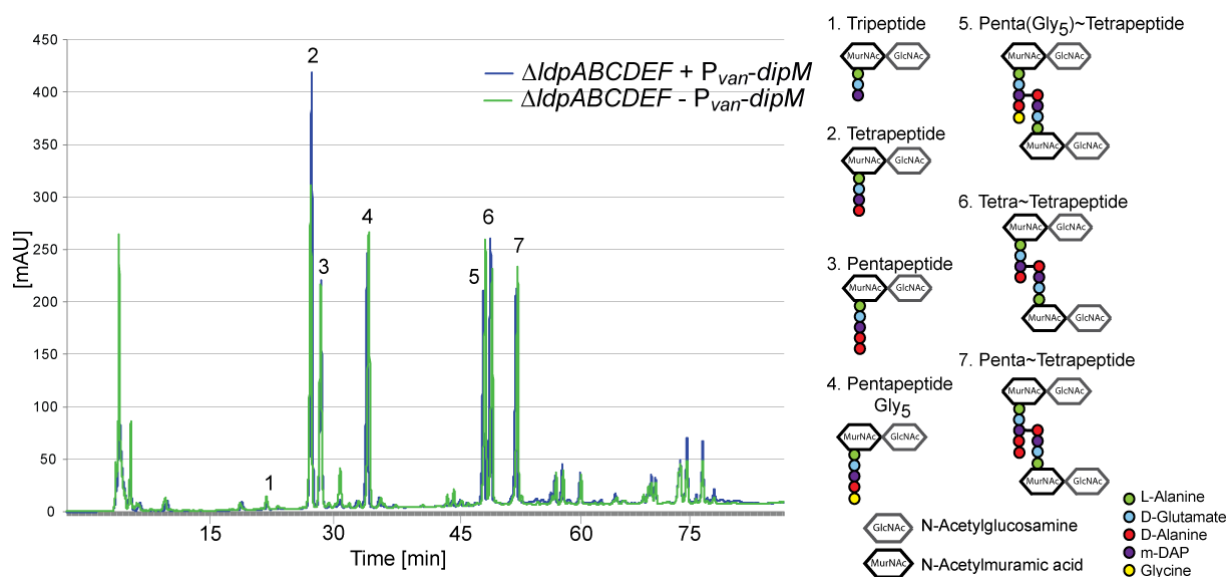
Figure 31. **Absence of LytMs factors affects cell wall architecture.** Overlay of HPLC profiles of muropeptides obtained from AZ65 (Δ*ldpABCDEF* P$_{dipM}$::P$_{van}$-dipM) before (blue track) and after (green track) 20 h of DipM depletion. The strain was grown in minimal medium (M2G) with and without vanillate to an OD$_{600}$ of 0.7. After lyophilization of the cells, cell walls were isolated (5-10 µg) and digested with muramidase. The resulting PG fragments were chromatographically separated and quantified. Their identity was determined by mass spectrometry (ESI – MS/MS). The numbers above the peaks are given on the right side, along with a graphical representations of the respective muropeptides.

Cell wall analysis performed for Δ*ldpABCDEF* cells revealed no dramatic changes when compared to the wild-type (described in section 2.4.2). Intrigued by the cumulative effect caused by depletion of

DipM in the the Δ*ldpABCDEF* background, I also analyzed cell wall composition. In DipM-depleted conditions, a shift in the fraction of terta-muropeptide was clearly noted (peak 2, Figure 31). Surprisingly, the other fraction did not differ significantly between permissive and non-permissive conditions (Figure 31). Furthermore, the decreased amount of tetra-peptides suggests that DipM may positively regulate the activity of a so-far unidentified DD-CPase, trimming the tetra-penta to tetra-tetra peptides.

Taken together, analysis of the phenotypes of the mutated strains demonstrated that DipM does not regulate the activity of neither SLTs nor LytM factors, resulting instead in synthetically lethal combinations. Most importantly, the collected data indicate that DipM acts in an alternative hydrolytic pathway. Moreover, the cell wall analysis of DipM depleted Δ*ldpABCDEF* cells, suggests CP-ase deficiency in non-permissive conditions. The active complexes of PG synthesis seemed to partially assemble at the most likely random positions, suggesting functional defects. The data from this chapter support the initial observation of functional redundancy of Ldps and collectively, robustness of the PG remodeling system of *C. crescentus*.

2.7.2   LdpF as a crucial component of the remodeling apparatus

Intrigued by the synthetic lethality caused by the absence of all seven LytM factors, I decided to determine whether the observed result was caused by the absence of all Ldps or rather a particular representative of this protein family. To this end, I tested the effect of DipM depletion in cells lacking one or more putatively active or inactive Ldps (Figure 32A). Specifically, I exchanged the native *dipM* gene for a vanillate-inducible allele in the Δ*ldpACDE* and Δ*ldpBF* backgrounds. Microscopic analysis showed that the morphology of the Δ*ldpACDE* mutant was greatly changed when depleted of DipM, as it formed elongated or shortened cells accompanied by progressing cell lysis (Figure 32BCE). In contrast, Δ*ldpBF* cells depleted of DipM formed multicompartmentalized cells connected often with elongated, thin protrusions characteristic for cell division defects at the separation stage (Figure 32BC). Moreover, stalk deformations such as thickening, and irregular or no outgrowth as well as cell lysis were noticed, indicating cell envelope disorganization (Figure 32B).

Notably, filamentation was often entailed with poor viability. To assess the extent to which the depletion of DipM affects the Δ*ldpACDE* and Δ*ldpBF* mutants, the growth experiments were performed on solid and in liquid media (Figure 32DF). On solid media supplemented with the inducer, the efficiency of colony formation of both tested strains was comparable to the wild type (Figure 32D). As expected, the extensive filamentation of Δ*ldpBF* strain depleted of DipM, correlated with the extent of growth inhibition (Figure 32D). Similar results were obtained for the DipM-depleted Δ*ldpACDE* mutant, although the inhibitory effect was less pronounced (Figure 32D). To confirm the obtained results, the growth in liquid media was monitored in real-time with automated plate reader. Analyses of the growth rates of both tested strains, revealed an evidently reduced growth rate of the cells with inactivated LdpB, LdpF and DipM*,* when compared to other tested strains (Figure 32F). DipM depletion combined with LdpACDE deletions caused slow growth phenotype, similar to the one of the

Δ*dipM* strain (Figure 32F). However, in contrast to the Δ*ldpBF* mutant, the Δ*ldpACDE* cells depleted of DipM were able to reach the stationary phase within the timeframe of the experiment.
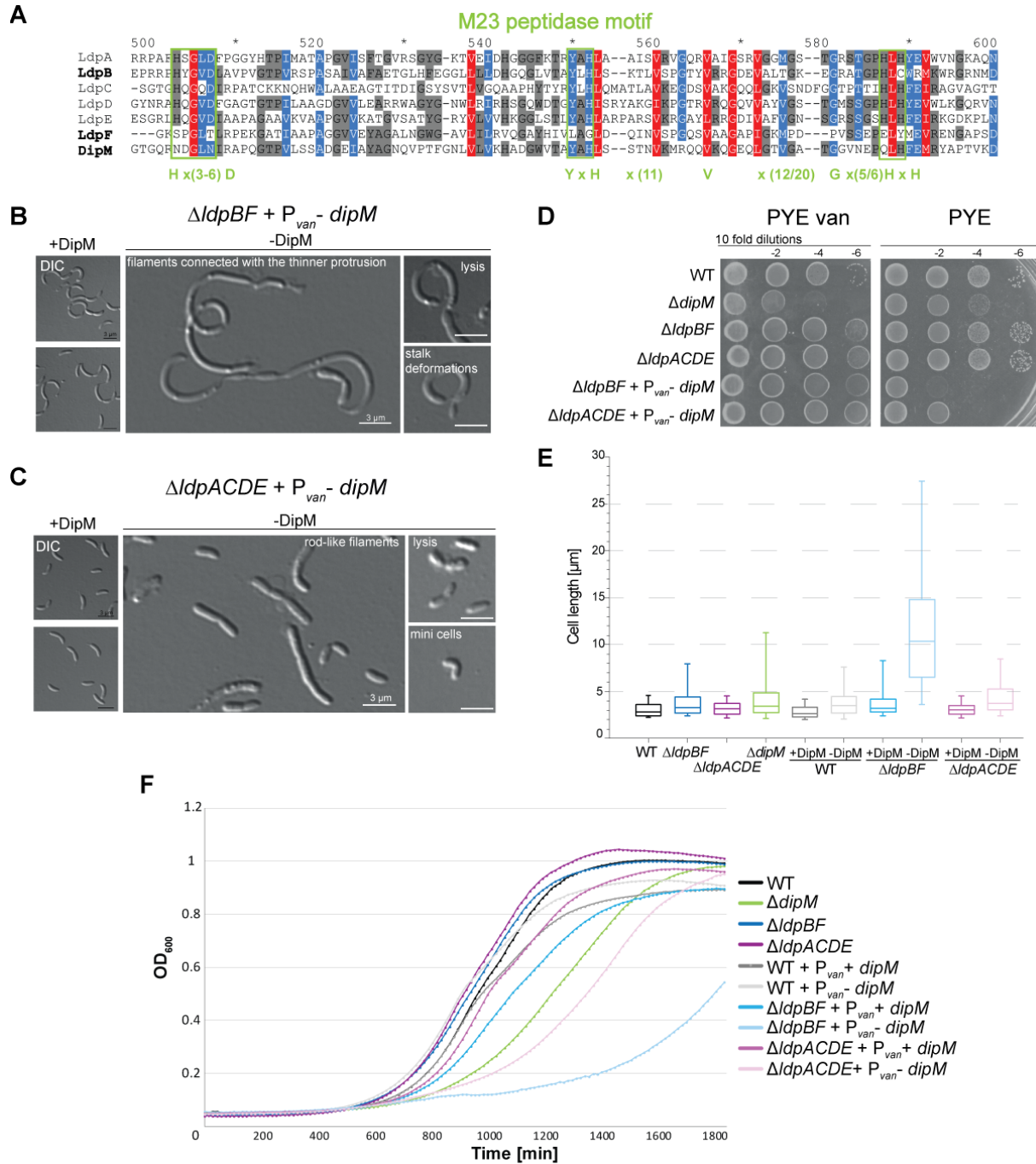
Figure 32. **The loss of LytM factors harboring either a full or partial M23 peptidase motif leads to severe physiological alterations upon DipM depletion.** **(A)** Alignment of the amino acid sequences of LytM factors from *C. crescentus*. The M23 peptidase motif is labeled in green. The proteins carrying a partial motif are depicted via bold font. **(B, C)** Morphology of the strains AZ99 (Δ*ldpBF* P*dipM*::P*van*-*dipM*) and AZ100 (Δ*ldpACDE* P*dipM*::P*van*-*dipM*) before and after DipM depletion. Cells were grown to exponential phase in PYE medium supplemented with 0.5 mM vanillate. Next, cultures were washed and depleted of DipM by incubation for 22 h in the absence of inducer, followed by DIC microscopy. Scale bar: 3 µm. **(D)** Loss of LdpB and LdpF is suppressed upon DipM depletion. Growth comparison of the strains MT258 (Δ*dipM*), AZ91 (Δ*ldpBF*), AM448 (Δ*ldpACDE*), AZ99 (Δ*ldpBF* P*dipM*::P*van*-*dipM*), and AZ100 (Δ*ldpACDE* P*dipM*::P*van*-*dipM*). Serial hundred-fold dilutions of cells in relation to CB15N (WT), plated on PYE agar and PYE agar supplemented with 0.5 mM vanillate, and

incubated for 2 d. **(E)** Statistical evaluation of cell lenghts of the strains analyzed in (D) in relation to WT (CB15N) and AZ35 (CB15N P_{dipM}::P_{van}-*dipM*). Cell body lengths were measured for 150 cells per strain using the MetaMorph program and visualized in box plots. Box plots show the median and the interquartile range (box), and the 5th and 95th percentile (whiskers), outliers are excluded. **(F)** Proliferation of the Δ*ldpBF* deprived of DipM is partially inhibited. Cells of the strains from (D) were grown o/n in rich medium supplemented with inducer if necessary, and transferred into fresh PYE medium. Growth was monitored by measuring the OD_{600} every 15 min for the total period of 31 h. Curves are color-coded to correlate with the box plots diagrams from (E).

Concluding from these experiments, Ldps carrying a partial M23 peptidase motif (LdpB, LdpF and DipM) seem to be crucial for sustaining proper cell division events, most likely by influencing the separation stage. On the other hand, LdpACDE seem to play a notable role in cell curvature, likely in concert with cytoskeleton elements, but a minor one in cell division. The substantial growth inhibition and morphological defects of cells with inactivated LdpB, LdpF and DipM prompted me to explore, whether the inactivation of LdpF or LdpB alone is able to emulate the observed phenotype.
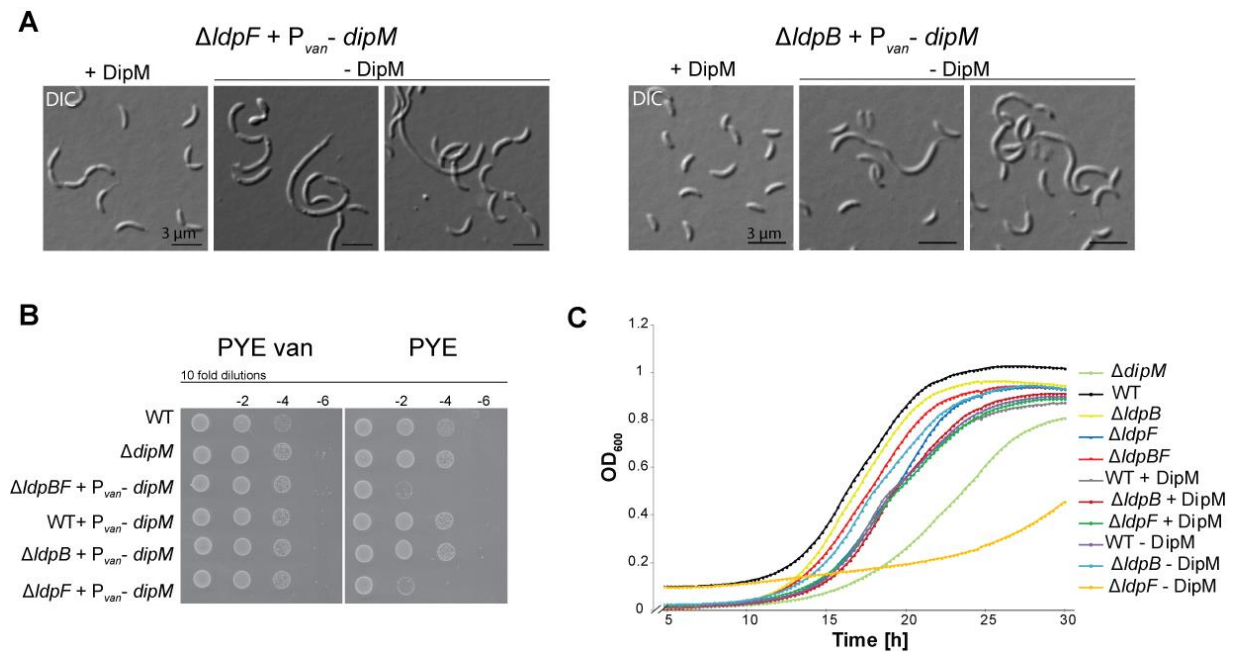
Figure 33. **Lack of LdpF resembles the phenotype of Δ*ldpBF* upon DipM depletion. (A)** Morphology of the strains AZ144 (Δ*ldpB* P_{dipM}::P_{van}-*dipM*) and AZ145 (Δ*ldpF* P_{dipM}::P_{van}-*dipM*) before and after DipM depletion. Cells were grown to exponential phase in PYE medium supplemented with 0.5 mM vanillate. Next, cultures were washed and depleted of DipM by incubation for 22 h in the absence of inducer, followed by DIC microscopy. Scale bar 3 µm. **(B)** Loss of LdpF triggers significant growth suppression. Growth comparison of the strains MT258 (Δ*dipM*), AZ99 (Δ*ldpBF* P_{dipM}::P_{van}-*dipM*), AZ35 (P_{dipM}::P_{van}-*dipM*), AZ144 (Δ*ldpB* P_{dipM}::P_{van}-*dipM*), and AZ145 (Δ*ldpF* P_{dipM}::P_{van}-*dipM*). Serial hundred fold dilutions of cells in relation to CB15N (WT) were plated on PYE agar and PYE agar supplemented with 0.5 mM vanillate, incubated for 2 d. Performed by Katharina Kremer. **(C)** Division rate of the Δ*ldpBF* cells deprived of DipM is significantly slowed down. Cells of the strains MT258 (Δ*dipM*), AM365 (Δ*ldpB*), AM369 (Δ*ldpF*), AZ91 (Δ*ldpBF*), AZ35 (P_{dipM}::P_{van}-*dipM*), AZ144 (Δ*ldpB* P_{dipM}::P_{van}-*dipM*), and AZ145 (Δ*ldpF* P_{dipM}::P_{van}-*dipM*) were grown o/n in rich medium supplemented with the inducer if necessary, following with the fresh PYE inoculation and OD_{600} measurements every 15 min for the total period of 31 h. Performed by Katharina Kremer.

Final experiments aiming to identify the component triggering the aberrant phenotype of the cells lacking LdpB and LdpF coupled with DipM depletion were performed by Katharina Kremer who sought to construct DipM conditional mutants in the Δ*ldpB* and Δ*ldpF* backgrounds (Kremer, 2015). Inactivation of DipM coupled with concurrent deletion of LdpB resulted in the morphology of the

parental strain (Figure 33B). In contrast, DipM depletion with concomitant loss of LdpF caused strong division defects, mimicking the phenotype obtained for deletion of both LytM facors Δ*ldpBF* (Figure 33A). The observed filamentous morphology of the strain lacking LdpF and DipM correlated with the growth inhibition on solid and in liquid media without inducer (Figure 33BC). Therefore, I concluded that LdpF is the LytM factor important to keep cells viability in the absence of DipM.

Altogether, analysis of the mutant phenotypes clearly suggests that LytM factors lacking catalytic residues are crucial for proper cell division, because inactivation of all of them results in inefficient proliferation and changes in morphology characteristic for defective cell constriction. Moreover, the data suggest that LdpF and DipM have a key role in orchestrating this process, likely in parallel functional pathways. Furthermore, LdpB seems to make only a minor contribution to cell division, whereas LdpACDE most likely do not contribute to the process at all. Instead, they might be involved in general PG turnover and the maintenance of proper cell shape.

2.7.3 AmiC, a putative PG hydrolase with unknown function

So far, experiments on AmiC have not led to the identification of its physiological function. The spatiotemporal localization dynamics of AmiC suggested an involvement in the late stages of the division process. This observation agrees with the predicted function of AmiC, which is to coordinate the cleavage of the cross-walls between the daughter cells. Since an in-frame deletion of *amiC* did not affect cell morphology, I decided to further characterize the protein, focusing on its possible regulatory mechanism and a potential functional redundancy of AmiC with other cell wall hydrolases.

To this end, first I depleted AmiC in the Δ*ldpABCDEF* background. Microscopic analysis showed that the cells have the same morphology as observed previously for the Δ*ldpABCDEF* mutant, suggesting that the concomitant lack of AmiC and Ldps does not yield synergistic effects (Figure 34A). Given that deletion of *ldpF* produced the most severe phenotype of all *ldp* mutations, I also depleted AmiC in cells lacking LdpF alone (Figure 34E). However, as expected again no synergistic effects were observed (Figure 34E).

I then went on to test the effects on AmiC depletion in Δ*sdpABC* cells. Interestingly, inactivation of all three SLTs in combination with AmiC depletion, resulted cells with unnatural swellings at the stalked pole (Figure 34B). This morphological feature was best observed when visualized via phase contrast microscopy. Despite these swellings, the average cell length was unaffected, resembling that of the Δ*sdpABC* mutant (Figure 34C). Labeling of the sites of active PG incorporation with HADA largely revealed the pattern previously observed for Δ*sdpABC* cells with a normal pattern in WT-sized cells and random incorporation in filaments (Figure 34D). However, in some cells the HADA signal accumulated at swellings suggesting more intensive incorporation at the cell poles (Figure 34D). Notably, none of the strains described in this chapter exhibited a significant decrease in growth rate (data not shown). Last, intrigued by the possibility that both proteins with predicted amidase activity may act in concert, I generated a double deletion mutant of *chap* and *amiC*. Notably, inactivation of both proteins yielded the morphology previously observed for the Δ*chap* mutant (Figure 34F).

Statistical analyses of the cell lengths confirmed the microscopy experiments and yielded the distribution similar to that of parental strain (Figure 34F).
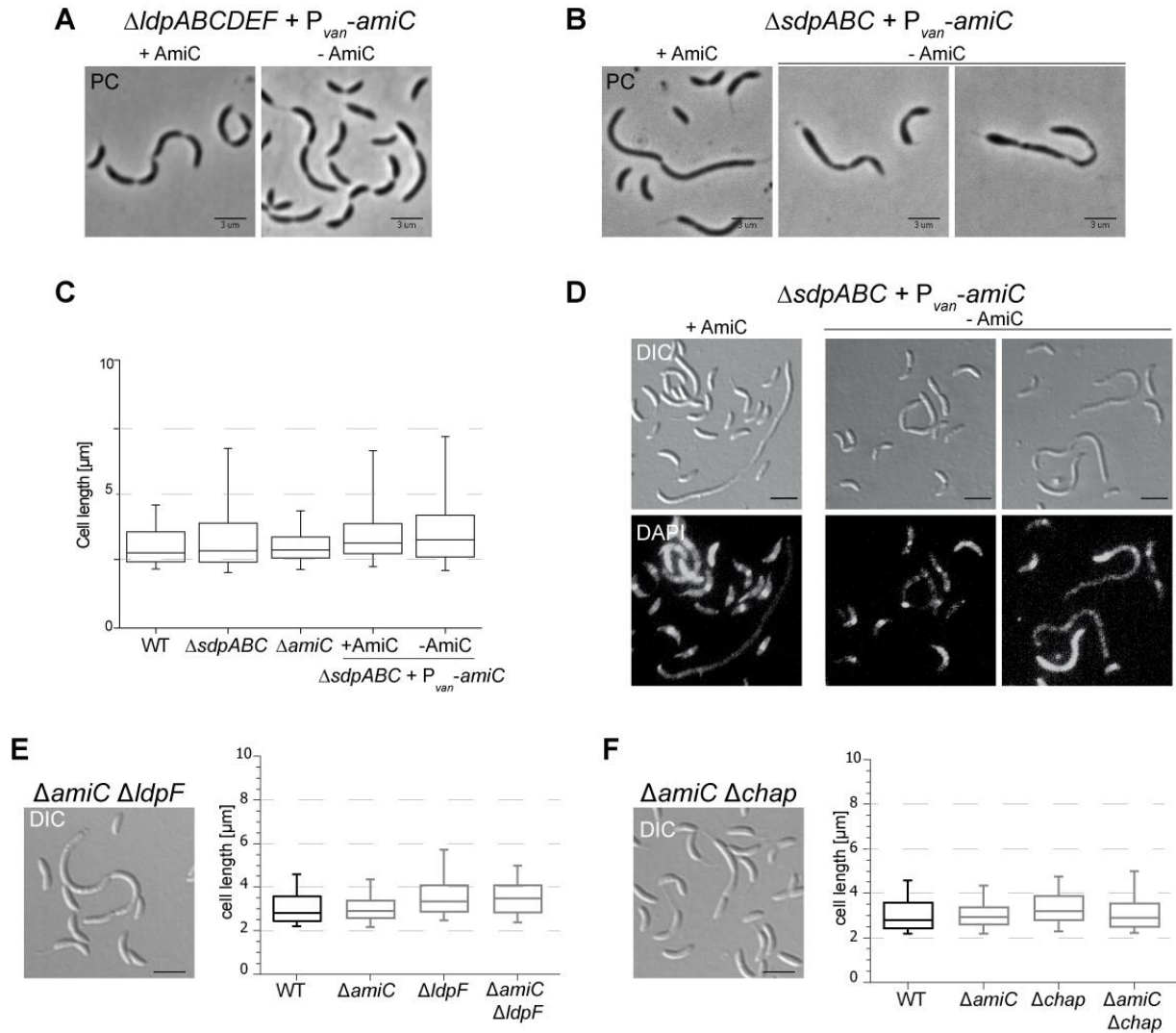
Figure 34. **Functional dependence of AmiC on other PG hydrolases.** Morphology of the strains AZ66 ($\Delta ldpABCDEF$ P_{amiC}::P_{van}-*amiC*). **(A)** and AZ42 ($\Delta sdpABC$ P_{amiC}::P_{van}-*amiC*) **(B)** before and after the depletion of DipM. Cells were grown to exponential phase in PYE medium supplemented with 0.5 mM vanillate. Next, cultures were washed and depleted of DipM by incubation for 22 h in the absence of inducer, followed by phase contrast microscopy. **(C)** Statistical evaluation of cell lenghts of the strains CB15N (WT), AM338 ($\Delta amiC$), AM440 ($\Delta sdpABC$) and AZ42 ($\Delta sdpABC$ P_{amiC}::P_{van}-*amiC*). Cell body lengths were measured for 150 cells per strain using the MetaMorph program and visualized in box plots. Box plots show the median and the interquartile range (box), and the 5th and 95th percentile (whiskers), outliers are excluded. **(D)** Labeling PG incorporation active sites. Cells of the strain from (B) were incubated with HADA, followed by fixation in ethanol, DIC and fluorescence microscopy. Scale bar: 3 μm. Morphology of the strains carrying a double deletion of AmiC coupled with either LdpF **(E)** or Chap **(F)** along with the statistical analyses of the cell length. Box plot description as in (C). DIC micrographs of the strains AZ166 (Δami $\Delta ldpF$) (E) and AZ165 ($\Delta amiC$ $\Delta chap$) (F) during exponential phase of growth cultivated in PYE medium. Cell body lengths measured and visualized as described in (C).

Altogether, the data obtained fail to reveal any detectable activity of AmiC, even in strains that have been sensitized by inactive action of Chap, the Ldps or the SLTs. Notably, the joint inactivation of SLTs and AmiC resulted in thickening of the cell poles, the origin of which must be elucidated in additional experiments.

2.7.4   Complementary activities of SLTs and Ldps

Based on their completely different specificities, SLTs and Lsps are likely to have independent activities. To test this hypothesis, deletion strains containing multiple in-frame deletions of genes encoding to SLTs and LytM factors were generated via step by step introductioin of single SLT gene deletions into Δ*ldpABCDEF* genetic background.

The construction of the mutant carrying in-frame deletion of all six *ldps* genes in combination with all three SLT genes was unsuccessful. However, I was able to introduce up to two in-frame deletion into the Δ*ldpABCDEF* genetic background. The morphology of the cells did not change significantly upon additional inactivation of SdpB and/or SdpC, when compared to the parental strain (Figure 35A), as supported by analysis of the cell lengths (Figure 35B). Notably, loss of SdpA in the Δ*ldpABCDEF* background resulted in strains with high length variation (Figure 35AB). The degree of cell length variation rose with the number of deleted genes. Notably, none of the strains mentioned in this section showed a decrease in its growth rate (data not shown).

Based on the additive effects of the mutations observed, I conclude that SLTs and LytM factors act in different pathways. Intriguingly, inactivation of up to eight genes did not influence the growth rate in mutant cells ultimately highlighting the redundancy of the investigated components of the PG remodeling machinery.
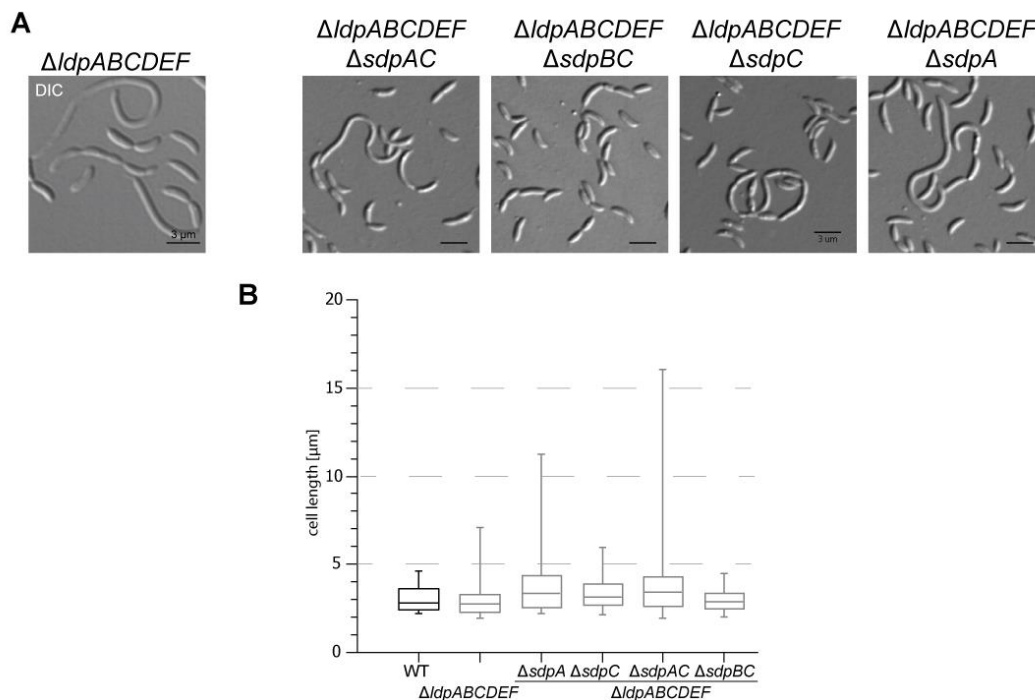
Figure 35. **SLTs and LytM factors act in independent pathways. (A)** Morphology of the strains carrying multiple SLTs and Ldps deletions. DIC micrographs of the strains AZ70 (Δ*ldpABCDEF* Δ*sdpC*), AZ71 (Δ*ldpABCDEF* Δ*sdpA*), AZ73 (Δ*ldpABCDEF* Δ*sdpAC*) and AZ74 (Δ*ldpABCDEF* Δ*sdpBC*) during exponential phase of growth cultivated in PYE medium. **(B)** Cell length analysis of SLTs and LytM factors deficient strains depicted in (A) in correlation to the wild type CB15N (WT). Cell body lengths were measured for 150 cells per strain using the MetaMorph program and visualized in box plots. Box plots show the median and the interquartile range (box), and the 5th and 95th percentile (whiskers), outliers are excluded.

3. DISCUSSION

3.1 Lytic transglycosylases

LTs are long known glycosidases cleaving the β-1,4 glycosidic bond between MurNAc and GlcNAc in PG (Holtje *et al.*, 1975). In *E. coli*, six out of seven LTs are OM-anchored (MltA-F), whereas Slt70 is soluble in the periplasm. None of them is divisome-associated, suggesting that LTs are active throughout the periplasm, maintaining proximinity to their substrate. They have been shown to play a rather moderate role in *E. coli's* PG remodeling process, based on the morphology of the strains lacking single and multiple copies of the genes encoding LTs (Heidrich *et al.*, 2002). Triple deletion of *mltA*, *mltB*, and *slt70* surprisingly led to no changes in the phenotype (Lommatzsch *et al.*, 1997), whereas Δ*mltCDE* cells formed short chains composed of three to six cells in 30 % of the population (Heidrich *et al.*, 2002). Inactivation of all LTs increased amount of chain-like cells to 50 % with concurrent slight shortening and rounding of the cell bodies (Heidrich *et al.*, 2002). Overall, this phenotype suggested impaired septum cleavage. The cells lacking murein hydrolases also appeared to be more tolerant towards ampicillin than the wild type (Tomasz, 1979).

The localization studies of the yet uncharacterized SLT homologues: SdpA, SdpB and SdpC in *C. crescentus*, revealed a dynamic localization of the first two proteins. Moreover, it was shown that the localization pattern of SdpA is FtsZ-, FtsN- and DipM- dependent. The subcellular distribution of SdpC remains known due to instability of the fluorescent protein fusion. In order to determine the pattern of SdpC, I generated a C-terminal fusion to a different fluorescent protein, super-folder GFP. However, again the resulting protein fusion was not stable (data not shown). Therefore, the question of whether SdpC can also associate with the divisome remains unanswered.

SdpA is evenly distributed throughout the periplasm until stalk synthesis is initiated. At this point, it forms a discrete focus at the stalked pole. Several minutes later, an additional midcell accumulation and a concomitant gradual loss of the protein from the lateral regions of the cell is visible, until it ultimately forms a distinct focus at the division plane once the cell enters the division phase. The polar localization of SdpA was observed, until the stalk was completely synthesized. In contrast, SdpB did not form a polar focus but only gradually condensed at midcell, which kinetics similar to those of SdpA (data not shown), suggesting no contribution of the latter to stalk biosynthesis. Collectively, the localization studies clearly suggest that at least two SLTs homologues in *C. crescentus* are integral parts of the divisome, presumably contributing to the final stages of the division process. The focus formed by SdpA early in the cell cycle at the stalked pole suggests that this SLT may be dynamically recruited to the locations of most intensive murein biosynthesis. Alternatively, it may be actively recruited to this position, by a thus-far unknown factor, to mediate lytic process specifically required for stalk formation. Consistently, it is known that PG hydrolases from other bacterial species adopt distinct localizations as a way to control their activity (Baba & Schneewind, 1998; Bernhardt & de Boer, 2003; Carballido-Lopez *et al.*, 2006; Peters *et al.*, 2011; Yamada *et al.*, 1996). However, the precise contribution of SdpA in stalk formation is still unclear.

Single and double in-frame deletions of SLT genes have no influence on cell morphology. In contrast, the triple Δ*sdpABC* mutant yielded cells with elongated cell bodies, accompanied with membrane blebbing, an indication of defects in OM metabolism. Interestingly, the blebs were either still attached to the cell bodies or shed to the surrounding milieu (data not shown). Vesiculation is a common phenomenon in Gram-negative bacteria grown in a variety of environments including liquid, solid and biofilm conditions (Beveridge, 1999). Previous studies suggest that the formation of blebs in *E. coli* may be triggered either by harsh environmental conditions (Katsui *et al.*, 1982) or by an imbalance in the division process. Consistent with a division defects, the formation of vesicles in the Δ*sdpABC* mutant preferentially occurred either close to midcell or at the cell poles. OM vesicles production was previously explained either by an increased PG turnover rate (Mug-Opstelten & Witholt, 1978) or by a loss of the connection between the PG and the OM leading to local disintegrity (Katsui *et al.*, 1982). In *C. crescentus* it was shown that depletion of the Tol-Pal components leads to extensive vesiculation, which was explained by the bridging function of this protein, which are required to maintain integrity of the cell envelope (Yeh *et al.*, 2010). The blebbing phenotype was also observed for DipM-deficient cells in *C. crescentus* (Goley *et al.*, 2010a; Moll *et al.*, 2010) and recently in *H. influenzae* lacking YebA, a LytM homologue with demonstrated PG hydrolytic activity (Ercoli *et al.*, 2015). The blebbing of Δ*dipM* cells was explained by thickening of the PG layer and consequent disruption of Tol-Pal-OM contacts (Goley *et al.*, 2010a). In agreement with an imbalance in the cell envelope biosynthesis, labeling experiments revealed that largely newly synthesized OM is implied in vesicle formation (Mug-Opstelten & Witholt, 1978). Notably, cells of *N. meningitidis* were recently reported to release OM vesicles in response to lower levels of three LTs, MltA, MltB, and Slt (Lappann *et al.*, 2013). Based on these findings it is tempting to hypothesize that the inhibition of SLT activity may disrupt the delicate balance between PG and OM biogenesis and/or lead to thickening of the PG layer thereby impairing the function of the Tol-Pal complex.

I provided several lines of evidence that the lack of SLTs affects the structure of murein by doubling the amount of murotetrapeptides and sensitizing the cells against the cell wall-targeting antibiotic ampicillin. Likely, the observed increase of murotetrapeptides may indicate thickening of the cell wall and concurrent accumulation of 'old' PG building blocks, which are mainly composed of these residues. Alternatively, the observed increase of the murotetrapeptide fraction may indicate the compensatory induction of a thus-far unidentified DD-CPase.

Interestingly, Δ*sdpABC* mutant is sensitive towards ampicillin, in contrary to the naturally resistant wild-type strain. Studies on *E. coli* revealed that the 1,6-anhydro-MurNAc molecule generated by the action of SLTs is necessary to trigger β-lactamase synthesis and to maintain proper PG recycling rate (Jacobs *et al.*, 1997). Hypothesizing that these regulatory pathways are conserved among bacterial species, inactivation of three SLTs in *C. crescentus* could significantly impair formation of 1,6-anhydroMurNAc and thus PG recycling. Therefore, the accumulation of particular fraction of muropeptides could be a consequence of an imbalance between PG biosynthesis and degradation. Surprisingly, in the mutant, overall percentage of the 1,6-anhydroMurNAc termini in the cell wall did not change when compared to the wild type, which is highly unlikely. Moreover, I showed that deletion of *sdpA* alone is sufficient to cause ampicillin sensitivity, which does not result from the

inhibition of natural β-lactamase activity. Therefore, I hypothesize that this effect is an outcome of modifications in the cell wall structure that make a normally redundant ampicillin-sensitive factors essential for survival. Alternatively, it is possible that SdpA is the SLT, whose activity alone is necessary to generate sufficient amounts of 1,6-anhydroMurNAc and sustain proper PG turnover rate. Therefore, the repetition of the cell wall composition of Δ*sdpABC* mutant along with analysis of the murein architecture of Δ*sdpA* strain must be performed. Based on these findings and previous localization studies I conclude that SdpA is a major SLT that contributes significantly to maintain the architecture and the turnover of the *C. crescentus* cell wall. The questions as to the extent to which SdpA contributes to the PG biogenesis and to its precise role remain unanswered.

In contrast to the SLTs, the MLTs of *C. crescentus* seem to have only a minor effect on cell division and/or cell wall biogenesis. It is rather unlikely that any of them is associated with the divisome, based on their predicted topology and/or the localization pattern obtained for the MtyD-mCherry fusion. Microscopic studies of cells carrying single and multiple deletion in MLT genes did not reveal any alteration in morphology or growth. However, *mta2* was the only gene out of the set of twenty putative hydrolases that was resistant to deletion, suggesting essentiality. Remarkably, Mta2 is mainly composed of an Ami_2 (PF01510) domain rendering N-acetyl-anhydromuramyl-L-alanine amidase activity and MltB (PF01471) domain known to bind PG. Based on sequence analysis, the MLT domain acts as an anchor to the OM and ensures sufficient proximity to the substrate, promoting effective cleavage. In order to clarify the consequences of the absence of Mta2, I attempted to construct a depletion strain in which the native copy, composed of Ami_2 domain was placed under the control of a vanillate-inducible promoter, allowing the control of its transcription. Unfortunately, in non-permissive conditions the strain exhibited the same morphology as the wild-type cells, suggesting that the protein is redundant or that the basal expression levels were sufficient for function. The *C. crescentus* genome encodes only two PG amidases, AmiC carrying an Ami_3 domain and Mta2 with a predicted Ami_2 domain. Since I could not detect any AmiC activity, Mta2 may be a promising candidate for an amidase required for cleaving the murein of *C. crescentus*.

3.2 Endopeptidases

C. crescentus encodes ten homologs with predicted LD-EPase activity, from two different groups, namely M23 metallopeptidases (LytM factors, Ldps) and NlpC/P60/CHAP homologues. Based on the deletion studies, individual EPases have only minor physiological functions. However, as a group, they have a significant role in the division process.

In *C. crescentus,* seven homologues with a predicted M23 metallopeptidase domain were identified and subjected to deletion and localization studies (Möll, 2011). None of the single deletions affected morphology, and none of the proteins showed a distinct localization pattern, except for DipM (Goley *et al.*, 2010a; Moll *et al.*, 2010; Poggio *et al.*, 2010). However, a moderate, chaining phenotype was observed when all six Ldps were deleted. In addition, mildly elongated cells were observed for the Δ*ldpF* strain (Möll, 2011). Additional experiments performed in this study showed that inactivation of both catalytically inactive LytM factors, LdpB and LdpF produced a phenotype similar to the one

observed for the sextuple Δ*ldpABCDEF* deletion, suggesting an important role in the division process. In contrast, inactivation of four Ldps with complete M23 peptidase catalytic motif resulted in wild-type morphology, suggesting that the analysis of the primary structure of LytM factors may serve as a way to conclude on a role in the division process. Notably, the depletion of DipM in the Δ*ldpBF* and Δ*ldpACDE* backgrounds revealed distinct effects of both groups on cell physiology. Inactivation of LdpB and LdpF combined with DipM depletion resulted in extensive division defects, as reflected by the presence of elongated and unseparated cells coupled with almost complete growth inhibition. In contrast, DipM depletion in the Δ*ldpACDE* mutant produced only slightly elongated cell bodies and occasional mini cells, with an interesting straight cell shape accompanied by a severe growth defect. Therefore, I presume that LdpACDE have a general role in PG biogenesis that may be required for establishing the characteristic cell curvature of *C. crescentus*. The growth defect observed for the DipM-depleted Δ*ldpACDE* mutant correlated with the growth rate of the Δ*dipM* strain in liquid medium, supporting the idea that LdpACDE are dispensable for cell constriction. Further experiments revealed that, in contrast to LdpB, inactivation of LdpF alone coupled with DipM inhibition was able to emulate the phenotype observed in the Δ*ldpBF* background (Kremer, 2015), indicating that LdpB is dispensable. Interestingly, apart from the defects in cell morphology and growth, the lack of LdpF triggers extreme halosensitivity. The low salt tolerance characteristic for *C. crescentus* decreased dramatically upon LdpF deactivation. Therefore, apart from the obvious contribution to the division process, LdpF may also play a crucial role in the resistance of the cell against osmotic stress (Kremer, 2015). This effect may be explained by a model in which the lack of salt-tolerant LdpF pathway makes a normally redundant salt-sensitive factors essential.
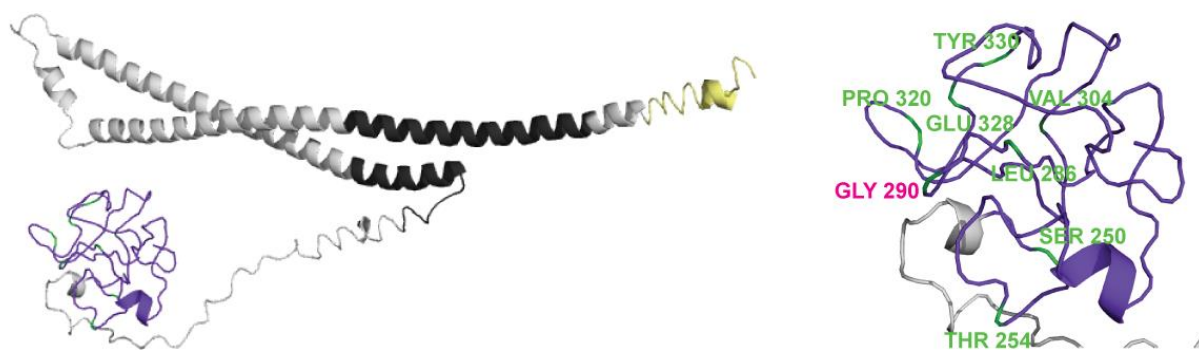
Figure 36. **LdpF has a structure similar to that of proteins modulated by FtsEX. (A)** Full-length LdpF modeled with I-TASSER. The protein consists of two coiled-coil (CC) regions (dark grey), the putative M23 peptidase catalytic domain (purple), and the signal peptide (yellow). (B) Zoom of the degenerated M23 peptidase domain. The residues crucial for substrate coordination are labeled in green (not conserved) and pink (conserved).

Catalytically inactive LytM factors are known to contribute to the division process as regulators of PG hydrolases (Yang *et al.*, 2012a). However, studies on various proteobacteria have revealed that despite sharing structural homology, LytM factors can have rather distinct functions in the division process (Ercoli *et al.*, 2015; Moll *et al.*, 2014; Yakhnina *et al.*, 2015). Two (EnvC, NlpD) out of four Ldps identified in *E. coli* that carry a degenerate catalytic M23 motif, activate PG amidases which are necessary for the separation of the daughter cells. EnvC and NlpD specifically activate AmiA/B and AmiC respectively, suggesting a selective regulatory mechanism (Uehara *et al.*, 2010). Structurally,

NlpD additionally harbors a LysM PG-binding domain, whereas EnvC features two coiled coil (CC) modules known to promote protein-protein interactions (Uehara *et al.*, 2009). Moreover, CC domain of EnvC is a regulatory domain, necessary and sufficient for recruitment to the divisome (Uehara *et al.*, 2010). Despite low sequence homologies and diverse hydrolytic activities, the function of the murein hydrolases CwlO and PcsB, which both carry coiled-coil domains, was shown to be controlled by FtsEX in *B. subtilis* (Meisner *et al.*, 2013) and *S. pneumoniae* (Sham *et al.*, 2011), respectively. Studies based on the crystal structure of PcsB suggested a molecular mechanism where the PscB dimer undergoes a conformational change, driven through ATP hydrolysis by FtsEX, leading to the release of the CHAP domain and thereby allowing precise cleavage of septal PG (Bartual *et al.*, 2014). Interestingly, LdpF in *C. crescentus* has the highest structural homology to EnvC (based on BLAST analysis) and two coiled-coil domains in addition to the C-terminally located M23 peptidase domain (Figure 36). Furthermore, the structures of LdpF (Figure 36) and PscB (Bartual *et al.*, 2014) show an analogous architecture, suggesting that LdpF might also be active as a dimer. Therefore, LdpF arose as a prominent candidate to mediate a similar type of regulation driven by ATP hydrolysis, possibly also involving FtsEX. It is likely that LdpF could regulate the activity of a thus-far uncharacterized hydrolase, in a similar way as described for *E. coli* (Figure 37). To test this possibility, further experiments involving FtsEX and LdpF must be performed. Collectively, based on the additive effects observed LdpF is active in a pathway that is independent of DipM. Therefore, a regulatory dependency between these two is highly unrealistic, automatically excluding DipM as a target for this type of regulation.
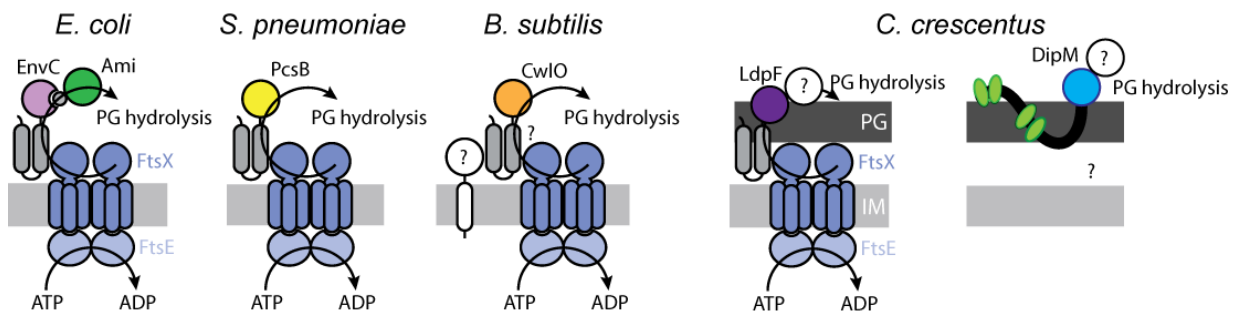
Figure 37. **FtsEX serves as a regulatory unit.** Graphical representation of FtsEX regulation in *E. coli*, *S. pneumoniae*, *B. subtilis*, and *C. crescentus*. The ATP hydrolysis conducted by FtsE in the cytoplasm drives PG hydrolysis through species-specific components with analogous functions. The hypothetical interactions between the components are labeled with question marks. The putative cell wall hydrolases regulated either by LdpF or DipM are depicted as white circles. The LysM-PG-binding tandems are colored in green. PG-peptidoglycan, IM-inner membrane. Adapted from (Meisner *et al.*, 2013).

The muropeptides composition of cell walls isolated from the Δ*ldpABCDEF* mutant revealed no difference when compared to the wild-type strain. Similar results were obtained for an *E. coli* strain carrying a quadruple deletion of LytM factors genes and triple deletion of key amidases (Heidrich *et al.*, 2001; Uehara *et al.*, 2009). Possibly, the fraction of septal PG, which is affected most prominently, is relatively small compared to the total cell wall background. Therefore, it would be interesting to perform a muropeptide analysis based on synchronized culture labeled with HADA. It is likely that the fraction of the fluorescently labeled muropeptides differ in the retention time, which could provide a direct way to specifically analyze the cell wall synthesized during cell division.

Cleavage of the crosslinks between the muropeptides is facilitated by a group of redundantly essential EPases from the NlpC/P60/CHAP family in *E. coli* (Singh *et al.*, 2012). Similarly, the data collected for the homologues found in *C. crescentus* clearly indicate their importance in sustaining proper cell division. Specifically, the absence of NlpA yielded a heterogeneous population of visibly elongated cells, which when additionally coupled with inactivation of Chap led to an almost complete block of proliferation. Conversely, the loss of Chap resulted in wild-type morphology but triggered sensitivity towards ampicillin, although the production of β-lactamase was not inhibited, suggesting an aberrant metabolism of PG. Moderate ampicillin sensitivity was also noted for every mutant carrying a deletion of *nlpA*. Collectively, NlpA is most likely involved, directly or indirectly, in cell division, whereas Chap may have a more general role in PG synthesis. Concurrent deactivation of a third Nlpc/P60/CHAP homologue, NlpB, did not yield a cumulative effect, suggesting a dispensable cellular function. Similar observation was made for *B. subtilis*, where LytE and CwlO despite carrying the same activity rendered by NlpC/P60 domain were not only different in their activities (Yamamoto *et al.*, 2008) but also appeared to be involved in different growth processes (Hashimoto *et al.*, 2012).

LD-TPases containing the YkuD domain were previously reported to play a central role in PG biogenesis in the α-proteobacterium *A. tumefaciens* (Cameron *et al.*, 2014)*.* The experiments aiming to characterize the functional homologues in *C. crescentus* revealed an involvement of YkuD homologues in the division process. Cells carrying a single deletion of *ykuD* resulted in a population of cells with by high cell length variations. Additional inactivation of the second identified LD-TPase homologue Mta2, did not produce any stronger defects in morphology, suggesting dispensability. Notably, concluding from the fact that the muropeptides profile of the wild-type *C. crescentus* strain revealing only a minor content of 3-3 crosslinks, it is unlikely that LD-TPases play a prominent role in the PG remodeling.

3.2.1   DipM and the riddle of its function

DipM arose as a key player of PG remodeling in *C. crescentus*, since changes in the protein level affect proper functioning of the cell division process and directly influence septal PG synthesis (Goley *et al.*, 2010a; Moll *et al.*, 2010; Poggio *et al.*, 2010). Studies focusing on finding direct DipM interaction partners may shed light on its function. It is known that its arrival at the divisome is FtsN dependent. However, other interaction partners are so far unknown. For that reason, I performed the Co-IP experiments coupled with MS analysis, using a tagged version of DipM as bait. These experiments yielded many unspecific hits (Table S5 and S6) along with two prominent candidates, which could be potential interaction partners of DipM, based on the predicted periplasmic topology (CCNA_00398) and catalytic domain organization (CCNA_02661). Unfortunately, labeling and microscopy experiments of these potential interaction partners did not show any implication in cell division and/or PG remodeling. Considering the dynamic nature of the divisome and the fact that it is constantly rearranged over the course of the cell cycle, trapping transient interactions between its components may be extremely difficult.

Analysis of the muropeptides profile of the Δ*dipM* strain did not reveal any compositional changes relative to the wild-type strain. As explained above, the fraction of the muropeptides building the septal PG may could be simply too small to be detected in the total muropeptide preparation.

3.3 Stress conditions highlight the importance of LytM factors

Multiple deletions of autolysin genes from individual enzymatic families resulted in rather mild morphological and physiological consequences. The phenotype caused by the lack of either SLTs or LytMs suggests a cell division defect, as reflected by the formation of filaments coupled with blebbing or the production of cells organized in chains, respectively. *In vivo* characterization of individual proteins or groups with overlapping functions is difficult due to the mildness or absence of morphological defects in optimal growth conditions. For this reason, I subjected the strains lacking whole enzymatic families to stress conditions, including osmotic pressure, temperature shock, and nutrient limitation.

C. crescentus displayed a very narrow range of osmotolerance in comparison to *E. coli*. It has been shown that the osmolality inhibiting the growth of *E. coli* is thirteen times higher than that inhibiting *C. crescentus* (Hocking *et al.*, 2012; Record *et al.*, 1998). I have established the threshold concentration of sodium chloride affecting cell morphology of wild-type *Caulobacter* to be 0.3 % (50 mM), whereas growth inhibition in liquid rich medium was observed at 0.45 % (85 mM), which agrees with the published data (Hocking *et al.*, 2012). A LytM factor-deficient strain (Δ*ldpABCDEF*) appeared to be extremely sensitive towards any type of osmotic stress and elevated temperature. As observed before, lack of LdpF alone promotes halosensitivity, therefore resulting phenotype of the Δ*ldpABCDEF* strain in the presence of salt not surprising (Kremer, 2015). It would be interesting to test the behavior of a strain lacking LdpF in other demanding growth conditions. The osmo-sensitive phenotype of Δ*ldpF* cells could arise from an altered structure of the cell wall, which for some reason, likely structural, is more sensitive to lysis in general. As stated before, the relaxed conformation of the cell wall does not positively influence its growth, since assembly of the biosynthetic complexes is favored the stretched configuration (Typas *et al.*, 2010). Therefore, the efflux of water, characterized by plasmolysis, loss of turgor pressure, shrinkage of the cytoplasmic space, and finally relaxation of the cell wall does not promote PG growth. In line with this hypothesis, a recent study of an *C. crescentus* revealed that PBP2, which is essential for cell elongation, is relocated to midcell upon an osmotic shift, which may be due to the mentioned relaxation of the cell wall architecture (Hocking *et al.*, 2012). In *E. coli*, the turgor pressure is important to maintain the size of the pores in PG, which is thought to be crucial for the activation of PBPs by their cognate lipoprotein activators (Lpo) and in turn, generating a homeostatic mechanism to control the rate of PG synthesis (Typas *et al.*, 2010). Accordingly, Ldps may require not only a favorable murein configuration but also assembly of other downstream components to create an active complex. Similarly, hypersensitivity towards high salt concentrations and high temperature was observed for an Δ*envC* mutant *E. coli* mutant, reflected by extensive chain formation (Ichimura *et al.*, 2002).

3.4 Properties of the cell envelope upon deactivation of PG hydrolases

The inhibition of hydrolytic enzymes generally leads to a defective PG architecture and, consequently, to an aberrant arrangement of the cell envelope. Furthermore, if the PG hydrolases of *C. crescentus* are necessary for normal PG biogenesis and/or scaffolds for the assembly of other biosynthetic complexes, their lack should lead to the mislocalization of the PG incorporation pattern. To test this prediction, cells carrying single and multiple deletions of PG hydrolase genes were labeled with a red fluorescent protein and fluorescent analogue of D-Ala (HADA), respectively. Furthermore, if the structure of the cell wall is affected, its physicochemical properties, including susceptibility to β-lactam antibiotics, could be changed. Therefore, sensitivity towards ampicillin was tested.

Visualization of the periplasm of the Δ*amiC* and Δ*ldpABCDEF* strains resulted in no obvious changes in the periplasmic diameter or organization. The blebbing phenotype of Δ*sdpABC* and Δ*dipM* cells was already explained in Section 3.1 and in (Moll *et al.*, 2010), respectively. Analysis of these two blebbing strains revealed a much higher frequency of OM vesicle formation in the Δ*sdpABC* strain than in Δ*dipM* strain. Inactivation of DipM led to enlargement of the periplasmic space at the site of division (Moll *et al.*, 2010), suggesting its involvement in PG remodeling during cell division. The SLTs instead, may be less important for proper division but critically contribute to the balance of PG and OM synthesis, or the attachment of the OM to PG layer.

Labeling of the sites of active PG incorporation with fluorescent derivative of D-Ala (HADA) revealed that the active zones dynamically relocate over the course of the cell cycle, fitting to a model of subsequent dispersed and zonal murein growth. Notably, the hallmark of *C. crescentus*, the stalk, demands considerable PG synthesis as manifested by a distinct, polar HADA focus. The spatiotemporal localization pattern of SdpA followed the pattern of PG incorporation, supporting the hypothesis of the coexistence and cooperation of the synthetic and hydrolytic activities driving PG remodeling. Aberrant positioning of the clusters was observed in every strain with filamentous morphology, likely because of divisome malfunction. Interestingly, the clusters rearranged into arrays of small foci that were at the first glance randomly distributed over the cell body (Δ*sdpABC*), or were creating zones of variable intensities (Δ*chap*). Interestingly, cells lacking DipM formed well-defined foci along the filaments, suggesting that the assembly of PG biosynthetic complexes is independent of DipM. The strain exhibiting the strongest morphological defect due to inactivation of the two putative PG hydrolases, NlpA and Chap, was still able to assemble the cell wall remodeling complexes, suggesting that these two proteins ensure the efficiency of the division process, but are not required for the proper assembly of the PG biosynthetic machinery. The normal pattern of PG incorporation in chaining cells of the Δ*ldpABCDEF* strain favors the idea that LytM factors fulfill rather accessory functions in the division process.

Ampicillin is a β-lactam antibiotic inhibiting a cross-peptidation step in cell wall biogenesis. It has been shown that the induction of bacteriolysis by β-lactams and other cell wall synthesis inhibitors require active growth of the cells and the activity of autolysins (Leduc & van Heijenoort, 1980; Leduc *et al.*,

1982; Tomasz, 1979). Ampicillin intolerance was observed for the strains lacking SdpA, Chap and DipM, in contrast to the wild-type control, which tolerates concentrations up to 150 µg/ml. Interestingly, this intolerance did not originate from the inhibition of the endogenous β-lactamase activity, since the deletion strains were still able to hydrolyse fluorescently labeled β-lactam nitrocefin. Thus, rather than down-regulating β-lactamase genes, the SdpA-, Chap- and DipM- deficient strains may display severe defects in cell wall architecture. Alternatively, lysis could result from an imbalance between biosynthetic and hydrolytic events, favoring uncontrolled degradation (Koch, 2000; Weidel & Pelzer, 1964), or it is a consequence of the activation of hydrolytic enzymes, which under normal growth conditions are inactive (de Pedro *et al.*, 2002). The intriguing point is that the data collected for *E. coli* PG hydrolase-deficient mutants indicates that inactivation of autolytic activity prevents lysis caused by penicillin and its derivatives (Goodell *et al.*, 1976; Heidrich *et al.*, 2002; Tomasz *et al.*, 1970; Tomasz, 1979; Uehara *et al.*, 2009), which is exactly the opposite to the effect observed in this study for *C. crescentus*.

3.5 Functional dependency of PG hydrolases in *Caulobacter crescentus*

Single and multiple deletions of genes encoding particular PG hydrolases from a distinct catalytic group resulted in either a mild or no phenotype, suggesting redundant functions. Therefore, studies based on the observation of changes in morphology did not provide many answers regarding the particular roles of PG hydrolase homologues in *C. crescentus*. For that reason, I decided to explore the functional pathways in which proteins act, by constructing strains lacking multiple genes from different enzymatic families. Importantly, such a global analysis may shed light on the regulatory network between the investigated elements. Several studies described a functional dependency between LytM factors and LytC-type amidases basing on cooperative activation (Moll *et al.*, 2014; Uehara *et al.*, 2009; Yakhnina *et al.*, 2015). Since DipM probably lacks catalytic activity, it was an obvious candidate to fulfill a regulatory function, as described for M23 peptidase homologues from several gamma-proteobacteria. Since the Δ*amiC* mutant shows wild-type morphology, whereas Δ*dipM* cells display severe division defects, DipM could act as an activator of AmiC. It was not the case. Combinations including DipM depletion coupled with deletion of either the six remaining LytM factors genes (*ldpA-F*) or three SLTs (*sdpA-C*) resulted in synthetic lethality, suggesting that DipM may have a role in the regulation of a pathway independent of Ldps ans SLTs. Interestingly, inactivation of LdpF coupled with depletion of DipM greatly reduce the vitality and growth rate of the cells, pointing out these two as the most important players in the PG remodeling machinery identified over the course of this work. The precise role of these two proteins still remain to be elucidated. Interestingly, analysis of the muropeptide profile of a DipM depleted Δ*ldpABCDEF* mutant revealed a significant difference in the amount of tetra-peptides, illustrating the high redundancy and, thus robustness of the hydrolytic system in *C. crescentus*. Since the loss of DipM alone did not affect the overall muropeptide composition, the observed change implies that DipM and other LytM factors, likely LdpF alone, could significantly influence the activity of a thus-far unknown DD-EPase responsible for generation of mentioned tetra-peptides. Most importantly, LytM factors are essential to maintain proper cell

division. Therefore, revealing the regulatory pathway/s that they constitute would have a great impact on an understanding of the PG remodeling process in *C. crescentus*.

The significance of DipM in the physiology of *C. crescentus* cells was finally established by creation of deletion strains lacking almost all identified PG hydrolase homologues, except for DipM. The resulting strain, which lacked LdpA-F and SdpA-C grew almost normally (data not shown).

AmiC is the only homologue of a LytC type amidases found in *C. crescentus* (Moll *et al.*, 2010). Lack of all three LytC-type amidases generates a severe division defects in *E. coli*, manifested by the formation of long, septated cell chains (Heidrich *et al.*, 2002). Generally, the lack of amidases in Gram-negative species is linked to OM dysfunctions, resulting in increased sensitivity towards detergents and anti-microbial agents, and thus induction of envelope stress responses aiming to alleviate this defect (Craig *et al.*, 2013; Weatherspoon-Griffin *et al.*, 2011). Interestingly, in *C. crescentus* none of the tested conditions triggered changes in morphology of the strain lacking AmiC, suggesting the presence of a so-far unidentified amidase or another enzyme with an equivalent function. Notably, Mta2 arose as a promising candidate for this role. However, more experiments need to be performed to clarify its function. Interesting is the fact that AmiC localizes to the division plane with an onset of visible constriction suggesting a role in division. To rule out the possibility that AmiC is regulated by either Chap, theoretically carrying the same activity and LdpF which arose as a prominent regulator of yet unknown hydrolase, the double deletion strains of the respective genes were generated. The double inactivation of AmiC and LdpF and AmiC and Chap resulted in unaffected morphology, suggesting no regulatory dependency between these proteins, consistent with the different phenotypes of the respective single mutants. Inactivation of LdpA-F coupled with AmiC depletion resulted in the same observation. In contrast, the inactivation of SLTs coupled with the loss of AmiC resulted in cells with obviously swollen cell poles. Thses swellings could originate from the accumulation of cell wall, due to the block in the cleavage of glycan strands.

3.6   Concluding remarks

Despite intensive research efforts, many cellular processes, including the growth of the cell wall still remain enigmatic. There is an impressive amount of mutational and phenomenological data, describing the process; but comprehensive studies are still very rare. In this work I aimed to characterize the set of putative cell wall hydrolases that specifically active at the late stages of cell division mediating ultimate separation of the daughter cells. Although I was able to identify some similarities to the intensively studied PG remodeling systems of *E. coli*, the enzymes and regulatory pathways involved in this process in *C. crescentus* seem to be different. Collectively, it is likely that the remodeling system of *C. crescentus* is controlled by the specie-specific components, even though similar modules could achieve the regulation of the process. Importantly, some components, such as DipM seem to be species- specific, which makes the perspective of further studies even more intriguing.

4. MATERIALS AND METHODS

4.1 Materials

4.1.1 Origin of the chemicals and enzymes

Chemical agents and enzymes used in this work were obtained from: Analytik Jena (Germany), Becton Dickinson (USA), Bioline (Germany), Carl-Roth (Germany), Difco (Spain), Fisher Scientific (Germany), GE Healthcare (Germany), Invitrogen (Germany), Life Technologies (USA), Merck Milipore (Germany), New England Biolabs (NEB, USA) PerkinElmer (USA), Peqlab (USA), Promega (USA), Sigma-Aldrich (USA), Stratagene (USA), Thermo scientific (former Fermentas, Canada) or Qiagen (Germany).

4.1.2 Buffers and solutions

Standard buffers and solutions were prepared as described by Ausubel et al (1988) and Sambrook et all (1982) on the basis on de-ionized water. Solutions and buffers were sterilized either by filtration (pore size 0.22 μm or 0.45 μm, Sarstedt, Germany) or autoclaved (20 min, 121°C, 2 bar) if needed. Specific solutions or buffers are described together with the respective method.

4.1.3 Media

Complex media were autoclaved (20 min, 121°C, 2 bar), minimal media were filter-sterilized (pore size 0.22 μm, Sarstedt, Germany). For the solid media 1.5 % (w/v) agar was added before autoclaving. Media supplements such as antibiotics (listed in Table 1 and Table 2), carbohydrates or organic inducers were filter-sterilized or added after autoclaving to pre-cooled media (~60 °C).

LB (Luria-Bertani) medium, Miller 1972

- 1 % (w/v) Tryptone
- 0.5 % (w/v) Yeast extract
- 1 % (w/v) NaCl
- 0.2 % (w/v) Bacto™Peptone

PYE (peptone - yeast - extract)

- 0.1 % (w/v) Yeast extract
- 1 mM $MgSO_4$
- 0.5 mM $CaCl_2$

M2G (M2-minimal medium supplemented with glucose)

- 6.1 mM Na_2HPO_4
- 3.9 mM KH_2PO_4
- 10 mM NH_4Cl
- 0.5 mM $MgSO_4$
- 0.5 mM $CaCl_2$
- 0.2 % (w/v) Glucose
- 0.1 % (v/v) $FeSO_4$/EDTA-Solution (Sigma-Aldrich)

NZY$^+$ Amine broth   1.0 % (w/v) NZ amine (casein hydrolysate)

0.5 % (w/v) yeast extract

0.5 % (w/v) NaCl

12.5 mM $MgCl_2$*

12.5 mM $MgSO_4$*

0.04 % (w/v) glucose*

                                        *added right before usage

4.1.3.1   Media additives

Antibiotics, carbohydrates and organic inducers were prepared as stock solutions and added to the media to a final concentration listed in the Table 1 and Table 2.

Table 1. Antibiotics used in this work.

ANTIBIOTIC	STOCK SOLUTION [mg/ml]	FINAL CONCENTRATION [µg/ml]			
		E. coli liquid media	*E. coli* solid media	*C. crescentus* liquid media	*C. crescentus* solid media
Ampicillin	100	200	200	10	50
Kanamycin	20	30	50	5	25
Gentamicin	1	15	20	0.5	5
Chloramphenicol (in 70 % ethanol)	10	20	30	2	1
Spectinomycin	20	50	100	25	50
Streptomycin	10	30	30	5	5

Table 2. Carbohydrates and organic additives used in this work.

SOLUTION	STOCK SOLUTION	FINAL CONCENTRATION			
		C. crescentus liquid media	*C. crescentus* solid media	*E. coli* liquid media	*E. coli* solid media
Xylose	20 %	0.3 %	0.3 %	-	-
Sucrose	100 %	-	3 %	-	-
Glucose	20 %	0.2 %	--	0.2 %	0.2 %
Vanillate	50 mM	0.5 mM	0.5 mM	-	-
IPTG	1 M	-	-	0.5 mM	20 mM

4.1.4   Primers for the PCR reactions

Primers for the PCR reactions used in this work were designed using GeneTool Lite 1.0 (BioTools Inc., Canada) and were synthesized either by Sigma-Aldrich (Germany) or Eurofins MWG Operon (Germany). The complete list of oligonucletides used in this study is found in appendix (Table S3 and S4).

4.2 Microbiological methods

4.2.1 Growth conditions of the bacterial strains

E. coli TOP10 (Invitrogen, Germany) was used for the general cloning purposes, *E. coli* Rosetta (DE3)/pLysS (Novagen, Germany) for the protein overproduction.

E. coli strains were cultivated either in liquid LB medium at 37 °C, with shaking at 220 rpm, or on solid LB medium. When necessary, supplements (listed on the Table 1 and Table 2) were added to the media.

All *C. crescentus* strains obtained and used in this study originated from the synchronizable wild-type strain CB15N (NA1000) (Evinger & Agabian, 1977). Unless indicated otherwise, strains were grown at 28 °C in either rich PYE or minimal M2G medium (Ely, 1991b), supplemented with additives (listed in Table 1 or Table 2), if needed. Liquid cultures were grown with shaking at 220 rpm.

4.2.2 Storage of cells

For short-term storage, bacterial strains were stored at 4 °C on the plates. For long-term storage, bacterial strains were grown overnight, mixed with 15 % (v/v) DMSO, and frozen at -80 °C.

4.2.3 Synchronization of C. *crescentus*

Synchronized populations of swarmer cells were obtained as described by Ely(Ely, 1991a). Briefly, 30 ml culture grown in M2G medium to an OD_{600} of 0.6 were harvest by centrifugation at 6500 rpm for 10 min at 4 °C. The cell pellet was resuspended in 750 µl of ice-cold M2 salts and mixed with an equal volume of Percoll (Sigma-Aldrich, Germany). The mixture was centrifuged for 20 min at 4 °C and 11000 rpm to separate stalked cells (upper band) from swarmer cells (lower band). After careful removal of the stalked cell fraction, the swarmer cells were transferred into a fresh tube and washed additionally with 1.5 ml M2 salts at 9000 rpm for 2 min at 4 °C. Remaining cell pellet was resuspended in 2 ml of the pre-warmed PYE medium.

4.2.4 Measurement of the growth curves

Growth experiments were performed either manually or automatically with a Tecan Infinite® M200 pro microplate reader. The strains to be analyzed, grown as a pre-culture in 5 ml PYE medium overnight at 28 °C with shaking at 220 rpm. Next, stationary or late-exponentially growing cells were diluted with PYE medium to an OD_{600} of 0.05 – 0.15, and cell densities (OD_{600}) were measured every 1 hour when monitored manually or every 15 min when monitored automatically, for a total time of 24-40 hours.

4.2.5 Spot test

The capacity of *C. crescentus* to grow on solid media was tested by spotting 15 µl of a cell cultures with an OD_{600} of 0.16 on the plates containing additives, followed by incubation for 48 hours at 28 °C.

4.2.6 Chemi-competent *E. coli* TOP 10 cells

Chemically competent *E. coli* TOP10 were prepared according to protocol described by (Sambrook, 1989). In short, an o/n *E. coli* culture was diluted 1:100 in 500 ml LB medium and cultivated until OD_{600} reached 0.6-0.8. Cells were cooled on ice for 10 min followed by harvesting at 4 °C (6500 rpm, 10 min) and resuspension in 8 ml 0.1 M ice-cold $CaCl_2$. The suspension was incubated on ice for additional 30 min. Next, cells were sedimented by centrifugation, followed by resuspension in 4 ml of ice-cold 0.1 M $CaCl_2$ supplemented with 15 % (v/v) glycerol. 150 µl aliquots were immediately snap-frozen in liquid nitrogen and stored at -80 °C.

4.2.7 Electro-competent *C. crescentus* cells

Electro-competent *C. crescentus* cells were prepared as described by (Ely, 1991a). In brief, cells were grown in two fold concentrated PYE to an OD_{600} of 1.0, followed by three washing steps using ice-cold 10 % (v/v) glycerol (6500 rpm, 4 °C and 10 min).The resulting cell pellet was resuspended in 1/50 volume of ice-cold 10 % glycerol. 80 µl aliquots were immediately snap-frozen in liquid nitrogen and stored at -80 °C.

4.2.8 Protein depletion from *C. crescentus*

To deplete proteins whose genes were expressed under the control of the xylose- and/or vanillate-inducible promoter (P_{xyl}, P_{van}), cells were grown in PYE medium supplemented with the respective inducer(s). 2 ml of the cultures, maintained in exponentiary phase were pelleted (9000 rpm, 2 min, 4 °C) and washed twice with 2 ml of the ice-cold M2-salts. Finally, the cells were resuspended in 1 ml of pre-warmed PYE medium for further cultivation. Samples were taken at various time-points to analyze the resulting phenotypes.

4.2.9 Test for β-lactamase activity

Cell cultures were grown in PYE to the exponential phase of growth, followed by addition of four drops of Nitrocefin® (500 µg/ml) to 2 ml of the cell suspension. The cells were spun down (1 min, RT, 11000 rpm) and 900 µl of the supernatant were measured spectrophotometrically at 390 nm and 468 nm. The cell pellet was suspended in the remaining 1 ml of the supernatant followed by incubation for 20 min at RT. After incubation, the cells were spun down and the 900 µl of supernatant were measured spectrofotometrically at 468 nm followed with the substraction of the value obtained before incubation.

4.2.10 Lyophilization of *C. crescentus* cells

To prepare cells for cell wall analyses, 250 ml PYE inoculated with an overnight culture, of the strain to be studied were cultivated to an OD_{600} of 0.7 followed by harvesting of the cells (6500 rpm, 10 min, 4 °C). The cell pellet was resuspended in 1 ml previously autoclaved water and incubated in a heating block for 10 min at 99 °C. Inactivated cells were cooled down, snap-frozen horizontally in liquid nitrogen and freeze-dried for 24 hours at -20 °C and 1.2 bar using the single-stage cooling system freeze dryer Alpha 1-4 (Christ, Germany).

4.3 Molecular cloning

4.3.1 *In silico* plasmid construction

Plasmids created in this work were designed using Vector NTI Advance™ 11 (Invitrogen, Germany). The complete list of vectors used in this study is found in the Appendix (Table S2). Sequence analysis was performed using VectorNTI (Germany) and SnapGene (GSL Biotech, USA).

4.3.1.1 Construction of plasmids encoding inducible C-terminal fluorescent protein fusions

Plasmids carrying fluorescent protein gene fusions were integrated at the chromosomal *xylX* or *vanA* locus of *C. crescentus* via single homologous recombination. To this end, the genes of interest were amplified with PCR using oligonucleotides containing restriction sites of pre-selected endonuclease at their 5' end. The size of the amplified product was confirmed with agarose gel electrophoresis, followed by its purification (Sigma-Aldrich, Germany). After restriction of both the insert and the vector backbone, and the product was used to transform competent cells, selection on the respective antibiotic and colony PCR for a final confirmation of integration into the desired locus.

pAZ1 Plasmid generated by PCR amplification of CC_1194 from pAM160 using primers 332f and 333r, cutting out *mCherry* of pXCHYC-2 by digestion with HindIII and XbaI, cutting the upstream region of CC_1194 out of pAM164 by restriction with XbaI and EcoRI, and ligation into HindIII and EcoRI-digested pNPTS138 vector.

pAZ7 Plasmid generated by PCR amplification of CCNA_03031 from CB15N chromosomal DNA using primers CCNA_03031f and CCNA_03031r, restricted with NdeI and EcoRI and ligated into NdeI and EcoRI-digested pXCHYC-2 vector.

pAZ8 Plasmid generated by PCR amplification of CCNA_00354 from CB15N chromosomal DNA using primers CCNA_00354f and CCNA_00354r, restricted with NdeI and EcoRI and ligated into NdeI and EcoRI-digested pXCHYC-2.

pAZ9 Plasmid generated by PCR amplification of CCNA_02863 from CB15N chromosomal DNA using primers CCNA_02863f and CCNA_02863r, restricted with NdeI and EcoRI and ligated into NdeI and EcoRI-digested pXCHYC-2.

pAZ14 Plasmid generated by PCR amplification of CC_1332 from CB15N chromosomal DNA using primers CC1332_271f and -272r, restrictied with NdeI and EcoRI and ligated into NdeI and EcoRI-digested pXTatCHYC-2.

pAZ15 Plasmid generated by PCR amplification of CC_2416 from CB15N chromosomal DNA using primers CC2416_273f and -274r, restricted with NdeI and EcoRI and ligated into NdeI and EcoRI-digested pXTatCHYC-2.

pAZ19 Plasmid generated by PCR amplification of CCNA_02661 from CB15N chromosomal DNA using primers CCNA_02661-f and CCNA_02661-r, restricted with NdeI and SacI and ligated into NdeI and SacI-digested pXCHYC-2.

pAZ20 Plasmid generated by PCR amplification of CCNA_00398 from CB15N chromosomal DNA using primers CCNA_00398-f and CCNA_00398-r, restricted with with NdeI and EcoRI and ligated into NdeI and EcoRI-digested pXCHYC-2.

pAZ23 Plasmid generated by PCR amplification of CCNA_02650 from CB15N chromosomal DNA using primers CCNA_02650-f and CCNA_02650-r, restricted with NdeI and EcoRI and ligated into NdeI and EcoRI-digested pXCHYC-2.

pAZ25 Plasmid generated by PCR amplification of CCNA_01579 from CB15N chromosomal DNA using primers CCNA_01579-f and CCNA_01579-r, restricted with NdeI and EcoRI and ligated into NdeI and EcoRI-digested pXCHYC-2.

pAZ29 Plasmid generated by PCR amplification of CCNA_03860 from CB15N chromosomal DNA using primers CCNA_03860-f and CCNA_03860-r, restricted with NdeI and EcoRI and ligated into NdeI and EcoRI-digested pXCHYC-2.

4.3.1.2 Construction of in-frame deletions based on pNPTS138 suicide vector

In-frame deletions of genes were generated by double homologues recombination using the suicide vector pNPTS138 (M.R.K. Alley, unpublished). In the first step, the upstream and downstream regions (450-600 bp each) of the target gene were PCR-amplified that contained the recognition sequences of selected restriction enzymes on their 5' end, which after digestion; enable triple ligation of the fragments into pre-digested pNPTS138 vector. The ligation product which carries a kanamycin resistance gene and the *sacB* gene for counter-selection was sequence-verified and used to transform electro-competent *C. crescentus* cells.

pAZ11 Plasmid generated by PCR amplification of upstream and downstream deletion regions of CCNA_00354 from CB15N chromosomal DNA using primers CCNA00354-1f/2r and CCNA00354-3f/4r, respectively. The upstream fragment was restricted with PstI and EcoRI, while the downstream fragment was restricted with EcoRI and NheI. Both fragments were ligated into PstI/NheI-digested pNPTS138.

pAZ12 Plasmid generated by PCR amplification of upstream and downstream deletion regions of CCNA_02863 from CB15N chromosomal DNA using primers CCNA02863-1f/2r and CCNA02863-3f/4r, respectively. The upstream fragment was restricted with HindIII and EcoRI, while the downstream fragment was restricted with EcoRI and NheI. Both fragments were ligated into HindIII/NheI-digested pNPTS138.

pAZ21 Plasmid generated by PCR amplification of upstream and downstream deletion regions of CCNA_02661 from CB15N chromosomal DNA using primers CCNA_2661-1/-2 and CCNA_02661-3/-4, respectively. The upstream fragment was restricted with MfeI and EcoRI, while the downstream fragment was restricted with with EcoRI and NheI. Both fragments were ligated into MfeI/NheI-digested pNPTS138.

pAZ22 Plasmid generated by PCR amplification of upstream and downstream deletion regions of CCNA_00398 from CB15N chromosomal DNA using primers CCNA_00398-1/-2 and CCNA_00398-3/-4, respectively. The upstream fragment was restricted with PstI and EcoRI, while the downstream fragment was restricted with EcoRI and NheI. Both fragments were ligated into PstI/NheI-digested pNPTS138.

pAZ24 Plasmid generated by PCR amplification of upstream and downstream deletion regions of CCNA_02650 from CB15N chromosomal DNA using primers CCNA_02650-1/-2 and CCNA_02661-3/-4, respectively. The upstream fragment was restricted with HindIII and EcoRI, while the downstream fragment was restricted with EcoRI and NheI. Both fragments were ligated into HindIII/NheI-digested pNPTS138.

pAZ26 Plasmid generated by PCR amplification of upstream and downstream deletion regions of CCNA_01579 from CB15N chromosomal DNA using primers CCNA_01579-1/-2 and CCNA_01579-3/4, respectively. The upstream fragment was restricted with PstI and EcoRI, while the downstream fragment was restricted with EcoRI and NheI. Both fragments were ligated into PstI/NheI-digested pNPTS138.

pAZ30 Plasmid generated by PCR amplification of upstream and downstream deletion regions of CCNA_03860 from CB15N chromosomal DNA using primers CCNA_03860-1/-2 and CCNA_03860-3/-4, respectively. The upstream fragment was restricted with HindIII and EcoRI, while the downstream fragment was restricted with EcoRI and NheI. Both fragments were ligated into HindIII/NheI-digested pNPTS138.

4.3.1.3 Construction of conditional C. *crescentus* mutants

To generate conditional mutants, non-replicating plasmids carrying the 5' region (400 – 600 bp) of the gene downstream of a short (123 bp) fragment containing the *vanA* promoter (Thanbichler et al, 2007) were integrated at the gene locus of selected *C. crescentus* strains. In this way, the native gene was truncated and a full-length version of the gene of interest was expressed from the *vanA* promoter in the presence of vanillate. The genotype was confirmed by PCR.

pAZ2 Plasmid generated by cutting *dipM* fragment (*dipM*$_{1-122aa}$) of pAM077 digested with NdeI/EcoRI and ligation into NdeI and EcoRI-digested pVMCS-4 vector.

pAZ3 Plasmid generated by cutting *sdpA* of pAM210 digested with NdeI/EcoRI and ligation into NdeI and EcoRI-digested pVCHYC-4 vector.

pAZ4 Plasmid generated by cutting *amiC* of pAM108 digested with NdeI/EcoRI and ligation into NdeI and EcoRI-digested pVCFPN-4 vector.

4.3.2   Polymerase chain reaction – PCR

The amplification of specific PCR fragments was performed using KOD Hot Start DNA Polymerase (Merck Milipore, Germany) together with the supplied reagents (Merck Milipore, Germany) and *C. crescentus* CB15 chromosomal DNA diluted 200 times, used as a template, described in Table 3

Colony PCR was performed as described in Table 4 using cells picked directly from the agar plate as a source of template DNA. In case of the strains grown on the plates supplemented with sucrose, cells were resuspended in 50 µl Tris-HCl (pH 7.5) and heated for 10 min at 95 °C, to avoid reaction inhibition. Next, 1 µl of the suspension was included in the PCR reaction.

In both cases, amplification of the desired genomic region was verified by agarose gel electrophoresis. Desired reaction products were purified with either the GeneElute™ PCR Clean-UpKit (Sigma-Aldrich, Germany) or the GeneElute™ Gel Extraction Kit (Sigma-Aldrich, Germany).

Table 3. Standard parameters for KOD polymerase PCR reactions.

REAGENT	CONCENTRATION	VOLUME [µl]	REACTION CONDITIONS		
			step	temperature [°C]	duration [min]
10xKOD Hot Start Polymerase buffer	1x	5	initial denaturation	94	3
MgSO$_4$	1 mM	2	denaturation	94	0.5
dNTPs	0.2 mM	5	annealing	62	0.5
DMSO	5 %	2.5	elongation	72	1 per 1kb
primers	0.5 µM	0.25 each			
KOD polymerase	2 units	0.5	final elongation	72	4
template	50-200 ng	1			
water	-	33.5	pause	12	∞

Table 4. Standard parameters for colony PCR reaction.

REAGENT	CONCENTRATION	VOLUME [µl]	REACTION CONDITIONS		
			step	temperature [°C]	duration [min]
Biomix™Red	1x	5	initial denaturation	94	3
			denaturation	94	0.5
DMSO	5 %	2.5	annealing	62	0.5
			elongation	72	1 per 1kb
primers	0.5 µM	0.25 each			
			final elongation	72	4
template	crude genomic DNA	1			
water	-	4.4	pause	12	∞

4.3.3   Agarose gel elecrophoresis

To purify or determine the size of DNA fragments the DNA solutions were mixed 1:6 with 6x DNA Loading dye (Thermo Scientific, Canada) if needed and applied to a 1 % agarose gel supplemented with 0.005 % ethidium bromide, using the GeneRuler™ 1kb Ladder (Thermo Scientific, Canada) as a size standard. Gels were prepared using 0.5 x TAE (20 mM Tris/HCl, pH 8, 0.175 % acetic acid, 0.5 mM EDTA,pH 8) as arunning buffer.The electrophoresis was performed at 160V for 20 min and DNA fragments were detected with a UV-Transilluminator (UVP-BioDoc-IT™ Imaging System, UniEquip, Germany).

4.3.4   Restriction digestion

The restriction of DNA fragments with suitable endonucleases (NEB, Germany; Thermo Scientific, Canada) was performed according to manufacturer's recommendations. 2-5 µg of DNA were digested for 2-12 hours at 37 °C. Reactions were supplemented with 0.1 mg/ml bovine serum albumine (BSA, NEB, Germany) if necessary. Dephosphorylation of the 5'-ends of linearized plasmid backbones was carried out using Shrimp Akaline Phosphatase (SAP or fastAP; Fermentas, Canada). The fragments were purified with either the GeneElute™ PCR Clean-Up Kit (Sigma-Aldrich, Germany) or the GeneElute™ Gel Extraction Kit (Sigma-Aldrich, Germany) after agarose gel electrophoresis.

4.3.5   Ligation

The ligation of DNA fragments was performed for 1-3 hours at RT using T4 DNA ligase (Thermo Scientific, Canada) at a molar ratio of 3:1 of the insert: recipient vector, in rapid ligation buffer (Thermo Scientific, Canada).

4.3.6   Plasmid DNA isolation

Plasmid DNA was isolated from *E. coli* using GenElute™ Plasmid Kit (Sigma-Aldrich, Germany) according to the manufacturer's instructions. The concentration and the purity of the samples were determined using a Nanodrop ND-1000 spectrophotometer (Nanodrop, USA).

4.3.7   DNA sequencing

DNA sequencing was performed by Eurofins MWG Operon (Germany). In general, 50-100 ng of DNA were provided along with suitable oligonucleotides. Sequencing results were analyzed using Vector NTI Advance™ 11 (Invitrogen, Germany).

4.3.8   Transformation of chemically competent *E. coli*

For transformation, 150 µl *E. coli* TOP10 (Invitrogen, Germany) or *E. coli* Rosetta(DE3)/pLysS (Merck Milipore, Germany) or 45 µl *E. coli* XL10 Gold competent cells were thawed on ice, mixed with 10 µl ligation mixture or 1-2 µl of isolated plasmid, and incubated on ice for 20 min. Subsequently, cells were heat-shocked at 42 °C for 45 sec, placed on ice for 2 min, and supplemented with 500 µl of LB (*E. coli* TOP10 and *E. coli* Rosetta(DE3)/pLysS) or 250 µl NZY+ medium (*E. coli* XL10 Gold) medium. The suspension was incubated at 37 °C for 1 hour with shaking at 200 rpm, followed by plating of 200 µl on LB/agar plates containing appropriate antibiotic.

4.3.9   Transformation of electrocompetent *C. crescentus*

For transformation, 80 µl of competent *C. crescentus* cells were mixed with 2-8 µl of isolated plasmid DNA (2 µl for replicative plasmids and 8 µl for integrating plasmids) and transferred to a precooled electroporation cuvette (Bio-Rad, Germany). Cells were transformed by an electric pulse at 1500 V, 800 W, and 25 µF (Gene Pulser Xcell, Bio-Rad, Germany) followed by addition of 900 µl cold, two fold concentrated PYE and incubation for 2-4 h at 28 °C with agitation at 220 rpm. After incubation, the cells were plated on selective medium and grown at 28 °C.

4.4   Microscopy

4.4.1   DIC and fluorescence microscopy

C. crescentus cells were analyzed microscopically at the mid-exponential phase of growth on 1 % agarose pads using an Axio Imager.M1 microscope (Zeiss, Germany), a Zeiss Plan Apochromat 100x/1.40 Oil DIC objective, and a Cascade:1K CCD camera (Photometrics, USA).
Fluorescence imaging was performed using an X-Cite®120PC metal halide light source (EXFO, Canada) in combination with ET-DAPI, ET-CFP (CFP), ET-YFP (eYFP), ET-GFP (eGFP) or ET-TexasRed (mCherry) filter cubes (Chroma, USA). Micrographs were processed with MetaMorph® 7.1.2 (Universal Imaging Group) and Adobe Illustrator CS5 and CS6. Cell lengths were measured using MetaMorph®. Unless indicated otherwise, the expression of fluorescent protein gene fusions under the control of the *vanA*

or *xylX* promoters in *C. crescentus* was induced during early-exponential phase with 0.5 mM vanillate or 0.3 % xylose for 2-3 h, respectively.

4.4.1.1   *In situ* probing with HADA/NADA

Staining of the *C. crescentus* cells was performed as described by Kuru et al., (2012). In brief, 250 µl of a cell culture in the exponential phase of growth were mixed with the fluorescent D-amino acids HADA (7-hydroxycoumarin 3-carboxylic acid conjugated with 3-amino-D-alanine, emission maximum of 450 nm, blue) or NADA (4-chloro-7-nitrobenzofurazan conjugated with 3-amino-D-alanine, emission maximum of 538 nm, green) to a final concentration of 0.5 mM and incubated for 1 min in 28 °C. Next, cells were fixed using ice cold ethanol in the final concentration of 70 % and incubated on ice for 20 min, followed with three steps washing (9000 rpm, RT, 2 min) in 500 µl PBS (137 mM NaCl, 2.7 mM KCl, 10 mM Na_2HPO_4, 2 mM KH_2PO_4. The resulting pellet was resuspended in 250 µl of PYE and analyzed immidiately.

4.4.1.2   BODIPY® staining

Staining of the outer membrane was performed using the fluorescent, sphingolipid dye BODIPY-FL-C12® (Molecular Probes, USA). In brief, 1 ml of a culture grown overnight was harvested (9000 rpm, 2 min, RT). The cells were resuspended in 300 µl Tris-HCl (pH 7.5), incubated on ice for 15 min, and mixed with BODIPY-FL-C12® to a final concentration of 50 µM. After 10 min incubation on ice, cells were analyzed using FITC filter.

4.4.1.3   DAPI staining

The bacterial nucleoid was stained with 0.5 µg/ml 4',6-diamidino-2-phenylindole (DAPI) for 15 min in the dark with shaking at 37 °C or 28 °C, respectively.

4.4.2   Time lapse microscopy

For time-lapse analysis, cells were transferred onto a 1 % agarose pad prepared in M2G medium, supplemented with inducer if necessary (Jacobs et al, 1999; Ryan et al, 2002). The edges of the cover glass and agarose pad were sealed with VLAP (1:1:1 Vaseline, lanolin and paraffin) to avoid evaporation of the liquids from the sample. Images were taken at defined timepoints for 8-24 hours.

4.4.3   Time course microscopy

For the time course microscopy, cell populations were synchronized (described in chapter 4.2.3), followed with microscopic analysis of the samples immobilized on the 1 % agarose pad at regular intervals.

4.4.4   Electron microscopy (EM)

Electron microscopy was performed by Dr. Katrin Bolte from the Faculty of Biology at the University of Marburg. Cells were applied onto carbon-coated grids, washed twice with distilled H_2O, and

contrasted with 2 % (w/v) uranyl acetate for 40 sec. Images were taken with a JEOL TEM 2100 operated at 80 kV using a fast-scan 2K x 2K CCD camera F214 (TVIPS, Gauting).

4.4.5 Cryo-Electron tomography (cryo-TEM)

Cryo-Electron tomography was performed by Dr. Ariane Briegel from the California Institute of Technology (USA). 2 ml of cell suspension were centrifuged for 5 min at 1500 x g, and the pellet was resuspended in 30–50 µl of the supernatant. A solution of 10-nm colloidal gold (Ted Pella, Redlands, CA) was added to the cells immediately before plunge freezing and after treatment with BSA to avoid aggregation of the gold particles (Iancu et al, 2006). A 4 µl droplet of the sample solution was transferred to a glow-discharged R2/2 copper/rhodium grid, then automatically blotted and plunge-frozen in liquid ethane or a liquid ethane/propane mixture (Tivol et al, 2008) using a Vitrobot (FEI Company, Hillsboro, OR). The grids were stored under liquid nitrogen until data collection. Images were acquired using the FEI Polara TM (FEI Company, Hillsboro, OR, USA) 300 kV FEG transmission electron microscope, equipped with a Gatan energy filter (slit width 20 eV) on a lens-coupled, cooled 4k x 4k Ultracam (Gatan, Pleasanton, CA). The pixel size on the specimen plane was 0.961 nm. Single-axis tilt series were recorded from -60 ° to 60 ° with an increment of 1 ° and an underfocus of 12 µm, using Leginon (Suloway et al, 2009). The cumulative dose was limited to 200 e/A2. Three-dimensional reconstructions were obtained using the IMOD software package (Mastronarde, 1997).

4.5 Biochemical methods

4.5.1 SDS-Polyacrylamide gel electrophoresis (SDS-PAGE)

SDS-PAGE to characterize protein levels was performed as described by (Laemmli, 1970). To this end, exponentially growing cells were pelleted and resuspended in 2x sodium dodecyl sulfate (SDS) sample buffer (125 mM Tris, 20 % (w/v) glycerol, 2 % (w/v) SDS, 0.05 % bromophenol blue, pH 6.8). The volume of added sample buffer was calculated based on the OD_{600} of the sample, with 1 ml of the culture being resuspended in 100 µl 2x sample buffer. The mixture was heated for 10 min at 95 °C and loaded on a polyacrylamide gel together with a molecular weight marker (PageRuler™ Prestained Protein Ladder, Fermentas, Canada). Samples of purified proteins were mixed with a sample buffer at a 1:10 ratio. The gels were composed out of a 5 % stacking and 11 % resolving gel (Table 5). Electrophoresis was performed in a Tris/Glycine buffer (25 mM Tris base, 192mM Glycine, 0.1 % SDS) at 20-30 mA per gel using a PerfectBlue™ Twin S system (Peqlab, USA). After electrophoresis, the proteins were either stained overnight in Coomassie blue (40 % methanol, 10 % acidic acid, 0.1 % (w/v) Brilliant Blue R 250) and destained in water to visualize proteins directly, or used for Western blot analysis.

4.5.2 Western blot analysis

Polyclonal antibodies against SdpA were generated by Eurogentec (Belgium) based on the purified SdpA used for the immunization of the rabbits.

Table 5. Composition of the gels used for SDS-PAGE.

COMPONENT	STACKING GEL 5 % 2.5 ml	RESOLVING GEL 11 % 5 ml
distilled water	1.43 ml	1.9 ml
4× stacking buffer (0.5 M Tris/HCl pH 6.8, 0.4 % (w/v) SDS)	625 µl	-
4× resolving buffer (1.5 M Tris/HCl pH 8.8, 0.4 % (w/v) SDS)	-	1.25 ml
30 % Rotiphorese® NR Acrylamide/Bis (29:1)	417 µl	1.9 ml
10 % w/v ammonium persulfat (APS)	25 µl	40 µl
TEMED (N,N,N',N'-Tetramethylethylenediamine)	1.9 µl	3 µl

For protein detection, specific samples were first separated by SDS-PAGE as described above, and next transferred onto polyvinylidene fluoride (PVDF) membrane (Millipore, USA) by a semi-dry transfer using a PerfectBlue™ Semi-Dry-Elektro Blotter (Peqlab, USA). To this end, PVDF membrane was activated by incubation in 100 % methanol for 15-20 sec and then washed with H_2O for 2 min. The membrane was next equilibrated in Western blot buffer (25 mM Tris, 192 mM glycine, 10 % methanol) for 10-30 min. The transfer onto the membrane was performed at 2 mA/cm² for 1.5-2 h. In the next step, the membrane was incubated in the solution containing 2.5-5% non-fat milk in 1× TBST buffer (10 mM Tris/HCl, pH 7.5, 150 mM NaCl, 0.1 % w/v Tween 20) to block non-specific interactions and incubated overnight with 40 rpm agitation at 4 °C. In the next step, the membrane was incubated with the primary antibody (Table 6) for 1.5 -3 h at RT with 50 rpm agitation and washed three times with 1× TBST buffer for 5 min. Subsequently, it was incubated with the anti-rabbit IgG conjugated with horseradish perioxidase (HRP) (Table 6), for another 1.5 -3 h at RT following with washing with 1×TBST buffer. For the detection of the proteins on the membrane Western Lightning™ Chemiluminescence Reagent Plus was used (Perkin Elmer, USA) according to the manufacturer's instruction and developed with a LAS-4000 Luminescent Image Analyzer (Fujifilm, Germany), with the exposure time adjusted to the strength and specificity of the interaction.

Table 6. Antibodies used for immunoblot analysis.

ANTIBODY	DILUTION	REFERENCE / COMMENTS
α-DipM	1: 20000	Möll *et.al*, 2010
α-SdpA	1: 2500	This work
α-CtrA	1: 10000	Domian *et al.*, 1997
α-RFP	1:10000	Chen *et al.*, 2005
α-His-HRP	1:4000	Abcam, United Kingdom
α-rabbit-HRP	1:20000	Perkin Elmer, USA
α-mCherry	1:10000	Biovision, USA

4.5.3   Coimmunoprecipitation (Co-IP) analysis

The *C. crescentus* strains SW59 (Δ*dipM* P*xyl*::P*xyl*-*dipM*) and tested AM409 (Δ*dipM* P*xyl*::P*xyl*-*dipM*-His10) were grown in 500 ml M2G medium to an OD_{600} of 0.45-0.6. Cells were incubated with formaldehyde, added to the cultures to a final concentration of 0.6 %, for 20 min at 37 °C. To terminate crosslinking

reaction, glycine was added to a final concentration of 125 mM, followed by incubation for 5 min at RT. Next, the suspension was centrifuged (6500 rpm, 4 °C for 10 min) and washed three times with ice-cold washing buffer (50 mM NaPO$_4$, pH 7.4, 5 mM MgCl$_2$). Cell pellets were weight and frozen at −80 °C. Afterwards, the cells were thawed on ice, washed and resuspended (with 100 ml and 2.5 ml/1 g of the cell pellet respectively) in Co-IP buffer (20 mM HEPES, pH 7.4, 100 mM NaCl, 0.5 % Triton X-100, 20 % Glycerine). The suspension was then supplemented with 10 mM MgCl$_2$, 10 mg/ml lysozyme, 10 U/ml DNaseI and 100 µg/ml PMSF and incubated for 30 min at 4 °C. Cells were disrupted through a French press (Thermo scientific, Canada) passages, followed with centrifugation for 5 min at 13000 rpm, 4 °C. The supernatant was aliquoted and frozen at -80 °C.

Magnetic beads were washed three times with either binding buffer 1 (20 mM Na$_2$HPO$_4$, pH 7.4, 500 mM NaCl, 10-60 mM imidazole) or binding/washing buffer 2 (20 mM Na$_2$HPO$_4$, pH 7.0, 300 mM NaCl). 0.5 – 1 ml of the respective lysate was mixed with 50 - 100 µl of the beads, and incubated at either RT or 4 °C with rotation for 1.5 – 3 hours. The mixture was washed three times with either binding buffer 1 or binding/washing buffer 2 and eluted with 100 µl elution buffer 1 (20 mM Na$_2$HPO$_4$, pH 7.4, 500 mM NaCl, 500 mM imidazole), 2 (pH 2-3, 100 mM glycine) or 3 (100 mM Tris, pH 12, 500 mM NaCl). After every step, 20 µl samples were collected and subjected to Western blot analysis.

4.5.4 Protein purification

Protein overproduction. To overproduce His-tagged CCNA_02152 (SdpA) *E. coli* Rosetta(DE3)/pLysS (Invitrogen) was transformed with pAM189 (P$_{IPTG}$-*sdpA*-His6) and cultivated at 37 °C in LB medium, supplemented with appropriate antibiotics to an OD$_{600}$ of 1.0. SdpA overproduction was induced for 3 h by addition of 0.5 mM IPTG. Next, cells were harvested by centrifugation (10 min at 6500 rpm, 4 °C), washed with 1/10 of the volume with lysis buffer (50 mM NaH$_2$PO$_4$, pH 8.0, 300 mM NaCl, 10 mM imidazole) and snap-frozen in liquid nitrogen.

Nickel affinity chromatography.
E. coli Rosetta(DE3)/pLysS cells were thawed an resuspended in lysis buffer supplemented with 100 µg/ml PMSF and 10 µg/ml DNaseI (2 ml / 1 g cell extract), and disrupted by two passages through a French press in at 16.000 psi. The lysate was centrifuged for 30 min at 16500 rpm and 4 °C. The supernatant was loaded on a His-Trap HP column, previously washed with 25 ml of water and equilibrated with 5 column volumes (CV) of wash buffer (50 mM NaH$_2$PO$_4$, pH 8.0, 300 mM NaCl, 20 mM imidazole). Next, loaded column was washed with 5CV wash buffer, followed with elution of the protein with linear imidazole gradient (20-250 mM) (50 mM NaH$_2$PO$_4$, pH 8.0, 300 mM NaCl, 250 mM imidazole) at 2 ml/min. After SDS-PAGE, fractions containing the desired protein were combined. The resulting protein solution was adjusted to 10 % glycerol, aliquoted and stored at -80 °C.

Protein concentrations were measured with the RotiNanoquant reagent (Carl-Roth, Germany), based on a modified Bradford assay (Bradford, 1976; Zor & Selinger, 1996).

Size exclusion chromatography. A protein sample was dialyzed overnight at 4 °C with gentle stirring, against dialysis buffer (50 mM NaH_2PO_4, pH 7.4, 150 mM NaCl, 5 mM $MgCl_2$). It was then loaded on a Superdex 75 GL10/300 column (GE Healthcare, Germany) equilibrated with dialysis buffer. The protein was eluted with 25 ml of dialysis buffer and 2 ml fractions were collected. SDS-PAGE analysis indicated samples containing the protein of interest. Appropriate fractions were pooled, supplemented with glycerol to final concentration of 10 %, frozen and stored at -80 °C.

4.5.5   High-performance liquid chromatography (HPLC)

The muropeptide profile of *C. crescentus* strains was analyzed by CeCo Labs (Tübingen, Germany). In brief, cell walls were isolated and treated with muraminidase digestion (5-10 mg of cell wall pro sample). Muropeptides were separated by HPLC using a 150 min linear gradient from 50 mM sodium phosphate buffer to 75 mM phosphate buffer in MeOH. The obtained peaks were analyzed by mass spetrometry.

4.6   Bioinformatic and statistical analyses

C. crescentus CB15N nucleotide and protein sequences were obtained from the National Center for Biotechnology Information (NCBI) (http://www.ncbi.nlm.nih.gov/). Sequences were compared and analyzed with either the NCBI Blastn-, Blastp-algorithm, or at the EMBL SMART (http://smart.embl-heidelberg.de/). Predictions for the transmembrane domains, signal peptides or subcellular protein localization were obtained using TOPCONS (www.topcons.cbr.su.se/), TMHMM and SignalP (www.cbs.dtu.dk/services/). Conserved domains of proteins were identified using the NCBI website (http://www.ncbi.nlm.nih.gov/). Sequence alignments were conducted by Clustal Omega (www.ebi.ac.uk/Tools/msa/clustalo), and the alignment results were analyzed by GeneDoc (Informer Technologies, Inc.)**.** Protein modeling was based on I-TASSER (University of Michigan, USA) prediction and graphically modified in PyMOL (Schrödinger Inc., USA).

Statystical analyses were performed using MetaMorph 7.1.2 (Universal Imaging Group) and visualized with QtiPlot® (IONDEV SLR, Romania).

MATERIALS AND METHODS

APPENDIX

Table S 1. *C. crescentus* strains.

NAME	GENOTYPE	REFERENCE / SOURCE
CB15N	Wild-type *C. crescentus* strain	Evinger and Agabian, 1977
AM52	CB15N Δ*vanA* Δ*ftsN* P*van*::P*van*-*ftsN*	Möll and Thanbichler, 2009
AM338	CB15N Δ*amiC*	Möll, 2011
AM364	CB15N Δ*ldpA*	Möll, 2011
AM365	CB15N Δ*ldpB*	Möll, 2011
AM366	CB15N Δ*ldpC*	Möll, 2011
AM369	CB15N Δ*ldpF*	Möll, 2011
AM370	CB15N Δ*ldpD*	Möll, 2011
AM371	CB15N Δ*ldpE*	Möll, 2011
AM383	CB15N Δ*ldpAB*	Möll, 2011
AM399	CB15N Δ*sdpA*	Möll, 2011
AM400	CB15N Δ*sdpC*	Möll, 2011
AM409	CB15N Δ*dipM* P*xyl*::P*xyl*-*dipM*-his10	Andrea Möll, unpublished
AM418	CB15N Δ*sdpB*	Möll, 2011
AM419	CB15N Δ*sdpAB*	Möll, 2011
AM438	CB15N Δ*ldpABCDE*	Möll, 2011
AM439	CB15N Δ*ldpABC*	Möll, 2011
AM440	CB15N Δ*sdpABC*	Möll, 2011
AM448	CB15N Δ*ldpABCD*	Möll, 2011
AM480	CB15N P*xyl*::P*xyl*-*sdpA*-*mCherry*	Möll, 2011
AZ11	CB15N P*xyl*::P*xyl*-*sdpB*-*mCherry*	Homologous recombination of pAM161 in CB15N
AZ12	CB15N P*xyl*::P*xyl*-*sdpC*-*mCherry*	Homologous recombination of pAM162 in CB15N
AZ28	CB15N Δ*sdpAC*	Double-homologous recombination of pAM162 in AM339
AZ29	CB15N Δ*sdpBC*	Double-homologous recombination of pAM162 in AM400
AZ35	CB15N P*dipM*::P*van*-*dipM*	Homologous recombination of pAZ2 in CB15N
AZ38	CB15N Δ*amiC* P*dipM*::P*van*-*dipM*	Homologous recombination of pAZ2 in AM338
AZ39	CB15N Δ*amiC* Δ*dipM*	Double-homologous recombination of pMT814 in AM338
AZ41	CB15N Δ*sdpABC* P*dipM*::P*van*-*dipM*	Homologous recombination of pAZ2 in AM440

APPENDIX

NAME	GENOTYPE	REFERENCE / SOURCE
AZ42	CB15N Δ*sdpABC* P$_{van}$-amiC	Homologous recombination of pAZ3 in AM440
AZ45	CB15N P$_{sdpA}$-*sdpA-mCherry*	Homologous recombination of pAZ1 in CB15N
AZ46	CB15N Δ*ftsN* P$_{van}$::P$_{van}$–*ftsN* P$_{xyl}$–*sdpA*–*mCherry*	Homologous recombination of pAM210 in AM52
AZ52	CB15N Δ*ldpABCDEF*	Double-homologous recombination of pAM157 in AM438
AZ57	CB15N Δ*sdpABC* pP$_{xyl}$-*torA′*-tdimer2	Transformation of AM440 with pEJ216
AZ58	CB15N Δ*ftsZ* P$_{xyl}$::P$_{xyl}$–*ftsZ* P$_{van}$::P$_{van}$–*sdpA*–*mCherry*	Homologous recombination of pAZ4 in YB1585
AZ63	CB15N Δ*sdpABC* P$_{xyl}$::P$_{xyl}$ -*venus-tolA*	Homologous recombination of pMT948 in AM440
AZ64	CB15N Δ*ldpABCDEF* P$_{xyl}$::P$_{xyl}$ –*sdpA-mCherry*	Homologous recombination of pAM210 in AZ52
AZ65	CB15N Δ*ldpABCDEF* P$_{dipM}$::P$_{van}$-*dipM*	Homologous recombination of pAZ2 in AZ52
AZ66	CB15N Δ*ldpABCDEF* P$_{van}$-amiC	Homologous recombination of pAZ3 in AZ52
AZ67	CB15N Δ*dipM* P$_{xyl}$::P$_{xyl}$–*sdpA*–*mCherry*	Homologous recombination of pAM210 in MT258
AZ70	CB15N Δ*ldpABCDEF* Δ*sdpC*	Double-homologous recombination of pAM166 in AZ52
AZ71	CB15N Δ*ldpABCDEF* Δ*sdpA*	Double-homologous recombination of pAM164 in AZ52
AZ73	CB15N Δ*ldpABCDEF* Δ*sdpAC*	Double-homologous recombination of pAM164 in AZ70
AZ74	CB15N Δ*ldpABCDEF* Δ*sdpBC*	Double-homologous recombination of pAM165 in AZ70
AZ80	CB15N P$_{xyl}$::P$_{xyl}$– *nlpA* – *mCherry*	Homologous-recombination of pAZ7 in CB15N
AZ81	CB15N P$_{xyl}$::P$_{xyl}$– *chap* – *mCherry*	Homologous-recombination of pAZ8 in CB15N
AZ82	CB15N P$_{xyl}$::P$_{xyl}$– *nlpB*– *mCherry*	Homologous-recombination of pAZ9 in CB15N
AZ85	CB15N Δ*nlpB*	Double homologous-recombination of pAZ12 in CB15N
AZ86	CB15N Δ*chap*	Double homologous-recombination of pAZ11 in CB15N
AZ89	CB15N Δ*nlpAB*	Double homologous-recombination of pAZ11 in AZ85
AZ91	CB15N Δ*ldpBF*	Double homologous-recombination of pAM157in AM365
AZ93	CB15N Δ*sdpABC* Δ*pleA*	Homologous recombination of pHPV120 in AM440
AZ96	CB15N pP$_{xyl}$-*tdimer2*	Transformation of CB15N with pEJ216
AZ97	CB15N Δ*amiC* pP$_{xyl}$-*tdimer2*	Transformation of AM338 with pEJ216
AZ98	CB15N Δ*ldpABCDEF* pP$_{xyl}$-*tdimer2*	Transformation of AZ52 with pEJ216
AZ99	CB15N Δ*ldpBF* P$_{dipM}$::P$_{van}$-*dipM*	Homologous recombination of pAZ2 in AZ91
AZ100	CB15N Δ*ldpACDE* P$_{dipM}$::P$_{van}$-*dipM*	Homologous recombination of pAZ2 in AM448
AZ111	CB15N P$_{xyl}$::P$_{xyl}$-CCNA_02661-*mCherry*	Homologous recombination of pAZ19 in CB15N

NAME	GENOTYPE	REFERENCE / SOURCE
AZ120	CB15N Δ*nlpA* Δ*chap*	Double-homologous recombination of pAZ11 in AZ167
AZ121	CB15N Δ*nlpB* Δ*chap*	Double-homologous recombination of pAZ12 in AZ167
AZ127	CB15N P$_{xyl}$::P$_{xyl}$-*torA-sdpB-mCherry*	Homologous-recombination of pAZ14 in CB15N
AZ129	CB15N P$_{xyl}$::P$_{xyl}$- *mta2 – mCherry*	Homologous-recombination of pAZ23 in CB15N
AZ130	CB15N P$_{xyl}$::P$_{xyl}$- *mtyD – mCherry*	Homologous-recombination of pAZ25 in CB15N
AZ132	CB15N ΔCCNA_00398	Double-homologous recombination of pAZ22 in CB15N
AZ137	CB15N Δ*mtyD*	Double-homologous recombination of pAZ26 in CB15N
AZ138	CB15N Δ*mtyD* Δ*ykuD*	Double-homologous recombination of pAZ30 in AZ137
AZ140	CB15N Δ*ykuD*	Double-homologous recombination of pAZ30 in CB15N
AZ144	CB15N Δ*ldpB* P$_{dipM}$::P$_{van}$-*dipM*	Single-homologous recombination of pAZ2 in AM365. (generated by Katharina Kremer)
AZ145	CB15N Δ*ldpF* P$_{dipM}$::P$_{van}$-*dipM*	Single-homologous recombination of pAZ2 in AM369. (generated by Katharina Kremer)
AZ164	CB15N Δ*mbtAB* Δ*mtyD*	Double-homologous recombination of pAZ26 in MAB251
AZ165	CB15N Δ*amiC* Δ*chap*	Double-homologous recombination of pAZ11 in AM338
AZ165	CB15N Δ*amiC* Δ*chap*	Double-homologous recombination of pAZ11 in AM338
AZ166	CB15N Δ*ami* Δ*ldpF*	Double-homologous recombination of pAM157 in AM338
AZ167	CB15N Δ*nlpA*	Double-homologous recombination of pMAB62 in CB15N
CS606	CB15N Δ*blaM*	West *et al.*, (2002)
MAB233	CB15N Δ*mbtB*	Maria Billini, unpublished
MAB239	CB15N Δ*mbtA*	Maria Billini, unpublished
MAB250	CB15N Δ*nlpAB* Δ*chap*	Maria Billini, unpublished
MAB251	CB15N Δ*mbtAB*	Maria Billini, unpublished
MT196	CB15N P$_{van}$:: P$_{van}$-*yfp-ftsZ*	Martin Thanbichler, unpublished
MT248	CB15N P$_{xyl}$::P$_{xyl}$-*amiC-mCherry*	Möll *et al.*, 2010
MT289	CB15N P$_{xyl}$::P$_{xyl}$-*venus-tolA*	Martin Thanbichler, unpublished
MT46	CB15N P$_{van}$::P$_{van}$-*ftsN-egfp*	Möll and Thanbichler, 2009
NR1371	CB15N Δ*bla* P$_{xyl}$::P$_{xyl}$-*tipN-gfp*	Huitema *et al.*, 2006

NAME	GENOTYPE	REFERENCE / SOURCE
SW59	CB15N Δ*dipM* P$_{xyl}$::P$_{xyl}$-*dipM*	Möll *et al.*, 2010
SS255	CB15N P$_{xyl}$::P$_{xyl}$-*gfp-fzlC*	Susan Schlimpert, unpublished
YB1585	CB15N P$_{ftsZ}$::P$_{xyl}$-*ftsZ*	Wang *et al.*, 2001

Table S 2. Plasmids used in this work.

PLASMIDS	DESCRIPTION	REFERENCE / SOURCE
pEJ216	Replicating plasmid carrying TAT-dimer2 under control of P$_{xyl}$, Cam^R	Judd *et al.*, 2005
pNPTS138	*sacB*-containing suicide vector used for double homologous recombination, Kan^R	M.R.K Alley, unpublished
pVMCS-4	Integrating plasmid for generating depletion strains encoded in *vanA* locus, Gent^R	Thanbichler *et al.*, 2007
pVCFPN-4	Plasmid for integrating genes encoding N-terminal fusion to the blue fluorescent protein CFP at the *vanA* locus, Gent^R	Thanbichler *et al.*, 2007
pVCHYC-4	Plasmid for integrating genes encoding C-terminal fusion to the red fluorescent protein mCherry at the *vanA* locus, Gent^R	Thanbichler *et al.*, 2007
pBXMCS-2	Replicating plasmid for generating inducible overexpression of genes in CB15N, Kan^R	Thanbichler *et al.*, 2007
pXCHYC-2	Plasmid for integrating genes encoding C-terminal fusions to the red fluorescent protein mCherry at the *xylX* locus, Kan^R	Thanbichler *et al.*, 2007
pVCHYC-2	Plasmid for integrating genes encoding C-terminal fusions to the red fluorescent protein mCherry at the *vanA* locus, Kan^R	Thanbichler *et al.*, 2007
pXTaTCHYC-2	Plasmid for integrating genes encoding C-terminal fusion to the red fluorescent protein mCherry with *torA^{ss}*	This study
pAM077	pXCHYC-2 carrying *dipM* $_{1-122aa}$ instead of *mCherry*	Möll, 2011
pAM108	pBXMCS-2 harboring *amiC*	Möll, 2011
pAM157	pNPTS138-based deletion-construct for *ldpF*	Möll, 2011
pAM161	pXCHYC-2 harboring *sdpB*	Möll, 2011
pAM162	pXCHYC-2 harboring *sdpC*	Möll, 2011
pAM164	pNPTS138-based deletion -construct for *sdpA*	Möll, 2011
pAM165	pNPTS138-based deletion -construct for *sdpB*	Möll, 2011
pAM166	pNPTS138-based deletion -construct for *sdpC*	Möll, 2011
pAM210	pXCHYC-2 harboring *sdpA*	Möll, 2011
pAM189	pET28a+ harboring *sdpA* $_{24-695aa}$	This study
pAZ1	pNPTS138 harboring *sdpA*	This study

PLASMIDS	DESCRIPTION	REFERENCE / SOURCE
pAZ2	pVMCS-4 harboring *dipM* $_{1\text{-}122aa}$	This study
pAZ3	pVCFPN-4 harboring *amiC*	This study
pAZ4	pVCHYC-4 harboring *sdpA*	This study
pAZ7	pXCHYC-2 harboring *nlpA*	This study
pAZ8	pXCHYC-2 harboring *chap*	This study
pAZ9	pXCHYC-2 harboring *nlpB*	This study
pAZ11	pNPTS138-based deletion -construct for *chap*	This study
pAZ12	pNPTS138-based deletion -construct for *nlpB*	This study
pAZ14	pXTatCHYC-2 harboring *sdpB*	This study
pAZ19	pXCHYC-2 harboring CCNA_02661	This study
pAZ20	pXCHYC-2 harboring CCNA_00398	This study
pAZ22	pNPTS138-based deletion -construct for CCNA_00398	This study
pAZ23	pNPTS138-based deletion -construct for CCNA_02661	This study
pAZ25	pXCHYC-2 harboring *mtyD*	This study
pAZ26	pNPTS138-based deletion -construct for *mtyD*	This study
pAZ30	pNPTS138-based deletion -construct for *ykuD*	This study
pMAB62	pNPTS138-based deletion -construct for *nlpA*	Maria Billini, unpublished
pMT814	pNPTS138-based deletion -construct for *dipM*	Möll et al., 2010
pMT948	pXVENN-1 harboring *tolA*	Martin Thanbichler, unpublished

Table S 3. General primers used for colony PCR.

LABEL	SEQUENCE 5'-3'
IntSpec-1 (RecUni-1)	atgccgtttgtgatggcttccatgtcg
IntXyl-2 (RecXyl-2)	tcttccggcaggaattcactcacgcc
M13for	gccagggttttcccagtcacga
M13rev	gagcggataacaatttcacacagg
PvanA-for	gacgtccgtttgattacgatcaagattgg
Pxyl-1	cccacatgttagcgctaccaagtgc
Pxyl-for	tgtcggcggcttctagcatggaccg
Pvan-for	tggactctagccgaccgactgagacgc
mCherry-up	ctcgccctcgccctcgatctcgaac
mCherry-down	ggcgcctacaacgtcaacatcaagttgg

APPENDIX

LABEL	SEQUENCE 5'-3'
REV-uni	ggggatgtgctgcaaggcgattaagttg
(IntVan-2) RecVan-2	cagccttggccacggtttcggtacc
pET-rev	cctttcagcaaaaaacccctcaagacccg
tdimer2-up	ggcggtctgggtgccctcgtag

Table S 4. Primers used for the generation of the strains.

NUMBER	LABEL	SEQUENCE 5'-3'
281	CC1194_281f	tttttgctagcacggccagcgcccagccttaagcg
282	CC1194_282r	tagaattcaggcttgtgggctacatgccgcagg
332	CC1194_332fr	ataaagcttccgctgctggaccaccatttcacgc
333	CC1194_332fr	aggtaccaggctgggcgctggccgtctcgg
(AZ)9	CCNA_03031f	ttttcatatgagcgcgtccgaccgccg
(AZ)10	CCNA_03031r	tagaattccgaacccgccgataccccagca
(AZ)11	CCNA_00354f	ttttcatatgcggcggccggagcgtgata
(AZ)12	CCNA_00354r	tagaattccggcgcggcgcggtcggcttg
(AZ)13	CCNA_02863f	ttttcatatgagcggcggggggcgcgcaatc
(AZ)14	CCNA_02863r	tagaattccggcctgaggtgcgcgctcctgagc
(AZ)15	CCNA_03031-1f	tataaagcttgcaataccgacgctgaaggccgc
(AZ)16	CCNA_03031-2r	taggatcctcggaccagggtgaggcggcg
(AZ)17	CCNA_03031-3f	taggatccacgggcggggtgctggggtat
(AZ)18	CCNA_03031-4r	tatagctagctgtctcgggcacgaacatgac
(AZ)19	CCNA_00354-1f	tactgcaggcgctgcgtatcgtgccgtgc
(AZ)20	CCNA_00354-2r	tagaattcaaaagagtgtttatcacgctc
(AZ)21	CCNA_00354-3f new	tagaattccccaacaacaagccgaccgcg
(AZ)22	CCNA_00354-4r new	tatagctagcaggcaggcgccgcgcatgtcg
(AZ)23	CCNA_02863-1f	tataaagcttcggcggctggagtcccggcgc
(AZ)24	CCNA_02863-2r	tagaattcggattgcgcgcccccgccgct
(AZ)25	CCNA_02863-3f	tagaattctcaggagcgcgcacctcaggctga
(AZ)26	CCNA_02863-4r	tatagctagccggccgatcccgtcgatcggg
(AZ)27	CCNA_03031-5f	taggatccggtgctggggtatcggcgggt

NUMBER	LABEL	SEQUENCE 5'-3'
(AZ)28	CCNA_03031-6r	tatagctagccgaccacctgtatgaattcct
(AZ)29	sfGFP-1	tagaattcatgagcaaaggagaagaact
(AZ)30	sfGFP-2	tatagctagctaaggatcctttgtagagctcat
(AZ)31	sf-GFP-f overhang	tatcaccggtcggccaccatgagcaaaggagaagaact
(AZ)32	sf-GFP-r	tatagctagcttaggatcctttgtagagctcat
(AZ)33	CCNA_03031 Nested-f	gcaagggtgtggtgttcgac
(AZ)34	CCNA_03031 Nested-r	cccgactggaacgccgtgct
(AZ)42	CCNA_03031f ko-nested new	cggcgatgacctcttgaa
(AZ)43	CCNA_03031r ko nested new	atcgcggtccaggaagaaag
(AZ)44	PleA-ko-1f	gcgaagagcggtggcggtgt
(AZ)45	PleA-ko-4r	ggccgctggatctgcttgct
(AZ)46	CCNA_03031f ko-nested new	cggcgatgacctcttgaa
(AZ)47	CCNA_03031r ko nested new	atcgcggtccaggaagaaag
(AZ)48	CCNA_02661-f	ttttcatatgggggagcgccctcctagcg
(AZ)49	CCNA_02661-r	tttgagctcgtttcgcaggattgccgtc
(AZ)50	CCNA_00398-f	ttttcatatgtatcccatgaggcctttcg
(AZ)51	CCNA_00398-r	tagaattccgggccttcggcttgttggtcg
(AZ)52	CCNA_02661-1	tatcaattgccctgatgttgcccgaccgg
(AZ)53	CCNA_02661-2	tagaattccttcatagtcattcccgct
(AZ)54	CCNA_02661-3	Tagaattccggatcatcgacgctgacgg
(AZ)55	CCNA_02661-4	tatagctagcggccgaccgtggacaagaagg
(AZ)56	CCNA_00398-1	tactgcagggccgatatggtccggatgc
(AZ)57	CCNA_00398-2	tagaattccgcgagggcggccgtcaggc
(AZ)58	CCNA_00398-3	tagaattcaagctgccgaccaacaagccg
(AZ)59	CCNA_00398-4	tatagctagcgtggcctgtccggaccgcaag
(AZ)60	CCNA_02650-f	ttttcatatgagcctgtccctgatcgag
(AZ)61	CCNA_02650-r	tagaattcgcgtcggccgccgcccgca
(AZ)62	CCNA_02650-1	tataaagcttcgcctcgtgggcctgctgcgg
(AZ)63	CCNA_02650-2	tagaattcgccgcgcaggagcccgtcgaa
(AZ)64	CCNA_02650-3	tagaattcagctgtcggcgggtctctgg
(AZ)65	CCNA_02650-4	tatagctagcgggcgacggggcctcgatca

NUMBER	LABEL	SEQUENCE 5'-3'
(AZ)66	CCNA_02650 deletion check-f	gcgcggtggtggtgatgtgga
(AZ)67	CCNA_02650 deletion check up-r	atcgctgtcggccttgttctg
(AZ)68	CCNA_01579-f	ttttcatatggtgatgcgatttacgagaac
(AZ)69	CCNA_01579-r	tagaattccggagtgcggcgatacgctgcaccag
(AZ)70	CCNA_01579-1	tactgcagaagaagaaggccatcaagtc
(AZ)71	CCNA_01579-2	tagaattcggcgccgcaggttctcgtaaa
(AZ)72	CCNA_01579-3	tagaattccgtgatctggtgcagcgtat
(AZ)73	CCNA_01579-4	tatagctagctggaacggccccttgctctg
(AZ)74	CCNA_02661-1 rev	tatagctagcccctgatgttgcccgaccgg
(AZ)75	CCNA_02661-4 rev	tatcaattgggccgaccgtggacaagaagg
(AZ)76	CCNA_01579-1 rev	tatagctagcaagaagaaggccatcaagtc
(AZ)77	CCNA_01579-4 rev	tactgcagtggaacggccccttgctctg
(AZ)78	pAZ28 inside-f	gccgcgccgacatcctgctg
(AZ)79	pAZ28 inside-r	tcaccatctaattcaacaag
(AZ)80	CCNA_03860-f	ttttcatatgctgtttcgagcccatg
(AZ)81	CCNA_03860-r	tagaattccggtccgcgagaatctggacg
(AZ)82	CCNA_03860-1	tataaagcttgcggaacggcttggtcacat
(AZ)83	CCNA_03860-2	tagaattcgcggccgtcagcatgggctc
(AZ)84	CCNA_03860-3	tagaattccccggcgacgccgtccagatt
(AZ)85	CCNA_03860-4	tatagctagccgtgaggcggtcggcttttt
(AZ)90	CCNA_02650 Ami_2-r	tactgcaggcccggatcgatcttgcg
(AZ)91	CCNA_00354-f shorter	tatggtaccatgacgaaacggacgaggaccc
(AZ)92	CCNA_00354-r shorter	tagaattcttagcgcggcgcggtcgg
(AZ)93	LysM QVR1-2PDGYK - rev	tagaattcgccttgtagccgtcgggcagaa
(AZ)94	pAZ37-f	gtcgaagtcgcgggcaagcc
(AZ)95	pAZ37 pAZ38-r	cggcgtgaagcgctgacccga
(AZ)96	pAZ38-r	ggcaagccccaggtgggtac
(AZ)97	CC_3434-r	tagaattcgcctatcgcgactcctgtttgagc
(AZ)98	CCNA_02650-STOP-rev	tagaattctcagtcggccgccgcccgca

Table S 5. Potential DipM interaction partners identified via Co-IP using Ni-magnetic beads (relevant hits).

NR.	PROTEIN NAME	ACCESION NR	MASS [kDa]	PEPTIDE COUNT	SCORE
1	peptidoglycan-specific endopeptidase, M23 family [*Caulobacter crescentus* NA1000]	gi|220964184|gb| ACL95540.1|	63.03	19	1822
22	cytochrome c oxidase polypeptide II coxB [*Caulobacter crescentus* NA1000]	gi|220965627|gb| ACL96983.1|	35.55	2	143
26	conserved hypothetical protein [*Caulobacter crescentus* NA1000]	gi|220962844|gb| ACL94200.1|	19.61	1	125
34	SSU ribosomal protein S6P [*Caulobacter crescentus* NA1000]	gi|220963850|gb| ACL95206.1|	14.56	2	112
36	pyruvate dehydrogenase complex, dihydrolipoamide acetyltransferase component [*Caulobacter crescentus*]	gi|220963912|gb| ACL95268.1|	43,98	2	104
39	phosphoribosylamidoimidazole-succinocarboxamide synthase [*Caulobacter crescentus* NA1000]	gi|220964685|gb| ACL96041.1|	28.6	2	95
42	3-oxoacyl-(acyl-carrier protein) reductase [*Caulobacter crescentus* NA1000]	gi|220963856|gb| ACL95212.1|	24.99	1	84
44	SSU ribosomal protein S1P [*Caulobacter crescentus* NA1000]	gi|220965811|gb| ACL97167.1|	62.06	2	79
45	ferric uptake regulation protein [*Caulobacter crescentus* NA1000]	gi|220962166|gb| ACL93522.1|	15.87	1	78
46	vitamin B12 receptor [*Caulobacter crescentus* NA1000]	gi|220963935|gb| ACL95291.1|	69.31	1	75
48	TonB-dependent outer membrane receptor [*Caulobacter crescentus* NA1000]	gi|220965217|gb| ACL96573.1|	121.76	1	73
51	hypothetical protein CCNA_00635 [*Caulobacter crescentus* NA1000]	gi|220962744|gb| ACL94100.1|	60.77	2	69
52	methyl-accepting chemotaxis protein [*Caulobacter crescentus* NA1000]	gi|220962550|gb| ACL93906.1|	70.83	1	69
58	UDP-N-acetylmuramoylalanyl-D-glutamate--2, 6-diaminopimelate ligase [*Caulobacter crescentus* NA1000]	gi|220964751|gb| ACL96107.1|	49.96	2	56

Table S 6. Potential DipM interaction partners identified via Co-IP using α-His conjugated magnetic beads (relevant hits).

NR.	PROTEIN NAME	ACCESION NR	MASS [kDa]	PEPTIDE COUNT	SCORE
1	peptidoglycan-specific endopeptidase, M23 family [*Caulobacter crescentus* NA1000]	gi|220964184|gb |ACL95540.1	63.03	22	2342
4	conserved hypothetical protein [*Caulobacter crescentus* NA1000]	gi|220962844|gb |ACL94200.1	19.61	1	121
5	hypothetical protein CCNA_00398 [*Caulobacter crescentus* NA1000]	gi|220962509|gb |ACL93865.1	46.4	1	83
9	peptidase, M16 family [*Caulobacter crescentus* NA1000]	gi|220964770|gb |ACL96126.1	100.3	2	57

Table S 7. Putative PG hydrolases in *C. crescentus*.

NAME	NUMBER CC	CCNA	PREDICTED ACTIVITY	LENGTH [aa]	SIZE [kDa]	ESSENTIALITY BASED ON Christen et. al 2011
ENDOPEPTIDASES						
DipM	CC_1996	CCNA_02075	peptidoglycan binding endopeptidase DipM	609	63.1	YES
LdpA	CC_1872	CCNA_01948	M23 family peptidoglycan-specific endopeptidase	383	41.2	NO
LdpB	CC_2248	CCNA_02331	peptidoglycan-specific endopeptidase, M23 family	266	26.9	NO
LdpC	CC_2297	CCNA_02382	membrane peptidase, M23 family	298	31	NO
LdpD	CC_3034	CCNA_03129	peptidoglycan-specific endopeptidase, M23 family	458	49.4	NO
LdpE	CC_3301	CCNA_03410	peptidoglycan-specific endopeptidase, M23 family	222	23.2	NO
LdpF	CC_3434	CCNA_03547	peptidoglycan-specific endopeptidase, M23 family	351	37.8	HIGH FITNESS COSTS
NlpC/P60 CHAP						
NlpA	CC_2936	CCNA_03031	gamma-D-glutamyl-meso-diaminopimelate peptidase	279	30.6	HIGH FITNESS COSTS
Chap	CC_0349	CCNA_00354	CHAP domain containing	235	24.9	YES
NlpB	CC_2775	CCNA_02863	Spr-family cell wall-associated hydrolase	206	22.1	NO
SOLUBLE LYTIC TRANSGLYCOSYLASES						
SdpA	CC_1194	CCNA_01252	soluble lytic murein transglycosylase	699	75.1	HIGH FITNESS COSTS
SdpB	CC_1332	CCNA_01393	soluble lytic murein transglycosylase	536	58	NO
SdpC	CC_2416	CCNA_02498	YjbJ-related lytic transglycosylase	218	23	NO
MEMBRANE BOUND LYTIC TRANSGLYCOSYLASES						
MbtA	CC_3740	CCNA_03856	membrane-bound lytic murein transglycosylase A	395	41.1	NO
MbtB	CC_3322	CCNA_03431	membrane-bound lytic murein transglycosylase B	433	46.1	NO
MtyD	CC_1511	CCNA_1579	cell wall degradation protein	502	54.7	NO
Mta2	CC_2567	CCNA_2650	anhydro-N-acetylmuramyl-tripeptide amidase	242	26.4	HIGH FITNESS COSTS
AMIDASES						
AmiC	CC_1876	CCNA_01952	N-acetylmuramoyl-L-alanine amidase	395	421	YES
L,D-TRANSPEPTIDASES (YkuD)						
MtyD	CC_1511	CCNA_1579	cell wall degradation protein	502	54.7	NO
YkuD	CC_3744	CCNA_3860	conserved hypothetical protein	169	18.3	NO

Figure S1. Set of putative PG hydrolases in *C. crescentus*. Schematic representation of lytic transglycosylases (LTs), amidases, endopeptidases (EP) and L,D-transpeptidases (LD-TP) based on SMART analyses (Schultz *et al.*, 1998).
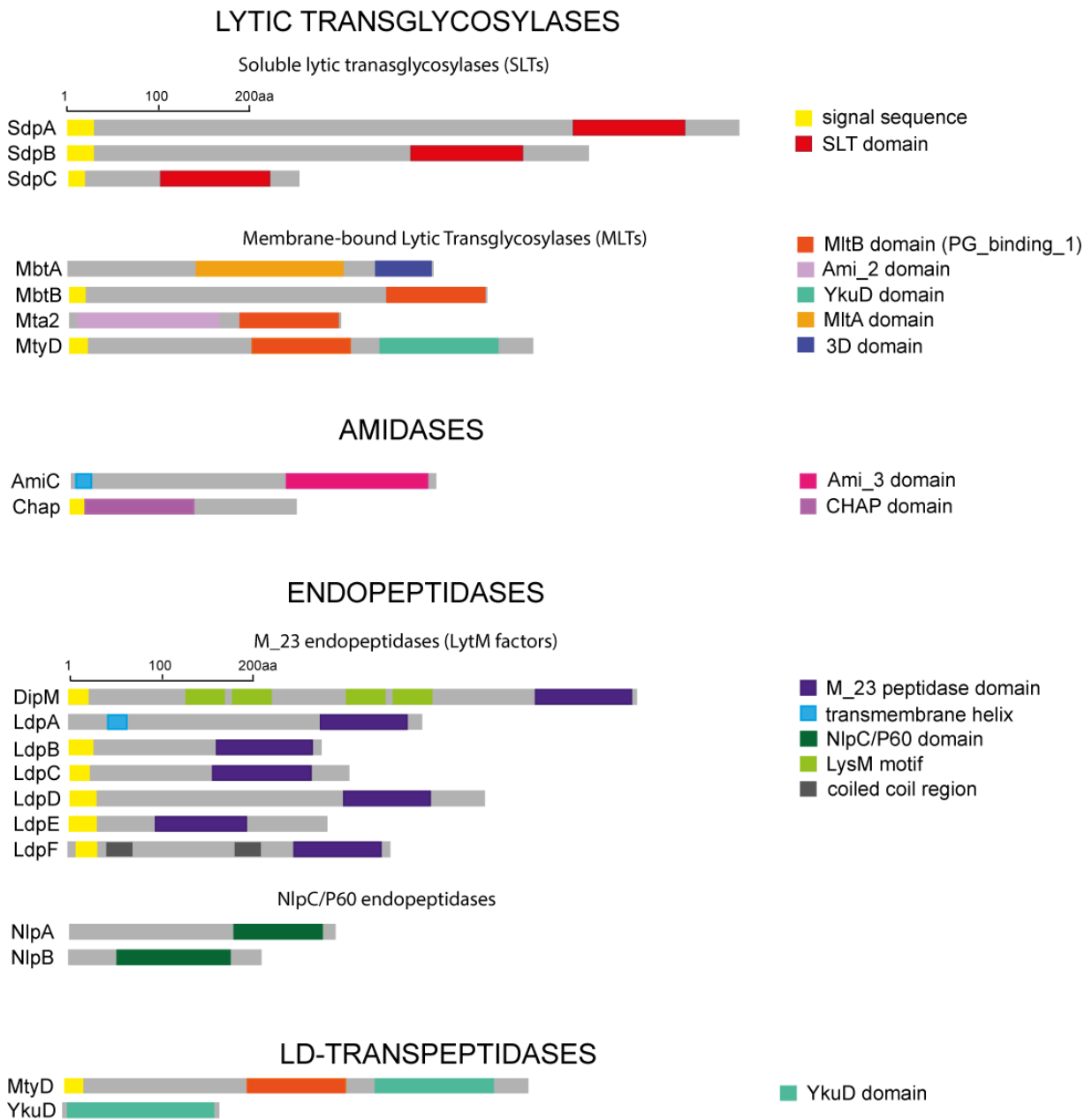
REFERENCES

Aaron, M., Charbon, G., Lam, H., Schwarz, H., Vollmer, W. & Jacobs-Wagner, C. (2007). The tubulin homologue FtsZ contributes to cell elongation by guiding cell wall precursor synthesis in *Caulobacter crescentus*. *Mol Microbiol* **64**, 938-952.

Aarsman, M. E. G., Piette, A., Fraipont, C., Vinkenvleugel, T. M. F., Nguyen-Disteche, M. & den Blaauwen, T. (2005). Maturation of the *Escherichia coli* divisome occurs in two steps. *Mol Microbiol* **55**, 1631-1645.

Adam, M., Fraipont, C., Rhazi, N. & other authors (1997). The bimodular G57-V577 polypeptide chain of the class B penicillin-binding protein 3 of Escherichia coli catalyzes peptide bond formation from thiolesters and does not catalyze glycan chain polymerization from the lipid II intermediate. *J Bacteriol* **179**, 6005-6009.

Addinall, S. G., Cao, C. & Lutkenhaus, J. (1997). FtsN, a late recruit to the septum in *Escherichia coli*. *Mol Microbiol* **25**, 303-309.

Allan, E. J., Hoischen, C. & Gumpert, J. (2009). Bacterial L-forms. *Adv Appl Microbiol* **68**, 1-39.

Anantharaman, V. & Aravind, L. (2003). Evolutionary history, structural features and biochemical diversity of the NlpC/P60 superfamily of enzymes. *Genome Biology* **4**.

Aramini, J. M., Rossi, P., Huang, Y. J. & other authors (2008). Solution NMR structure of the NlpC/P60 domain of lipoprotein Spr from *Escherichia coli:* structural evidence for a novel cysteine peptidase catalytic triad. *Biochemistry* **47**, 9715-9717.

Artola-Recolons, C., Llarrull, L. I., Lastochkin, E., Mobashery, S. & Hermoso, J. A. (2011). Crystallization and preliminary X-ray diffraction analysis of the lytic transglycosylase MltE from *Escherichia coli*. *Acta Crystallogr Sect F Struct Biol Cryst Commun* **67**, 161-163.

Atrih, A., Zollner, P., Allmaier, G. & Foster, S. J. (1996). Structural analysis of *Bacillus subtilis* 168 endospore peptidoglycan and its role during differentiation. *J Bacteriol* **178**, 6173-6183.

Aussel, L., Barre, F. X., Aroyo, M., Stasiak, A., Stasiak, A. Z. & Sherratt, D. (2002). FtsK Is a DNA motor protein that activates chromosome dimer resolution by switching the catalytic state of the XerC and XerD recombinases. *Cell* **108**, 195-205.

Baba, T. & Schneewind, O. (1998). Targeting of muralytic enzymes to the cell division site of Gram-positive bacteria: repeat domains direct autolysin to the equatorial surface ring of *Staphylococcus aureus*. *EMBO J* **17**, 4639-4646.

Baba, T., Ara, T., Hasegawa, M. & other authors (2006). Construction of *Escherichia coli* K-12 in-frame, single-gene knockout mutants: the Keio collection. *Mol Syst Biol* **2**, 2006 0008.

Barendt, S. M., Land, A. D., Sham, L. T., Ng, W. L., Tsui, H. C. T., Arnold, R. J. & Winkler, M. E. (2009). Influences of Capsule on Cell Shape and Chain Formation of Wild-Type and pcsB Mutants of Serotype 2 *Streptococcus pneumoniae*. *Journal of Bacteriology* **191**, 3024-3040.

Barreteau, H., Kovac, A., Boniface, A., Sova, M., Gobec, S. & Blanot, D. (2008). Cytoplasmic steps of peptidoglycan biosynthesis. *FEMS Microbiol Rev* **32**, 168-207.

Bartual, S. G., Straume, D., Stamsas, G. A., Munoz, I. G., Alfonso, C., Martinez-Ripoll, M., Havarstein, L. S. & Hermoso, J. A. (2014). Structural basis of PcsB-mediated cell separation in *Streptococcus pneumoniae*. *Nat Commun* **5**, 3842.

Bateman, A. & Bycroft, M. (2000). The structure of a LysM domain from *E. coli* membrane-bound lytic murein transglycosylase D (MltD). *J Mol Biol* **299**, 1113-1119.

Bateman, A. & Rawlings, N. D. (2003). The CHAP domain: a large family of amidases including GSP amidase and peptidoglycan hydrolases. *Trends Biochem Sci* **28**, 234-237.

Bernadac, A., Gavioli, M., Lazzaroni, J. C., Raina, S. & Lloubes, R. (1998). *Escherichia coli* tol-pal mutants form outer membrane vesicles. *J Bacteriol* **180**, 4872-4878.

Bernard, C. S., Sadasivam, M., Shiomi, D. & Margolin, W. (2007). An altered FtsA can compensate for the loss of essential cell division protein FtsN in *Escherichia coli*. *Mol Microbiol* **64**, 1289-1305.

Bernhardt, T. G. & de Boer, P. A. J. (2003). The *Escherichia coli* amidase AmiC is a periplasmic septal ring component exported via the twin-arginine transport pathway. *Molecular Microbiology* **48**, 1171-1182.

Bertsche, U., Kast, T., Wolf, B. & other authors (2006). Interaction between two murein (peptidoglycan) synthases, PBP3 and PBP1B, in *Escherichia coli*. *Mol Microbiol* **61**, 675-690.

Beveridge, T. J. (1999). Structures of gram-negative cell walls and their derived membrane vesicles. *J Bacteriol* **181**, 4725-4733.

Bisicchia, P., Noone, D., Lioliou, E., Howell, A., Quigley, S., Jensen, T., Jarmer, H. & Devine, K. M. (2007). The essential YycFG two-component system controls cell wall metabolism in *Bacillus subtilis*. *Mol Microbiol* **65**, 180-200.

Biteen, J. S., Goley, E. D., Shapiro, L. & Moerner, W. E. (2012). Three-dimensional super-resolution imaging of the midplane protein FtsZ in live *Caulobacter crescentus* cells using astigmatism. *Chemphyschem* **13**, 1007-1012.

Blackburn, N. T. & Clarke, A. J. (2001). Identification of four families of peptidoglycan lytic transglycosylases. *J Mol Evol* **52**, 78-84.

Bochtler, M., Odintsov, S. G., Marcyjaniak, M. & Sabala, I. (2004). Similar active sites in lysostaphins and D-Ala-D-Ala metallopeptidases. *Protein Sci* **13**, 854-861.

Bodenmiller, D., Toh, E. & Brun, Y. V. (2004). Development of surface adhesion in *Caulobacter crescentus*. *J Bacteriol* **186**, 1438-1447.

Born, P., Breukink, E. & Vollmer, W. (2006). In vitro synthesis of cross-linked murein and its attachment to sacculi by PBP1A from *Escherichia coli*. *J Biol Chem* **281**, 26985-26993.

Bouhss, A., Trunkfield, A. E., Bugg, T. D. & Mengin-Lecreulx, D. (2008). The biosynthesis of peptidoglycan lipid-linked intermediates. *FEMS Microbiol Rev* **32**, 208-233.

Braun, V. (1973). Molecular organization of the rigid layer and the cell wall of *Escherichia coli*. *J Infect Dis* **128**, Suppl:9-16.

Brown, P. J., de Pedro, M. A., Kysela, D. T., Van der Henst, C., Kim, J., De Bolle, X., Fuqua, C. & Brun, Y. V. (2012). Polar growth in the Alphaproteobacterial order *Rhizobiales*. *Proc Natl Acad Sci U S A* **109**, 1697-1701.

Buddelmeijer, N., Judson, N., Boyd, D., Mekalanos, J. J. & Beckwith, J. (2002). YgbQ, a cell division protein in *Escherichia coli* and Vibrio cholerae, localizes in codependent fashion with FtsL to the division site. *Proceedings of the National Academy of Sciences of the United States of America* **99**, 6316-6321.

Buddelmeijer, N. & Beckwith, J. (2004). A complex of the *Escherichia coli* cell division proteins FtsL, FtsB and FtsQ forms independently of its localization to the septal region. *Mol Microbiol* **52**, 1315-1327.

Buist, G., Steen, A., Kok, J. & Kuipers, O. P. (2008). LysM, a widely distributed protein motif for binding to (peptido)glycans. *Mol Microbiol* **68**, 838-847.

Burman, L. G. & Park, J. T. (1984). Molecular-Model for Elongation of the Murein Sacculus of *Escherichia coli*. *Proceedings of the National Academy of Sciences of the United States of America-Biological Sciences* **81**, 1844-1848.

Busiek, K. K. & Margolin, W. (2014). A role for FtsA in SPOR-independent localization of the essential *Escherichia coli* cell division protein FtsN. *Mol Microbiol* **92**, 1212-1226.

Cameron, T. A., Anderson-Furgeson, J., Zupan, J. R., Zik, J. J. & Zambryski, P. C. (2014). Peptidoglycan synthesis machinery in *Agrobacterium tumefaciens* during unipolar growth and cell division. *MBio* **5**, e01219-01214.

Caparros, M., Torrecuadrada, J. L. & de Pedro, M. A. (1991). Effect of D-amino acids on *Escherichia coli* strains with impaired penicillin-binding proteins. *Res Microbiol* **142**, 345-350.

Carballido-Lopez, R., Formstone, A., Li, Y., Ehrlich, S. D., Noirot, P. & Errington, J. (2006). Actin homolog MreBH governs cell morphogenesis by localization of the cell wall hydrolase LytE. *Dev Cell* **11**, 399-409.

Carson, M. J., Barondess, J. & Beckwith, J. (1991). The FtsQ protein of *Escherichia coli*: membrane topology, abundance, and cell division phenotypes due to overproduction and insertion mutations. *J Bacteriol* **173**, 2187-2195.

Cascales, E., Bernadac, A., Gavioli, M., Lazzaroni, J. C. & Lloubes, R. (2002). Pal lipoprotein of *Escherichia coli* plays a major role in outer membrane integrity. *J Bacteriol* **184**, 754-759.

Cava, F., Lam, H., de Pedro, M. A. & Waldor, M. K. (2011). Emerging knowledge of regulatory roles of D-amino acids in bacteria. *Cell Mol Life Sci* **68**, 817-831.

Chen, J. C. & Beckwith, J. (2001). FtsQ, FtsL and FtsI require FtsK, but not FtsN, for co-localization with FtsZ during *Escherichia coli* cell division. *Mol Microbiol* **42**, 395-413.

Chen, J. C., Viollier, P. H. & Shapiro, L. (2005). A membrane metalloprotease participates in the sequential degradation of a *Caulobacter* polarity determinant. *Mol Microbiol* **55**, 1085-1103.

Cheng, Q., Li, H., Merdek, K. & Park, J. T. (2000). Molecular characterization of the beta-N-acetylglucosaminidase of *Escherichia coli* and its role in cell wall recycling. *J Bacteriol* **182**, 4836-4840.

Christen, B., Abeliuk, E., Collier, J. M., Kalogeraki, V. S., Passarelli, B., Coller, J. A., Fero, M. J., McAdams, H. H. & Shapiro, L. (2011). The essential genome of a bacterium. *Mol Syst Biol* **7**, 528.

Cloud-Hansen, K. A., Peterson, S. B., Stabb, E. V., Goldman, W. E., McFall-Ngai, M. J. & Handelsman, J. (2006). Breaching the great wall: peptidoglycan and microbial interactions. *Nat Rev Microbiol* **4**, 710-716.

Cohen, D. N., Sham, Y. Y., Haugstad, G. D., Xiang, Y., Rossmann, M. G., Anderson, D. L. & Popham, D. L. (2009). Shared catalysis in virus entry and bacterial cell wall depolymerization. *J Mol Biol* **387**, 607-618.

Costa, T., Priyadarshini, R. & Jacobs-Wagner, C. (2008). Localization of PBP3 in *Caulobacter crescentus* is highly dynamic and largely relies on its functional transpeptidase domain. *Molecular Microbiology* **70**, 634-651.

Craig, M., Sadik, A. Y., Golubeva, Y. A., Tidhar, A. & Slauch, J. M. (2013). Twin-arginine translocation system (tat) mutants of *Salmonella* are attenuated due to envelope defects, not respiratory defects. *Mol Microbiol* **89**, 887-902.

Curtis, P. D. & Brun, Y. V. (2010). Getting in the loop: regulation of development in *Caulobacter crescentus*. *Microbiol Mol Biol Rev* **74**, 13-41.

Dai, K., Xu, Y. F. & Lutkenhaus, J. (1993). Cloning and Characterization of Ftsn, an Essential Cell-Division Gene in *Escherichia coli* Isolated as a Multicopy Suppressor of Ftsa12(Ts). *Journal of Bacteriology* **175**, 3790-3797.

Daniel, R. A. & Errington, J. (2000). Intrinsic instability of the essential cell division protein FtsL of *Bacillus subtilis* and a role for DivIB protein in FtsL turnover. *Mol Microbiol* **36**, 278-289.

de Boer, P. A., Crossley, R. E. & Rothfield, L. I. (1989). A division inhibitor and a topological specificity factor coded for by the minicell locus determine proper placement of the division septum in *E. coli*. *Cell* **56**, 641-649.

de Boer, P. A. (2010). Advances in understanding *E. coli* cell fission. *Curr Opin Microbiol* **13**, 730-737.

de Jonge, R., van Esse, H. P., Kombrink, A. & other authors (2010). Conserved fungal LysM effector Ecp6 prevents chitin-triggered immunity in plants. *Science* **329**, 953-955.

de Leeuw, E., Graham, B., Phillips, G. J., ten Hagen-Jongman, C. M., Oudega, B. & Luirink, J. (1999). Molecular characterization of *Escherichia coli* FtsE and FtsX. *Mol Microbiol* **31**, 983-993.

de Pedro, M. A., Holtje, J. V. & Schwarz, H. (2002). Fast lysis of *Escherichia coli* filament cells requires differentiation of potential division sites. *Microbiology* **148**, 79-86.

de Pedro, M. A., Young, K. D., Holtje, J. V. & Schwarz, H. (2003). Branching of *Escherichia coli* cells arises from multiple sites of inert peptidoglycan. *J Bacteriol* **185**, 1147-1152.

Demchick, P. & Koch, A. L. (1996). The permeability of the wall fabric of *Escherichia coli* and *Bacillus subtilis*. *J Bacteriol* **178**, 768-773.

Den Blaauwen, T., Aarsman, M. E., Vischer, N. O. & Nanninga, N. (2003). Penicillin-binding protein PBP2 of *Escherichia coli* localizes preferentially in the lateral wall and at mid-cell in comparison with the old cell pole. *Mol Microbiol* **47**, 539-547.

den Blaauwen, T., de Pedro, M. A., Nguyen-Disteche, M. & Ayala, J. A. (2008). Morphogenesis of rod-shaped sacculi. *FEMS Microbiol Rev* **32**, 321-344.

Derouiche, R., Benedetti, H., Lazzaroni, J. C., Lazdunski, C. & Lloubes, R. (1995). Protein complex within *Escherichia coli* inner membrane. TolA N-terminal domain interacts with TolQ and TolR proteins. *J Biol Chem* **270**, 11078-11084.

Doerrler, W. T. (2006). Lipid trafficking to the outer membrane of Gram-negative bacteria. *Mol Microbiol* **60**, 542-552.

Domian, I. J., Quon, K. C. & Shapiro, L. (1997). Cell type-specific phosphorylation and proteolysis of a transcriptional regulator controls the G1-to-S transition in a bacterial cell cycle. *Cell* **90**, 415-424.

Duncan, T. R., Yahashiri, A., Arends, S. J., Popham, D. L. & Weiss, D. S. (2013). Identification of SPOR domain amino acids important for septal localization, peptidoglycan binding, and a disulfide bond in the cell division protein FtsN. *J Bacteriol* **195**, 5308-5315.

Duong, F., Eichler, J., Price, A., Leonard, M. R. & Wickner, W. (1997). Biogenesis of the gram-negative bacterial envelope. *Cell* **91**, 567-573.

Durand-Heredia, J., Rivkin, E., Fan, G., Morales, J. & Janakiraman, A. (2012). Identification of ZapD as a cell division factor that promotes the assembly of FtsZ in *Escherichia coli*. *J Bacteriol* **194**, 3189-3198.

Egan, A. J. & Vollmer, W. (2013). The physiology of bacterial cell division. *Ann N Y Acad Sci* **1277**, 8-28.

Egan, A. J., Jean, N. L., Koumoutsi, A. & other authors (2014). Outer-membrane lipoprotein LpoB spans the periplasm to stimulate the peptidoglycan synthase PBP1B. *Proc Natl Acad Sci U S A* **111**, 8197-8202.

Ely, B. (1991a). Genetics of *Caulobacter crescentus*. *Methods Enzymol* **204**, 372-384.

Ely, B. (1991b). Genetics of Caulobacter-Crescentus. *Methods in Enzymology* **204**, 372-384.

Ercoli, G., Tani, C., Pezzicoli, A. & other authors (2015). LytM proteins play a crucial role in cell separation, outer membrane composition, and pathogenesis in nontypeable *Haemophilus influenzae*. *MBio* **6**, e02575.

Erickson, H. P., Anderson, D. E. & Osawa, M. (2010). FtsZ in bacterial cytokinesis: cytoskeleton and force generator all in one. *Microbiol Mol Biol Rev* **74**, 504-528.

Errington, J. (2015). Bacterial morphogenesis and the enigmatic MreB helix. *Nat Rev Microbiol*.

Evinger, M. & Agabian, N. (1977). Envelope-associated nucleoid from *Caulobacter crescentus* stalked and swarmer cells. *J Bacteriol* **132**, 294-301.

Fan, D. P. (1970). Autolysin(S) of *Bacillus subtilis* as Dechaining Enzyme. *Journal of Bacteriology* **103**, 494-&.

Figge, R. M., Divakaruni, A. V. & Gober, J. W. (2004). MreB, the cell shape-determining bacterial actin homologue, co-ordinates cell wall morphogenesis in *Caulobacter crescentus*. *Mol Microbiol* **51**, 1321-1332.

Fraipont, C., Alexeeva, S., Wolf, B., van der Ploeg, R., Schloesser, M., den Blaauwen, T. & Nguyen-Disteche, M. (2011). The integral membrane FtsW protein and peptidoglycan synthase PBP3 form a subcomplex in *Escherichia coli*. *Microbiology-Sgm* **157**, 251-259.

Gan, L., Chen, S. & Jensen, G. J. (2008). Molecular organization of Gram-negative peptidoglycan. *Proc Natl Acad Sci U S A* **105**, 18953-18957.

Garcia, D. L. & Dillard, J. P. (2006). AmiC functions as an N-acetylmuramyl-l-alanine amidase necessary for cell separation and can promote autolysis in *Neisseria gonorrhoeae*. *J Bacteriol* **188**, 7211-7221.

Geissler, B., Elraheb, D. & Margolin, W. (2003). A gain-of-function mutation in ftsA bypasses the requirement for the essential cell division gene zipA in *Escherichia coli*. *Proc Natl Acad Sci U S A* **100**, 4197-4202.

Gerding, M. A., Ogata, Y., Pecora, N. D., Niki, H. & de Boer, P. A. J. (2007). The trans-envelope Tol-Pal complex is part of the cell division machinery and required for proper outer-membrane invagination during cell constriction in *E. coli*. *Molecular Microbiology* **63**, 1008-1025.

Gerding, M. A., Liu, B., Bendezu, F. O., Hale, C. A., Bernhardt, T. G. & de Boer, P. A. J. (2009). Self-Enhanced Accumulation of FtsN at Division Sites and Roles for Other Proteins with a SPOR Domain (DamX, DedD, and RlpA) in *Escherichia coli* Cell Constriction. *Journal of Bacteriology* **191**, 7383-7401.

Ghigo, J. M. & Beckwith, J. (2000). Cell division in *Escherichia coli*: Role of FtsL domains in septal localization, function, and oligomerization. *Journal of Bacteriology* **182**, 116-129.

Glauner, B. (1988). Separation and quantification of muropeptides with high-performance liquid chromatography. *Anal Biochem* **172**, 451-464.

Glauner, B., Holtje, J. V. & Schwarz, U. (1988). The composition of the murein of *Escherichia coli*. *J Biol Chem* **263**, 10088-10095.

Goehring, N. W. & Beckwith, J. (2005). Diverse paths to midcell: assembly of the bacterial cell division machinery. *Curr Biol* **15**, R514-526.

Goley, E. D., Comolli, L. R., Fero, K. E., Downing, K. H. & Shapiro, L. (2010a). DipM links peptidoglycan remodelling to outer membrane organization in *Caulobacter*. *Mol Microbiol* **77**, 56-73.

Goley, E. D., Dye, N. A., Werner, J. N., Gitai, Z. & Shapiro, L. (2010b). Imaging-based identification of a critical regulator of FtsZ protofilament curvature in *Caulobacter*. *Mol Cell* **39**, 975-987.

Goley, E. D., Yeh, Y. C., Hong, S. H., Fero, M. J., Abeliuk, E., McAdams, H. H. & Shapiro, L. (2011). Assembly of the *Caulobacter* cell division machine. *Mol Microbiol* **80**, 1680-1698.

Gonzalez, M. D. & Beckwith, J. (2009). Divisome under construction: distinct domains of the small membrane protein FtsB are necessary for interaction with multiple cell division proteins. *J Bacteriol* **191**, 2815-2825.

Gonzalez, M. D., Akbay, E. A., Boyd, D. & Beckwith, J. (2010). Multiple interaction domains in FtsL, a protein component of the widely conserved bacterial FtsLBQ cell division complex. *J Bacteriol* **192**, 2757-2768.

Goodell, E. W., Lopez, R. & Tomasz, A. (1976). Suppression of lytic effect of beta lactams on *Escherichia coli* and other bacteria. *Proc Natl Acad Sci U S A* **73**, 3293-3297.

Goodell, E. W. & Schwarz, U. (1985). Release of cell wall peptides into culture medium by exponentially growing *Escherichia coli*. *J Bacteriol* **162**, 391-397.

Gray, A. N., Egan, A. J., Van't Veer, I. L. & other authors (2015). Coordination of peptidoglycan synthesis and outer membrane constriction during *Escherichia coli* cell division. *Elife* **4**.

Gueiros-Filho, F. J. & Losick, R. (2002). A widely conserved bacterial cell division protein that promotes assembly of the tubulin-like protein FtsZ. *Genes Dev* **16**, 2544-2556.

Hale, C. A. & deBoer, P. A. J. (1997). Direct binding of FtsZ to ZipA, an essential component of the septal ring structure that mediates cell division in *E. coli*. *Cell* **88**, 175-185.

Hale, C. A., Shiomi, D., Liu, B., Bernhardt, T. G., Margolin, W., Niki, H. & de Boer, P. A. (2011). Identification of *Escherichia coli* ZapC (YcbW) as a component of the division apparatus that binds and bundles FtsZ polymers. *J Bacteriol* **193**, 1393-1404.

Haney, S. A., Glasfeld, E., Hale, C., Keeney, D., He, Z. & de Boer, P. (2001). Genetic analysis of the *Escherichia coli* FtsZ.ZipA interaction in the yeast two-hybrid system. Characterization of FtsZ residues essential for the interactions with ZipA and with FtsA. *J Biol Chem* **276**, 11980-11987.

Hantke, K. & Braun, V. (1973). Covalent Binding of Lipid to Protein - Diglyceride and Amide-Linked Fatty-Acid at N-Terminal End of Murein-Lipoprotein of *Escherichia coli* Outer Membrane. *European Journal of Biochemistry* **34**, 284-296.

Hashimoto, M., Ooiwa, S. & Sekiguchi, J. (2012). Synthetic lethality of the *lytE cwlO* genotype in *Bacillus subtilis* is caused by lack of D,L-endopeptidase activity at the lateral cell wall. *J Bacteriol* **194**, 796-803.

Heidrich, C., Templin, M. F., Ursinus, A., Merdanovic, M., Berger, J., Schwarz, H., de Pedro, M. A. & Holtje, J. V. (2001). Involvement of N-acetylmuramyl-L-alanine amidases in cell separation and antibiotic-induced autolysis of *Escherichia coli*. *Mol Microbiol* **41**, 167-178.

Heidrich, C., Ursinus, A., Berger, J., Schwarz, H. & Holtje, J. V. (2002). Effects of multiple deletions of murein hydrolases on viability, septum cleavage, and sensitivity to large toxic molecules in *Escherichia coli*. *Journal of Bacteriology* **184**, 6093-6099.

Hobot, J. A., Carlemalm, E., Villiger, W. & Kellenberger, E. (1984). Periplasmic Gel - New Concept Resulting from the Reinvestigation of Bacterial-Cell Envelope Ultrastructure by New Methods. *Journal of Bacteriology* **160**, 143-152.

Hocking, J., Priyadarshini, R., Takacs, C. N., Costa, T., Dye, N. A., Shapiro, L., Vollmer, W. & Jacobs-Wagner, C. (2012). Osmolality-dependent relocation of penicillin-binding protein PBP2 to the division site in *Caulobacter crescentus*. *J Bacteriol* **194**, 3116-3127.

Holden, S. J., Pengo, T., Meibom, K. L., Fernandez Fernandez, C., Collier, J. & Manley, S. (2014). High throughput 3D super-resolution microscopy reveals *Caulobacter crescentus* in vivo Z-ring organization. *Proc Natl Acad Sci U S A* **111**, 4566-4571.

Holtje, J. V., Mirelman, D., Sharon, N. & Schwarz, U. (1975). Novel type of murein transglycosylase in *Escherichia coli*. *J Bacteriol* **124**, 1067-1076.

Holtje, J. V., Kopp, U., Ursinus, A. & Wiedemann, B. (1994). The negative regulator of beta-lactamase induction AmpD is a N-acetyl-anhydromuramyl-L-alanine amidase. *FEMS Microbiol Lett* **122**, 159-164.

Holtje, J. V. (1995). From growth to autolysis: the murein hydrolases in *Escherichia coli*. *Arch Microbiol* **164**, 243-254.

Holtje, J. V. (1998). Growth of the stress-bearing and shape-maintaining murein sacculus of *Escherichia coli*. *Microbiol Mol Biol Rev* **62**, 181-203.

Horsburgh, G. J., Atrih, A. & Foster, S. J. (2003). Characterization of LytH, a differentiation-associated peptidoglycan hydrolase of *Bacillus subtilis* involved in endospore cortex maturation. *Journal of Bacteriology* **185**, 3813-3820.

Huitema, E., Pritchard, S., Matteson, D., Radhakrishnan, S. K. & Viollier, P. H. (2006). Bacterial birth scar proteins mark future flagellum assembly site. *Cell* **124**, 1025-1037.

Ichimura, T., Yamazoe, M., Maeda, M., Wada, C. & Hiraga, S. (2002). Proteolytic activity of YibP protein in *Escherichia coli*. *J Bacteriol* **184**, 2595-2602.

Iwaya, M. & Strominger, J. L. (1977). Simultaneous deletion of D-alanine carboxypeptidase IB-C and penicillin-binding component IV in a mutant of *Escherichia coli* K12. *Proc Natl Acad Sci U S A* **74**, 2980-2984.

Ize, B., Stanley, N. R., Buchanan, G. & Palmer, T. (2003). Role of the *Escherichia coli* Tat pathway in outer membrane integrity. *Mol Microbiol* **48**, 1183-1193.

Jacobs, C., Huang, L. J., Bartowsky, E., Normark, S. & Park, J. T. (1994). Bacterial cell wall recycling provides cytosolic muropeptides as effectors for beta-lactamase induction. *EMBO J* **13**, 4684-4694.

Jacobs, C., Joris, B., Jamin, M. & other authors (1995). AmpD, essential for both beta-lactamase regulation and cell wall recycling, is a novel cytosolic N-acetylmuramyl-L-alanine amidase. *Mol Microbiol* **15**, 553-559.

Jacobs, C., Frere, J. M. & Normark, S. (1997). Cytosolic intermediates for cell wall biosynthesis and degradation control inducible beta-lactam resistance in gram-negative bacteria. *Cell* **88**, 823-832.

Jean, N. L., Bougault, C. M., Egan, A. J., Vollmer, W. & Simorre, J. P. (2015). Solution NMR assignment of LpoB, an outer-membrane anchored Penicillin-Binding Protein activator from *Escherichia coli*. *Biomol NMR Assign* **9**, 123-127.

Johnson, J. W., Fisher, J. F. & Mobashery, S. (2013). Bacterial cell-wall recycling. *Ann N Y Acad Sci* **1277**, 54-75.

Journet, L., Rigal, A., Lazdunski, C. & Benedetti, H. (1999). Role of TolR N-terminal, central, and C-terminal domains in dimerization and interaction with TolA and tolQ. *J Bacteriol* **181**, 4476-4484.

Judd, E. M., Comolli, L. R., Chen, J. C., Downing, K. H., Moerner, W. E. & McAdams, H. H. (2005). Distinct constrictive processes, separated in time and space, divide *Caulobacter* inner and outer membranes. *J Bacteriol* **187**, 6874-6882.

Kajimura, J., Fujiwara, T., Yamada, S. & other authors (2005). Identification and molecular characterization of an N-acetylmuramyl-L-alanine amidase Sle1 involved in cell separation of *Staphylococcus aureus*. *Mol Microbiol* **58**, 1087-1101.

Katsui, N., Tsuchido, T., Hiramatsu, R., Fujikawa, S., Takano, M. & Shibasaki, I. (1982). Heat-induced blebbing and vesiculation of the outer membrane of *Escherichia coli*. *J Bacteriol* **151**, 1523-1531.

Kerff, F., Petrella, S., Mercier, F. & other authors (2010). Specific structural features of the N-acetylmuramoyl-L-alanine amidase AmiD from *Escherichia coli* and mechanistic implications for enzymes of this family. *J Mol Biol* **397**, 249-259.

Klieneberger, E. (1935). The natural occurrence of pleuropneumonia-like organisms in apparent symbiosis with *Streptobacillus moniliformis* and other bacteria. *Journal of Pathology and Bacteriology* **40**, 93-105.

Koch, A. L., Higgins, M. L. & Doyle, R. J. (1981). Surface tension-like forces determine bacterial shapes: *Streptococcus faecium*. *J Gen Microbiol* **123**, 151-161.

Koch, A. L. (1983). The surface stress theory of microbial morphogenesis. *Adv Microb Physiol* **24**, 301-366.

Koch, A. L. (1990). Additional arguments for the key role of "smart" autolysins in the enlargement of the wall of gram-negative bacteria. *Res Microbiol* **141**, 529-541.

Koch, A. L. & Woeste, S. (1992). Elasticity of the sacculus of *Escherichia coli*. *J Bacteriol* **174**, 4811-4819.

Koch, A. L. (2000). The exoskeleton of bacterial cells (the sacculus): still a highly attractive target for antibacterial agents that will last for a long time. *Crit Rev Microbiol* **26**, 1-35.

Koraimann, G. (2003). Lytic transglycosylases in macromolecular transport systems of Gram-negative bacteria. *Cell Mol Life Sci* **60**, 2371-2388.

Korat, B., Mottl, H. & Keck, W. (1991). Penicillin-Binding Protein-4 of *Escherichia coli* - Molecular-Cloning of the *dacB* Gene, Controlled Overexpression, and Alterations in Murein Composition. *Molecular Microbiology* **5**, 675-684.

Kraft, A. R., Templin, M. F. & Holtje, J. V. (1998). Membrane-bound lytic endotransglycosylase in Escherichia coli. *J Bacteriol* **180**, 3441-3447.

Kremer, K. (2015). Characterization of LytM factors in *Caulobacter crescentus*.

Kumar, P., Arora, K., Lloyd, J. R., Lee, I. Y., Nair, V., Fischer, E., Boshoff, H. I. & Barry, C. E., 3rd (2012). Meropenem inhibits D,D-carboxypeptidase activity in Mycobacterium tuberculosis. *Mol Microbiol* **86**, 367-381.

Kuru, E., Hughes, H. V., Brown, P. J., Hall, E., Tekkam, S., Cava, F., de Pedro, M. A., Brun, Y. V. & van Nieuwenhze, M. S. (2012). In Situ Probing of Newly Synthesized Peptidoglycan in Live Bacteria with Fluorescent D-Amino Acids. *Angewandte Chemie* **51**.

Labischinski, H., Goodell, E. W., Goodell, A. & Hochberg, M. L. (1991). Direct proof of a "more-than-single-layered" peptidoglycan architecture of Escherichia coli W7: a neutron small-angle scattering study. *J Bacteriol* **173**, 751-756.

Laemmli, U. K. (1970). Cleavage of structural proteins during the assembly of the head of bacteriophage T4. *Nature* **227**, 680-685.

Lam, H., Schofield, W. B. & Jacobs-Wagner, C. (2006). A landmark protein essential for establishing and perpetuating the polarity of a bacterial cell. *Cell* **124**, 1011-1023.

Lappann, M., Otto, A., Becher, D. & Vogel, U. (2013). Comparative proteome analysis of spontaneous outer membrane vesicles and purified outer membranes of *Neisseria meningitidis*. *J Bacteriol* **195**, 4425-4435.

Lara, B., Rico, A. I., Petruzzelli, S., Santona, A., Dumas, J., Biton, J., Vicente, M., Mingorance, J. & Massidda, O. (2005). Cell division in cocci: localization and properties of the *Streptococcus pneumoniae* FtsA protein. *Mol Microbiol* **55**, 699-711.

Laub, M. T., McAdams, H. H., Feldblyum, T., Fraser, C. M. & Shapiro, L. (2000). Global analysis of the genetic network controlling a bacterial cell cycle. *Science* **290**, 2144-2148.

Layec, S., Gerard, J., Legue, V., Chapot-Chartier, M. P., Courtin, P., Borges, F., Decaris, B. & Leblond-Bourget, N. (2009). The CHAP domain of Cse functions as an endopeptidase that acts at mature septa to promote *Streptococcus thermophilus* cell separation. *Molecular Microbiology* **71**, 1205-1217.

Leduc, M. & van Heijenoort, J. (1980). Autolysis of *Escherichia coli*. *J Bacteriol* **142**, 52-59.

Leduc, M., Kasra, R. & van Heijenoort, J. (1982). Induction and control of the autolytic system of *Escherichia coli*. *J Bacteriol* **152**, 26-34.

Lee, M., Hesek, D., Llarrull, L. I., Lastochkin, E., Pi, H., Boggess, B. & Mobashery, S. (2013). Reactions of all *Escherichia coli* lytic transglycosylases with bacterial cell wall. *J Am Chem Soc* **135**, 3311-3314.

Letunic, I., Doerks, T. & Bork, P. (2012). SMART 7: recent updates to the protein domain annotation resource. *Nucleic Acids Res* **40**, D302-305.

Levdikov, V. M., Blagova, E. V., McFeat, A., Fogg, M. J., Wilson, K. S. & Wilkinson, A. J. (2012). Structure of components of an intercellular channel complex in sporulating *Bacillus subtilis*. *Proc Natl Acad Sci U S A* **109**, 5441-5445.

Levin, P. A., Shim, J. J. & Grossman, A. D. (1998). Effect of minCD on FtsZ ring position and polar septation in *Bacillus subtilis*. *J Bacteriol* **180**, 6048-6051.

Liepinsh, E., Genereux, C., Dehareng, D., Joris, B. & Otting, G. (2003). NMR structure of *Citrobacter freundii* AmpD, comparison with bacteriophage T7 lysozyme and homology with PGRP domains. *J Mol Biol* **327**, 833-842.

Liu, B., Persons, L., Lee, L. & de Boer, P. A. (2015). Roles for both FtsA and the FtsBLQ subcomplex in FtsN-stimulated cell constriction in *Escherichia coli*. *Mol Microbiol* **95**, 945-970.

Lommatzsch, J., Templin, M. F., Kraft, A. R., Vollmer, W. & Holtje, J. V. (1997). Outer membrane localization of murein hydrolases: MltA, a third lipoprotein lytic transglycosylase in *Escherichia coli*. *J Bacteriol* **179**, 5465-5470.

Lowe, J., Ellonen, A., Allen, M. D., Atkinson, C., Sherratt, D. J. & Grainge, I. (2008). Molecular mechanism of sequence-directed DNA loading and translocation by FtsK. *Mol Cell* **31**, 498-509.

Lutkenhaus, J., Pichoff, S. & Du, S. (2012). Bacterial cytokinesis: From Z ring to divisome. *Cytoskeleton (Hoboken)* **69**, 778-790.

Ma, X. & Margolin, W. (1999). Genetic and functional analyses of the conserved C-terminal core domain of *Escherichia coli* FtsZ. *J Bacteriol* **181**, 7531-7544.

Madoori, P. K. & Thunnissen, A. M. (2010). Purification, crystallization and preliminary X-ray diffraction analysis of the lytic transglycosylase MltF from *Escherichia coli*. *Acta Crystallogr Sect F Struct Biol Cryst Commun* **66**, 534-538.

Magnet, S., Dubost, L., Marie, A., Arthur, M. & Gutmann, L. (2008). Identification of the L,D-transpeptidases for peptidoglycan cross-linking in *Escherichia coli*. *J Bacteriol* **190**, 4782-4785.

Mainardi, J. L., Morel, V., Fourgeaud, M. & other authors (2002). Balance between two transpeptidation mechanisms determines the expression of beta-lactam resistance in *Enterococcus faecium*. *J Biol Chem* **277**, 35801-35807.

Mainardi, J. L., Fourgeaud, M., Hugonnet, J. E., Dubost, L., Brouard, J. P., Ouazzani, J., Rice, L. B., Gutmann, L. & Arthur, M. (2005). A novel peptidoglycan cross-linking enzyme for a beta-lactam-resistant transpeptidation pathway. *J Biol Chem* **280**, 38146-38152.

Markiewicz, Z., Glauner, B. & Schwarz, U. (1983). Murein structure and lack of DD- and LD-carboxypeptidase activities in *Caulobacter crescentus*. *J Bacteriol* **156**, 649-655.

Marks, M. E., Castro-Rojas, C. M., Teiling, C., Du, L., Kapatral, V., Walunas, T. L. & Crosson, S. (2010). The genetic basis of laboratory adaptation in *Caulobacter crescentus*. *J Bacteriol* **192**, 3678-3688.

Martin, M. E., Trimble, M. J. & Brun, Y. V. (2004). Cell cycle-dependent abundance, stability and localization of FtsA and FtsQ in *Caulobacter crescentus*. *Mol Microbiol* **54**, 60-74.

Matias, V. R., Al-Amoudi, A., Dubochet, J. & Beveridge, T. J. (2003). Cryo-transmission electron microscopy of frozen-hydrated sections of *Escherichia coli* and *Pseudomonas aeruginosa*. *J Bacteriol* **185**, 6112-6118.

Matias, V. R. & Beveridge, T. J. (2007). Cryo-electron microscopy of cell division in *Staphylococcus aureus* reveals a mid-zone between nascent cross walls. *Mol Microbiol* **64**, 195-206.

Matias, V. R. F. & Beveridge, T. J. (2005). Cryo-electron microscopy reveals native polymeric cell wall structure in *Bacillus subtilis* 168 and the existence of a periplasmic space. *Molecular Microbiology* **56**, 240-251.

Meisner, J. & Moran, C. P., Jr. (2011). A LytM domain dictates the localization of proteins to the mother cell-forespore interface during bacterial endospore formation. *J Bacteriol* **193**, 591-598.

Meisner, J., Montero Llopis, P., Sham, L. T., Garner, E., Bernhardt, T. G. & Rudner, D. Z. (2013). FtsEX is required for CwlO peptidoglycan hydrolase activity during cell wall elongation in *Bacillus subtilis*. *Mol Microbiol* **89**, 1069-1083.

Mesnage, S., Dellarole, M., Baxter, N. J. & other authors (2014). Molecular basis for bacterial peptidoglycan recognition by LysM domains. *Nat Commun* **5**, 4269.

Modell, J. W., Hopkins, A. C. & Laub, M. T. (2011). A DNA damage checkpoint in *Caulobacter crescentus* inhibits cell division through a direct interaction with FtsW. *Genes Dev* **25**, 1328-1343.

Mohammadi, T., Sijbrandi, R., Lutters, M., Verheul, J., Martin, N. I., den Blaauwen, T., de Kruijff, B. & Breukink, E. (2014). Specificity of the transport of lipid II by FtsW in *Escherichia coli*. *J Biol Chem* **289**, 14707-14718.

Moll, A. & Thanbichler, M. (2009). FtsN-like proteins are conserved components of the cell division machinery in proteobacteria. *Mol Microbiol* **72**, 1037-1053.

Moll, A., Schlimpert, S., Briegel, A., Jensen, G. J. & Thanbichler, M. (2010). DipM, a new factor required for peptidoglycan remodelling during cell division in *Caulobacter crescentus*. *Mol Microbiol* **77**, 90-107.

Moll, A., Dorr, T., Alvarez, L., Chao, M. C., Davis, B. M., Cava, F. & Waldor, M. K. (2014). Cell separation in Vibrio cholerae is mediated by a single amidase whose action is modulated by two nonredundant activators. *J Bacteriol* **196**, 3937-3948.

Möll, A. (2011). Anatomy of the divisome during late stages of the cell division in the assymetric α-proteobacterium *Caulobacter crescentus*. *PhD thesis*.

Mravljak, J., Monasson, O., Al-Dabbagh, B., Crouvoisier, M., Bouhss, A., Gravier-Pelletier, C. & Le Merrer, Y. (2011). Synthesis and biological evaluation of a diazepanone-based library of liposidomycins analogs as MraY inhibitors. *Eur J Med Chem* **46**, 1582-1592.

Mug-Opstelten, D. & Witholt, B. (1978). Preferential release of new outer membrane fragments by exponentially growing *Escherichia coli*. *Biochim Biophys Acta* **508**, 287-295.

Nelson, D. E. & Young, K. D. (2001). Contributions of PBP 5 and DD-carboxypeptidase penicillin binding proteins to maintenance of cell shape in *Escherichia coli*. *J Bacteriol* **183**, 3055-3064.

Neuhaus, F. C. & Baddiley, J. (2003). A continuum of anionic charge: structures and functions of D-alanyl-teichoic acids in gram-positive bacteria. *Microbiol Mol Biol Rev* **67**, 686-723.

Nierman, W. C., Feldblyum, T. V., Laub, M. T. & other authors (2001). Complete genome sequence of *Caulobacter crescentus*. *Proc Natl Acad Sci U S A* **98**, 4136-4141.

Nikaido, H. (2003). Molecular basis of bacterial outer membrane permeability revisited. *Microbiol Mol Biol Rev* **67**, 593-656.

Ohta, N., Ninfa, A. J., Allaire, A., Kulick, L. & Newton, A. (1997). Identification, characterization, and chromosomal organization of cell division cycle genes in *Caulobacter crescentus*. *J Bacteriol* **179**, 2169-2180.

Oldmixon, E. H., Glauser, S. & Higgins, M. L. (1974). Two proposed general configurations for bacterial cell wall peptidoglycans shown by space-filling molecular models. *Biopolymers* **13**, 2037-2060.

Olshausen, P. V., Defeu Soufo, H. J., Wicker, K., Heintzmann, R., Graumann, P. L. & Rohrbach, A. (2013). Superresolution imaging of dynamic MreB filaments in *B. subtilis*--a multiple-motor-driven transport? *Biophys J* **105**, 1171-1181.

Osawa, M., Anderson, D. E. & Erickson, H. P. (2009). Curved FtsZ protofilaments generate bending forces on liposome membranes. *EMBO J* **28**, 3476-3484.

Paradis-Bleau, C., Markovski, M., Uehara, T., Lupoli, T. J., Walker, S., Kahne, D. E. & Bernhardt, T. G. (2010). Lipoprotein cofactors located in the outer membrane activate bacterial cell wall polymerases. *Cell* **143**, 1110-1120.

Park, J. T. (1993). Turnover and recycling of the murein sacculus in oligopeptide permease-negative strains of *Escherichia coli*: indirect evidence for an alternative permease system and for a monolayered sacculus. *J Bacteriol* **175**, 7-11.

Park, J. T. (1995). Why does *Escherichia coli* recycle its cell wall peptides? *Mol Microbiol* **17**, 421-426.

Park, J. T. & Uehara, T. (2008). How bacteria consume their own exoskeletons (turnover and recycling of cell wall peptidoglycan). *Microbiol Mol Biol Rev* **72**, 211-227, table of contents.

Parsons, L. M., Lin, F. & Orban, J. (2006). Peptidoglycan recognition by Pal, an outer membrane lipoprotein. *Biochemistry* **45**, 2122-2128.

Pazos, M., Natale, P. & Vicente, M. (2013). A specific role for the ZipA protein in cell division: stabilization of the FtsZ protein. *J Biol Chem* **288**, 3219-3226.

Peters, N. T., Dinh, T. & Bernhardt, T. G. (2011). A Fail-Safe Mechanism in the Septal Ring Assembly Pathway Generated by the Sequential Recruitment of Cell Separation Amidases and Their Activators. *Journal of Bacteriology* **193**, 4973-4983.

Pichoff, S. & Lutkenhaus, J. (2002). Unique and overlapping roles for ZipA and FtsA in septal ring assembly in *Escherichia coli*. *EMBO J* **21**, 685-693.

Pichoff, S. & Lutkenhaus, J. (2007). Identification of a region of FtsA required for interaction with FtsZ. *Mol Microbiol* **64**, 1129-1138.

Pichoff, S., Shen, B., Sullivan, B. & Lutkenhaus, J. (2012). FtsA mutants impaired for self-interaction bypass ZipA suggesting a model in which FtsA's self-interaction competes with its ability to recruit downstream division proteins. *Mol Microbiol* **83**, 151-167.

Pisabarro, A. G., Prats, R., Vaquez, D. & Rodriguez-Tebar, A. (1986). Activity of penicillin-binding protein 3 from *Escherichia coli*. *J Bacteriol* **168**, 199-206.

Poggio, S., Takacs, C. N., Vollmer, W. & Jacobs-Wagner, C. (2010). A protein critical for cell constriction in the Gram-negative bacterium *Caulobacter crescentus* localizes at the division site through its peptidoglycan-binding LysM domains. *Mol Microbiol* **77**, 74-89.

Poindexter, J. S. (1964). Biological Properties and Classification of the *Caulobacter* Group. *Bacteriol Rev* **28**, 231-295.

Priyadarshini, R., de Pedro, M. A. & Young, K. D. (2007). Role of peptidoglycan amidases in the development and morphology of the division septum in *Escherichia coli*. *J Bacteriol* **189**, 5334-5347.

Raetz, C. R. H. & Whitfield, C. (2002). Lipopolysaccharide endotoxins. *Annual Review of Biochemistry* **71**, 635-700.

Record, M. T., Jr., Courtenay, E. S., Cayley, S. & Guttman, H. J. (1998). Biophysical compensation mechanisms buffering *E. coli* protein-nucleic acid interactions against changing environments. *Trends Biochem Sci* **23**, 190-194.

Reddy, M. (2007). Role of FtsEX in cell division of *Escherichia coli*: viability of ftsEX mutants is dependent on functional SufI or high osmotic strength. *Journal of Bacteriology* **189**, 98-108.

Rigden, D. J., Jedrzejas, M. J. & Galperin, M. Y. (2003). Amidase domains from bacterial and phage autolysins define a family of gamma-D,L-glutamate-specific amidohydrolases. *Trends in Biochemical Sciences* **28**, 230-234.

Robson, S. A., Michie, K. A., Mackay, J. P., Harry, E. & King, G. F. (2002). The *Bacillus subtilis* cell division proteins FtsL and DivIC are intrinsically unstable and do not interact with one another in the absence of other septasomal components. *Mol Microbiol* **44**, 663-674.

Rocaboy, M., Herman, R., Sauvage, E., Remaut, H., Moonens, K., Terrak, M., Charlier, P. & Kerff, F. (2013). The crystal structure of the cell division amidase AmiC reveals the fold of the AMIN domain, a new peptidoglycan binding domain. *Mol Microbiol* **90**, 267-277.

Royet, J. & Dziarski, R. (2007). Peptidoglycan recognition proteins: pleiotropic sensors and effectors of antimicrobial defences. *Nat Rev Microbiol* **5**, 264-277.

Salje, J., van den Ent, F., de Boer, P. & Lowe, J. (2011). Direct membrane binding by bacterial actin MreB. *Mol Cell* **43**, 478-487.

Sambrook, J. (1989). Molecular Cloning. A Laboratory Manual. *Cold Spring Harbor Laboratory Press*

Sanders, A. N. & Pavelka, M. S. (2013). Phenotypic analysis of *Eschericia coli* mutants lacking L,D-transpeptidases. *Microbiology* **159**, 1842-1852.

Sauvage, E., Kerff, F., Terrak, M., Ayala, J. A. & Charlier, P. (2008). The penicillin-binding proteins: structure and role in peptidoglycan biosynthesis. *FEMS Microbiol Rev* **32**, 234-258.

Schindler, C. A. & Schuhardt, V. T. (1964). Lysostaphin: A New Bacteriolytic Agent for the *Staphylococcus*. *Proc Natl Acad Sci U S A* **51**, 414-421.

Schleife.Kh & Kandler, O. (1972). Peptidoglycan Types of Bacterial Cell-Walls and Their Taxonomic Implications. *Bacteriological Reviews* **36**, 407-477.

Schmidt, K. L., Peterson, N. D., Kustusch, R. J., Wissel, M. C., Graham, B., Phillips, G. J. & Weiss, D. S. (2004). A predicted ABC transporter, FtsEX, is needed for cell division in *Escherichia coli*. *J Bacteriol* **186**, 785-793.

Schultz, J., Milpetz, F., Bork, P. & Ponting, C. P. (1998). SMART, a simple modular architecture research tool: identification of signaling domains. *Proc Natl Acad Sci U S A* **95**, 5857-5864.

Sham, L. T., Barendt, S. M., Kopecky, K. E. & Winkler, M. E. (2011). Essential PcsB putative peptidoglycan hydrolase interacts with the essential FtsXSpn cell division protein in *Streptococcus pneumoniae* D39. *Proc Natl Acad Sci U S A* **108**, E1061-1069.

Sham, L. T., Butler, E. K., Lebar, M. D., Kahne, D., Bernhardt, T. G. & Ruiz, N. (2014). Bacterial cell wall. MurJ is the flippase of lipid-linked precursors for peptidoglycan biogenesis. *Science* **345**, 220-222.

Sherratt, D. J., Arciszewska, L. K., Crozat, E., Graham, J. E. & Grainge, I. (2010). The *Escherichia coli* DNA translocase FtsK. *Biochem Soc Trans* **38**, 395-398.

Siegrist, M. S., Whiteside, S., Jewett, J. C., Aditham, A., Cava, F. & Bertozzi, C. R. (2013). (D)-Amino acid chemical reporters reveal peptidoglycan dynamics of an intracellular pathogen. *ACS Chem Biol* **8**, 500-505.

Singh, S. K., SaiSree, L., Amrutha, R. N. & Reddy, M. (2012). Three redundant murein endopeptidases catalyse an essential cleavage step in peptidoglycan synthesis of *Escherichia coli* K12. *Molecular Microbiology* **86**, 1036-1051.

Snowden, M. A. & Perkins, H. R. (1990). Peptidoglycan cross-linking in *Staphylococcus aureus*. An apparent random polymerisation process. *Eur J Biochem* **191**, 373-377.

Spratt, B. G. (1977). Properties of the penicillin-binding proteins of *Escherichia coli* K12. *Eur J Biochem* **72**, 341-352.

Stohl, E. A., Chan, Y. A., Hackett, K. T., Kohler, P. L., Dillard, J. P. & Seifert, H. S. (2012). *Neisseria gonorrhoeae* virulence factor NG1686 is a bifunctional M23B family metallopeptidase that influences resistance to hydrogen peroxide and colony morphology. *J Biol Chem* **287**, 11222-11233.

Strobel, W., Moll, A., Kiekebusch, D., Klein, K. E. & Thanbichler, M. (2014). Function and localization dynamics of bifunctional penicillin-binding proteins in *Caulobacter crescentus*. *J Bacteriol* **196**, 1627-1639.

Sturgis, J. N. (2001). Organisation and evolution of the tol-pal gene cluster. *J Mol Microbiol Biotechnol* **3**, 113-122.

Suginaka, H., Blumberg, P. M. & Strominger, J. L. (1972). Multiple penicillin-binding components in *Bacillus subtilis*, *Bacillus cereus*, *Staphylococcus aureus*, and *Escherichia coli*. *J Biol Chem* **247**, 5279-5288.

Sundararajan, K., Miguel, A., Desmarais, S. M., Meier, E. L., Casey Huang, K. & Goley, E. D. (2015). The bacterial tubulin FtsZ requires its intrinsically disordered linker to direct robust cell wall construction. *Nat Commun* **6**, 7281.

Szwedziak, P., Wang, Q., Freund, S. M. & Lowe, J. (2012). FtsA forms actin-like protofilaments. *EMBO J* **31**, 2249-2260.

Szwedziak, P., Wang, Q., Bharat, T. A., Tsim, M. & Lowe, J. (2014). Architecture of the ring formed by the tubulin homologue FtsZ in bacterial cell division. *Elife* **4**.

Takacs, C. N., Poggio, S., Charbon, G., Pucheault, M., Vollmer, W. & Jacobs-Wagner, C. (2010). MreB drives de novo rod morphogenesis in *Caulobacter crescentus* via remodeling of the cell wall. *J Bacteriol* **192**, 1671-1684.

Takacs, C. N., Hocking, J., Cabeen, M. T., Bui, N. K., Poggio, S., Vollmer, W. & Jacobs-Wagner, C. (2013). Growth medium-dependent glycine incorporation into the peptidoglycan of *Caulobacter crescentus*. *PLoS One* **8**, e57579.

Tatusov, R. L., Natale, D. A., Garkavtsev, I. V. & other authors (2001). The COG database: new developments in phylogenetic classification of proteins from complete genomes. *Nucleic Acids Res* **29**, 22-28.

Thanbichler, M. & Shapiro, L. (2006). MipZ, a spatial regulator coordinating chromosome segregation with cell division in *Caulobacter*. *Cell* **126**, 147-162.

Thanbichler, M., Iniesta, A. A. & Shapiro, L. (2007). A comprehensive set of plasmids for vanillate- and xylose-inducible gene expression in *Caulobacter crescentus*. *Nucleic Acids Res* **35**, e137.

Thunnissen, A. M., Isaacs, N. W. & Dijkstra, B. W. (1995). The catalytic domain of a bacterial lytic transglycosylase defines a novel class of lysozymes. *Proteins* **22**, 245-258.

Tidhar, A., Flashner, Y., Cohen, S. & other authors (2009). The NlpD lipoprotein is a novel *Yersinia pestis* virulence factor essential for the development of plague. *PLoS One* **4**, e7023.

Tomasz, A., Albino, A. & Zanati, E. (1970). Multiple antibiotic resistance in a bacterium with suppressed autolytic system. *Nature* **227**, 138-140.

Tomasz, A. (1979). The mechanism of the irreversible antimicrobial effects of penicillins: how the beta-lactam antibiotics kill and lyse bacteria. *Annu Rev Microbiol* **33**, 113-137.

Tsang, M. J. & Bernhardt, T. G. (2015a). A role for the FtsQLB complex in cytokinetic ring activation revealed by an ftsL allele that accelerates division. *Mol Microbiol* **95**, 925-944.

Tsang, M. J. & Bernhardt, T. G. (2015b). Guiding divisome assembly and controlling its activity. *Curr Opin Microbiol* **24**, 60-65.

Turner, R. D., Hurd, A. F., Cadby, A., Hobbs, J. K. & Foster, S. J. (2013). Cell wall elongation mode in Gram-negative bacteria is determined by peptidoglycan architecture. *Nat Commun* **4**, 1496.

Turner, R. D., Vollmer, W. & Foster, S. J. (2014). Different walls for rods and balls: the diversity of peptidoglycan. *Mol Microbiol* **91**, 862-874.

Typas, A., Banzhaf, M., van den Berg van Saparoea, B. & other authors (2010). Regulation of peptidoglycan synthesis by outer-membrane proteins. *Cell* **143**, 1097-1109.

Typas, A., Banzhaf, M., Gross, C. A. & Vollmer, W. (2012). From the regulation of peptidoglycan synthesis to bacterial growth and morphology. *Nat Rev Microbiol* **10**, 123-136.

Uehara, T., Dinh, T. & Bernhardt, T. G. (2009). LytM-Domain Factors Are Required for Daughter Cell Separation and Rapid Ampicillin-Induced Lysis in *Escherichia coli*. *Journal of Bacteriology* **191**, 5094-5107.

Uehara, T., Parzych, K. R., Dinh, T. & Bernhardt, T. G. (2010). Daughter cell separation is controlled by cytokinetic ring-activated cell wall hydrolysis. *EMBO J* **29**, 1412-1422.

Ursinus, A., van den Ent, F., Brechtel, S., de Pedro, M., Holtje, J. V., Lowe, J. & Vollmer, W. (2004). Murein (peptidoglycan) binding property of the essential cell division protein FtsN from *Escherichia coli*. *J Bacteriol* **186**, 6728-6737.

van Asselt, E. J., Dijkstra, A. J., Kalk, K. H., Takacs, B., Keck, W. & Dijkstra, B. W. (1999a). Crystal structure of Escherichia coli lytic transglycosylase Slt35 reveals a lysozyme-like catalytic domain with an EF-hand. *Structure* **7**, 1167-1180.

van Asselt, E. J., Thunnissen, A. M. & Dijkstra, B. W. (1999b). High resolution crystal structures of the *Escherichia coli* lytic transglycosylase Slt70 and its complex with a peptidoglycan fragment. *J Mol Biol* **291**, 877-898.

van Asselt, E. J., Kalk, K. H. & Dijkstra, B. W. (2000). Crystallographic studies of the interactions of *Escherichia coli* lytic transglycosylase Slt35 with peptidoglycan. *Biochemistry* **39**, 1924-1934.

van den Bogaart, G., Hermans, N., Krasnikov, V. & Poolman, B. (2007). Protein mobility and diffusive barriers in *Escherichia coli*: consequences of osmotic stress. *Mol Microbiol* **64**, 858-871.

van Heijenoort, J. (2011). Peptidoglycan hydrolases of *Escherichia coli*. *Microbiol Mol Biol Rev* **75**, 636-663.

van Straaten, K. E., Dijkstra, B. W., Vollmer, W. & Thunnissen, A. M. (2005). Crystal structure of MltA from *Escherichia coli* reveals a unique lytic transglycosylase fold. *J Mol Biol* **352**, 1068-1080.

van Straaten, K. E., Barends, T. R., Dijkstra, B. W. & Thunnissen, A. M. (2007). Structure of *Escherichia coli* Lytic transglycosylase MltA with bound chitohexaose: implications for peptidoglycan binding and cleavage. *J Biol Chem* **282**, 21197-21205.

van Teeffelen, S., Wang, S., Furchtgott, L., Huang, K. C., Wingreen, N. S., Shaevitz, J. W. & Gitai, Z. (2011). The bacterial actin MreB rotates, and rotation depends on cell-wall assembly. *Proc Natl Acad Sci U S A* **108**, 15822-15827.

Viollier, P. H. & Shapiro, L. (2003). A lytic transglycosylase homologue, PleA, is required for the assembly of pili and the flagellum at the *Caulobacter crescentus* cell pole. *Mol Microbiol* **49**, 331-345.

Virudachalam, R. & Rao, V. S. R. (1979). Theoretical Studies on Peptidoglycans .2. Conformations of the Disaccharide-Peptide Subunit and the 3-Dimensional Structure of Peptidoglycan. *Biopolymers* **18**, 571-589.

Vollmer, W. (2008). Structural variation in the glycan strands of bacterial peptidoglycan. *FEMS Microbiol Rev* **32**, 287-306.

Vollmer, W. & Bertsche, U. (2008). Murein (peptidoglycan) structure, architecture and biosynthesis in *Escherichia coli*. *Biochim Biophys Acta* **1778**, 1714-1734.

Vollmer, W., Blanot, D. & de Pedro, M. A. (2008). Peptidoglycan structure and architecture. *FEMS Microbiol Rev* **32**, 149-167.

Vollmer, W. & Seligman, S. J. (2010). Architecture of peptidoglycan: more data and more models. *Trends Microbiol* **18**, 59-66.

Wang, L., Khattar, M. K., Donachie, W. D. & Lutkenhaus, J. (1998). FtsI and FtsW are localized to the septum in *Escherichia coli*. *J Bacteriol* **180**, 2810-2816.

Wang, S. C., West, L. & Shapiro, L. (2006). The bifunctional FtsK protein mediates chromosome partitioning and cell division in *Caulobacter*. *J Bacteriol* **188**, 1497-1508.

Wang, T. S., Manning, S. A., Walker, S. & Kahne, D. (2008). Isolated peptidoglycan glycosyltransferases from different organisms produce different glycan chain lengths. *J Am Chem Soc* **130**, 14068-14069.

Weatherspoon-Griffin, N., Zhao, G., Kong, W., Kong, Y., Morigen, Andrews-Polymenis, H., McClelland, M. & Shi, Y. (2011). The CpxR/CpxA two-component system up-regulates two Tat-dependent peptidoglycan amidases to confer bacterial resistance to antimicrobial peptide. *J Biol Chem* **286**, 5529-5539.

Weidel, W. & Pelzer, H. (1964). Bagshaped Macromolecules--a New Outlook on Bacterial Cell Walls. *Adv Enzymol Relat Areas Mol Biol* **26**, 193-232.

Weigand, R. A., Vinci, K. D. & Rothfield, L. I. (1976). Morphogenesis of the bacterial division septum: a new class of septation-defective mutants. *Proc Natl Acad Sci U S A* **73**, 1882-1886.

Weiss, D. S. (2015). Last but not least: new insights into how FtsN triggers constriction during *Escherichia coli* cell division. *Mol Microbiol* **95**, 903-909.

West, L., Yang, D. & Stephens, C. (2002). Use of the *Caulobacter crescentus* genome sequence to develop a method for systematic genetic mapping. *Journal of Bacteriology* **184**, 2155-2166.

Whisstock, J. C. & Lesk, A. M. (1999). SH3 domains in prokaryotes. *Trends Biochem Sci* **24**, 132-133.

Yahashiri, A., Jorgenson, M. A. & Weiss, D. S. (2015). Bacterial SPOR domains are recruited to septal peptidoglycan by binding to glycan strands that lack stem peptides. *Proc Natl Acad Sci U S A* **112**, 11347-11352.

Yakhnina, A. A. & Gitai, Z. (2013). Diverse functions for six glycosyltransferases in Caulobacter crescentus cell wall assembly. *J Bacteriol* **195**, 4527-4535.

Yakhnina, A. A., McManus, H. R. & Bernhardt, T. G. (2015). The cell wall amidase AmiB is essential for *Pseudomonas aeruginosa* cell division, drug resistance and viability. *Mol Microbiol* **97**, 957-973.

Yamada, S., Sugai, M., Komatsuzawa, H., Nakashima, S., Oshida, T., Matsumoto, A. & Suginaka, H. (1996). An autolysin ring associated with cell separation of *Staphylococcus aureus*. *J Bacteriol* **178**, 1565-1571.

Yamamoto, H., Hashimoto, M., Higashitsuji, Y., Harada, H., Hariyama, N., Takahashi, L., Iwashita, T., Ooiwa, S. & Sekiguchi, J. (2008). Post-translational control of vegetative cell separation enzymes through a direct interaction with specific inhibitor IseA in *Bacillus subtilis*. *Mol Microbiol* **70**, 168-182.

Yang, D. C., Peters, N. T., Parzych, K. R., Uehara, T., Markovski, M. & Bernhardt, T. G. (2011). An ATP-binding cassette transporter-like complex governs cell-wall hydrolysis at the bacterial cytokinetic ring. *Proceedings of the National Academy of Sciences of the United States of America* **108**, E1052-E1060.

Yang, D. C., Tan, K., Joachimiak, A. & Bernhardt, T. G. (2012a). A conformational switch controls cell wall-remodelling enzymes required for bacterial cell division. *Mol Microbiol* **85**, 768-781.

Yang, D. C., Tan, K. M., Joachimiak, A. & Bernhardt, T. G. (2012b). A conformational switch controls cell wall-remodelling enzymes required for bacterial cell division. *Molecular Microbiology* **85**, 768-781.

Yao, X., Jericho, M., Pink, D. & Beveridge, T. (1999). Thickness and elasticity of gram-negative murein sacculi measured by atomic force microscopy. *Journal of Bacteriology* **181**, 6865-6875.

Yeh, Y. C., Comolli, L. R., Downing, K. H., Shapiro, L. & McAdams, H. H. (2010). The *Caulobacter* Tol-Pal complex is essential for outer membrane integrity and the positioning of a polar localization factor. *J Bacteriol* **192**, 4847-4858.

Yousif, S. Y., Broome-Smith, J. K. & Spratt, B. G. (1985). Lysis of *Escherichia coli* by beta-lactam antibiotics: deletion analysis of the role of penicillin-binding proteins 1A and 1B. *J Gen Microbiol* **131**, 2839-2845.

EINVERSTANDNISERKLÄRUNG

Ich versichere, dass ich meine Dissertation:

„Comprehensive analysis of peptidoglycan hydrolases in *Caulobacter crescentus*"

selbstständig, ohne unerlaubte Hilfe angefertigt und mich dabei keiner anderen als der von mir ausdrücklich bezeichneten Quellen und Hilfen bedient habe. Die Dissertation wurde in der jetzigen oder einer ähnlichen Form noch bei keiner anderen Hochschule eingereicht und hat noch keinen sonstigen Prüfungszwecken gedient.

Marburg, den ___.___.2016   Aleksandra Zielińska